THE INTERACTION BETWEEN FIBRILLAR BETA-2 MICROGLOBULIN AND SERUM AMYLOID P COMPONENT

Garrick Foster Taylor

THESIS SUBMITTED TO THE CENTRE FOR BIOLOGICAL SCIENCES GRADUATE SCHOOL IN PARTIAL FULFILMENT OF THE REQUIREMENTS FOR AWARD OF THE DEGREE OF DOCTOR OF PHILOSOPHY BY THE UNIVERSITY OF SOUTHAMPTON

CENTRE FOR BIOLOGICAL SCIENCES

UNIVERSITY OF SOUTHAMPTON

OCTOBER 2011

UNIVERSITY OF SOUTHAMPTON

ABSTRACT

FACULTY OF NATURAL AND ENVIRONMENTAL SCIENCES

Biological Sciences

Doctor of Philosophy

THE INTERACTION BETWEEN FIBRILLAR BETA-2 MICROGLOBULIN AND SERUM AMYLOID P COMPONENT

Garrick Foster Taylor

Dialysis Related Amyloidosis (DRA) is a serious complication of long term haemodialysis. Amyloid deposits accumulate in the joints causing great pain & restricting mobility of sufferers. The main constituent of these amyloid deposits is fibrillar β_2-microglobulin (β_2m), although additional components are found which are thought to affect the formation and stability of the β_2m fibrils.

β_2m fibrils formed *in vitro* under acidic conditions appear to have the same morphology as fibrils formed *in vivo* under pathological conditions when studied using electron microscopy and atomic force microscopy. However, the *in vitro* formed fibrils are not stable at neutral pH and quickly dissociate into monomeric and low oligomeric species. This raises the question as to why fibrils do not dissociate *in vivo* at physiological pH.

In vivo serum amyloid P component (SAP) is always found associated with β_2m fibrils and thought to stabilise the fibrils by preventing dissociation. Here we present evidence from pull-down assays that SAP binds tightly to acid produced β_2m fibrils.

The behaviour of the acid produced fibrils with and in the absence of SAP at neutral pH has being characterised using Thioflavin T fluorescence studies and has revealed that SAP does have a small stabilising effect on acid produced fibrils at the concentrations tested. The studies also imply that ionic strength as well as free protein concentration are important determining factors into the longevity of the fibrils at neutral pH.

Studies of β_2m in inclusion bodies prior to refolding demonstrate that they are not identical to β_2m fibrils but that NMR studies do show areas of structural homogeneity with fibrils suggesting that the inclusion bodies may have structure and are not amorphous aggregate as previously thought.

Soluble β_2m has been assigned using solution-state NMR to identify regions of structural transition between soluble and fibrillar forms of β_2m. Solid-state NMR spectra of acid produced fibrils have been acquired at both acidic and neutral pH and reveal that at a molecular level the fibrils are structurally homogenous, giving rise to spectra with site specific resolution. Sequential assignment of fibrillar β_2m has therefore been possible using specific labelling techniques to overcome spectral crowding.

To identify the interaction interface between β_2m fibrils and SAP we have undertaken solid-state NMR studies of β_2m with and without SAP bound. Comparing the chemical shifts from these studies has allowed us to identify that SAP is interacting with the side chain carboxylates of fibril aspartates and glutamates. Subsequent chemical modification of these carboxylates to remove their charge resulted in complete inhibition of SAP binding; confirming that they are essential for SAP binding to occur. However there is no strong interaction between monomeric β_2m and SAP occurring demonstrating that a collective action of these acidic side chains is needed for binding to occur. Fibrils provide this in the form of acidic strips along the fibril axis brought about by the parallel and anti-parallel beta-strand structure of fibrils.

Table of Contents

List of Tables

List of Figures

Academic Thesis: Declaration Of Authorship

I, Garrick Foster Taylor,

declare that this thesis and the work presented in it are my own and has been generated by me as the result of my own original research.

THE INTERACTION BETWEEN FIBRILLAR BETA-2 MICROGLOBULIN AND SERUM AMYLOID P COMPONENT

I confirm that:

1. This work was done wholly or mainly while in candidature for a research degree at this University;

2. Where any part of this thesis has previously been submitted for a degree or any other qualification at this University or any other institution, this has been clearly stated;

3. Where I have consulted the published work of others, this is always clearly attributed;

4. Where I have quoted from the work of others, the source is always given. With the exception of such quotations, this thesis is entirely my own work;

5. I have acknowledged all main sources of help;

6. Where the thesis is based on work done by myself jointly with others, I have made clear exactly what was done by others and what I have contributed myself;

7. Either none of this work has been published before submission, or parts of this work have been published as:

Taylor, G. F., Wood, S. P., Mörs, K., Glaubitz, C., Werner, J. M., and Williamson, P. T. F. (2011) Morphological Differences between β2-Microglobulin in Fibrils and Inclusion Bodies, *ChemBioChem 12*, 556-558.

Signed:

Date:

Acknowledgements

Firstly, I would like to thank my primary supervisor Phil Williamson for all his support, both academic and pastoral, during my 4 years of PhD studies. I'm fully aware that Phil couldn't have ended up with his first ever PhD student coming from a more unconventional background. Phil has been an amazing supervisor and I couldn't have been better looked after. Phil has managed to look after me while also, along with Jeanne, looking after little Zoë, who I'm sure will be grateful that she'll no longer have to compete for her Daddy's attention with me!

I would also like to express my sincerest gratitude to my supervisors, Jörn Werner and Steve Wood, whose experience and genius have been of so much help in completing my studies and dealing with some really very challenging academic subject areas.

I need to thank Phedra Marius, Stuart Findlow and Neville Wright without whom I would have been wandering around the lab not knowing what to do (and most probably alight!).

For inspiring and encouraging me to do a PhD I thank (blame?) Lindy Holden-Dye, John Chad and Vincent O'Connor, three truly inspirational figures at the University of Southampton.

I'd like to sincerely acknowledge the help and support of Neil Smyth, Lorraine Prout and all the members of the graduate school and admin staff, without whom all the PhD students, I especially, would be wandering around like penniless headless chickens.

Thanks go to the UK 850 MHz Solid-State NMR Facility in Warwick and the Frankfurt Facility for Biomolecular NMR and EPR for allowing me to play with their incredibly expensive magnets. Thanks especially go to Prof. Clemens Glaubitz and Prof. Steven Brown for allowing this to happen. For looking after me, treating me with such kindness and making Frankfurt like a second home to me, I would like to thank the entire Glaubitz group but especially Lenica Reggie and Jakob Lopez for their excellent sense of humour and many fascinating and hysterical conversations.

There are many past and present lab and office members who have provided valuable academic assistance and drinking companionship over the 4 years. To name but a few: Michael Knight, Nik Rogers, Helen Watson, Juan Bolivar-Gonzalez, Sam Hill, Chris Ford, John Butler and Natalie Smithers. Special thanks go to Annie Cardew who will always be a close friend.

I've had the pleasure of looking after many project students in my time at Southampton and a big thanks to all of you for making my job so easy; however one student will always be remembered as my Padawan and that is Sarah Stephens, a truly gifted individual who will one day no doubt be trying to avoid me as I pester her for a job!

On a wider school and faculty basis there have been many people who have enhanced my PhD experience through nights out and in, friendship and providing me meals so that I didn't exist on a diet of solely steak and pasta. Franky Lock, Mike Blackney, Hazel Smith, Helga Groll, Kirstin Williamson, Chih-Hua Huang, Mandela Fernandez-Grandon, Jo Bailey, Gabrielle Lockett, Tom Secker, Becky Stead, Nash Matinyarare, Nancy Wong,

Scott Kimber and many more whom I would mention but fear going over the allowed word count!

PhDs are stressful; I found that throwing myself out of planes helped relieve some of this stress. A huge thanks goes to the University of Southampton Skydive Club which I had the honour of being Captain of for so many years. Special thanks go to my committees over the years and in particular Hannah Lever and Sam Cady who have been rocks to me. Of course I also have to thank my team mates from the mighty Team Jesters, Matt Gottwald, Tom 'TB' Bennet and Jakob Aungiers. I'll always prefer to have Jakob flying flat beside me rather than head down through me! Amielia Katze, you are one of my most talented friends and you are destined for great things!

Sean Hughes, Chris Holmes, Jen Lemon and Lauren Davies have been essential in being some of my only friends of similar age. Sometimes it's just too tiring being around 20 year olds!

A special mention goes to my family who, even through the toughest of times, never seemed to lose faith in me. Special thanks go to my mum, sisters Donna and Jade, and my Uncle George and Aunt Lorraine who have always been there for me. In this section I also include Neil Thaxter, who I class as family and without whose support I would never have been able to make it through my undergraduate years to make it to my PhD studies.

University is about more than getting qualifications and the most valuable thing I'll be leaving with is not a Doctorate but a fantastic group of friends who, had I not embarked upon higher education, I would never have met. These friends are numerous but two stick out beyond measure, one is Sammy Hibberd who has been a true friend ever since I met her studying nutrition as an undergrad; the other much newer friend, but who is possibly the dearest to me, is Nicola 'The Sea' Jackson. Nicola you've been the friend that made me realise what the true definition of a friend is and if it wasn't for you and our friend Katy, this last year probably would have been so stressful I would have gone quite mad!

Life can change a lot in eight years and mine certainly has, I'm so glad that you have all been there to witness that change!

Abbreviations and acronyms

ADDL: Alzheimer's Disease Diffusible Ligand

Aβ: Amyloid beta (Alzheimer's disease)

AGE: Advanced glycation end products

ApoE: Apolipoprotein E

β_2m: Beta-2 microglobulin

BCA: Bicinchoninic acid

CMC: Carboxymethyl cellulose

CP: Cross-polarisation

CPHPC: R-1-[6-[R-2-carboxy-pyrrolidin-1-yl]-6-oxohexanoyl] pyrrolidine-2-carboxylic acid

Cryo-EM: Cryogenic electron microscopy

CSA: Chemical shift anisotropy

CSI: Chemical shift index

CTS: Carpal tunnel Syndrome

DRA: Dialysis related amyloidosis

DSA: Destructive spondyloarthopathy

E.coli: *Escherichia coli*

EDTA: Ethylenediaminetetraacetic acid

EM: Electron microscopy

FID: Free induction decay

GAG: Glycosaminoglycan

HEPES: 4-(2-hydroxyethyl)-1-piperazineethanesulfonic acid

HSQC: Heteronuclear single-quantum correlation

IB: Inclusion body

INEPT: Insensitive nuclei enhanced by polarisation transfer

K1-9: Peptide fragments produced by lysyl endopeptidase digestion of β_2m

MAS: Magic angle spinning

MHC I: Majorhistocompatibility complex 1

MPL: Mass per unit length

NMR: Nuclear magnetic resonance

PAGE: Polyacrylamide gel electrophoresis

PHF: Paired helical filaments

RF: Radio frequency

SAP: Serum amyloid P component

SDS: Sodium dodecyl sulphate

SEC: Size exclusion chromatography

SPINAL: Small phase incremental alternation

STEM: Scanning transmission electron microscopy

T_1: Longitudinal relaxation time

T_2: Transverse relaxation time

TEM: Transmission electron microscopy

TFE: Tetrafluoroethanol

ThT: Thioflavin T

TNCa: Tris, sodium chloride and calcium containing buffer

TPPM: Time proportional phase modulated

US: Ultra shield

WB: Wide bore

Chapter 1

1 Introduction

1.1 Amyloid

1.1.1 What is amyloid?

Amyloid is the term given to insoluble plaques that have formed from normally soluble proteins that have misfolded, aggregated and deposited as highly ordered fibrils. This deposition can eventually cause disruption to the structure and function of organs and tissues affected, although deposition may be asymptomatic (*1*). These fibrils are the main constituent of plaques which also usually contain other constituents such as proteoglycans, heparan and dermatan sulphated glycosaminoglycans (GAG) and serum amyloid P component (SAP) amongst others. In humans, all instances of amyloid formation are associated with disease states and there are over 20 proteins that are associated with types of amyloidosis.

The classical criterion for classification of deposits as amyloid is for them to show apple green birefringence when stained with Congo red dye and viewed under cross polarised light as was demonstrated by Divry and Florkin in the 1920s (*2*). This assay still remains the gold standard in clinical settings but typically amyloidosis is diagnosed through histology of biopsy or autopsy specimens, however modern criteria would also include the observation of long unbranched fibrils using negative stain transmission electron microscopy.

The exact processes that leads normally soluble proteins to transition into insoluble amyloid *in vivo* remain elusive in most cases but based on *in vitro* findings it is generally

agreed that it is at least a two step, nucleation dependent process that requires a partial unfolding event in the case of natively globular proteins (*3*) or in the case of natively unfolded proteins such as α-synuclein, a partial folding event. Familial amyloidoses are usually caused by a mutation that causes the expressed protein to become partially unfolded.

1.1.2 Diseases associated with amyloid

Broadly speaking there are two main types of disease associated with amyloid, systemic and localised or tissue specific amyloidoses. In the systemic amyloidoses amyloid deposits accumulate in the parenchyma of the viscera and of all other tissues except the brain; diseases include reactive systemic amyloidosis and monoclonal immunoglobulin light chain amyloidosis (*1, 3*). Localised amyloidoses occur in certain organs only, including the brain. Diseases such as Alzheimer's, Parkinson's and Huntington's are all localised and all have amyloid associated with them although there is debate as to whether it is the amyloid causing the major symptoms of the disease in these cases (*3-6*). All currently known amyloidoses are listed in Table 1 and Table 2.

The mechanisms by which amyloid causes pathogenesis are not fully understood. A large amount of amyloid deposited in organs is structurally disruptive and can compromise normal function and so their presence alone can cause pathological effects, however the correlation between amount of amyloid present and the severity of symptoms is sometimes poor. For instance visualisation of amyloid load on organs using radioisotopically labelled SAP scintigraphy has shown poor correlation with the amount of amyloid within an organ and the organ's resultant dysfunction (*7*). In addition similar amounts of amyloid from different precursor proteins can cause differing severity of symptoms. Cardiac amyloid

deposits in light chain amyloidosis cause worse functional and prognostic impact than in patients with similar quantities of cardiac amyloid deposits in transthyretin amyloidosis (*8*). The type of amyloid must therefore play a role in pathogenesis, ruling out a simple space occupying hypothesis in at least some cases.

Table 1 Human neurodegenerative diseases associated with amyloid or intracellular inclusions

Adapted from Chiti *et al.* (2006) (*3*)

Disease	Aggregating protein	Number of residues	Native structure of protein
Neurodegenerative diseases			
Alzheimer's disease	**Amyloid β peptide**	**40 or 42**	**Natively unfolded**
Amyotrophic lateral sclerosis	**Superoxide dismutase I**	**153**	**All β, Ig like**
Dementia with Lewy bodies	**α-synuclein**	**140**	**Natively unfolded**
Familial British dementia	**ABri**	**23**	**Natively unfolded**
Familial Danish dementia	**ADan**	**23**	**Natively unfolded**
Frontotemporal dementia with Parkinsonism	**Tau**	**352-441**	**Natively unfolded**
Hereditary dentatorubral-pallidoluysian atrophy	**Atrophin-1 with polyQ expansion**	**1185**	**Unknown**
Huntington's disease	**Huntingtin with polyQ expansion**	**3144**	**Largely natively unfolded**
Parkinson's disease	**α-synuclein**	**140**	**Natively unfolded**
Spongiform encephalopathies	**Prion proteins or fragments**		**Natively unfolded (residues 1-120) and α-helical (residues 121-230)**

Table 2 Human non neuropathic diseases associated with amyloid or intracellular inclusions
Adapted from Chiti *et al.* (2006) (*3*)

Disease	Aggregating protein	Number of residues	Native structure of protein
Nonneuropathic systemic amyloidoses			
AA amyloidosis	**Serum amyloid A fragments**	**76-104**	**All α, unknown fold**
AL amyloidosis	**Immunoglobulin light chain or fragments**	**~90**	**All β, Ig like**
ApoAI amyloidosis	**N-terminal fragments of apolipoprotein AI**	**80-93**	**Natively unfolded**
ApoAII amyloidosis	**N-terminal fragments of apolipoprotein AII**	**98**	**Unknown**
ApoAIV amyloidosis	**N-terminal fragments of apolipoprotein AIV**	**~70**	**Unknown**
Dialysis related amyloidosis	**Beta-2 microglobulin**	**99**	**All β**
Familial amyloidotic polyneuropathy	**Mutants of transthyretin**	**127**	**All β, prealbumin like**
Familial Mediterranean fever	**Serum amyloid A protein fragments**	**76-104**	**All α, unknown fold**
Fibrinogen amyloidosis	**Fibrinogen α-chain variants**	**27-81**	**Unknown**
Finnish hereditary amyloidosis	**Gelsolin mutant fragments**	**71**	**Natively unfolded**
Icelandic hereditary cerebral amyloid angiopathy	**Cystatin C mutant**	**120**	**α + β, cystatin like**
Lysozyme amyloidosis	**Lysozyme mutants**	**130**	**α + β, lysozyme fold**
Senile systemic amyloidosis	**Wild-type transthyretin**	**127**	**All β, prealbumin like**
Nonneuropathic localised diseases			
Aortic medial amyloidosis	**Medin**	**50**	**Unknown**
Atrial amyloidosis	**Atrial natriuretic factor**	**28**	**Natively unfolded**
Calcifying epithelial **o**dontogenic tumours	**Unknown**	**~46**	**Unknown**
Cataract	**γ-crystallins**	**Variable**	**All β, γ-crystallin like**
Corneal amyloidosis associated with trichiasis	**Lactoferrin**	**692**	**α + β, periplasmic-binding protein like II**
Cutaneous lichen amyloidosis	**Keratins**	**Variable**	**Unknown**
Hereditary cerebral haemorrhage with amyloidosis	**Amyloid β peptide mutants**	**40 or 42**	**Natively unfolded**
Hereditary lattice corneal dystrophy	**Mainly C-terminal fragments of kerato-epithelin**	**50-200**	**Unknown**
Inclusion body myositis	**Amyloid β peptide**	**40 or 42**	**Natively unfolded**
Injection-localised amyloidosis	**Insulin**	**21 + 30**	**All α, insulin like**
Medullary carcinoma of the thyroid	**Calcitonin**	**32**	**Natively unfolded**
Pituitary prolactinoma	**Prolactin**	**199**	**All α, 4 helical cytokines**
Pulmonary alveolar proteinosis	**Lung surfactant protein C**	**35**	**Unknown**
Type II diabetes	**Amylin**	**17**	**Natively unfolded**

Additional evidence that amyloid is not simply causing damage by occupying space comes through studies on the neurotoxicity of amyloid. Lorenzo and Yanker (*9*) demonstrated that Aβ fibrils cause profound neurodegenerative changes in rat hippocampal cell cultures including dystrophic neuritis, shrinkage of the neuronal soma and neuronal death. This is in contrast to amorphous Aβ aggregate which did not. More recently attention has switched from the fibrils themselves to prefibrillar, soluble aggregates being the causative agent in neurodegeneration. These intermediate species such as Alzheimer's disease diffusible ligands (ADDLs) and protofibrils can cause neuronal injury *in vitro.* ADDLs caused more than 20% cell death in 24 hours in organotypic hippocampal cell cultures at only 5 nM concentration; at 5 μM over 40% of cells were killed. In contrast 20 μM of $A\beta_{1-42}$ fibrils caused no cell death (*10*). It has been demonstrated that protofibrils can induce death in cultured cortical neurons over a period of days and that they can acutely increase the electrical activity of cortical neurons at sub micromolar concentrations (*11*).

1.1.3 The structure of amyloid fibrils

As previously mentioned fibrils show apple green birefringence under cross polarised light when bound to Congo red dye. This birefringence is a property only shown when light passes through a highly ordered structure such as a crystal and is doubly refracted. This was the first clue that fibril structure has a high degree of order. Studies by transmission electron microscopy reveal that fibrils can range from 7-20 nm in diameter, have indefinite length and they are unbranched (*12, 13*).

High resolution studies of fibrils have proved difficult due to fibrils lacking long range three-dimensional order which precludes detailed study by X-ray crystallography. Liquid state NMR is not possible due to fibril size and the resultant slow molecular tumbling which means anisotropic interactions are not averaged out and results in severe line broadening. Fibre diffraction studies exploring long range two-dimensional order have revealed all tested fibrils have a cross-β structure; these fibrils include *ex vivo* fibrils from Alzheimer's and diabetes patients. They give a diffraction pattern of two characteristic reflections, a strong sharp 4.7 Å meridional reflection from the repeating electron density in strands separated by hydrogen bonding and a diffuse equatorial reflection of 10-12 Å from the spacing between β-sheets (*14, 15*).

Atomic level structural information is now becoming available through solid-state NMR. Solid-state NMR overcomes the broadening of the resonances associated with slowly tumbling molecules in solution through the mechanical reintroduction of the motion through techniques such as magic-angle spinning; a more detailed discussion of studying proteins in the solid-state is presented in section 1.8.1 Magic Angle Spinning (MAS)

There have now been several solid-state studies of fibrils published. A tertiary structure of fibrils formed from $A\beta_{1-40}$ has been put forward by Tycko and co-workers using solid state NMR and computational energy minimisation procedures. Each Aβ molecule displays a strand-turn-strand structure; these molecules are stacked on top of each other so that the strands are parallel and in-register. The stacking of the strand-turn-strand structures on top of each other forms two adjacent and parallel β-sheets; this motif can be seen in the structures in Figure 1. Measurements from different techniques such as transmission electron microscopy and scanning transmission electron microscopy have led to suggestions that a single protofilament consists of four β-sheets each separated by a distance of ~10Å (*16-18*).

The group of Oschkinat (*19*) solved the structure of the 26 residue CA150 (WW2) domain that forms fibrils and is co-deposited with Huntingtin fibrils in Huntington's disease using solid-state NMR and electron microscopy methods. The monomer units form a beta-hairpin and these stack on top of each other to form two beta-sheets as can be seen in Figure 1 (yellow) and is similar to the motif found in Aβ1-40 and 1-42. The side-chains are closely packed in a steric zipper arrangement.

Meier and co-workers have solved the structure of the prion forming domain of HET-s (218-289) and found it to be a β-solenoid with a triangular hydrophobic core (*20*); this structure can be seen in Figure 1 (red). The group of Baldus and co-workers has proposed a model for the paired helical filaments of tau involving a β-core of three major β-strands (*21*).

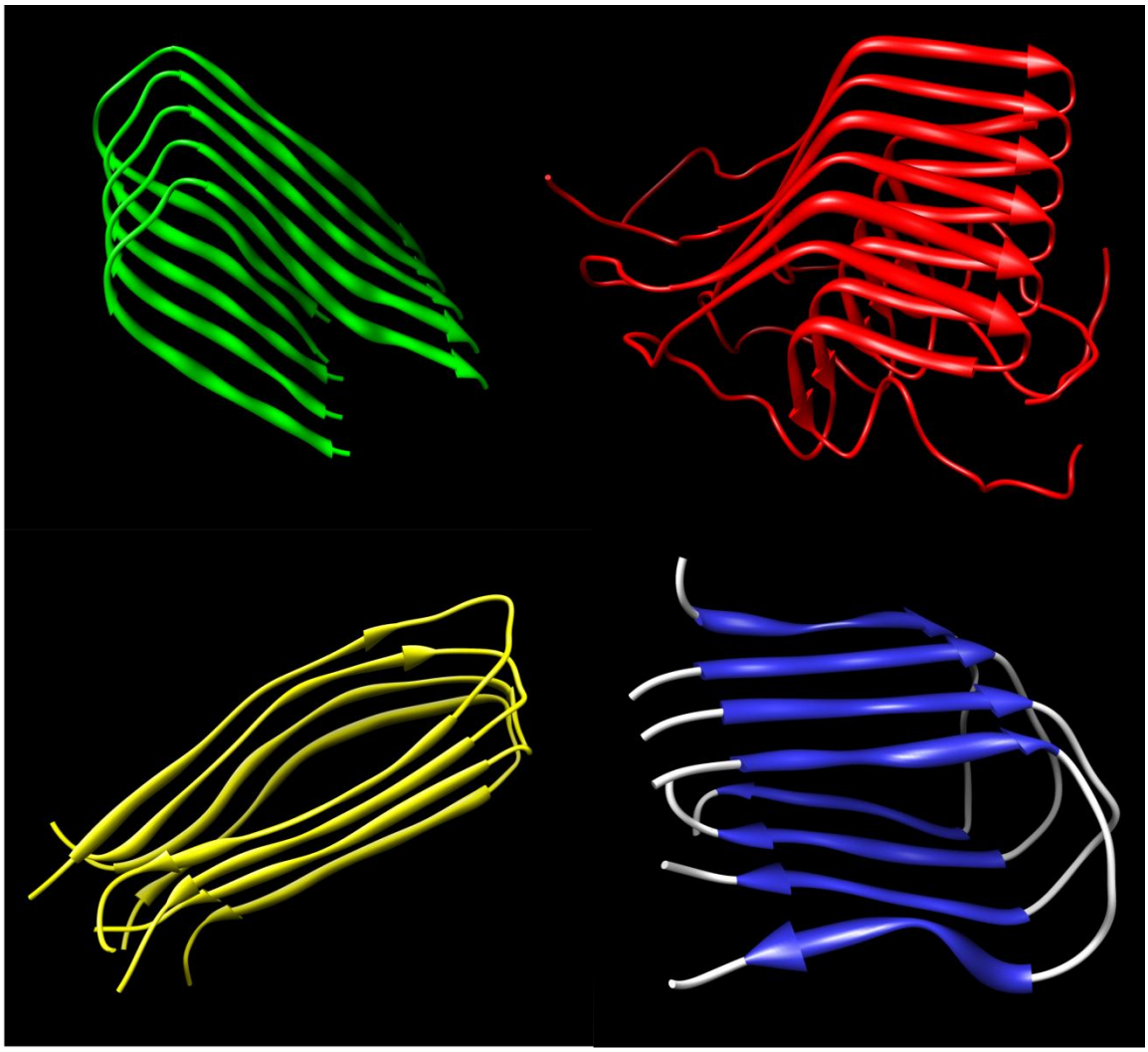

Figure 1 Solid –state NMR derived structures of amyloid fibrils
Structures of amyloid fibrils from the literature. In green: Aβ(1-42) by Luhrs *et al.* (*161*). In red: HET-S (218-289) by Van Melkebecke *et al.* (*20*). In yellow: Human CA150 (WW2) by Ferguson e*t al.* (*19*). In blue: K3 fragment of β_2m by Iwata *et al.* (*84*). Arrows represent β-strands pointing towards the C-terminus. Non-arrows are connecting loops.

1.2 Dialysis Related Amyloidosis

Dialysis related amyloidosis is a class of amyloidosis almost unique to those who are undergoing long term haemodialysis due to kidney failure. It will affect all those on haemodialysis if they remain on it long enough. There are currently over 800000 chronic haemodialysis patients globally and this figure is increasing by 10% each year (*1*).

1.2.1 Symptoms

The clinical symptoms of DRA predominantly manifest themselves in the joints and surrounding areas. One of the first clinical symptoms to usually present is carpal tunnel syndrome (CTS). CTS is caused by compression of the median nerve in the carpal tunnel located in the wrist, this results in parathesia of the palmar surfaces of the first 3-4 fingers which leads to sensory disturbance, muscle weakness and muscle atrophy. The pain of this condition is usually worse during the night and can be exacerbated during dialysis sessions. CTS is not exclusive to DRA and often manifests itself in other diseases such as hyperparathyroidism and chronic synovitis. In DRA it is the accumulation of β_2m amyloid in the carpal tunnel that causes the compression of the median nerve, and surgical removal of the β_2m plaque has been shown to relieve the symptoms of CTS. Presence of β_2m in the carpal tunnel is used to determine that the CTS is due to DRA and not associated with another disease (*22*).

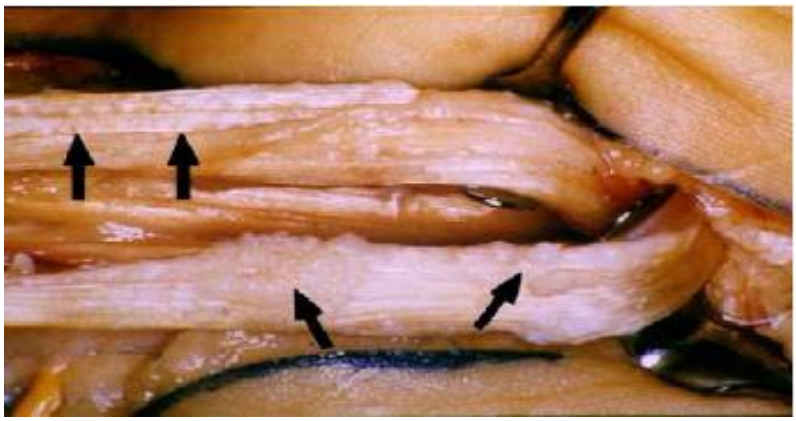

Figure 2 β_2m in the carpal tunnel
This picture was taken during surgery on the Carpal tunnel to remove β_2m amyloid deposits (marked with black arrows). Picture taken from Yamamoto, 2005 (*22*).

Chronic arthralgias and arthropathy are the other main symptoms of DRA. Amyloid deposition on cartilage, tendons, synovia and joint capsules leads to macrophage invasion (*23*).This is at least in part due to the modification of β_2m with advanced glycation end products (AGE). These are a heterogeneous group of compounds produced by the Maillard reaction, an irreversible non enzymatic reaction (*24*). Proteins with long half lives such as fibrils are more susceptible to modification by AGE. Indeed β_2m removed from patients with DRA has been found to be AGE modified in this fashion whilst β_2m from the sera of healthy subjects is free of such modifications (*25*). AGE modified β_2m has been shown to increase monocyte chemotaxis and secretion of tumour necrosis factor alpha and interleukin-1β and therefore induces an inflammatory state (*24*).The cytokines released by the macrophages cause expression of collagenase in synovial cells (*26*), continual expression would lead to bone and joint destruction.

Deposition of amyloid without inflammation is usually asymptomatic. Like CTS the arthralgias are usually exacerbated at night and during dialysis (*22*). Occasionally amyloid deposition occurs around the discovertebral bones; if this subsequently causes inflammation then destructive spondyloarthopathy (DSA) can occur. This leads to

discovertebral destruction and narrowing of the disc space which is often asymptomatic or the cause of mild pain in the spine. Rarely this may lead to nerve root compression and subsequent paraplegia (*27*). There have also been reported fatal cases of cervical DSA (*28, 29*).

Subchondral bone cysts can develop in advanced cases of DRA; they are a serious complication of the disease as they can lead to bone fractures which can seriously limit the daily life of patients, especially older ones, and can require long periods of hospitalisation (*30*). β_2m amyloid can also deposit in visceral organs in long term dialysis patients; these deposits are, more often than not, asymptomatic but can often cause serious complications such as heart failure (*31*) when deposited in the heart, or bowel complications when deposited in the gastrointestinal tract (*32*).

1.2.2 Etiology

The exact cause of DRA is unclear but the accumulation of soluble β_2m is a pre requisite for DRA (*33*). In addition to accumulation due to inefficient removal by the kidneys and dialysis, production of β_2m may be increased in patients on dialysis due to mononuclear cells coming into contact with dialysis membranes (*34, 35*). In addition inflammatory states (*36*), metabolic acidosis (*37*) and calcitriol treatment (*38*) may all cause increased production. Serum concentrations of β_2m in symptomatic and asymptomatic dialysis patients are the same and *in vitro* at neutral pH raised concentrations of soluble β_2m are not sufficient to cause the transition into amyloid (*39*). This suggests that direct precipitation is an unlikely cause and there are other factors involved in fibrillogenesis. It certainly means that serum concentrations cannot be used as a marker of DRA (*40*).

Dialysis itself may not be a pre-requisite for DRA as β_2m amyloid may occasionally be observed in patients with severe renal dysfunction who are not yet receiving dialysis or related procedures (*41*). Dialysis may just be keeping patients with renal dysfunction alive long enough so they are able to develop the mature amyloidosis; cases of this are rare however and there is evidence that dialysis may play a role through copper. Dialysis allows the opportunistic interaction of Cu^{2+} with β_2m. Although copper is present in the serum of all humans it is normally tightly bound to plasma proteins and is therefore unavailable to interact with β_2m. Dialysis can make copper available to β_2m in two ways; the first is that copper is present in the dialysate up to the value of 1.6µM (*42*) and the second is that cuprophan membranes, one of the most common membranes used during dialysis due to their low cost, contain ~2mg of copper per m^2; most dialysis membranes are 1-2m^2. These membranes do not release Cu^{2+} in the saline prewash of the membrane but readily release Cu^{2+} when incubated in plasma at body temperature (*43*).

Further evidence that membrane derived copper plays an important role in fibril formation comes from studies that have found that there is a more than a 50% lower incidence of DRA in patients treated with membranes not containing copper (*44*). The predominant deposition of β_2m amyloid in the joints could be a clue as to the other factors that are required for the transition of soluble β_2m to its fibrillar form. The joint capsule is rich in components that could potentially enhance fibrillogenesis; these include collagen, proteoglycans and glycosaminoglycans (*45*). These factors will be discussed more fully in section 1.4.

1.2.3 Current treatments

Currently there is no cure for DRA and the only way to completely halt progression of symptoms is for the patient to have a renal transplant which will immediately bring serum concentrations of β_2m back to normal levels. There is good evidence that a renal transplant will also cause relief from arthralgias and CTS (*46*), regression of deposits has also been reported (*47*), but bone cysts seem to persist (*48*). Other treatments revolve around the alleviation of symptoms, the pain associated with carpal tunnel syndrome and arthralgias is usually effectively alleviated with adrenocorticosteroids (*22*). In severe cases surgical removal of amyloid deposits from the carpal tunnel and joints often gives immediate relief from symptoms although this could be due to the powerful anti inflammatories used after surgery (*22*).

A lot of effort has centralised around the production of adsorption columns that can remove more β_2m from the blood than conventional dialysis techniques. At this moment the most successful column has been Lixelle™ with reported lowering of serum β_2m by a mean of 74% in the first treatment. Lixelle columns are not completely specific for β_2m and also remove inflammatory cytokines such as interleukin-1-β and interleukin-6 which have also been proposed to be involved in DRA and therefore this could also help to alleviate symptoms and prevent progression of the disease (*49*).

These treatments again demonstrate the importance of raised serum β_2m concentrations in DRA and that β_2m is a causal factor in DRA and not just an epiphenomenon.

1.3 Beta-2 Microglobulin

In 1985 the major constituent of amyloid in DRA was discovered to be beta-2 microglobulin (β_2m) by 2 separate groups (*50, 51*). Beta-2 microglobulin is a normally soluble protein, found in the major histocompatibility complex I (MHC I) and is therefore ubiquitously expressed in most mononuclear cells and is released from the surface of these cells as part of its normal catabolic cycle (*52*). Typically β_2m is removed from the body by glomerular filtration, however in patients with renal dysfunction this process fails to occur and serum β_2m concentration rises by an order of magnitude from 1-3 mg/L to in excess of 30 mg/L (*33*).

Wild type human β_2m is 99 residues in length (*53*) and has been the subject of both crystallographic and NMR studies (*54, 55*). These studies have revealed that β_2m, like other proteins of the immunoglobulin family, has a "Greek key" topology comprising of a seven stranded antiparallel β-sandwich. These form two β sheets that are connected with a disulphide bridge linking cysteines 25 and 80 in the human wild type version. The strands are conventionally labelled I-VII starting with I at the N-terminus. I, II, IV and V form the first β-sheet while III, VI and VII form the second. The III-IV loop contains 2 residues in a β-strand denoted III'. The protein is stabilised by around 60 intramolecular hydrogen bonds (*56*). While in complex with the MHC I heavy chain it is the loop region between strands V and VI that interacts with the MHC I heavy chain through hydrophobic interactions and hydrogen bonds; a list of the contacts can be found in Table 3.

MET-0	ILE-1	GLN-2	ARG-3	THR-4	PRO-5	LYS-6	ILE-7	GLN-8	VAL-9
TYR-10	SER-11	ARG-12	HIS-13	PRO-14	ALA-15	GLU-16	ASN-17	GLY-18	LYS-19
SER-20	ASN-21	PHE-22	LEU-23	ASN-24	CYS-25	TYR-26	VAL-27	SER-28	GLY-29
PHE-30	HIS-31	PRO-32	SER-33	ASP-34	ILE-35	GLU-36	VAL-37	ASP-38	LEU-39
LEU-40	LYS-41	ASN-42	GLY-43	GLU-44	ARG-45	ILE-46	GLU-47	LYS-48	VAL-49
GLU-50	HIS-51	SER-52	ASP-53	LEU-54	SER-55	PHE-56	SER-57	LYS-58	ASP-59
TRP-60	SER-61	PHE-62	TYR-63	LEU-64	LEU-65	TYR-66	TYR-67	THR-68	GLU-69
PHE-70	THR-71	PRO-72	THR-73	GLU-74	LYS-75	ASP-76	GLU-77	TYR-78	ALA-79
CYS-80	ARG-81	VAL-82	ASN-83	HIS-84	VAL-85	THR-86	LEU-87	SER-88	GLN-89
PRO-90	LYS-91	ILE-92	VAL-93	LYS-94	TRP-95	ASP-96	ARG-97	ASP-98	MET-99

Figure 3 Beta-2 microglobulin primary structure

Most crystal structures and original NMR studies of β_2m were performed while it was still bound as part of the MHC I complex. In these studies strand IV contains a β bulge which divides strand IV into two portions, IV-1 and IV-2. Residues 53-62, which comprise the β bulge, strand IV-2 and the following loop have been shown to be dynamic and are not uniquely structured in solution in this study and in others (*54, 57*). In a recent crystal study on monomeric β_2m Trinh *et al.* (*58*) found that strand IV formed a continuous 6 residue strand with no β-bulge however when using 2D NMR they found that, as in the studies where β_2m was bound as part of the MHC I complex, strand IV had the β bulge splitting it into two portions. They proposed that the crystal structure could be representative of a rarely populated state that could be more amyloidogenic. This is due to the proposal that the β-bulge protects against intermolecular association of β-strands and results in a shift in the H-bonding between strands IV and V; which itself results in His51 rotating 180˚ from an inwardly pointing position to an outwardly pointing position. Histidine would be at least partially charged at pH 7 and below; potentially facilitating interactions with other molecules in its surroundings.

β_2m contact	side/main	MHC contact	side/main	Type of interaction
Asp-53 CO2-	**sc**	**Gln-32 NH2**	**sc**	**H-bond**
Asp-53 CO2-	**sc**	**Arg-35 NH2+**	**sc**	**H-bond**
Phe-56 CH	**sc**	**Phe-8 CH**	**sc**	**Hydrophobic**
Tyr-63 OH	**sc**	**Tyr-27 OH**	**sc**	**H-bond**
Ile-1 N-terminus	**mc**	**Asp-119 C=O**	**mc**	**H-bond**
His-31 NH	**sc**	**Gln-96 C=O**	**sc**	**H-bond**
Trp-60 C=O	**mc**	**Gln-96 NH2**	**sc**	**H-bond**
Trp-60 NH	**sc**	**Asp-122 CO2**	**sc**	**H-bond**
Phe-62	**sc**	**Gln-96 NH2**	**sc**	**H-bond**
Lys-6 NH3+	**sc**	**Glu-232 CO2-**	**sc**	**Ionic**
Gln-8 NH2	**sc**	**Glu-232 C=O**	**mc**	**H-bond**
Gln-8 C=O	**sc**	**Arg-234 NH2**	**sc**	**H-bond**
Tyr-10 OH	**sc**	**Pro-235 C=O**	**mc**	**H-bond**
Ser-11 CO	**mc**	**Gln-242 NH2**	**sc**	**H-bond**
Arg-12 NH2	**sc**	**Gly-237 C=O**	**mc**	**H-bond**
Arg-12 C=O	**mc**	**Gln-242 NH2**	**sc**	**H-bond**
Asn-24 NH2	**sc**	**Ala-236 C=O**	**mc**	**H-bond**
Tyr-26 CH	**sc**	**Pro-235 CH**	**sc**	**Hydrophobic**
Asp-98 C=O	**mc**	**Arg-202 NH**	**sc**	**H-bond**
Asp-98 C=O	**mc**	**Arg-202 NH2**	**sc**	**H-bond**
Met-99 C-terminus	**mc**	**Arg-234 NH2+**	**sc**	**Ionic**

Table 3 β_2m contacts with MHC I heavy chain

β_2m contacts with the MHC I alpha domain. Contact data from Tysoe-Calnon, 1991 (*59*).

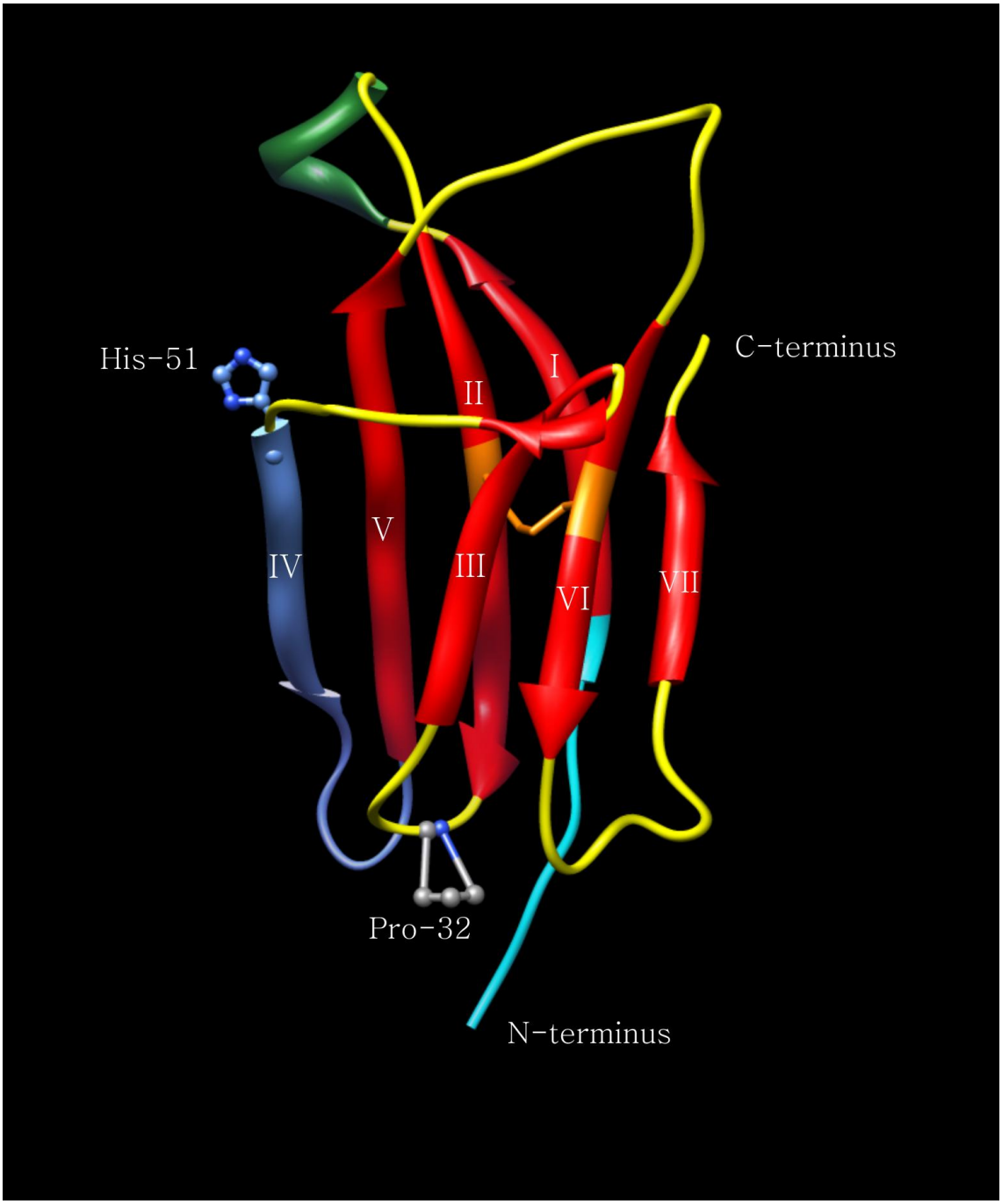

Figure 4 Crystal structure of monomeric β_2m as determined by Trinh *et al.* in 2002
Tertiary structure of β_2m derived from X-ray data acquired by Trinh *et al.* (*58*). Arrows represent β-strand structure. Roman numerals depict β-strand number. In green is alpha-helical structure. Orange shows the disulphide bridge between cysteines 25 and 80. In blue is strand D and loop DE. Cyan marks the first 6 N-terminal residues often truncated *in vivo*. Rendered using Chimera (PDB code: 1LDS)

1.4 The formation of fibrillar beta-2 microglobulin

The *in vivo* mechanism by which soluble β_2m is converted to its fibrillar pathogenic form still eludes the scientific community, however *in vitro* formation of β_2m fibrils has been achieved by many groups.

By far the quickest and easiest way to produce fibrils *in vitro* is to lower the pH of the β_2m solution. This has been the preferred method for many groups who want to produce fibrils that can be analysed using NMR, negative stain transmission electron microscopy and atomic force microscopy (*60, 61*). It has been demonstrated that fibrils have different morphologies depending on the pH and ionic strength at which they were formed. Formation of fibrils between pH 3.0-4.5 at less than 50mM salt concentration results in short 200-600nm highly curved fibrils. Similar fibrils are produced at pH 1.0-4.0 at high salt concentration of 400mM. These two species form rapidly within 1 day without a lag phase. At pH $\leq$3 and low salt concentration $\leq$100mM long straight fibrils easily exceeding 600nm in length are formed This species forms with a lag phase and takes in the region of six days (*60*).

In order to try and determine which parts of β_2m are amyloidogenic, Kozhukh (*62*) attempted to make fibrils from peptide fragments produced through the digestion of β_2m with a lysyl endopeptidase. This resulted in 9 fragments denoted K1 to K9. These fragments were then put under acid precipitation conditions; of the 9 fragments only K3, which corresponds to β-strands II and III and is shown in blue in Figure 5, was able to form fibrils on its own. Without the reduction of the disulphide bridge K3 remains attached to K7, which was β-strand VII of β_2m before digestion, and the pair also form fibrils under acid conditions. The K3, K7 pairing showed a longer lag phase in fibril

formation than K3 alone but both had a shorter lag phase than intact β_2m. However upon increasing pH the K3 fibrils rapidly dissociated as did K3, K7 but not as rapidly as K3 alone. Intact β_2m took the longest time to dissociate back into monomeric β_2m. These results suggest that the essential region for fibril formation lies within this K3 peptide and hence within strands II and III in the native form.

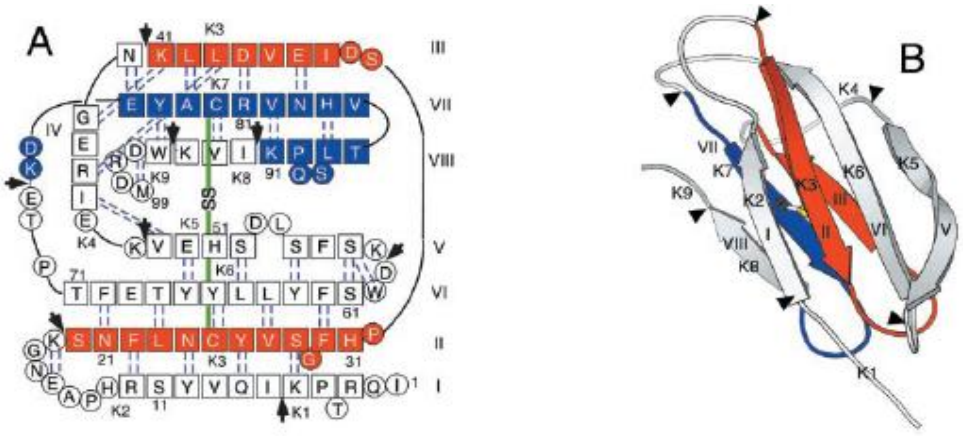

Figure 5 Structure of β_2m in context of peptides K1-K9 from Kozhukh's study in 2002
A shows the primary structure of β_2m. **B** shows the secondary and tertiary structure. Highlighted in red is the K3 peptide and in blue the K7. Arrows mark the cleavage sites of the lysyl endopeptidase used to digest β_2m in the study. Squares represent residues within β-strand, circles residues within non-β-strand structure. Dashed lines represent hydrogen boding between strands. The green line depicts the disulphide bridge between Cys-25 and Cys-80. Figure modified from Kozhukh, 2002 (*62*).

In vivo there are locations with lowered pH accessible to β_2m, namely macrophage lysosomes. Macrophage lysosomes normally have a pH of around 4.8 (*63*). Therefore in theory they could provide an acidic compartment for acid precipitation of β_2m. However in a study by Morten *et al.* in 2007 (*64*) soluble β_2m was completely degraded within macrophage lysosomes by proteases and did not get the chance to undergo fibrillogenesis. Interestingly in the same study live-cell imaging experiments performed on macrophages

in vitro showed that β_2m fibrils do get internalised to macrophage lysosomes but that the macrophages are unable to degrade the fibrils. This adds to the finding in a previous electron microscopy study of β_2m fibrils in macrophage lysosomes that the density of intracellular staining of β_2m fibrils was not reduced compared to extracellular deposits in *ex vivo* material. This suggests that macrophages may not be able to degrade β_2m fibrils *in vivo* (*65*). This could imply that macrophage infiltration into β_2m amyloid deposits may actually help prevent the extension of fibrils by decreasing the local concentration of β_2m although as already discussed macrophage infiltration is probably responsible for most of the clinical symptoms of DRA. What these findings do reiterate is the importance of preventing the stabilisation of fibrils as once the fibrils are formed they prove to be resistant to removal.

Many groups have tried to form fibrils at neutral pH which is more likely to be the environment that β_2m is in when fibrillogenesis is initiated. Efforts have concentrated around the addition of factors that are associated with dialysis or have been found associated with deposits from patients such as Cu^{2+}, glycosaminoglycans, apolipoprotein E and collagen. More recently the ability of ΔN6-β_2m to convert β_2m to an amyloid competent form has been used to create β_2m amyloid fibrils at neutral pH. These efforts are described in more detail below.

1.4.1 Factors contributing to fibrillogenesis at neutral pH

As discussed previously Cu^{2+} is associated with dialysis and it has been proposed to be a factor in fibrillogenesis in DRA. This is because β_2m can act as a Cu^{2+} specific binding protein with a dissociation constant of 2.7 ± 0.6 μM (*39*) and binding can promote amyloid assembly under near native conditions (*66*). Divalent cation interactions have been

implicated in the formation or alteration of ordered aggregates in several amyloid diseases including Alzheimer's and prion disease (*67, 68*).

In vitro fibrils have been formed at neutral pH using copper (II) chloride and non denaturing concentrations of urea (*39*). It has been proposed that only transient encounter with copper is needed in order to form the fibrils and once past a critical stage the copper ion is no longer needed. This was observed when fibrils were grown in the presence of copper and then the metal chelator EDTA added, thus removing the copper available to the β_2m. This did not result in the fibrils returning to their monomeric form as would be expected but instead forming chelate resistant oligomers. It has been proposed by Calabrese that Cu^{2+} catalyses the isomerisation of the *cis*-proline 32 to its *trans* conformation which converts the β_2m into an intermediate activated state that is able to go on to form fibrils (*69*). This study complements one by Jahn *et al.* in 2006 (*70*) finding that the rate of fibril elongation correlates directly with the concentration of the *trans* intermediate. There is a large energy barrier to overcome in converting the *cis* P32 to the *trans* variety, however at equilibrium the intermediate state is still populated, be it sparsely. This would help explain why elevated concentrations of β_2m are required as this would increase the total amount of the amyloidogenic intermediate and it would also explain why dialysis can contribute as the extra Cu^{2+} would decrease the energy barrier needed to form the intermediate state, increasing the population of β_2m that is able to form fibrils.

Highly sulphated glycosaminoglycans (GAGs) have been identified in all tissues containing β_2m deposits and heparan sulphate has been found specifically localised to the deposits themselves (*71*). *In vitro* the presence of 20% TFE or SDS allows amyloid fibrils to be produced and stabilised using heparan. It has been suggested by Naiki *et al.* that the TFE initially unfolds the soluble β_2m so that it may form its beta sheet rich form and

heparin may aid extension of fibrils by inhibiting depolymerisation which occurs rapidly at neutral pH (*72*).

Apolipoprotein E (apoE), a cholesterol transport protein that serves as a ligand for low density lipoprotein receptors (*73*), is co-localised with all types of localised and systemic amyloid deposits which have so far been examined, these include those found in prion disease, Alzheimer's (*74*), amyloid A protein amyloidosis, immunoglobulin light chain amyloidosis and dialysis related amyloidosis (*75*). *In vitro* studies have shown that depolymerisation of β_2m fibrils from patients occurs spontaneously and rapidly at neutral pH and above. The addition of apoE inhibits depolymerisation in a dose dependent fashion. Yamaguchi proposes a model where this could be due to specific and direct binding of apoE to the β_2m fibrils therefore stabilising the structure (*76*).

Collagen is found localised with amyloid deposits in DRA and soluble β_2m has a K_d for collagen type I of 410 μM and for collagen type II of 2.3 mM (*77*). Attempts at *in vitro* β_2m fibrillogenesis at pH 6.4 and 37.4˚C in a study by Relini fail to produce β_2m fibrils however attempts in the same conditions with the addition of collagen do result in β_2m fibrils. These fibrils are of very similar morphology to fibrils from patients as confirmed by atomic force microscopy (AFM) (*78*). In the same study evidence is presented showing that exposure of the β_2m to the positively charged regions can enhance rate of fibril formation. Fibrils were successfully grown on positively charged mica (the surface used to study material with AFM) but attempts at doing the same on mica with a negatively charged surface failed. These experiments were also highly dependent on temperature and no fibrils were formed if incubation at 40˚C did not take place. In addition to this, β_2m with the first 6 residues truncated at the N terminus has ten times higher affinity for type 1 collagen at pH 6.4 than at pH 7.4; this species is found to make up over 20% of the β_2m

found within amyloid deposits (*79*). In cases of acidosis, which are well documented in the synovial fluid (*80-82*), this may represent an effective method to increase the local concentration of the truncated β_2m at the collagen surface which would allow the critical concentration for β_2m oligermerisation to be reached (*77*). Recently it has been demonstrated that truncated β_2m can form fibrils by incubation at pH 7.2 (t_{lag}=35 ±4 days) without the use of additives (*83*). In the same study it was also demonstrated that ΔN6-β_2m converts more rapidly into fibrils at pH 6.2 (t_{lag}=15 ±4 days) and that ΔN6-β_2m can convert full length β_2m to an amyloid-competent state; this is an incredibly interesting finding as it means that ΔN6-β_2m effectively acts as a prion. These recent findings may explain how β_2m fibrils initially form *in vivo*, which until recently had eluded the scientific community.

The experiments with GAG, apoE and collagen all required a method of partial unfolding of the native β_2m before fibril extension took place. It is therefore likely that they all stabilise and allow the extension of fibril protomers.

Further evidence for this is the fact that fibrils can be formed with these factors in the absence of a method of partial unfolding if β_2m fibril seeds are used. In this case, fibrils form slowly over the course of weeks. Figure 6 shows a model of how stabilising factors could potentially promote fibrillogenesis; concentrations of β_2m rise due to inefficient removal of β_2m by the kidneys and dialysis. Some as yet unknown factor causes partial unfolding of the native β_2m and fibril seeds are then formed. This may be aided by Cu^{2+} from the dialysis procedure. These fibril seeds are then stabilised by factors present in the synovium such as collagen, ApoE, GAG and SAP. This stabilisation prevents the fibril seeds from reverting back to monomeric β_2m and allows their extension by further β_2m into full length fibrils. SAP then forms an endogenous protein coating for the fibrils masking them from the body's protein scavenging mechanisms and inhibiting degradation

by proteinases (*45*). In the study serum amyloid P component was able to increase thioflavin T fluorescence demonstrating that it can enhance fibril formation in seeded reactions but there is a lot more evidence than this alone implicating SAP in amyloidosis as will be discussed in section 1.6.1.

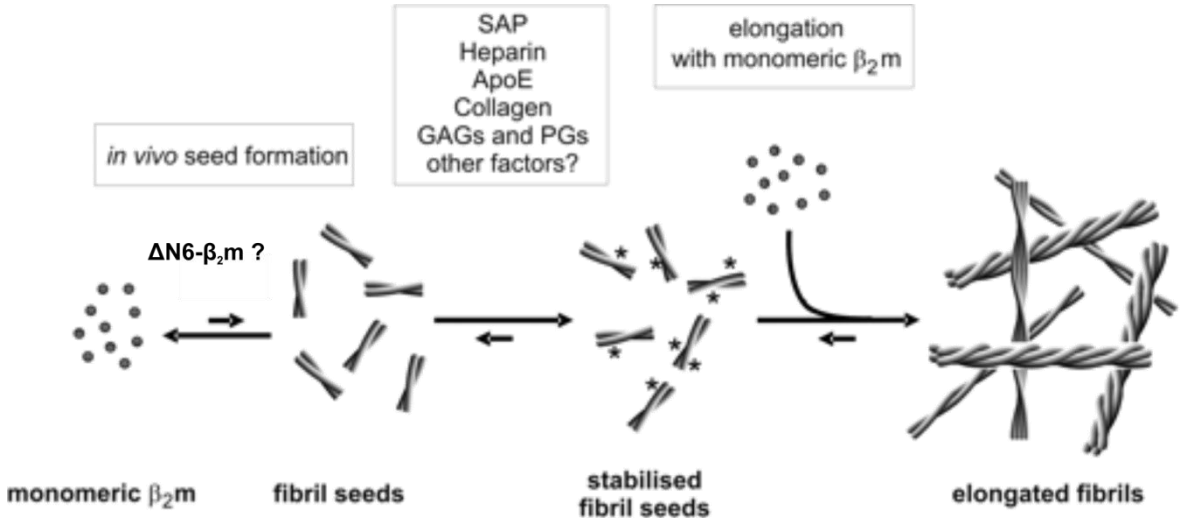

Figure 6 A model of potential factors involved in β_2m fibrillogenesis
Arrows represent equilibrium between different forms of β_2m, filled circles represent monomeric β_2m and stars represent stabilising factors. From Myers *et al.* (2006) (*45*).

1.5 The structure of fibrillar beta-2 microglobulin

There have been several structural models proposed for fibrils formed from β_2m or its fragments. A combination of solid state NMR, X-ray fibre diffraction and atomic force microscopy studies of the 22 residue K3 fragment of β_2m has revealed a conformation of β-strand-loop-β-strand with each K3 fibril packed in a parallel, staggered arrangement (*84*) (Figure 7). A zipper spine model was proposed by Ivanova *et al.* in 2004 (*85*). This model involved the full length β_2m; most of the protein retained its native structure while residues 83-89 formed a central β-spine (Figure 8). Interestingly these residues form part of the K7 fragment, which while able to form fibrils when covalently bound to K3 via a disulphide bond, is unable to form them while dissociated.

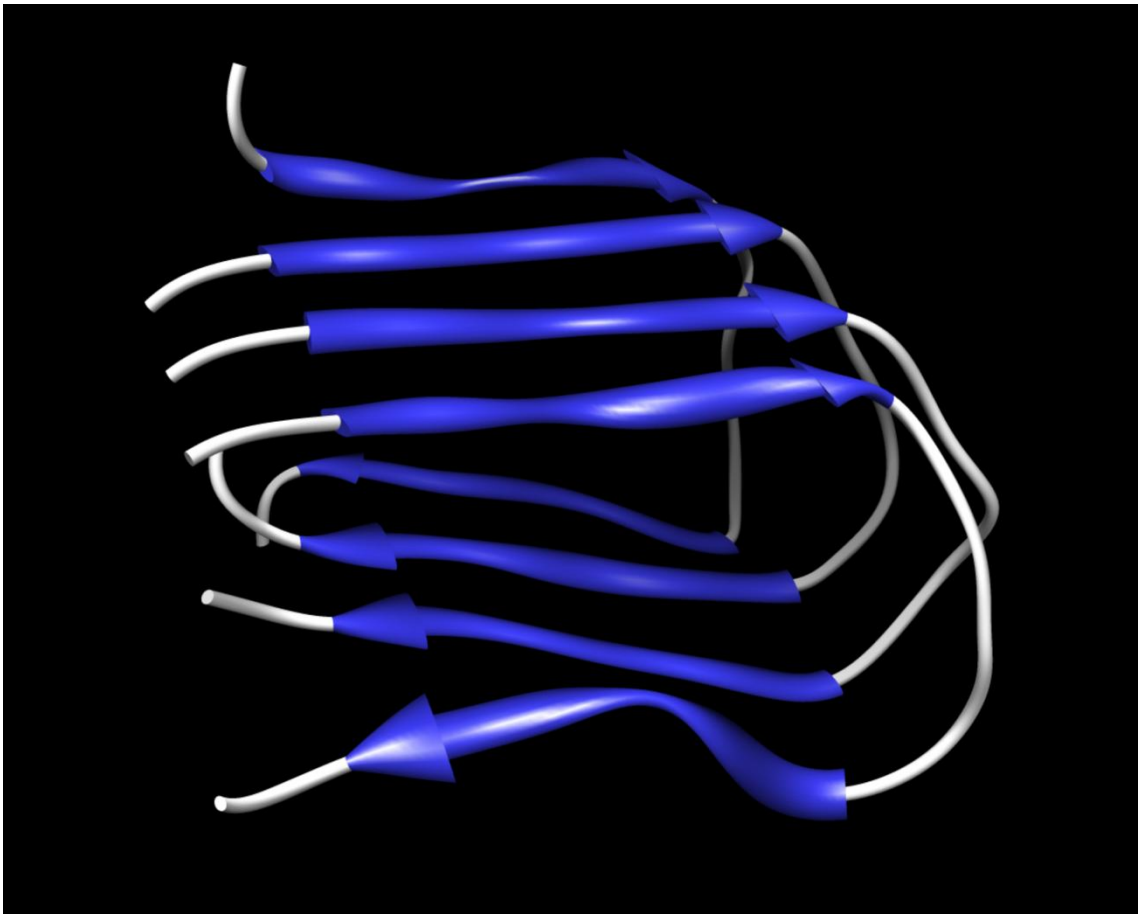

Figure 7 Iwata's three dimensional structure of the fibril formed from the K3 fragment of β_2m

K3 is the 22 residue peptide (Ser20-Lys41) created by digestion of β_2m with lysyl endopeptidase. Under acidic conditions it forms fibrils. Through a combination of solid state NMR, X-ray diffraction and atomic force microscopy techniques this structure was published in the protein data bank (PDB ID:2E8D)(*84*). The blue arrows represent β-strand secondary structure. The white portions are loop regions.

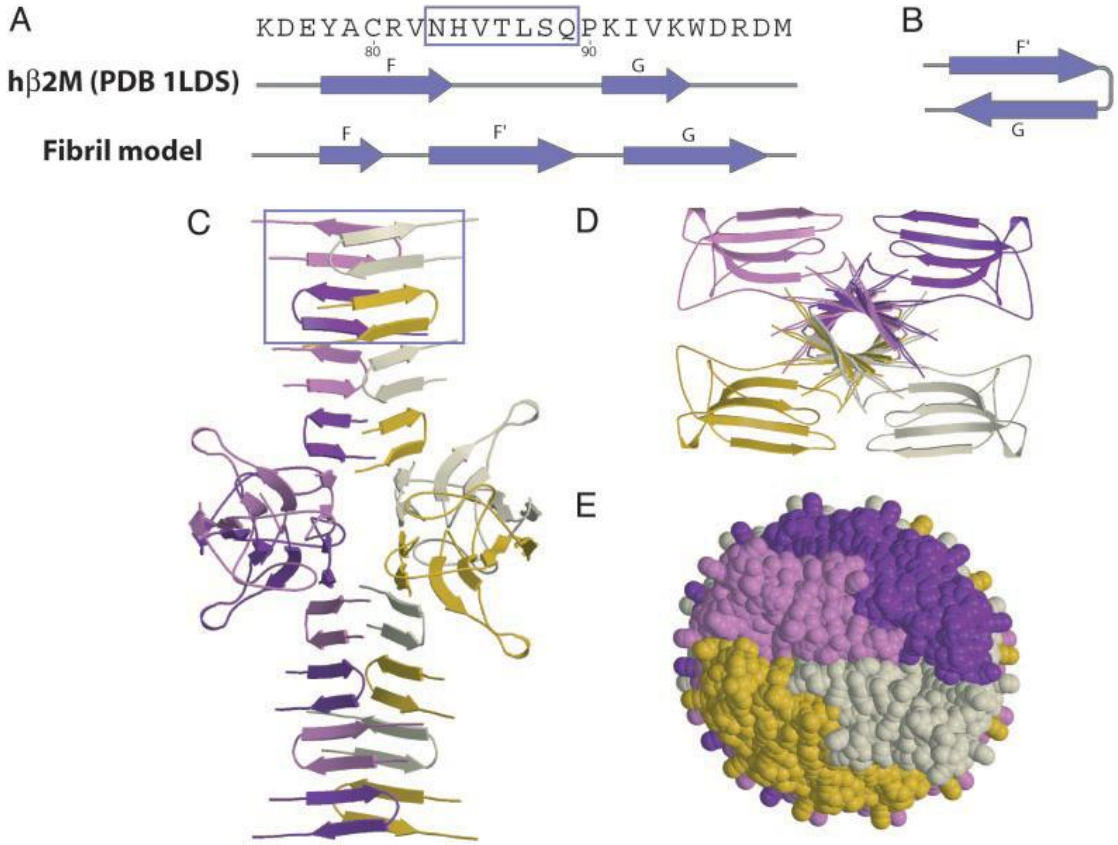

Figure 8 Ivanova's speculative Zipper-spine model for the β_2m protofilament
(A) The C-terminal segment of β_2m is the portion of the structure to rearrange during fibril formation and the amyloid-forming hβ_2m7mer (boxed) forms a new β-strand F'. (B) In the fibril model, residues Pro 90 and Lys 91 form a type I β-turn. Thus the β-strand G is hydrogen bonded with the new β-strand F' rather than with the β-strand F of the native structure. (C) Two such F'-G hairpins stack to form the asymmetric unit of one of the sheets of the spine. Each sheet is built with a small (7°) twist between β-strands, stacked 4.7 Å apart, so that the spine has a pitch of~242 Å. The sheets are separated by ~11 Å. β-Strands A–E and part of F retain their native structure with the disulfide bond between β-strands B and F intact. These native-like core domains decorate the periphery of the double β-sheet spine, with only four molecules shown for clarity. (D) The view down the fibre axis shows the double β-sheet spine. The rest of the β_2m molecules, which remain folded, are packed closely around the β-sheet spine. (E) A space-filling model (view of the fibril down its axis) shows that each of the four molecules, represented with different colours, is tightly packed within the fibril, with no space for solvent. Thus, the core domains shield the spine from solvent. Figure modified from Ivanova, 2004 (*85*).

Perhaps the most rigorous study of β_2m fibril macro-structure published to date was undertaken by a collaborative effort between Helen Saibil's and Sheena Radford's groups. In their study they used cryo-EM to create 3D maps of the fibrils and used scanning

transmission EM (STEM) to make mass measurements. They identified two main fibril types within one sample which we shall call type 1 and 2 for the remainder of this thesis.

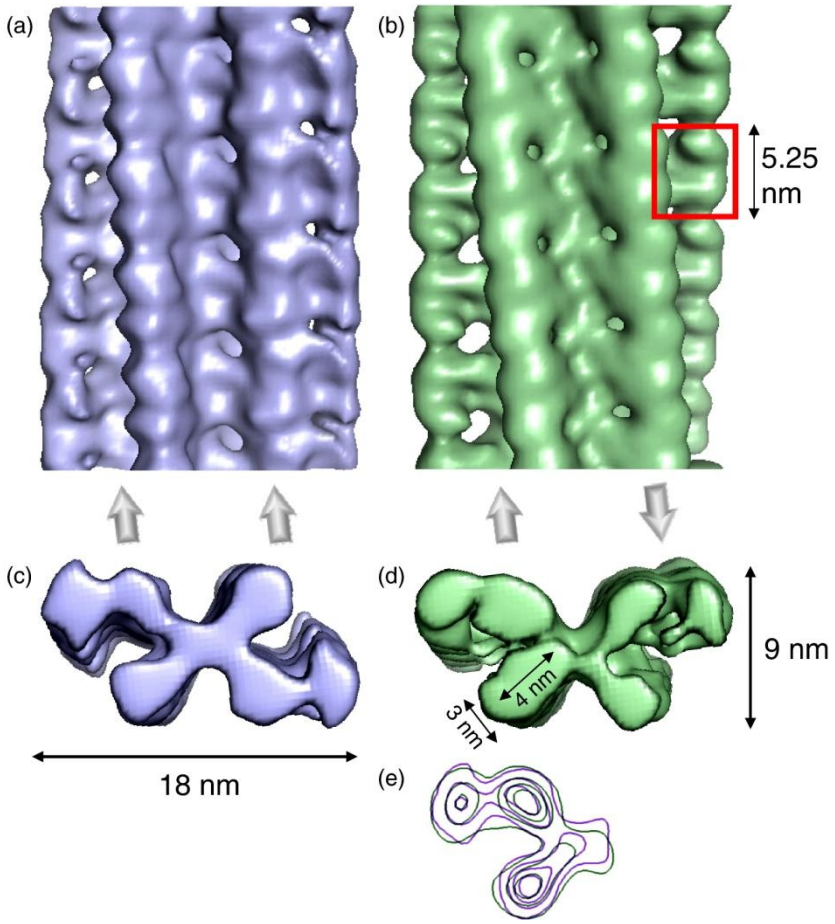

Figure 9 Saibil's three-dimensional reconstructions of the type 1 and type 2 forms of β_2m fibrils

Side views of a type 1 fibril (a) and a type 2 fibril (b). The maps are contoured at a volume corresponding to an MPL of 53 kDa/nm. One dimeric density unit is indicated by a red box in (b). The directions of the half-fibrils are indicated by arrows below the maps. Cross sections of the type 1 (c) and type 2 fibrils (d) show that the structures are formed of crescent-shaped units stacked back-to-back. (e) Superposed contour plots of the 1 (lilac) and 2 (green) repeat units, showing that the two fibril types have the same underlying organisation that differs only in the orientation of the two stacks, either parallel or anti-parallel.

Both fibril types consist of two half fibrils of the same morphology joined back to back and the only difference between type 1 and 2 is that they run parallel in type 1 and anti-parallel in type 2. They propose a dimer of dimers repeat unit in complex hierarchical fibril assembly (Figure 9).

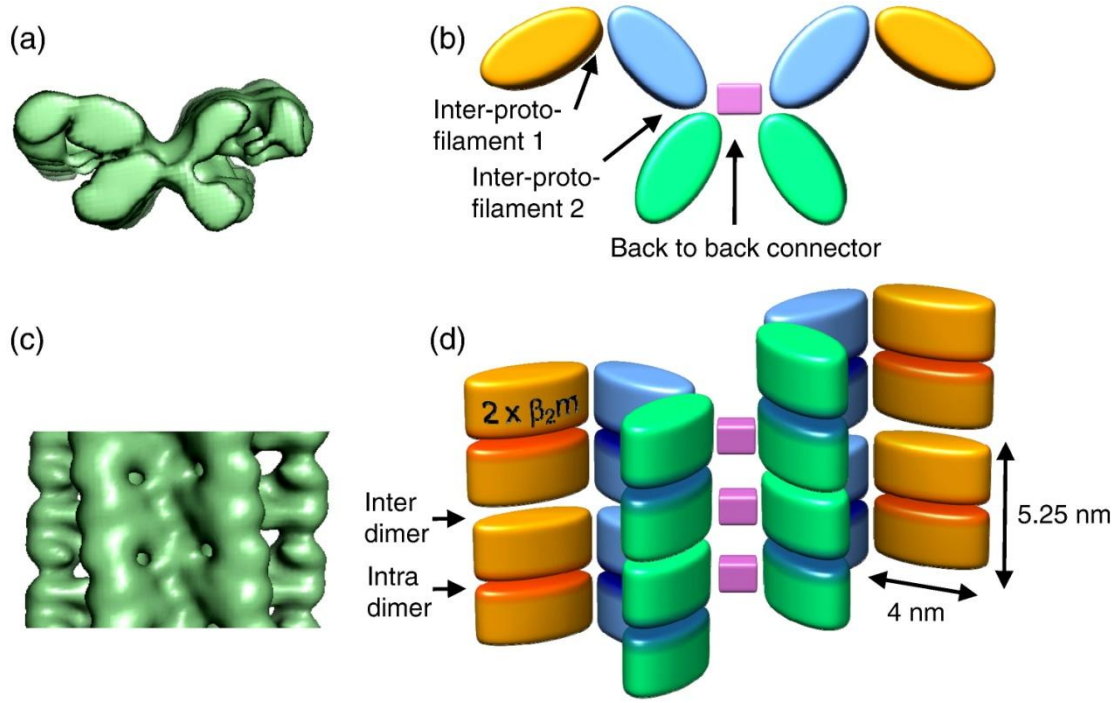

Figure 10 Schematic of subunit packing and interfaces in Saibil's type 2 fibril.
(a and c) Cross section and side view of a type 2 fibril. (b and d) Schematic representation of the dimer-of-dimers subunit packing for the same fibril orientation; each elliptical cylinder corresponds to two β_2m monomers. The outermost (orange) protofilaments in the model are disordered in the map, so that their full density is not reconstructed. It is possible, although unlikely, that pairs of protein subunits are threaded through all three protofilaments in one crescent with flexible hinge regions between the protofilaments. Figure modified from White, 2009 (*13*).

There are two symmetrically arranged stacks connected by a short connector (purple block in Figure 10) The stacks consist of a series of three dimers of dimers arranged in a crescent shape that are stacked on top of each other. This creates two types of interfaces in

the plane of the stack, one between the stacks – called inter dimer (Figure 10d) and intra dimer (Figure 10d).

The many different models for β_2m fibrils suggest that the fibril architecture is a lot more complicated than was previously thought.

1.6 Serum Amyloid P Component

1.6.1 Serum amyloid P component and amyloid

SAP is found associated with all types of amyloid deposits however this alone is not evidence that it contributes to pathogenesis and is not just an epiphenomenon in amyloidosis. There is evidence that amyloidosis is more closely related to circulating levels of SAP rather than amount of precursor protein available. In experimental murine reactive systemic amyloidosis, deposition of serum amyloid A protein as amyloid was found to correlate better with levels of SAP than that of serum amyloid A protein (*86*). In studies in the Syrian hamster, females developed reactive systemic amyloidosis much more readily than males. The relevant difference between males and females in this case was that SAP is under female sex hormone control (*87*).

Catabolism of SAP only occurs in the hepatocytes and so when associated with amyloid deposits no degradation of SAP takes place. This has been demonstrated by Pepys by using radiolabelled ^{125}I-SAP as it persists in the deposits for prolonged periods. SAP from both blood and amyloid deposits are indistinguishable from each other. These findings support the concept that SAP provides a protein coating to the fibrils masking them from the body's protein scavenging mechanisms (*1*). SAP itself is also highly resistant to proteolysis (*88*). In 1995, Tennent demonstrated that SAP binding to Aβ deposits from Alzheimer's, and AA fibrils from reactive systemic amyloidosis, conferred resistance to

proteolysis during *in vitro* tests. SAP could only prevent the degradation while bound to the fibrils, and when the SAP was dissociated from the fibrils using cyclic pyruvate acetal the proteinases cleaved the fibrils to the same extent as with no SAP present. This demonstrates that SAP prevents proteolysis through steric hindrance and it is not a protease inhibitor (*89*).

SAP knockout mice show retarded and reduced induction of experimental reactive systemic amyloidosis (*90*) demonstrating that SAP definitely does contribute to this type of amyloidosis, and presumably, as SAP binds to β_2m amyloid as well as proved by scintigraphy of DRA patients (*47*), contributes to DRA as well.

As SAP retards and reduces induction of amyloidosis in animals, screens were undertaken for drugs which could prevent SAP from binding to amyloid. A drug was found that prevented murine SAP from binding to amyloid in mice with experimentally induced murine amyloidosis. When these mice were engineered with a copy of human SAP not only did the drug stop binding of SAP to amyloid but also caused the depletion of amyloid from the system. Human trials are now underway for the drug R-1-[6-[R-2-carboxy-pyrrolidin-1-yl]-6-oxohexanoyl] pyrrolidine-2-carboxylic acid (CPHPC) (*90*). CPHPC's mechanism of action is by blocking ligand binding sites on SAP whilst cross linking pairs of pentameric SAP molecules forming a decameric molecule which is rapidly cleared from the body by the liver. This rapid depletion of SAP from the plasma leads to SAP dissociating from amyloid deposits into the plasma as SAP in the two components are in dynamic equilibrium. As SAP stabilises fibrils and prevents proteolytic degradation *in vitro* it is hoped that this reduction of SAP will lead to the removal of amyloid deposits in amyloidoses including DRA.

1.6.2 Structure and function of serum amyloid P component

The physiological role of SAP is not known for certain but it is thought to be involved in binding apoptotic cells as well as binding DNA and chromatin arising from cell necrosis (*91*); this prevents an auto immune response to self-nuclear material as shown by the finding that SAP knockout mice develop anti-nuclear autoimmunity (*92*). More recently DNA-SAP complexes have been identified in the serum of healthy humans via ELISA demonstrating that SAP does bind DNA *in vivo* in humans (*93*). SAP has been shown to bind to certain types of bacteria including *Streptococcus pyogenes* via the cyclic pyruvate acetals of sugars in their cell walls (*94*), but during *in vivo* tests on mice SAP has been shown to actually contribute to the pathogenicity of a number of bacterial strains due to giving resistance to phagocytosis (*95*).

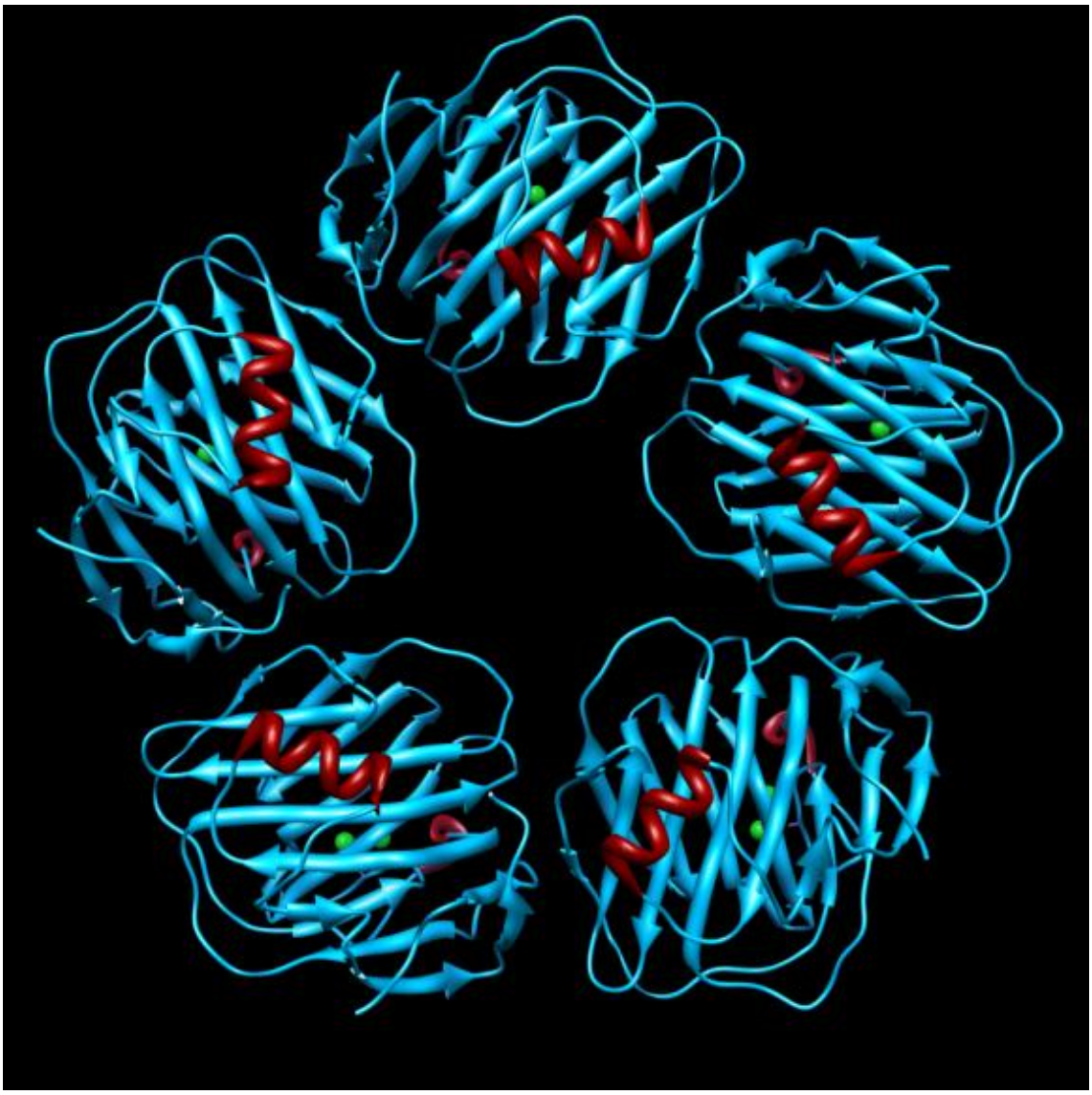

Figure 11 Pentameric SAP as determined by crystallography showing the alpha helix "A" face

Arrow shapes represent β-strands, red twists represent α-helices. Green spheres represent Ca^{2+} ions. Rendered using Chimera (PDB code:3KQR) (*96*).

Under normal serum conditions SAP forms a pentamer of identical non-covalently bound 25462 Da subunits. In the absence of Ca^{2+} SAP forms a decameric complex; *in vitro* in the presence of calcium, SAP pentamers auto aggregate and become insoluble however this precipitation is prevented by physiological concentrations of albumin and by calcium dependent ligands of SAP hence in the body SAP will always be found as a pentamer (*97*).

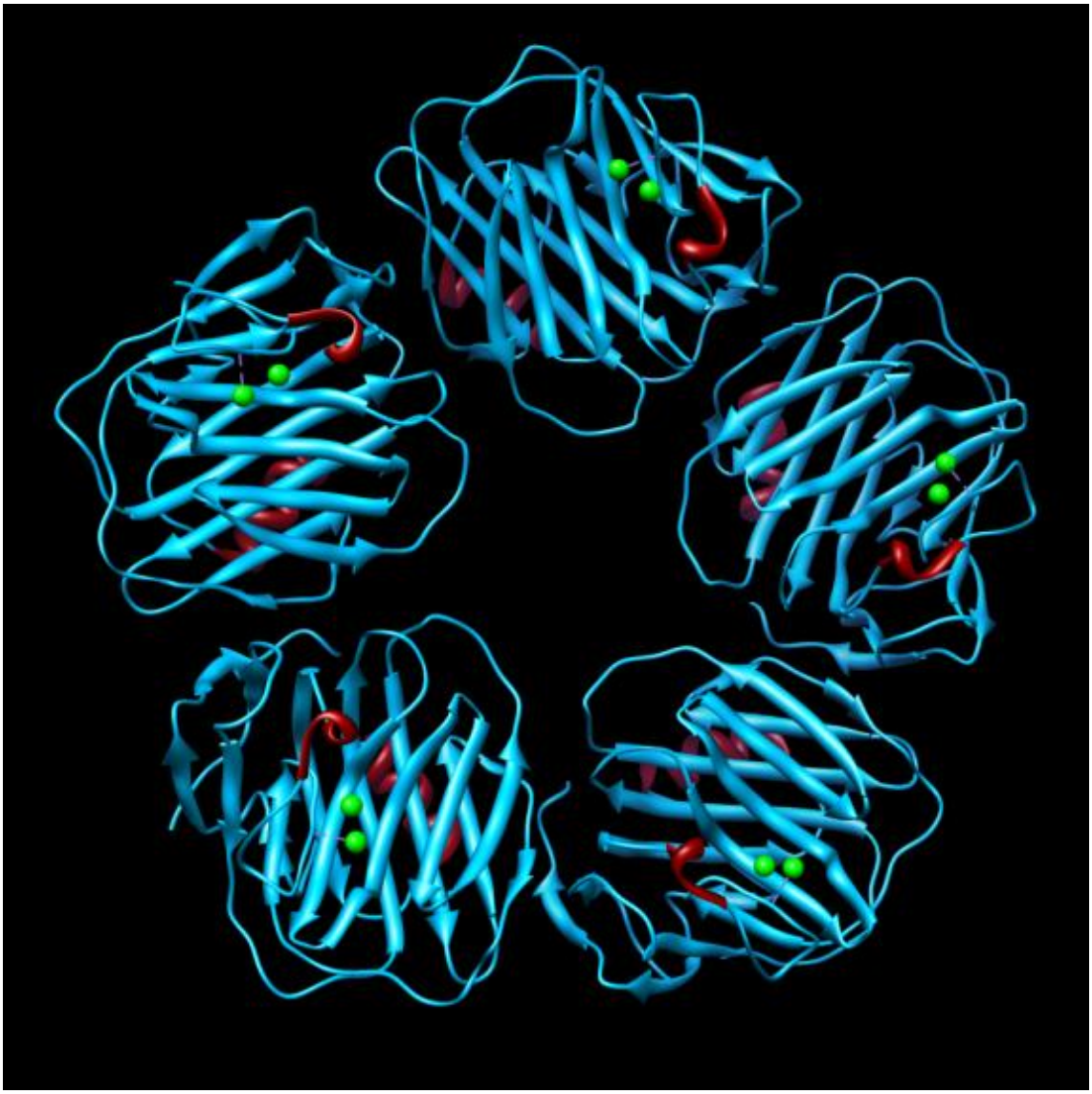

Figure 12 Pentameric SAP showing the calcium binding "B" face
In pentameric SAP all calcium binding sites are located on the same face of the molecule; creating a total of 10 calcium binding sites available. These are occupied above by calcium ions in green. Rendered using Chimera (PDB code:3KQR) (*96*).

Crystal studies of the native pentameric form by Emsley in 1994 revealed that it has a diameter of approximately 100Å and depth of 35Å forming a ring like structure. Each monomer contains 204 residues with a jelly roll topology of two beta-sheet layers. One of the sheets contains an alpha-helix (Figure 11) while the other sheet which makes the other

face contains two calcium binding sites (Figure 12). These sites are 3.93 Å apart from each other; calcium site 1 is high affinity while site 2 is lower (*98*). When present in site 1, X-ray diffraction studies reveal that the calcium ion is co-ordinated to the carboxyl groups of the side-chains of Asp-58, Asn-59, Glu-136, Asp-138 and the main chain carbonyl of Glu-137 (Figure 13). Distortion of the start of strand E sends the above residues looping towards calcium binding site 1. An additional co-ordination site is filled by buffer acetate in 4 of 5 protomers but occupied by Glu-167 of an adjacent molecule in the crystal lattice in one. This opens up the possibility of glutamates from external molecules co-ordinating with calcium ion 1. Calcium ion 2 is bridged to ion 1 via the oxygens of Glu-136 and Asp-138. Co-ordination is completed by the oxygen of Gln-148 and 2 water molecules (Figure 13). Calcium ion 2 is more loosely bound than ion 1 and can be displaced by cerium ions in cerium sulphate soaked crystals and is also removed if crystals are soaked in calcium free buffers. This is consistent with the position being more solvent accessible and having less ligands donated from the protein. When the SAP monomers associate all the alpha-helices are on the same side as each other and hence the pentamer has one face with five alpha helices present named the A face and one face with ten calcium binding sites named the B face (*98*). Calcium is essential for SAP to bind to ssDNA and dsDNA as well as chromatin, as has been shown *in vitro* by binding assays while DNA has been both immobilised on gels and at physiological concentration in vitro (*91*). Calcium is also essential for SAP binding to all types of fibrils; *in vitro* tests show that while SAP will bind to fibrils when incubated in the presence of Ca^{2+}, if no Ca^{2+} is present in the incubation buffer or EDTA is present then no binding between SAP and fibrils will occur (*99*).

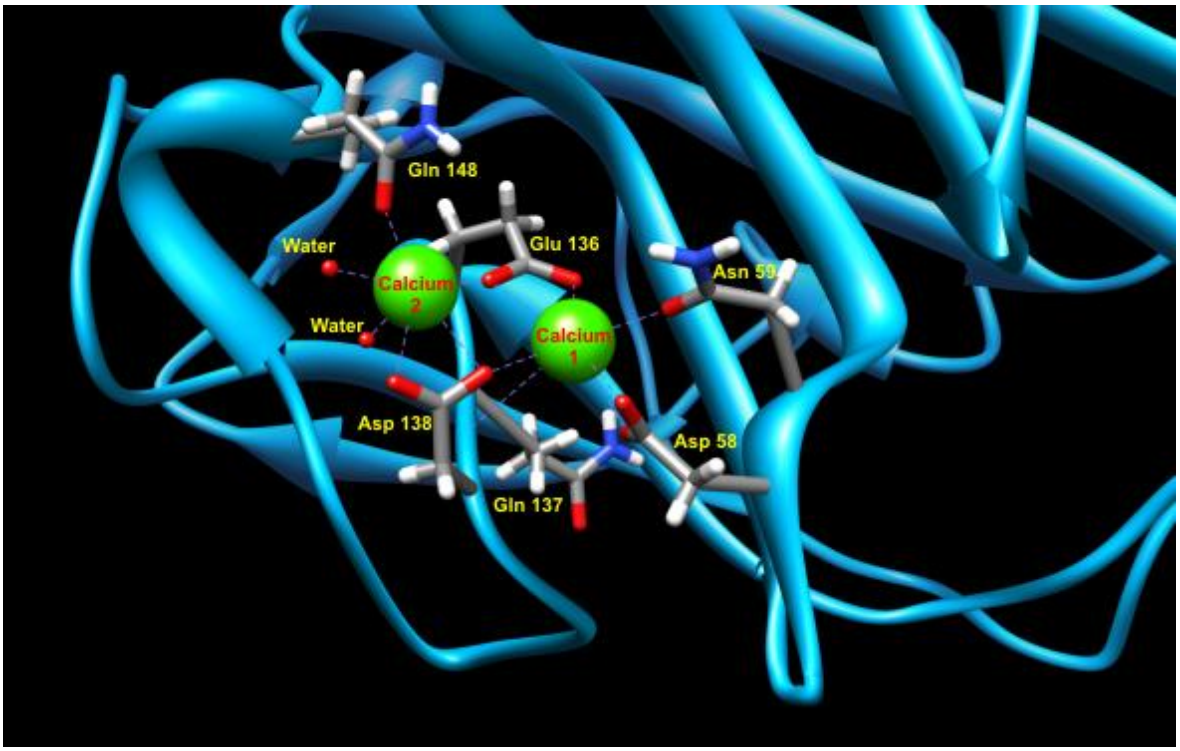

Figure 13 Calcium binding sites of Serum Amyloid P component
Calcium 1 has a high affinity interaction with SAP mediated through co-ordination to the oxygen atoms of the carboxyl groups of the sidechains of D58, N59, E136, D138 and to the main chain carbonyl of Q137. The seventh co-ordination site in this particular protomer, by Mikolajek *et al.* in 2011, is filled with phosphoethanolamine (not shown) (*96*) Calcium 2 is bridged to calcium 1 via E136 and D138. Co-ordination is completed by Q148 and two water molecules. Rendered in Chimera (PDB code: 3KQR).

The evidence from the literature points towards an interaction between serum amyloid P component and fibrillar β_2m being causative in dialysis related amyloidosis (DRA) and so characterising this interaction at atomic resolution is essential for a complete understanding of how SAP causes the persistence of amyloid in DRA. Due to the non-crystalline nature of fibrils, nuclear magnetic resonance (NMR) is the only viable high-resolution technique appropriate for the detailed study of the interaction between fibrillar β_2m and SAP. An introduction to NMR is given in the following section.

1.7 Introduction to nuclear magnetic resonance

1.7.1 Introduction

The material found within this section is well explained in various textbooks and focuses only on theory which is particularly relevant to the project. For a more detailed explanation of the theory discussed please see Spin Dynamics (2nd edn.) by Malcolm Levitt (2008) (*100*). Nuclear magnetic resonance (NMR) occurs due to the property of nuclear spin; which is a form of angular momentum. Nuclear spin is an intrinsic property of the some nuclei. In the absence of an external magnetic field the energy levels of the spins are degenerate. However in the presence of a magnetic field these degenerate energy levels split; the magnitude of energy split depends on the strength of the magnetic field. This splitting of energy levels allows the nucleus to absorb an electromagnetic radiation wave of an energy matching the difference between energy levels. It is the absorption of this energy that produces a signal that can be detected by a spectrotometer. The resonance frequency for a given nucleus is dependent on the interaction between the nuclear spin and the local magnetic field making it an excellent reporter on the local structure and environment. This will be discussed in detail later.

In the liquid-state NMR spectrum narrow lines result from the rapid tumbling of the molecule in solution. This is due to the averaging of anisotropic interactions that are dependent on the orientation of the molecule with respect to the applied magnetic field. NMR of fibrils is made difficult due to their size and the resultant slow molecular tumbling which means the anisotropic interactions are not averaged out; this results in severe line broadening as each orientation of the molecule produces its own unique signal making structural and dynamic studies difficult. However the anisotropy present in the solid-state

NMR spectrum can provide valuable structural and dynamic information. The key to this is understanding the origin of the anisotropic interactions which requires knowledge of the nuclear spin Hamiltonian.

1.7.2 The nuclear spin Hamiltonian

The position and form of the signal that a nucleus will produce in a spectrum depends on the total nuclear spin Hamiltonian:

$$\hat{H} = \hat{H}_Z + \hat{H}_J + \hat{H}_D + \hat{H}_{CS}$$

where H_Z is the Hamiltonian for the Zeeman effect, H_{CS} is the chemical shift Hamiltonian, H_J is the J-coupling Hamiltonian and H_D is the dipolar coupling Hamiltonian.

The Zeeman effect describes the interaction of the nucleus with the external magnetic field causing previously degenerate energy levels to split into different energy levels.

$$\hat{H}_Z = \gamma B_0 \hat{I}_{jz}$$

where γ is the gyromagnetic ratio of the nucleus (rad s^{-1}), B_0 is the external magnetic field (Tesla) and $\hat{I}_{jz}$ is the spin angular momentum operator.

When placed in a magnetic field, electrons will circulate around the nucleus and produce a magnetic field which opposes the applied magnetic field. The field experienced by a nucleus will therefore differ depending on the electrons surrounding that nucleus. As the Larmor frequency is dependent on field strength this results in a perturbation of the resonance frequency. The chemical shift anisotropy comes about through the uneven

electron distribution surrounding nuclei. In solution this uneven distribution gets averaged out due to the fast molecular tumbling. In solids the nuclei will experience a different field depending on the orientation of the molecule, so nuclei in the exact same electronic environments will be experiencing different fields.

$$\widehat{H}_{CS} = \pm\gamma_j B_0(\sigma_{\text{iso}} + \frac{\sigma_{zz} - \sigma_{\text{iso}}}{2}(3\cos^2\theta - 1) - \eta\sin^2(\theta)\cos(2\phi))\hat{I}_{jz}$$

where σ_{iso} is the isotropic shift $\frac{1}{3}(\sigma_{yy}+\sigma_{xx}+\sigma_{zz})$. σ_{ii} being the principle components of the chemical shielding tensor. The anisotropy is σ_{zz}-σ_{iso} and η the asymmetry parameter is:

$$\frac{\sigma_{yy}-\sigma_{xx}}{\sigma_{zz}-\sigma_{iso}}$$

Nuclear spins are associated with a magnetic moment and as such produce their own magnetic fields. These magnetic fields are able to interact through space with other nearby spins, resulting in so called dipolar interactions. In solution these dipolar interactions are averaged out through the rapid tumbling of the molecule resulting in sharp lines. In solids the spectra will show a distribution of lines, each corresponding to a different local field which depends on the orientation of the internuclear vector, distance between nuclei and the magnetic moments of the nuclei.

The Hamiltonian describing the interaction of two spins *j* and *k* takes the form of:

$$\widehat{H}^{D}_{Homo} = -\frac{b_{jk}}{2}(3\cos^2\theta - 1)\,(3\hat{I}_{jz}\hat{I}_{kz} - \hat{\mathbf{I}}_j.\hat{\mathbf{I}}_k)$$

for a homonuclear spin pair and:

$$\widehat{H}^{D}_{Hetero} = -\frac{b_{jk}}{2}\,(3\cos^2\theta - 1)I_{jz}I_{kz}$$

for a heteronuclear spin pair.

where b_{jk} is the magnitude of the dipolar interaction between spins *j* and *k* and is determined by:

$$b_{jk} = -\frac{\mu_0}{4\pi}\frac{\gamma_j\gamma_k\hbar}{r^3_{jk}}$$

where μ_0 is the vacuum permeability (4π x 10^{-7} H m^{-1}), γ_j and γ_k are the gyromagnetic ratios (rad s^{-1}) of the nuclei and r_{jk} is the inter spin distance (m).

J-coupling is the through bond coupling between two nuclei. The J-coupling contains isotropic and anisotropic components, but the anisotropic component is small and not readily discernable from the dipolar couplings and thus only the isotropic scalar couplings are usually considered. The isotropic J-coupling Hamiltonian (heteronuclear case) is:

$$\widehat{H}^{J}_{jk} = 2\pi J_{jk}\hat{I}_{jz}.\hat{I}_{kz}$$

where J is the magnitude of the J-coupling. J-couplings are not as important in solid-state NMR as in liquid-state NMR as they are typically significantly smaller than dipolar

couplings and contributions from the CSA and thus not routinely observed in the solid-state NMR spectra.

1.8 Solid-State NMR studies of fibrillar proteins

1.8.1 Magic Angle Spinning (MAS) NMR

Fibrillar proteins are insoluble and experience very limited, if any, molecular tumbling. For this reason the anisotropic interactions that they experience do not get averaged out by fast molecular tumbling as perhaps they would in their monomeric form; and as such solid state spectra of unorientated static samples are of poor resolution. An understanding of the total nuclear spin Hamiltonian can provide an answer to this problem. As can be seen from the Hamiltonians in 1.7.2, the anisotropic interactions all have an angular dependence of $\frac{1}{2}(3\cos^2\theta-1)$ which leads to a distribution of resonance lines due to the random orientation of the molecules within the magnetic field. When $\theta = 54.7^\circ$ (known as the magic angle) then $\frac{1}{2}(3\cos^2\theta-1)=0$. It is not practical in these samples to align all the molecules at the magic angle such that the anisotropic terms disappear leaving only the isotropic chemical shift and the J-coupling. However, if we rapidly rotate the sample (such that ω_r>anisotropic interaction) at 54.7° (so called magic-angle spinning) then on average these anisotropic interactions are projected onto the magic angle resulting in contributions containing a $\frac{1}{2}(3\cos^2\theta-1)$ dependence (e.g. CSA, dipolar) being averaged (*101*). The resulting NMR spectrum is similar to that found in liquid state NMR with the resonance position dependent on the isotropic chemical shift and in favourable cases by the isotropic J-coupling.

1.8.2 Improving detection of low γ nuclei ($^{13}C/^{15}N$) in solid-state NMR

Carbon, nitrogen, oxygen and hydrogen are the main constituents of amino acids and therefore protein and as such it is obviously desirable to be able to study them using NMR when investigating proteins. ^{1}H is almost 100% abundant and is spin ½ and therefore causes no problems from a detection point of view; although strong $^{1}H/^{1}H$ homonuclear dipolar coupling that are not readily averaged by MAS lead to poor spectral resolution. The most naturally abundant form of carbon is carbon-12 which is 98.9% abundant and this, along with oxygen-16 which is 99.96% abundant, unfortunately has no spin. Nitrogen-14 is 99.6% abundant and has spin 1 making it a quadrupolar nucleus, which, for reasons that go beyond the scope of this thesis, make it difficult to study by NMR. Carbon-13 which is 1.1 % abundant and nitrogen-15 which is 0.37% abundant are both spin ½ and therefore are easily detectable by NMR.

As well as their low natural abundances, ^{13}C and ^{15}N only have gyromagnetic ratios of 10.71 MHz/T and -4.32 MHz/T respectively as opposed to 42.58 MHz/T for hydrogen.

The lower value of γ, which is an intrinsic property of the nucleus, for $^{13}C/^{15}N$ means that the energy gap between states is smaller and the difference in population between the energy states is smaller resulting in lower sensitivity. The result of this is that carbon-13 NMR is a factor of 4 less sensitive than proton NMR and nitrogen-15 NMR is a factor of 10 less sensitive.

We can enhance the polarisation of $^{13}C/^{15}N$ using cross-polarisation. In short this is where magnetisation from abundant spins such as hydrogen is transferred over to the carbon spins using the pulse sequence in Figure 14.

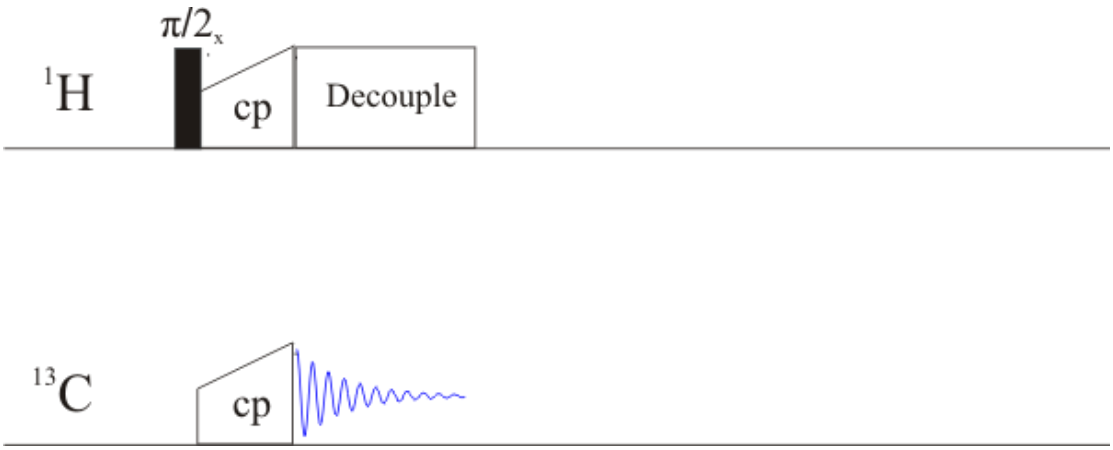

Figure 14 Cross-polarisation pulse sequence
Cross-polarisation is a much used method in solid-state NMR for transferring magnetisation between nuclei. The black rectangle represents a 90˚ pulse along the x axis. The ramped boxes represent contact pulses used for matching the Hartmann-Hahn condition. The box containing 'Decouple' is a decoupling pulse. The blue wave symbol represents the collection of an FID.

The 90˚ pulse applied to the proton along the X-axis rotates the hydrogen magnetisation vector onto the y axis. A contact pulse is now applied along the y axis, this one in the range of milliseconds rather than microseconds like the 90˚ pulse. The pulse 'spin-locks' and precesses about the y axis. At the same time a contact pulse is applied on the ^{13}C channel causing the ^{13}C magnetisation to precess along the y axis.

The frequency of the precession under the spin lock is dependent on the radio frequency field (B_1) and gyromagnetic ratio (γ) in the following manner:

$$\omega_1 = (\gamma B_1)$$

If the both magnetisations precess at the same angular frequency (ω_1) and have J or dipolar coupling between them then mutual spin flips or mutual relaxation can occur.

The frequencies of the precessions have to be matched stringently in order for magnetisation transfer to take place and this is called the Hartmann-Hahn condition where:

$$(\gamma B_1)_{\mathrm{C}} = (\gamma B_1)_{\mathrm{H}}$$

As most the magnetisation is on the hydrogens due to its higher gyromagnetic ratio the magnetisation is transferred onto carbon. The contact pulse on the hydrogen channel is then replaced with a decoupling field and the contact pulse on the carbon channel is switched off and a FID acquired.

The low gyromagnetic ratio of carbon-13 can be compensated for by increasing the field strength applied to the sample. Magnets up to 23.5 Tesla (1 GHz) are now commercially available. The low natural abundance of carbon-13 can be overcome in recombinant proteins by growing the bacterial expression systems on minimal media and using a ^{13}C labelled glucose (or glycerol in some cases) as the only carbon source for the bacteria.

1.8.3 Improving resolution in NMR through decoupling

A problem with observing the ^{13}C nucleus when studying proteins is that dipolar coupling of ^{13}C to hydrogen nuclei causes a distribution of resonance frequencies and makes the spectra hard to interpret. This problem can be solved by applying a continuous wave irradiation at the hydrogen frequency which causes the proton polarisation to rapidly precess around either the x or y axis causing an averaging of proton polarisation observed by the carbon-13. Typically we use Time Proportional Phase Modulated (TPPM) or SPINAL (*102*) decoupling which improve the efficiency of decoupling through the application of rapid switching of the decoupler phase.

1.8.4 Magnetisation exchange through dipolar recoupling

As discussed in section 1.8.1, magic angle spinning (MAS) enables narrowing of powder line-shapes in solid-state NMR spectra often leading to, in the case of chemical shifts, a single spectral line for each molecular site. However MAS also attenuates or removes homo- and heteronuclear dipolar couplings within the sample. These dipolar couplings are the basis for most structural techniques in solid-state NMR, including spectral assignments and using distance and torsion angle measurements to constrain structures; therefore in order to obtain information from dipolar coupling, the couplings must be re-introduced by interfering with the MAS averaging process.

Spin exchange can be promoted by any of three methods: 1) RF-driven spin exchange which relies on RF pulse trains to reintroduce dipolar coupling. 2) Rotor-driven spin exchange that relies on spinning the sample at multiple integers of the difference in isotropic chemical shift between carbons. In practice a combination of RF- and rotor-driven spin exchange is often used so that reduced RF power can be employed which prevents RF overheating of the sample 3) Proton driven spin diffusion which relies on line-broadening due to proton-carbon dipolar couplings that are incompletely averaged by MAS.

Spin-diffusion describes polarisation exchange in a strongly coupled spin system, which under appropriate conditions can resemble a diffusion process. Typically the rate of spin-diffusion is dependent on two properties. Firstly the strength of the dipolar couplings that exist between the labelled sites within the biopolymers, with stronger couplings and more extensive labelling resulting in a higher rate of spin-diffusion and secondly, the distribution of chemical shifts with small variation making the exchange process energy conserving and thereby increasing the rate of spin diffusion. Typically low-γ nuclei, such as carbon-

13, have weak couplings and a large distribution of chemical shifts. These conditions make the measurement of spin-diffusion between low-γ nuclei unfavourable, however in the case of proton-driven spin-diffusion, by coupling the low-γ nuclei to an external reservoir such as the surrounding protons with their strong network of dipolar couplings and relatively small chemical shift dispersion, the rate spin diffusion is significantly enhanced (*103*). Proton driven spin diffusion is one of the main techniques used in this thesis and is discussed in more detail in chapter 4.

1.8.5 Reducing the lossiness of samples

High ionic strength is often required in order to keep some biological samples stable at the concentrations required for good signal in solid-state NMR; this leads to elevated conductivity, resulting in longer pulse lengths and less efficient detection. This is particularly problematic when decoupling for extended periods of time as this can lead to a significant amount of sample heating. This is particularly true when working at higher magnetic fields when the radiowaves irradiating the protons are more readily absorbed by the sample. The combination of this less efficient detection and the sample heating means that sample lossiness is a major factor in determining the quality of the spectra acquired in solid-state NMR. One method of reducing the lossiness of samples is to alter sample preparation and try and use the minimum amount of ionic buffer components possible in the sample, but as mentioned above these components are often needed in order to keep the protein stable. Recent advances in probe technology have led to the development of E^{free} probes which reduce the E-field at the location of the sample. In this project we use both altered sample preparation and E^{free} technology to overcome the high ionic strength conditions required to keep SAP stable during NMR experiments.

1.9 Aims of thesis

SAP is always found associated with β_2m amyloid deposits *in vivo* therefore we know it has the opportunity and does interact with β_2m; although this alone does not necessarily mean it is not an epiphenomenon. Evidence has been presented that SAP is able to enhance the elongation of β_2m fibrils *in vitro* and this leads to the possibility that it could potentially do it *in vivo* as well. There is *in vivo* evidence, through SAP knockout mice, that without SAP it is difficult to induce experimental amyloidosis. There is also *in vitro* evidence that SAP prevents the proteolytic degradation of amyloid fibrils and therefore it could be providing a mechanism by which the balance between fibril elongation and degradation is vastly tipped in the favour of elongation.

There is strong evidence that SAP plays a pathogenic role in amyloid diseases and that it may be do this by preventing degradation of amyloid by the body's protein scavenging systems through binding to amyloid fibrils. SAP binds to amyloid irrespective of its precursor protein; there therefore has to be a common feature or motif of all amyloid fibril types that SAP recognises. The work presented in this thesis aims to characterise the properties and characteristics of β_2m fibrils and in particular the specific nature of the fibrils' interaction with SAP. By identifying the mechanism of binding between β_2m fibrils and SAP this thesis hopes to draw wider conclusions about the common mechanism of binding that SAP must display towards all fibrils types.

Chapter 2

2 Biochemical Studies of Beta-2 Microglobulin and Serum Amyloid P Component

2.1 Introduction

In the introduction, it is explained how we intended to use biochemical, biophysical and nuclear magnetic resonance (NMR) techniques in order to characterise β_2m and its interaction with SAP. The study of proteins by NMR requires large amounts of protein enriched with magnetic isotopes. Although most nuclei possessing spin can be studied by NMR, only spin-½ nuclei can be studied easily. This precludes the use of material from patients as the only abundant spin one-half magnetic nuclei belong to hydrogen and protons have strong dipolar couplings not readily manipulated by MAS and this makes assignment and structural studies difficult. The number of proton resonances in large macromolecules such as proteins also means that in the solid-state single resonance experiments produce crowded spectra. Due to this requirement recombinant protein has to be expressed in a system which allows addition of isotopes with a magnetic moment such as carbon-13 and nitrogen-15. Although yeast in now a feasible expression system (*104*), prokaryotes such as *Escherichia coli* still offer the simplest and fastest way to express enough protein to provide enough material for study by NMR. Accordingly we have undertaken the expression of β_2m in *E.coli*. Under the control of the T7 promoter, large concentrations of protein are produced which form inclusion bodies. The protein therefore has to be resolubilised and refolded back to its native fold. An efficient protocol for the formation of monomeric β_2m was therefore developed. For solid-state studies milligrams

of β_2m fibrils have to be produced from monomeric β_2m; we therefore developed an efficient protocol for the conversion of monomeric β_2m to fibrillar β_2m that resembles β_2m fibrils from DRA patients.

Amyloid deposits in DRA contain a number of other components as well as β_2m fibrils. These components include collagen, proteoglycans, glycosaminoglycans and serum amyloid P component. Serum amyloid P component is thought to play a key role in the prevention of clearance of fibrils by the body's protein scavenging mechanisms. The association of SAP and fibrillar β_2m has been demonstrated *in vivo* using scintigraphy (*47*) and prevention of enzymatic proteolysis of fibrils in the presence of SAP has been demonstrated *in vitro.* SAP has also previously been identified as being able to enhance the rate of β_2m fibril formation at neutral pH (*45*).

In order to characterise the interaction between SAP and fibrillar β_2m the interaction had to be recreated *in vitro*. There were several difficulties that had to be overcome in order to achieve this. The main difficulty was that acid produced fibrils are unstable at neutral pH and SAP, like most proteins, becomes partially unfolded at the pH levels at which β_2m acid produced fibrils are stable. This raises the question as to whether the interaction between β_2m fibrils and SAP at neutral pH is strong enough to stabilise the fibrils during the time course of a solid-state NMR experiment. A second difficulty was SAP's requirement for high concentrations of calcium in order to both bind fibrils and stay soluble concurrently, this leading to unphysiological concentrations of salt which as well as changing the morphology of fibrils, can also cause sample heating and reduce signal to noise in the NMR spectrum. In this chapter we describe how we have proven a definite and strong interaction between *in vitro* produced fibrillar β_2m and SAP using binding assays.

Most *in vitro* studies of fibrillar β_2m to date have focussed on the low salt, acid produced variety. There are a number of questions that have to be addressed regarding the stability of these fibrils under physiological-like conditions; currently the general consensus is that they are unstable at neutral pH. We have undertaken a number of fluorescence and electron microscopy dissociation studies to establish the conditions under which acid produced fibrils may be stable at neutral pH, the role that SAP may play in stabilising these fibrils at neutral pH, and under which conditions it binds. These studies also look at the effect of macromolecular crowding on fibril stability; the dilute conditions used in the depolymerisation study do not truly represent the environment that fibrils would find themselves either in an intra or intercellular environment, where concentrations of macromolecules can reach ~400 mg/ml (*105*). These environments are not normally referred to as concentrated, as no one species tends to be in high concentration, but molecularly crowded. Molecular crowding leads to volume exclusion effects and it has been suggested that volume exclusion *in vivo* could modulate the rate and extent of fibril formation (*106, 107*). Studies of the phenomenon *in vitro* using molecular crowding agents such as Ficoll 70 and dextran, as well as proteins such as BSA and lysozyme, have demonstrated that the rate of fibrillogenesis of α-synuclein and apolipoprotein C-II can be enhanced in the presence of high concentrations of molecular crowding agents (*108, 109*). As molecular crowding effects can promote fibrillogenesis, we investigated whether it would be able to inhibit the depolymerisation of fibrils. These studies have revealed that the buffer conditions and the soluble protein concentration in particular may play an important role in determining fibril morphology and stability.

This chapter describes the efforts undertaken to produce fibrillar β_2m and characterise its morphology and stability under a variety of conditions including in the presence of SAP.

2.2 Materials & Methods

2.2.1 Expression and purification of soluble beta-2 microglobulin

In order to characterise beta-2 microglobulin (β_2m) and its interaction with SAP large amounts of β_2m were needed. Due to this requirement recombinant human β_2m was expressed in *E.coli*. This allowed the expression of enough β_2m to complete all necessary studies.

Expression of β_2m

Competent BL21 (DE3) *E.coli* were transformed using a pET11a vector containing the β_2m gene. The *E.coli* were grown on Luria Broth (Sigma-Aldrich) containing 0.1 mg/ml ampicillin for biochemical and biophysical analysis.

For isotopically labelled β_2m, minimal media (see appendix 1) containing one of the following combinations of labelled media was used:

^{15}N labelled ammonium chloride

^{13}C labelled glucose

^{15}N labelled ammonium chloride and ^{13}C labelled glucose

[1,3-^{13}C]-glycerol and ^{15}N labelled ammonium chloride

[2-^{13}C]-glycerol and ^{15}N labelled ammonium chloride

The following protocol was used:

Glycerol stock of BL21 *E.coli* transformed with human β_2m gene in pET11a plasmid vector was added to 2 x 10ml of Luria Broth supplemented with 6µl of 100mg/ml ampicillin in each. The starter cultures were then incubated with shaking at 25˚C for approximately 8 hours. The starter cultures were then spun at 1922*g* for 10 minutes,

supernatant removed and discarded and pellets resuspended in 1ml minimal M9 growth medium each. This suspension was then split equally between 4 x 25ml minimal M9 media. The cultures were then incubated with shaking at 25˚C overnight for approximately 16 hours. Two flasks each containing 500ml minimal M9 medium were prepared and 250µl of 100mg/ml ampicillin added to each. Two of the 25ml cultures were then added to each flask and the flasks incubated at 37˚C with shaking for approximately 6 hours. OD 600 measurements were taken on a Jenway 6100 spectrophotometer each hour to monitor for mid log growth phase.

Irrespective of media used expression of β_2m was induced using IPTG (1 mM final conc.) once an optical density of ~1.0 at 600 nm was reached.

E.coli were harvested by centrifugation (20 min, 8983 *g*) when an optical density of ~1.6 at 600 nm was reached. The *E.coli* were lysed by sonication (30 seconds on, 30 seconds, power level 8, 10 min process time off) using a stud sonicator (Heat systems) in an ice bath.

Washing of inclusion bodies

Inclusion bodies were washed as follows: β_2m inclusion bodies (IB) were harvested by centrifugation (20 min, 16000 *g*) and homogenised and incubated at 37˚C for 1 hour in lysis buffer (10 ml per gram of original cell paste) containing lysozyme and DNase I (10 mM Tris-HCl pH 7.5, 2.5 mM $MgCl_2$, 0.5 mM $CaCl_2$, 0.013 mg/ml DNase I, 4 x 10^{-3} mg/ml lysozyme). The IB were centrifuged (20 min, 16000 *g*) and the pellet homogenised in 30 ml Triton buffer (50 mM Tris-HCl pH 8.0, 100 mM NaCl, 0.5% Triton X-100) before centrifugation (20 min, 5000 *g*). This was followed by homogenisation in 1:10 Triton buffer and centrifugation (20 min, 8000 *g*). The subsequent pellet was homogenised in 1:10 Triton buffer and centrifuged (20 min, 16000 *g*).

Solubilisation of inclusion bodies

The inclusion body pellet was solubilised in solubilisation buffer (10 ml per gram of original cell paste) containing 8 M urea (8 M Urea, 50 mM MES pH 6.5, 0.1 mM EDTA, 0.1 mM DTT) and left for 12 hours minimum and centrifuged (20 min, 16000 *g*) to remove any non-solubilised material. The supernatant (solubilised β_2m) was retained, concentration was determined spectrophotometrically at 280 nm ($A^{1cm}_{1\%}$ = 16.91) via nanodrop (Thermo scientific) and any pellet discarded.

Refolding of β_2m

The solubilised β_2m was refolded by dilution at 4˚C. The solubilised β_2m was first diluted 1:1 with refold buffer (100 mM Tris-HCl pH 8.0, 400 mM L-Arginine-HCl, 2 mM EDTA, 5 mM Glutathione- Reduced, 0.5 mM Glutathione- Oxidised, 0.1 mM PMSF) by addition of the refold buffer to the solubilised β_2m drop by drop at 0.1 ml/min using a peristaltic pump. The β_2m/refold buffer was subsequently added overnight drop by drop at 0.1 ml/min to a volume of refold buffer in which the final concentration of β_2m would be less than or equal to 5 μM (2 litres of refold buffer generally used for 100 mg of solubilised protein).

Concentration & gel filtration

After refold the β_2m is concentrated using a 5000 MWCO Kvick filtration system (GE Healthcare) to a concentration of ~2 mg/ml as determined by nanodrop. A Sephadex 75 filled Hiload 16/60 column (GE Healthcare) was equilibrated with eluent (10 mM HEPES pH 7.4, 50 mM KCl, 0.1 % Sodium azide) and 5 ml of the concentrated β_2m was loaded onto the column per run; the eluent was run through at 1 ml/min. The fractions were collected using an automated fraction collector and the fraction containing monomeric β_2m

(determined by SDS PAGE and comparison of elution profile with known standards) was retained. The monomeric β_2m was subsequently concentrated to 1 mg/ml by centrifugal filtration using 10000 MWCO Vivaspin 20 filtration units (Sartorius). The β_2m was either stored at 4˚C for up to a month or lyophilised for storage for longer periods.

2.2.2 Beta-2 microglobulin fibrillogenesis

The characterisation of β_2m fibrils and their interaction with SAP was undertaken using fibrils formed *in vitro* from recombinant β_2m expressed and purified as described in the previous section. Two types of fibrils were produced, for most experiments characterising β_2m fibrils and their interaction with SAP, fibrils were produced under relatively low ionic strength conditions and henceforth described as low salt fibrils. Fibrils were also grown under conditions of relatively high ionic strength for characterisation of fibrils with non-standard morphologies; these fibrils will henceforth be referred to as high salt fibrils. For low salt fibrils soluble β_2m was mixed 1:1 with a low pH sodium citrate buffer to lower its pH to 2.5 (Reaction composition: 42 μM β_2m, 25 mM sodium citrate, 25 mM KCl, 12.5 mM HEPES, pH 2.5). For high salt fibrils, potassium chloride was added (84 μM β_2m, 50 mM sodium citrate, 500 mM KCl, pH 2.5). The solutions were then incubated at 37˚C with 200rpm orbital shaking for 1 week. Once formed fibrils were stored at ambient temperature. Fibril formation was confirmed with the Congo red spectrophotometric assay recording at 403 and 541 nm and thioflavin T fluorescence assay exciting at wavelength 420 nm and monitoring emissions at wavelength 485 nm.

Negative stain transmission electron microscopy of fibrils for determining morphology

Negative stain transmission electron microscopy was used to determine fibril morphology. 5µl of 0.5 mg/ml fibril suspension was put onto a 200 mesh formvar-carbon coated copper grid for 30 seconds. The suspension was then blotted off with absorbent paper and 5µl 2% uranyl acetate put on grid for 10 seconds. Grids were inspected with a transmission electron microscope operated at 120 kV (Hitachi).

Monitoring fibrillogenesis using thioflavin T fluorescence

The time course of fibrillogenesis of β_2m fibrils was monitored using ThT fluorescence. 20 µl of 1mg/ml acidic fibril suspension was added to low salt and high salt ThT containing buffers. These buffers were:

- Low salt (reaction composition: 8.4 µM β_2m, 9 µM ThT, 22.5 mM sodium citrate, 22.5 mM KCl, 11.25 mM HEPES, pH 2.5)
- High salt (reaction composition: 8.4 µM β_2m, 9 µM ThT, 540 mM NaCl, 180 mM $CaCl_2$, 90 mM Tris-HCl, 0.09% NaN_3, pH 2.5)

Experiments were performed in triplicate and mean of results taken.

2.2.3 Fibrillar beta-2 microglobulin-SAP pull down assay

The interaction between amyloid fibrils has been well established and radiolabelled SAP is used clinically to detect the presence of amyloid, including β_2m amyloid, in patients. In order to prove that an interaction exists between the *in vitro* produced fibrils that we would be using during the project and SAP, we undertook a pull-down assay between the two proteins.

Fibrils were produced in low pH, low salt conditions (reaction composition: 49.3 μM β_2m, 50 mM sodium citrate, 25 mM KCl, 15 mM HEPES, pH 2). Fibrils (1 ml suspension) were spun down for 10 minutes at 17000 *g* and supernatant removed. Fibrils were resuspended in 1 ml TNCa buffer (100 mM Tris-HCl, 600 mM NaCl, 200 mM $CaCl_2$) and divided into two aliquots of 500 μl. Aliquots were then spun down for 10 minutes at 17000 *g*, supernatant removed and fibrils resuspended in 100 μl of either 79 μM SAP in TNCa buffer or TNCa buffer alone (control); after an hour of incubation they were each spun down at 17000 *g* and the supernatant removed. The aliquots were then suspended upside down with absorbent paper inserted to remove any excess supernatant. SDS PAGE was run on the final pellet and supernatant.

2.2.4 Fibril depolymerisation in presence of SAP

One of the aims of this thesis is to determine whether or not SAP binding to fibrillar β_2m stabilises the fibrils. Acid produced fibrils are known to be unstable at neutral pH, quickly depolymerising to soluble species (*110*). This normally hinders the study of *in vitro* fibrils under physiological like conditions however it also provides a unique opportunity for determining whether SAP can stabilise β_2m fibrils as if the presence of SAP slows the depolymerisation of fibrils it can be ascertained that SAP does stabilise them. The amount

of fibrils present in a sample can be monitored by the addition on thioflavin T, a fluorescent dye that when excited at 440 nm emits at 485 nm when bound to fibrils (*111, 112*). Monitoring the decay of ThT fluorescence over a time period allows a rate of depolymerisation to be calculated assuming certain factors.

The depolymerisation of β_2m fibrils was monitored using ThT fluorescence. 1mg/ml acidic fibril suspension (20µl) was added to one of six different ThT containing buffers. These buffers were:

- Low pH, low salt (reaction composition: 8.4 µM fibrillar β_2m, 9 µM ThT, 22.5 mM sodium citrate, 22.5 mM KCl, 11.25 mM HEPES, pH 2.5)
- Low pH, high salt (reaction composition: 8.4 µM fibrillar β_2m, 9 µM ThT, 540 mM NaCl, 180 mM $CaCl_2$, 90 mM Tris-HCl, 0.09% NaN_3, pH 2.5)
- Neutral pH, low salt (reaction composition: 8.4 µM fibrillar β_2m, 9 µM ThT, 90 mM Tris, 45 mM KCl, pH 7.4)
- Neutral pH, high salt (reaction composition: 8.4 µM fibrillar β_2m, 9 µM ThT, 540 mM NaCl, 180 mM $CaCl_2$, 90 mM Tris-HCl, 0.09% NaN_3, pH 7.4)
- Neutral pH, calcium (reaction composition: 8.4 µM fibrillar β_2m, 9 µM ThT, 180 mM $CaCl_2$, 90 mM Tris-HCl, pH 7.4)
- Neutral pH, SAP, calcium (reaction composition: 8.4 µM fibrillar β_2m, 9 µM ThT, 35 µM SAP, 180 mM $CaCl_2$, 90 mM Tris-HCl, pH 7.4)

The ThT fluorescence (excitation = 440 nm, emission = 485 nm) was then monitored on a Fluostar optima 96 well fluorimeter (BMG Labtech) over a time course of 24 hours recording every 600 seconds with 300 seconds of orbital shaking after each measurement.

Samples were made in triplicate and the mean was taken. Controls of buffer alone and buffer with soluble β_2m were used for each experiment. Measurements were taken at 30˚C.

Immediately after the fluorescence experiment the samples were frozen to -18˚C to stop any further depolymerisation. Subsequently the samples were unfrozen and negative stain transmission electron microscopy was used to determine the morphology of any remaining material in the sample. The sample (5 µl) was loaded onto a 200 mesh formvar-carbon coated copper grid for 30 seconds. The suspension was then blotted off with absorbent paper and 5µl 2% uranyl acetate put on grid for 10 seconds. Grids were inspected with a transmission electron microscope operated at 120 kV (Hitachi).

2.2.5 Fibril depolymerisation with different concentrations of soluble protein

During the study of SAP binding to fibrils under neutral conditions, β_2m fibrils are pelleted by centrifugation. During these studies it was observed that the control pellets of β_2m, which contained no SAP, did not quickly depolymerise into soluble species. It was hypothesised that any depolymerisation that occurred would have led to extremely high local concentrations of soluble β_2m; this perhaps caused a shift in equilibrium between soluble and fibrillar β_2m so that the high concentration of soluble β_2m forced the fibrillar β_2m to remain as fibrils. To investigate this ThT monitored fibril depolymerisation experiments were run in the presence of increasing amounts of soluble β_2m. The experiments were also repeated with bovine serum albumin (BSA), chosen as a generic protein with no known interaction with β_2m, to determine if any effect was unique to β_2m being in the buffer.

The depolymerisation of β_2m fibrils at neutral pH was monitored using ThT fluorescence. Acidic fibril suspension (20µl of 59 µM) was added to a ThT containing buffer. These buffers were:

- Soluble β_2m (reaction composition: 5.9 µM fibrillar β_2m, 0-12 mg/ml soluble β_2m, 50 µM ThT, 25 mM sodium citrate, 25 mM KCl, 5 mM HEPES, 100 mM Tris-HCl, pH 7.4)
- Soluble BSA (reaction composition: 5.9 µM fibrillar β_2m, 0-12 mg/ml soluble BSA, 50 µM ThT, 25 mM sodium citrate, 25 mM KCl, 5 mM HEPES, 100 mM Tris-HCl, pH 7.4)

The ThT fluorescence (excitation = 440 nm, emission = 485 nm) was then monitored on a Fluostar Optima 96 well fluorimeter (BMG Labtech) over a time course of 24 hours recording every 600 seconds with 30 seconds of double orbital 600 rpm shaking before each measurement. The plates were covered with an adhesive plate cover to prevent loss of volume through agitation or evaporation. Samples were made in triplicate and the mean was taken. Controls of buffer alone and buffer with soluble β_2m were used for each experiment. Measurements were acquired at 30˚C.

After the depolymerisation experiments the trays were quick frozen in a dry ice/ethanol ice bath at -72˚C to halt depolymerisation and then stored at -18˚C. The 12 mg/ml β_2m and BSA samples then underwent negative stain transmission electron microscopy. The samples were defrosted and 5 µl of sample placed on a 200 mesh formvar coated copper grid. After 30 seconds the excess sample was removed with absorbent paper. Distilled water (5 µl) was placed on the grid to remove soluble protein. After 10 seconds the distilled water was removed with absorbent paper. Uranyl acetate 2% stain (5 µl) was

placed on the grid; after 10 seconds excess was removed with absorbent paper. Grids were allowed to air dry and inspected with a transmission electron microscope operated at 120 kV (Hitachi).

2.2.6 Fibril depolymerisation with molecular crowding agent

The results from the fibril depolymerisation in the presence of soluble β_2m and soluble BSA show that thioflavin T fluorescence increases in both the experiments. The increase in fluorescence did not agree with our hypothesis that the β_2m was being kept in a fibrillar state through equilibrium with the high concentrations of soluble β_2m. A possible explanation for this result was through molecular crowding. To investigate whether this was the case we undertook fibril depolymerisation experiments in the presence of the molecular crowding agent Ficoll 70, an inert extended polysaccharide. The depolymerisation of β_2m fibrils at neutral pH was monitored using ThT fluorescence. Acidic fibril suspension (20µl of 59 µM) was added to a ThT containing buffer:

- Ficoll 70 (reaction composition: 5.9 µM fibrillar β_2m, 0-300 mg/ml Ficoll 70, 50 µM ThT, 25 mM sodium citrate, 25 mM KCl, 5 mM HEPES, 100 mM Tris-HCl, pH 7.4)

The ThT fluorescence (excitation = 440 nm, emission = 485 nm) was then monitored on a fluostar optima 96 well fluorimeter (BMG Labtech) over a time course of 24 hours recording every 600 seconds with 30 seconds of double orbital 600 rpm shaking before each measurement. The plates were covered with an adhesive plate cover; to prevent loss of volume through agitation or evaporation. Samples were made in triplicate and the mean was taken. Controls of buffer alone and buffer with soluble β_2m were used for each experiment. Measurements were acquired at 30˚C.

2.3 Results

2.3.1 Expression and purification of soluble beta-2 microglobulin

β_2m was successfully expressed in *E.coli* as shown by SDS-PAGE of pre-induction and post-induction *E.coli* samples (Figure 15A). Inclusion bodies were washed of all soluble protein (Figure 15B). Solubilisation of inclusion bodies resulted in approximately 200 mg of protein per litre growth of *E.coli* when grown in Luria broth and 100 mg of protein when grown in minimal media with ^{13}C and ^{15}N isotopically enriched substrates; refolding and concentration of the solubilised β_2m results in ~95% of the protein being retained. Size exclusion chromatography (SEC) of the refolded protein results in 5 distinct peaks (Figure 15C) of which 4 are β_2m (determined by SDS PAGE) and the fifth is residual DNA and the refold buffer components (determined by absorbance at 260 nm and comparison with SEC of refold buffer alone). Peak D is the monomeric form as determined by comparison with SEC of known protein standards. Around 50% of the protein is eluted in peak D. Total yield of monomeric β_2m from solubilised inclusion bodies is typically 50% per preparation.

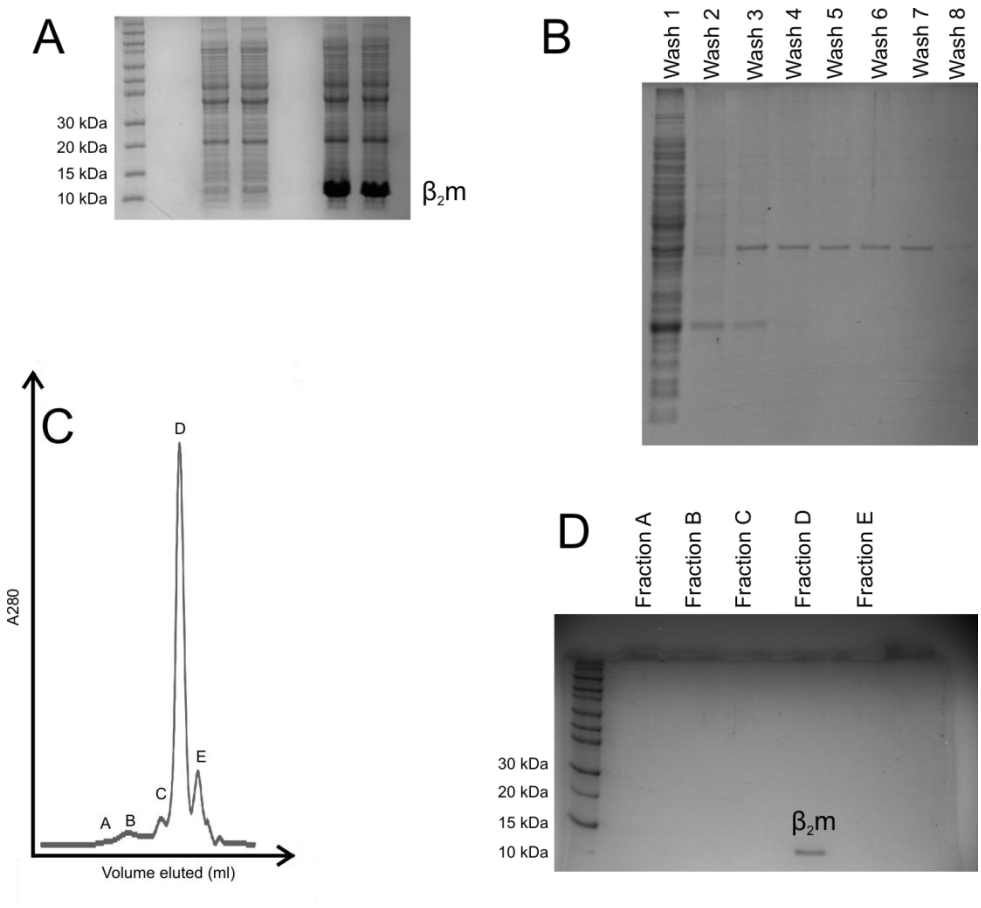

Figure 15 Assay results from key points in β_2m expression and purification
A) SDS PAGE gel of *E.coli* pre and post induction with IPTG. A large protein band corresponding to the molecular weight of β_2m is clearly present in the post induction sample which was not previously there. **B)** SDS PAGE of supernatants from the inclusion body washes. The protein bands can be seen to get less intense after each wash as the soluble proteins are removed from the inclusion bodies. **C)** Plot of OD_{280} from SEC, 5 main peaks are present; A-C correspond to multimers of β_2m while D is the monomeric version. E is residual DNA and refold buffer components. **D)** SDS PAGE gel of peaks from SEC showing purity of final monomeric product.

2.3.2 Fibrillogenesis of beta-2 microglobulin

Fibrils were formed *in vitro* under acidic conditions for analysis as described in section 2.2.2. The incubation of a solution of 42 μM β_2m in low salt/low pH conditions results in the appearance of insoluble material at around 24 hours. Within a week these aggregates had reached a size where they would quickly settle to the bottom of the reaction tube if shaking was stopped. When this suspension was tested with Congo red dye, the dye exhibited the characteristic red shift that occurs on binding to fibrillar material (Figure 16A). On testing with ThT, the dye emitted strongly at 485 nm when excited at 440 nm which is characteristic of the formation of fibrillar material. Together these results indicate that the sample contains fibrillar material and is not an amorphous aggregate as non-fibrillar material does not cause ThT to emit significantly at 485 nm (Figure 16B) and does not cause a red shift when Congo Red binds.

In the ThT monitored experiment, fluorescence started increasing after ~260 minutes suggesting that β_2m rapidly forms structures capable of binding ThT which then slowly convert to fibrils visible to the naked eye in the time frame witnessed in initial non ThT monitored experiments. Maximum fluorescence is observed after ~800 minutes at which point it plateaus (Figure 17).

After the initial fibril preparations all subsequent preparations were seeded with fibrils from the previous preparation. This removed the lag phase and fibrillogenesis went to completion in all cases within 4 hours.

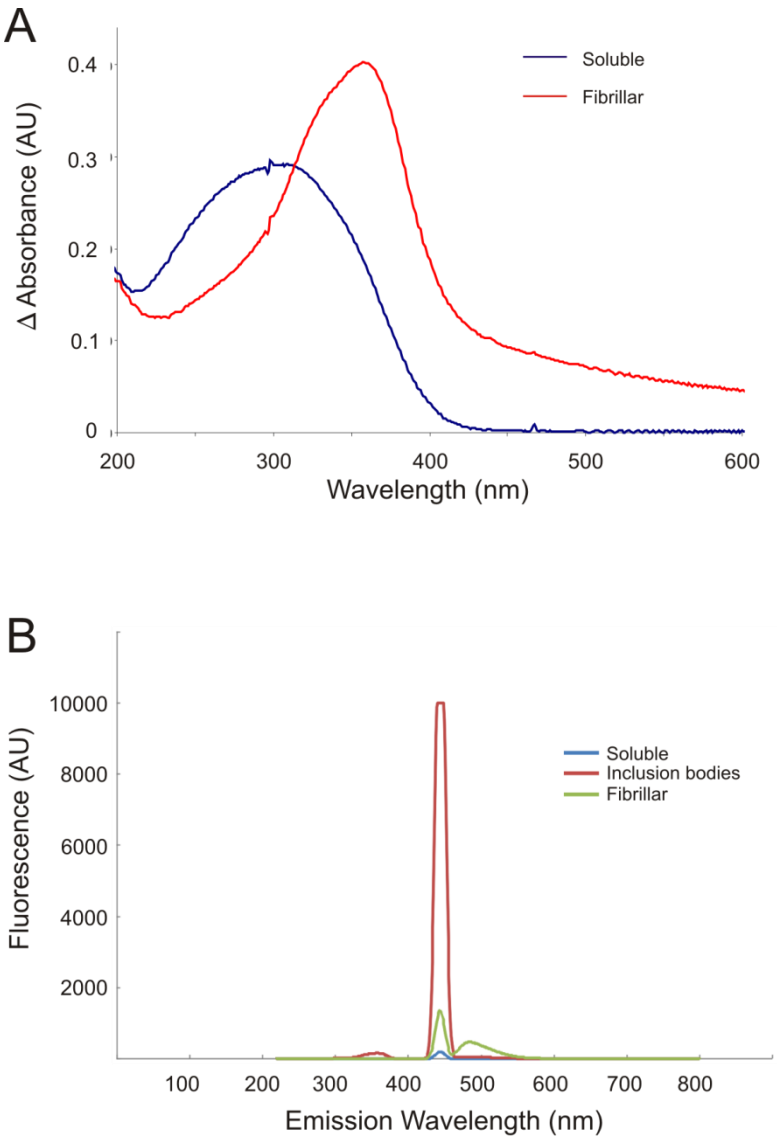

Figure 16 Dye assays for confirmation of fibrils.

A) Change in light absorbance of Congo red in presence of soluble β_2m (blue) and fibrillar β_2m (red). B) Wavelength scan of fluorescence emitted by ThT dye in presence of β_2m in its soluble, inclusion body or fibrillar forms. In presence of fibrils the ThT emits light of 485 nm when excited at 440 nm. The peak shown by all 3 forms at 440 nm is due to the excitation beam being scattered into the fluorimeter's detector. All protein was at a concentration of 1mg/ml as deduced by the BCA protein assay.

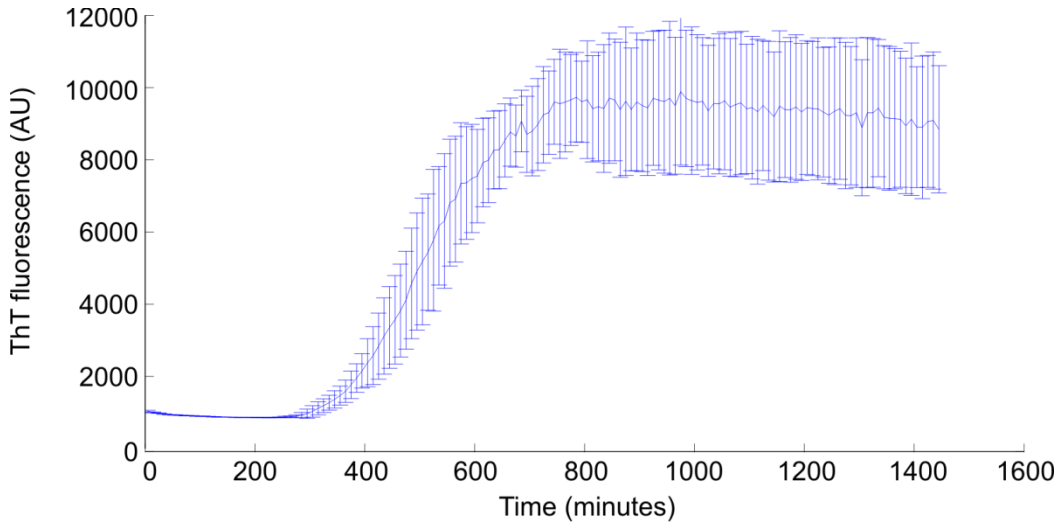

Figure 17 β_2m fibrillogenesis at pH 2.5 monitored over 24 hours with ThT dye
The pH of β_2m was reduced to 2.5 and then ThT fluorescence at 485 nm monitored to follow the formation of fibrillar aggregates. ThT fluorescence starts to increase after 260 minutes and reaches a maximum after ~800 minutes. Error bars are 95% confidence bounds.

Transmission electron micrographs of negatively stained fibrils show a heterogeneous mix of fibril morphologies (Figure 18). Most are less than 20 nm in width, long and straight and range from less than 100 nm in length to over 600 nm (Figure 19B). They consist of multiple protofilaments that are ~5 nm in width and some fibrils clearly display a helical twist with a periodicity of ~100 nm (Figure 19E). None of the fibrils are branched. Structures that match descriptions of protofibrils (circled in red) can be seen in some images (Figure 18) but only make up a small percentage of the total sample. These observations are consistent with the morphologies previously observed by other groups (*60*).

In the high salt, low pH reaction conditions insoluble aggregate formed in the same time frame as the low salt fibrils and tested positive for fibrils with Congo red and ThT.

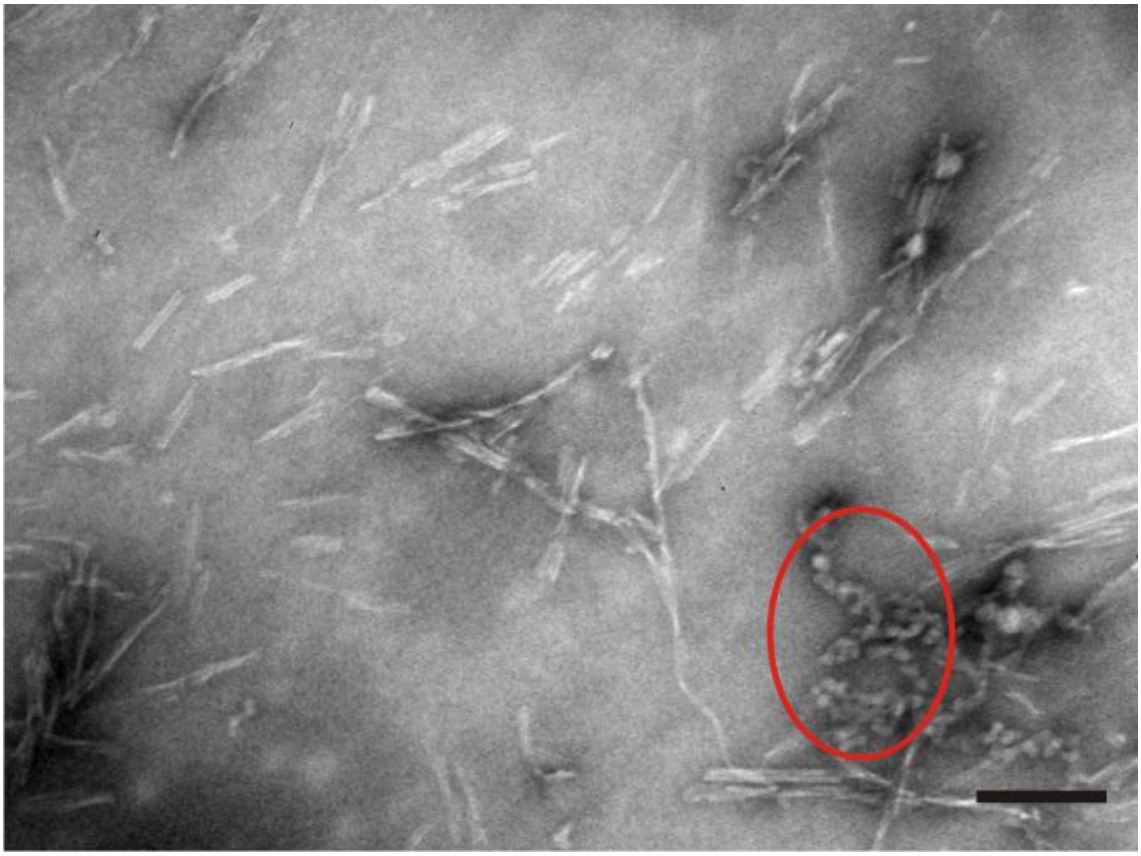

Figure 18 Transmission electron micrograph of low salt fibrils at 60000x magnification
This overview of fibrils produced in 25 mM KCl. A range of morphologies can be seen. Circled in red are what are most probably protofibrils. The bar represents 200 nm.

Transmission electron micrographs of the negatively stained fibrils showed that they appeared to be homogeneous and of a different morphology to the low salt fibrils; however there appears to be a lot more amorphous aggregate. The images of the high salt fibrils are of low quality due the high salt concentration that results in a loss of resolution in the image due to salt crystallising out when the sample is dried on the grid. All the fibrils appear to be highly curved and in the region of 100 nm in length (Figure 20). The width of the fibrils is around 10 nm but because of the low resolution it cannot be discerned whether or not this is one or more protofilaments. A scan of the entire copper grid revealed that the whole grid was covered in these fibrils and that unlike the low salt fibrils they showed a lower propensity to aggregate together.

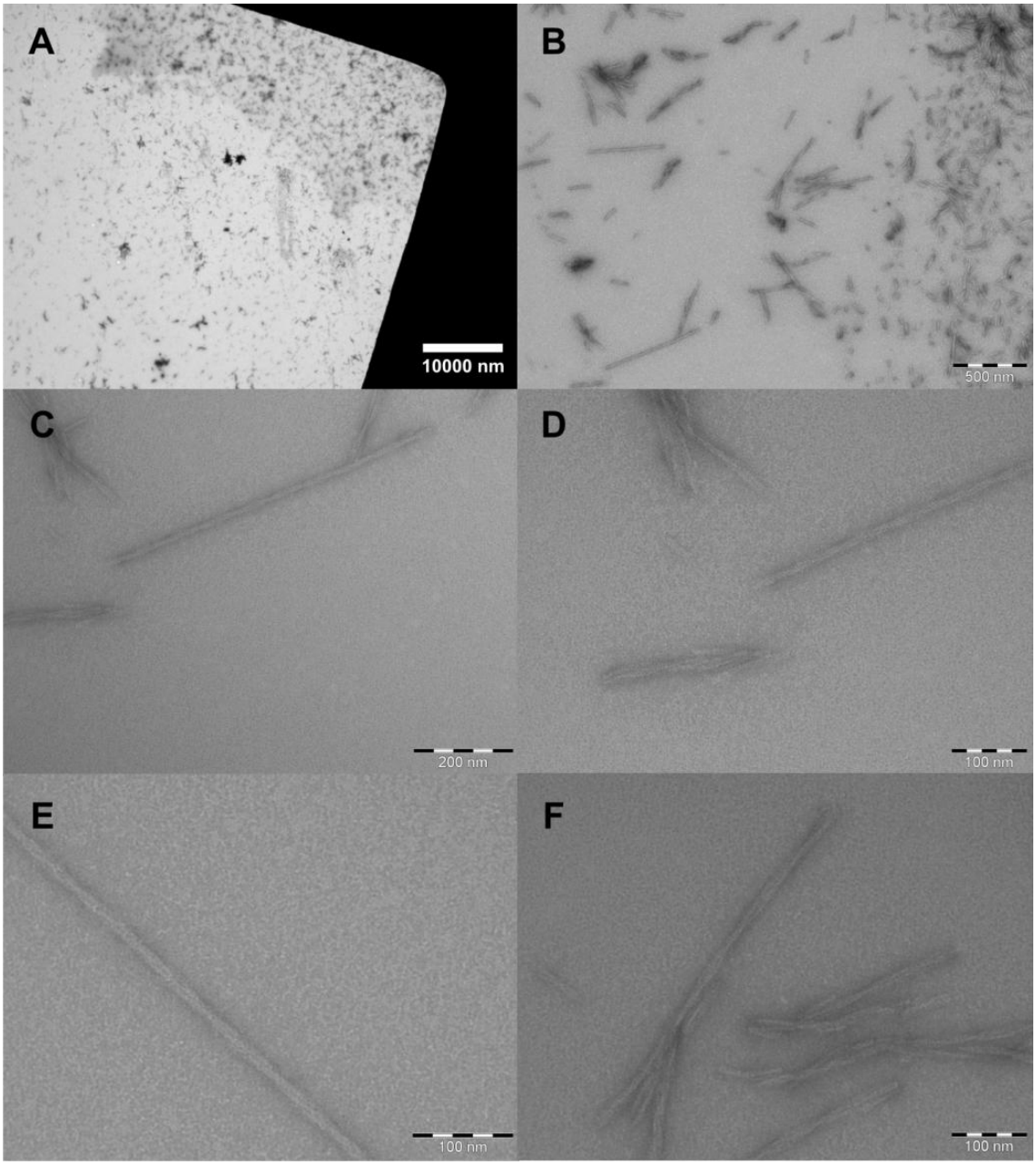

Figure 19 Transmission electron micrographs of fibrils produced under low salt acidic conditions

Selection of micrographs of negatively stained fibrils produced under low salt acidic conditions. A) Shows a section of the grid at 1000 x magnification, a lot of material can be seen; this is representative of the entire grid. B) Is from the same section of the grid at 30000 x magnification, at this magnification the material on the grid can be seen to fibrils, the fibrils are all straight and show great variety in length from <100 nm to >600 nm. C) At 100000 x magnification it becomes possible to see that the fibrils consist of at least 2 protofilaments displaying a helical twist in the main fibril however in the fibril on the centre left it appears as if there are more than 2 protofilaments, this can be seen more clearly in D at 150000 x magnification. E & F show fibrils from other parts of the grid. The fibril in E is at 200000 x magnification and is well resolved. The periodicity of the helical twist can be seen to be approximately 40 nm.

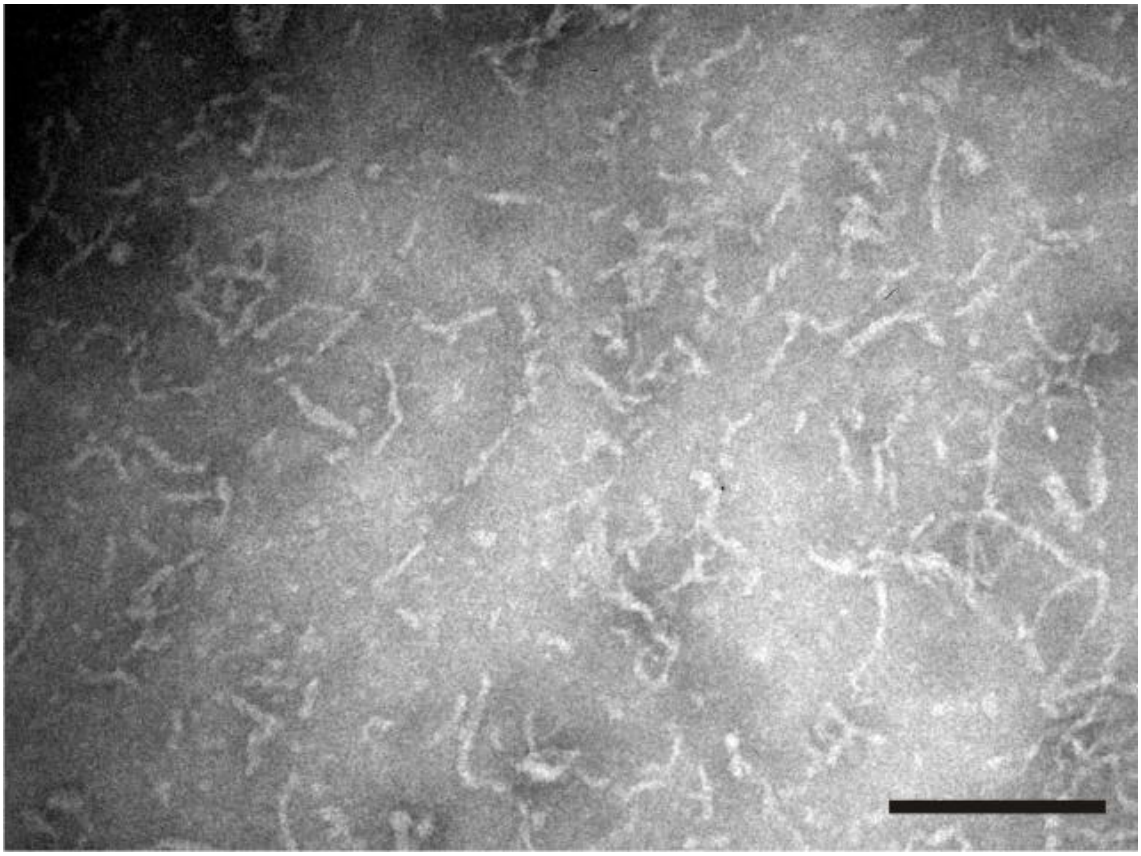

Figure 20 Transmission electron micrograph of fibrils produced under high salt acidic conditions at 100000 x magnification.
Fibrils incubated with 500 mM KCl and show a distinct morphology from the low salt produced fibrils. They can be seen to be highly curved and in the region of 100 nm in length. The bar represents 200 nm.

2.3.3 Pull-down of SAP

To demonstrate that there is an interaction between fibrillar β_2m and SAP and to establish the conditions of optimal binding; a pull-down assay was undertaken as described in section 2.2.4. Centrifugation of a suspension of fibrils and SAP results in 2 fractions, soluble and insoluble. If there is a stable interaction between the two then SAP should be found in the insoluble fraction with the fibrils. The pull-down fractions confirmed that SAP had been pulled down with the fibrils. SAP was present in both pelleted fraction (Figure 21, lane 5) and the supernatant Figure 21, lane 6). More SAP is present in the

pelleted fraction than could be expected from any residual supernatant trapped within the pellet. In the control experiment without SAP, β_2m was present in the pelleted fraction (Figure 21, lane 8). In the control supernatant (Figure 21, lane 9) there is a faint band corresponding to β_2m, this indicates that in the hour of incubation at neutral pH some β_2m transitioned from its fibrillar form to a soluble species. This is in contrast to the SAP sample in which no β_2m was present in the supernatant (Figure 21, lane 6) indicating that no β_2m transitioned from its fibrillar form to a soluble species in the hour of incubation.

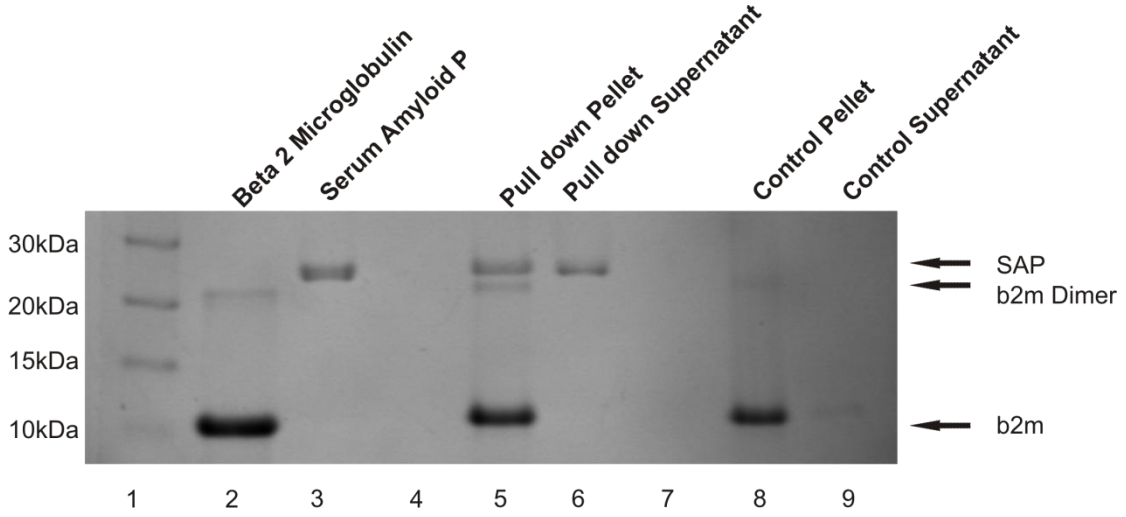

Figure 21 SDS PAGE gel of SAP-fibril pull-down assay

Fibrils were incubated with SAP and then centrifuged to separate the soluble and insoluble fractions. If a strong interaction is present between SAP and fibrillar β_2m then SAP should be pulled down with the fibrils upon centrifugation. Lane 5 contains the pelleted fraction of the pull-down assay. Bands corresponding to both β_2m and SAP can be seen in the lane. Lane 6 contains the supernatant from the pull-down; SAP is present but no β_2m. Lane 8 is the pellet from the control experiment in which SAP was not present in the buffer, it contains β_2m as expected. Lane 9 is the supernatant from the control experiment it also contains a very faint band of β_2m which means that some β_2m transitioned from insoluble to soluble in the hour of incubation in neutral buffer. No β_2m is present in lane 6 demonstrating that in the presence of SAP all β_2m remained insoluble during the hour of incubation at neutral pH.

2.3.4 Depolymerisation of fibrillar β_2-microglobulin-Effect of SAP and ionic strength

Depolymerisation assays were run on fibrillar β_2m to determine the effect of SAP and ionic strength on the stability of fibrils at neutral pH. An interaction between SAP and *in vitro* produced fibrillar β_2m was proven with the use of pull-down assays (Figure 21), the second important step was to determine if SAP stabilised these fibrils at neutral pH; which the ThT monitored depolymerisation assays would be able to determine. The presence of salts in NMR samples negatively affects the quality of spectra in a concentration dependent manner, it was therefore also important to determine to what extent the presence of salt was needed in order to stabilise fibrils at neutral pH.

Results from the depolymerisation assays show acid produced fibrils to be highly unstable at neutral pH. ThT fluorescence rapidly decreases from its maximum in an exponential manner when fibrils are first added in all buffer conditions tested, a second slower exponential decay component is also present and the data fit the following equation:

$$\boldsymbol{f(t) = A_1 . e^{-R_1 t} + A_2 . e^{-R_2 t}}$$

where A_1 and A_2 represent the amplitudes of the fast and slow decays respectively and R_1 and R_2 represent the rate constants of the fast and slow delays respectively. Results of fitting these decays are given in Table 4.

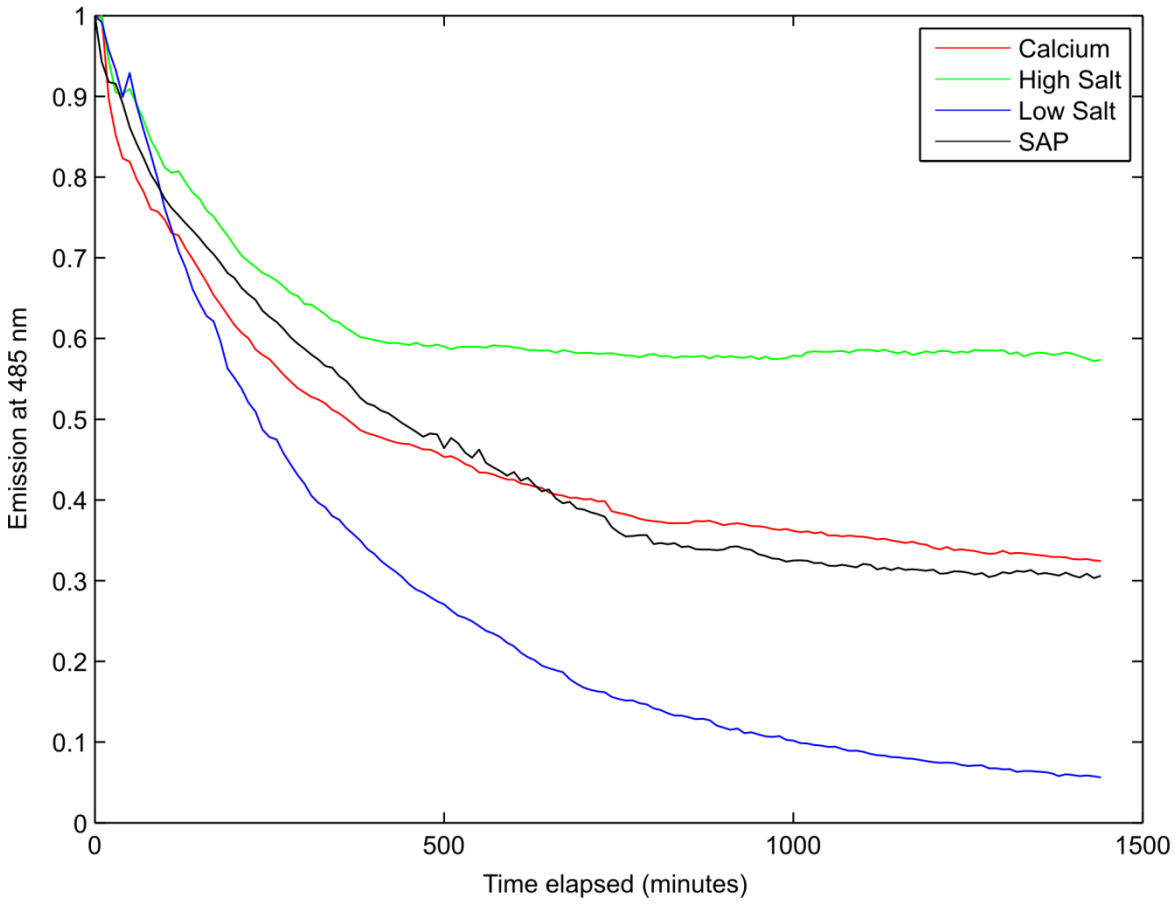

Figure 22 ThT fluorescence in presence of fibrils and SAP
Depolymerisation of fibrils at neutral pH is monitored using ThT fluorescence which is positively correlated with the amount of fibrils present. In low salt buffer (blue) ThT fluorescence decays to 6% of its maximum in 24 hours. It decays rapidly in a bi-exponential manner consisting of a dominating rapid decay followed by a slow decay. In high salt buffer (green) there is a rapid decrease in fluorescence before it plateaus at ~58%. In SAP (black) and calcium (red) buffers fluorescence decays to ~32% of its maximum following a bi-exponential decay.

Depolymerisation under low salt conditions is characterised by a bi-exponential decay whose fast component (R_1= 41.76*10^{-4} min^{-1}) contributes to over 70% of the overall decay of fluorescence. A slower component (R_2= 12.79*10^{-4} min^{-1}) results in the almost complete dissolution of the fibrils during the time course of the experiment. In contrast under high salt conditions, the process appears to be characterised by a bi-exponential decay in which there is a fast component (R_1= 60.26*10^{-4} min^{-1}) similar to the low salt but also an extremely slow rate very near to zero which results in around 60% of the original ThT fluorescence being present after 24 hours incubation at neutral pH. Assuming that the

fibrillar species formed has a similar quantum yield to the initial fibrils, this suggests that under high salt conditions approximately 60% of the fibrils remain at neutral pH.

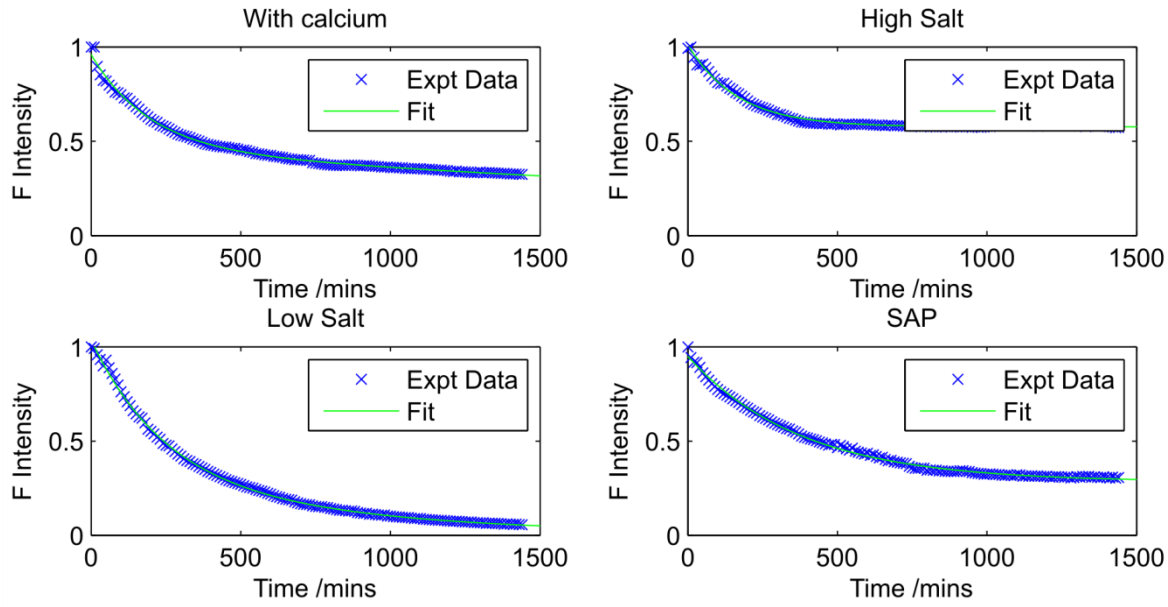

Figure 23 Data fits of ThT fluorescence over 24 hours incubation of β_2m fibrils in low salt, high salt, calcium and SAP buffers at neutral pH
These graphs show the data fits (green) of each of the depolymerisation experiments. This can be modelled as $\boldsymbol{f(t) = A_1.e^{-R_1 t} + A_2.e^{-R_2 t}}$ where *t* is time elapsed, A_1 is the amplitude of the fluorescence decay and R_1 the rate constant of the fluorescence decay.

Depolymerisation in the calcium buffer conditions is characterised by a bi-exponential decay whose fast component (R_1= 51.7*10^{-4} min^{-1}) contributes ~50% to the overall decay of the fluorescence. A slower component (R_2= 2.6*10^{-4} min^{-1}) results in the fluorescence decreasing to ~32% of its maximum over the 24 hour time course of the experiment. Still assuming that the quantum yield of formed fibrils remains the same then this suggests that 32% of the fibrils remain at neutral pH after 24 hours.

In the presence of SAP depolymerisation is characterised by a bi-exponential decay consisting of a fast component (R_1=26.4*10^{-4} min^{-1}) and an extremely slow component of near zero which results in ~32% of fibrils remaining at neutral pH after 24 hours. At this

concentration of SAP and fibrils no significant reduction in rate is seen over the calcium control.

SAMPLE	A_1	A_2	R_1 $(/10^4)$ min^{-1}	R_2 $(/10^4)$ min^{-1}
LOW SALT	0.70	0.33	41.76	12.79
HIGH SALT	0.43	0.57	60.26	~0
CALCIUM	0.49	0.46	51.73	2.57
SAP	0.67	0.28	26.40	~0

Table 4 Amplitudes and rate constants from fibril depolymerisation experiment
A_1 and A_2 are the amplitudes of the fast and slow decays respectively. R_1 and R_2 are the rate constants on the fast and slow decays respectively. Low salt and High salt refer to the depolymerisations carried out in low and high salt buffers respectively. Calcium and SAP refer to the depolymerisations carried out in calcium buffer without and with the presence of SAP respectively.

Negative stain transmission electron microscopy was used to study the morphologies of remaining fibrils following the depolymerisation assay. The negative stain pools around fibrils and into any relief the fibril may have. Electrons cannot transmit through the stain and therefore a negative image is created. TEM images were obtained of the fibrils at the end point of the experiment in order to confirm the presence and determine the morphology of any remaining fibrillar material.

Negative stain TEM of the low salt sample at 24 hours reveals fibrillar like material still present although it is very sparse and hard to find on the grid. Most of the material left of the grid matched the description of protofibrils described by other groups (*113*). These can be seen in Figure 24A which is at 70000 x magnification. The fibril-like material found on the grid was mainly in one area and from visual inspection was estimated to make up only a small percentage on the total material on the grid. At 30000 x magnification (Figure 24B) the filaments appear to be curved and are similar in morphology to those fibrils created under high salt conditions (Figure 20). The filaments surround what appears to be an

extremely large fibril composed of many protofilaments and which looks as though it is 'unravelling' at its ends (Figure 24B). In Figure 24C it can be seen that the filaments vary in length from <100 nm to >500 nm. The negative stain pools around the filaments and is not absorbed by the material. In Figure 24D the filaments are at 100000 x magnification and show no sign of being composed of several protofilaments as with fibrils incubated at acidic pH; as these filaments appear to be breaking off the large fibril in Figure 24B they could be protofilaments.

Negative stain TEM of the high salt sample after 24 hours at neutral pH reveals fibril like material. The grid is well covered with the material (Figure 25A). Most of the material appears to be 100-200 nm in length and <10 nm wide (Figure 25B). The exact morphology of this material is difficult to determine due to the diffuse nature of the negative staining. The high ThT fluorescence levels at the end of the 24 hour incubation period would suggest that this material is able to bind to and cause ThT to emit at 485 nm.

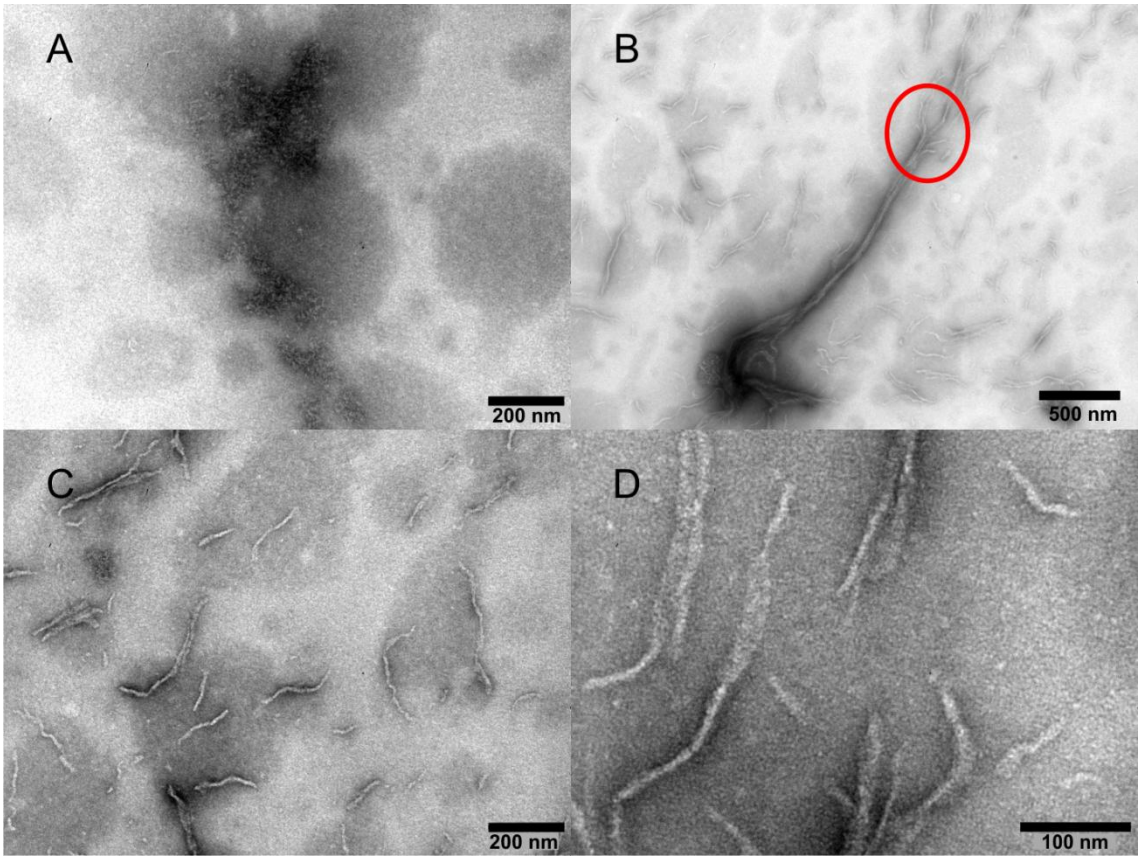

Figure 24 Transmission electron micrographs of β_2m fibrils incubated in low salt neutral pH buffer for 24 hours

These transmission electron micrographs were taken after β_2m fibrils were incubated in low salt, neutral pH buffer for 24 hours. **A** is of protofibrils at 70000 x magnification. Panels B, C and D show fibril like material at 30000, 70000 and 100000 x magnification respectively. A fibril which appears to be 'unravelling' is circled in red.

Negative stain TEM of the calcium only sample at 24 hours reveals abundant fibril like material covering the grid (Figure 25C). This material is of the same form as the high salt neutral pH depolymerisation (Figure 25D); like in the high salt incubation, the ThT fluorescence is still high after 24 hours suggesting that the material is fibril-like and able to bind ThT and cause it to fluoresce at 485 nm.

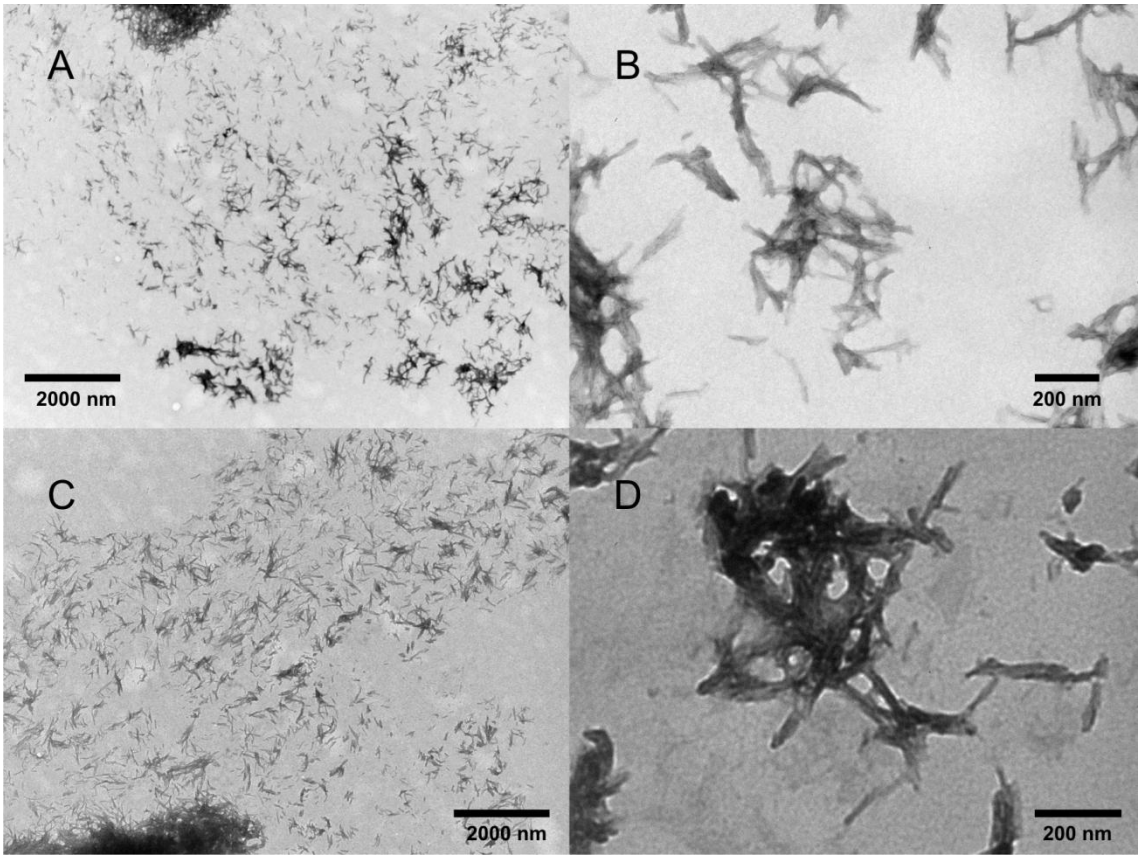

Figure 25 Transmission electron micrographs of β_2m fibrils incubated in high salt or calcium containing neutral pH buffer for 24 hours.
These transmission electron micrographs were taken after β_2m fibrils were incubated in high salt, neutral pH buffer for 24 hours. **A**) This micrograph is at 10000 x magnification and indicates how much material was present after the high salt buffer depolymerisation experiment. The micrograph is representative of the entire grid. **B**) Same as A at 70000 x magnification **C**) Micrograph of calcium incubated fibrils at 10000 x magnification; the micrograph is representative of the entire grid. **D**) Calcium incubated fibrils at 80000 x magnification.

Negative stain TEM of the SAP containing sample at 24 hours gave no usable images due to the high concentration of soluble protein interfering with the staining.

2.3.5 Depolymerisation of fibrillar β_2-microglobulin-Effect of native proteins and molecular crowding agents

The effects of high concentrations of β_2m, BSA and Ficoll 70 on the stability of β_2m fibrils at neutral pH were investigated using the methods described in sections 2.2.5 and 2.2.6. Figure 26 shows the ThT intensity against time results from the incubation of fibrils in increasing concentrations of soluble β_2m. The intensities of ThT emissions in all buffers containing soluble β_2m can be seen to sharply rise towards high maxima within 4 hours before reducing slowly over the next 20 hours to an intensity which is still significantly higher than that at the start of the experiment.

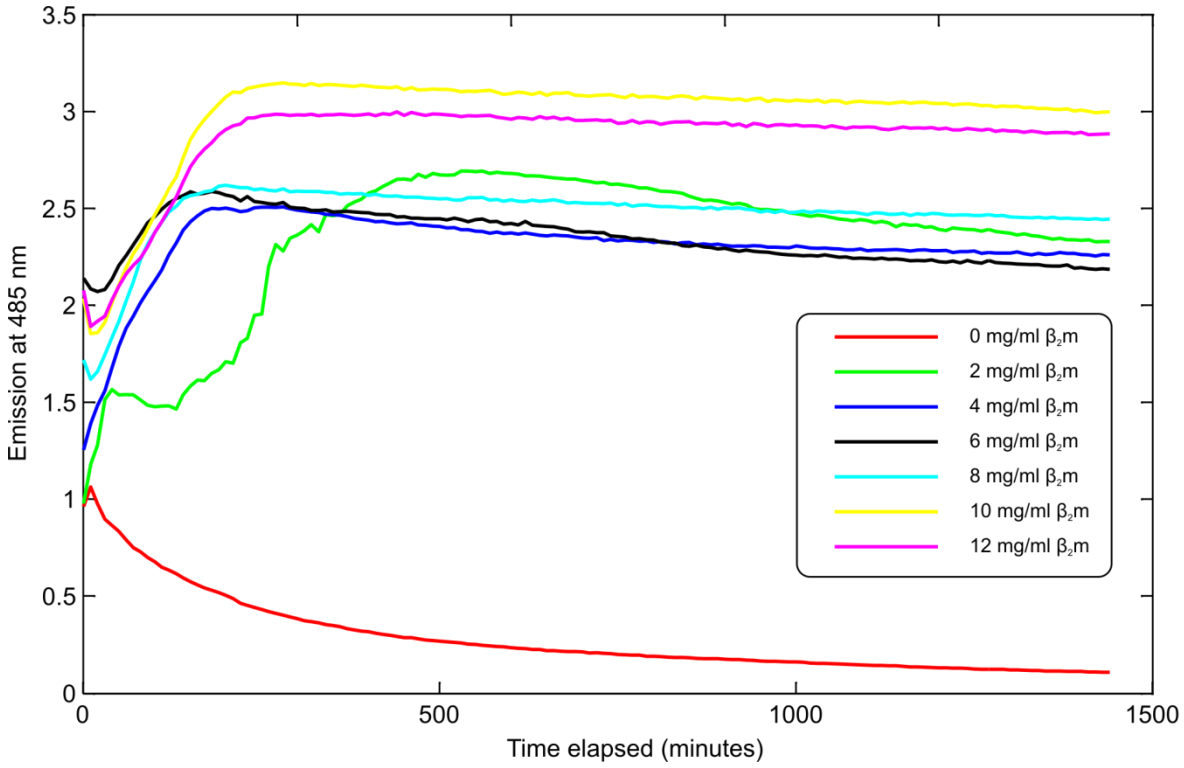

Figure 26 Incubation of β_2m fibrils in free native β_2m at neutral pH followed by ThT fluorescence

Above shows the ThT intensity against time results from the incubation of fibrils in increasing concentrations of soluble β_2m. The data are normalised to the first data point of the 0 mg/ml sample which is treated as an intensity of 1.

The data are normalised to the first data point of the 0 mg/ml sample which is treated as an intensity of 1. We can model this behaviour as the sum of two exponentials, the first charactering the initial build-up of fluorescence intensity, the second the decay, using the following relationship:

$$\boldsymbol{f(t) = A_1.(1 - e^{-R_1 t}) + A_2.e^{-R_2 t}}$$

where *t* is time elapsed, A_1 is the amplitude of the first component, R_1 the rate constant of the first component (corresponding to the build-up of fluorescence intensity), A_2 the amplitude of the second component and R_2 the rate constant of the second component (characterising the subsequent decay of the fluorescence intensity).

As can be seen a good agreement is observed between the model and experiments data (See Figure 27 Data fits of ThT fluorescence over 24 hours incubation of β_2m fibrils in native β_2m at neutral pH) and can be seen to fit well in all cases except the 2 mg/ml β_2m sample which displayed an atypical evolution of ThT fluorescence relative to the other free β_2m buffered samples. Analysis of the amplitudes and rates of the two components as a function of free β_2m is shown in Figure 31. This reveals that there is an upward trend in the amplitudes of both components with increasing soluble β_2m concentration. The amplitude of the first component in the 6 mg/ml is an outlier compared with the trend of the other experiments; this could be due to experimental error, such as more fibrils being present however the experiments were performed in triplicate and the mean taken. Both rate constants stay relatively constant and do not show any free β_2m concentration dependent upwards or downwards trends. Experimentally these results indicate that there is a process causing a fast increase in ThT fluorescence, the amplitude of which is dependent on the amount of free β_2m present; however the rate of this process is not dependent on the

concentration of free β_2m present. A second process is causing a slow decrease in ThT fluorescence the amplitude of which is dependent on free β_2m concentration but the rate of which is not.

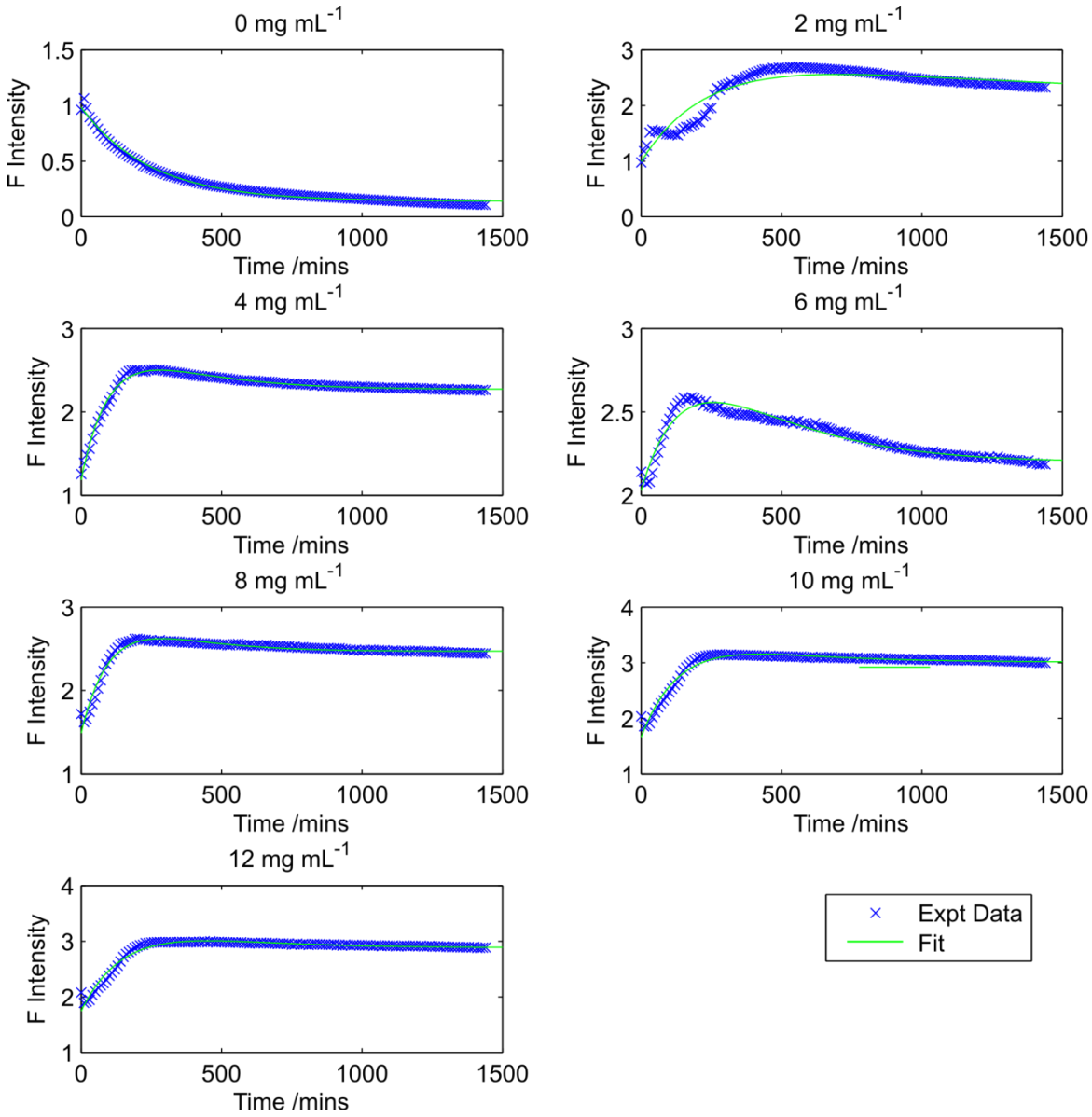

Figure 27 Data fits of ThT fluorescence over 24 hours incubation of β_2m fibrils in native β_2m at neutral pH

These graphs show the data fits (green) of each of the depolymerisation experiments. This can be modelled as $f(t) = A_1.(1 - e^{-R_1 t}) + A_2.e^{-R_2 t}$ where t is time elapsed, A_1 is the amplitude of build-up of fluorescence intensity, R_1 the rate constant of the build up of fluorescence intensity, A_2 the amplitude of the decay of fluorescence intensity and R_2 the rate constant of the decay of fluorescence intensity.

The results from this experiment are not as expected, we hypothesised that the addition of high concentrations of free β_2m would slow or halt the depolymerisation of fibrillar β_2m due to a shift in equilibrium between the two forms. Instead, assuming that ThT fluorescence is positively correlated with the amount of fibrillar material present, there has been an increase in the amount of fibrils present in each of the samples containing the free β_2m. It would be possible for this to happen as the high concentration of free β_2m along with the presence of existing fibrils could provide a fibrillogenic environment in which the free β_2m gets added to the fibrils.

TEM images of the fibrils incubated in 12 mg/ml β_2m for 24 hours do not rule out the possibility that the free β_2m was converted to fibrillar β_2m. The grids were extensively covered in stainable material (Figure 28A) which could be stain absorbing fibril-like material (Figure 28C & D) approximately 100-200 nm in length and less than 10 nm in diameter. It can be said with certainty however that no typical, long straight fibril types were found.

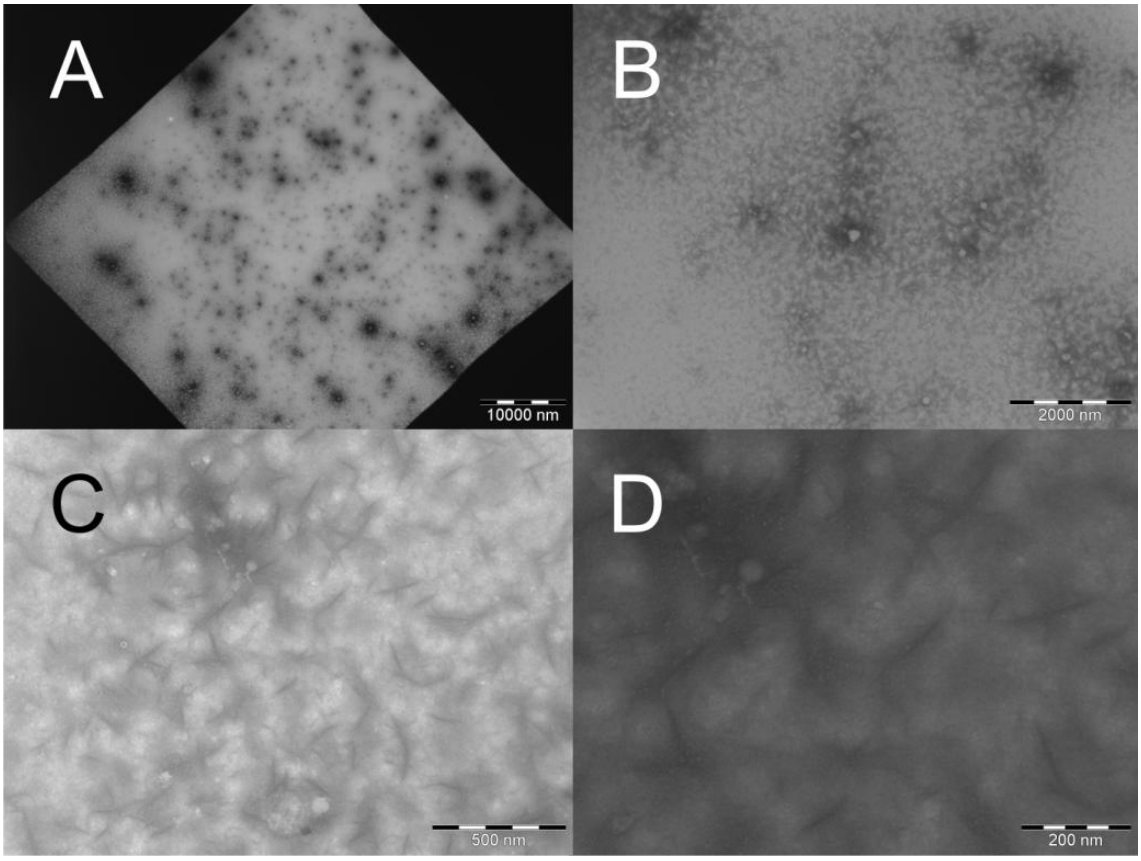

Figure 28 Transmission electron micrographs of fibril sample incubated in neutral pH native β_2m for 24 hours

TEM images of the fibrils incubated in 12 mg/ml β_2m for 24 hours show the grids were extensively covered in stainable material. A) Overview of 1 grid compartment at 1000 x magnification. This compartment is representative of all compartments on the grid. B) Grid at 10000 x magnification. C) Grid at 50000 x magnification. D) Grid at 100000 x magnification.

As β_2m persisting in its fibrillar form when in fibrils was hypothesised to be due to fibrillar and free β_2m being in equilibrium a control set of experiments was used under exactly the same conditions but using soluble BSA in the buffer instead of free β_2m. Figure 29 shows the variation of ThT intensity against time results from the incubation of fibrils in increasing concentrations of soluble BSA. The intensities of ThT emissions in all buffers containing soluble BSA can be seen to sharply rise towards high maxima within 4 hours before reducing slowly over the next 20 hours to a still high intensity; as was the case with the β_2m experiment. The rate of the exponential growth in the 8 mg/ml sample was

atypically fast and seems to be an outlier relative to the other results. The results of the individual experiments that make up the mean had a wide range and so this may have contributed to the atypical result.

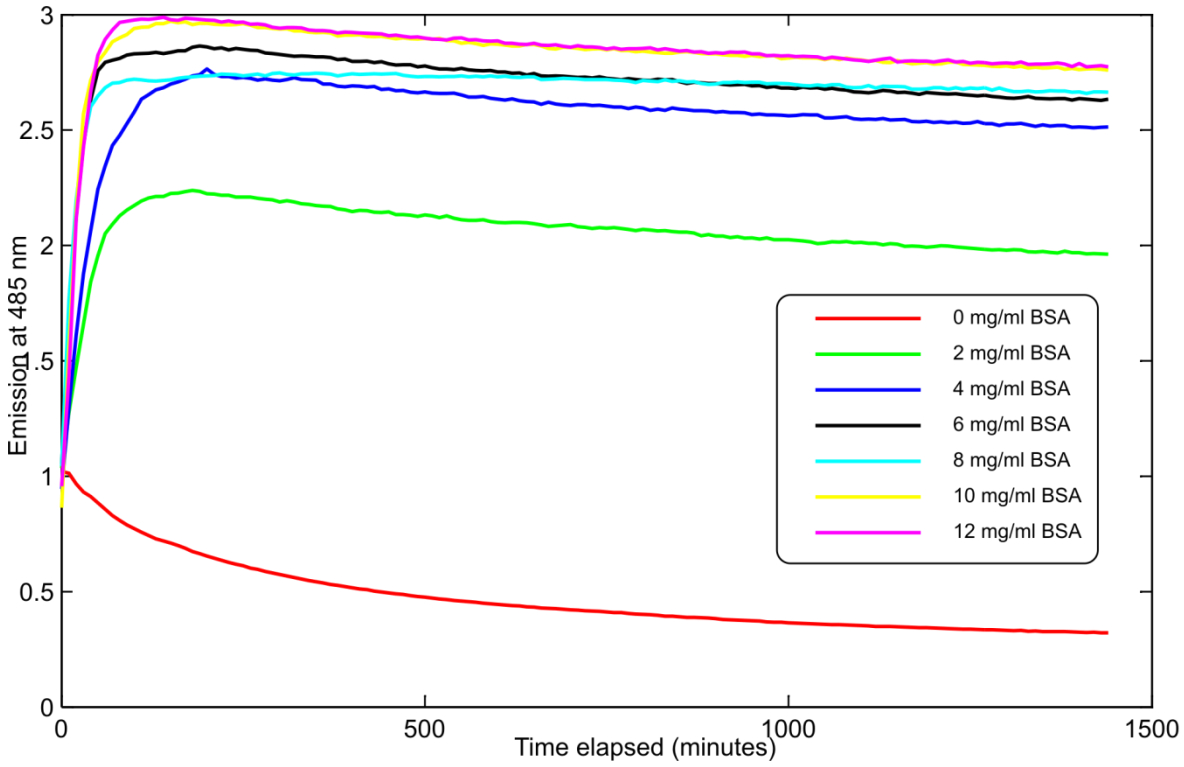

Figure 29 Incubation of β_2m fibrils in native bovine serum albumin at neutral pH followed by ThT fluorescence

Above shows the ThT intensity against time results from the incubation of fibrils in increasing concentrations of soluble BSA. The data are normalised to the first data point of the 0 mg/ml sample which is treated as an intensity of 1.

The data are normalised to the first data point of the 0 mg/ml sample which is treated as an intensity of 1. We can model this behaviour as the sum of two exponentials, the first charactering the initial build-up of fluorescence intensity, the second the decay, using the following relationship:

$$\boldsymbol{f(t) = A_1.(1 - e^{-R_1 t}) + A_2.e^{-R_2 t}}$$

Where *t* is time elapsed, A_1 is the amplitude of the first component, R_1 the rate constant of the first component (corresponding to the build-up of fluorescence intensity), A_2 the amplitude of the second component and R_2 the rate constant of the second component (characterising the subsequent decay of the fluorescence intensity).

The data fits can be seen in Figure 30 and the model fits the experimental data well. Comparison of the amplitudes and rate constants for the different conditions can be found in Figure 31. The amplitudes of the build up of fluorescence intensity show a positive correlation with the concentration of BSA, whilst the amplitudes of the decay of fluorescence intensity show a negative correlation with the concentration of BSA. The rate constants characterising both the build-up and decay of fluorescence intensity increase until a BSA concentration of 8 mg/mL above which they are observed to descrease slightly. It is important to note at this point that the rate constants for the 8 mg/ml experiment are extremely fast relative to the rest of the experiments and if it were discounted a positive correlation between the first components' rate constants and BSA concentration would be seen up until the 12 mg/ml experiment where a slight decrease in rate occurs. The second components' rate constants would, to the most degree, stay constant relative to each other.

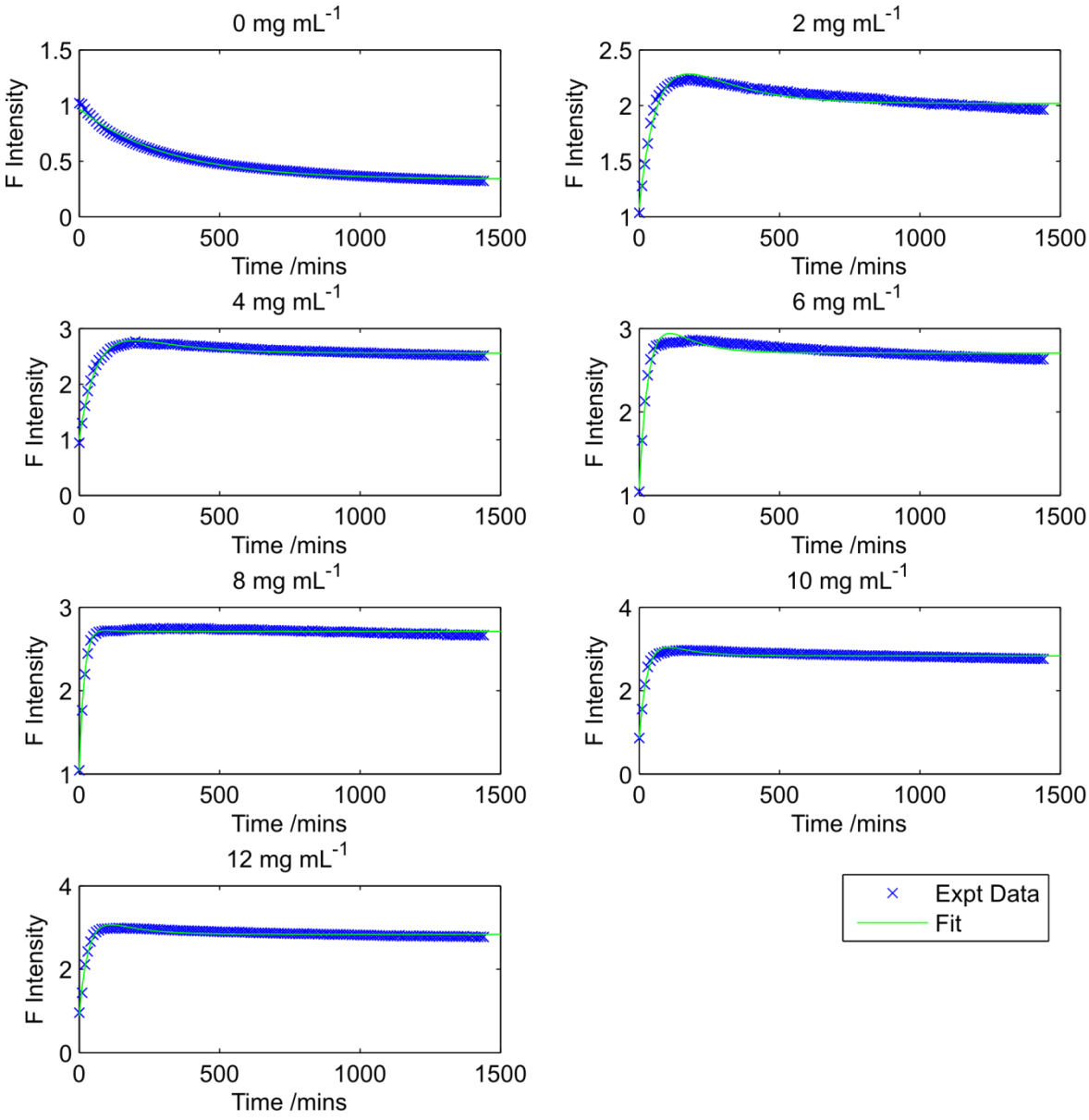

Figure 30 Data fits of ThT fluorescence over 24 hours incubation of β_2m fibrils in native BSA at neutral pH

These graphs show the data fits (green) of each of the depolymerisation experiments. This can be modelled as $f(\boldsymbol{t}) = \boldsymbol{A_1}.(\boldsymbol{1} - \boldsymbol{e^{-R_1 t}}) + \boldsymbol{A_2}.\boldsymbol{e^{-R_2 t}}$ where t is time elapsed, A_1 is the amplitude of build-up of fluorescence intensity, R_1 the rate constant of the build up of fluorescence intensity, A_2 the amplitude of the decay of fluorescence intensity and R_2 the rate constant of the decay of fluorescence intensity.

Experimentally this indicates that there is a process causing an increase in ThT fluorescence whose amplitude and rate are dependent on the concentration of soluble BSA present. There is a second process causing a decrease in ThT fluorescence whose amplitude and rate are not dependent on BSA concentration.

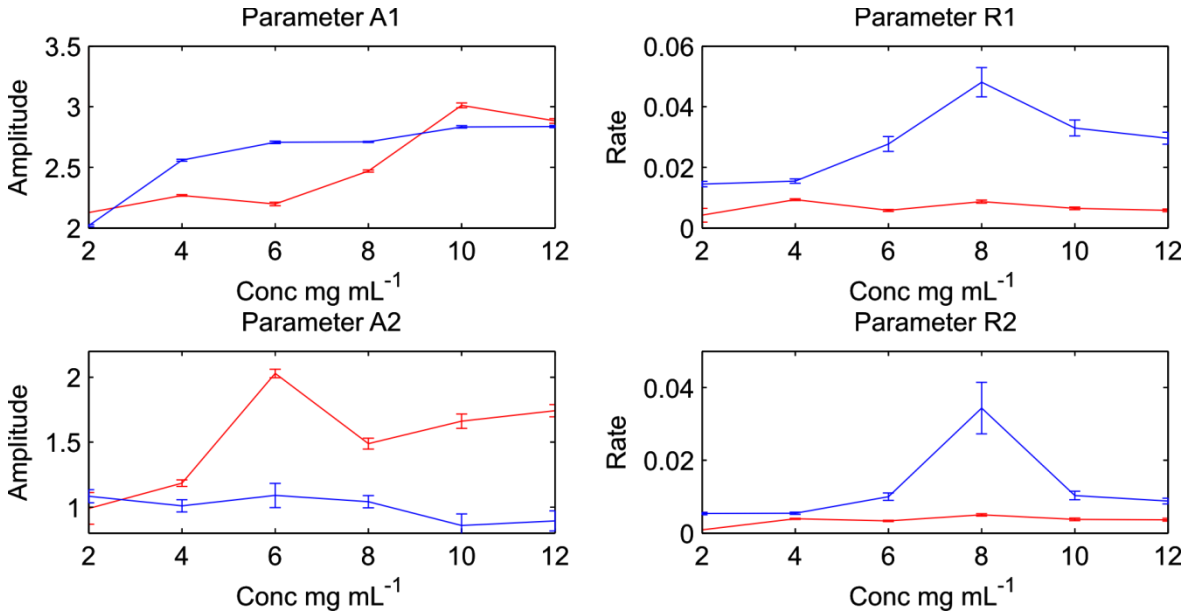

Figure 31 Comparison of amplitudes and rate constants of ThT fluorescence evolution during fibril incubation in different concentrations of free β_2m (red) or BSA (blue)
Parameter A1 and A2 refer to the amplitudes of the exponential growth and decay of ThT fluorescence respectively. Parameter R1 and R2 refer to the rate constants of the exponential growth and decay respectively.

The results from this experiment are not as expected. BSA is not known to be fibrillogenic and so an increase in ThT fluorescence due to BSA forming fibrils, although not impossible, is not very likely with β_2m fibril seeds and no method of partial unfolding. BSA has been shown to promote fibrillogenesis of α-synuclein when used as a molecular crowding agent (*108*) and it has been demonstrated that β_2m can form fibrils at neutral pH in the presence of β_2m fibril seeds and other physiological factors (*45*); so molecular crowding could cause fibril depolymerisation to slow and this was investigated and will be described in this section; however it should not be able to cause ThT fluorescence to

increase through causing more fibrillar material to be present without the addition of more β_2m. This leaves the possibility that the BSA is causing the conversion of fibrillar β_2m into a form that can either bind more ThT through an increase in area accessible to ThT or conversion into a form where ThT exhibits a higher quantum yield.

The TEM data reveal a grid covered in protofibril like material and the image in Figure 32A taken at 30000 x magnification is representative of the entire grid. This image contains an abundance of protofibril like material and also some fibril-like material. The fibril-like material appear as in Figure 32B (30000 x magnification) & C (50000 x magnification) and are typically between 50 and 100 nm in diameter and vary greatly in length from less than 100 nm to greater than 500 nm. The diameter along the length of the fibril-like fibres shows variability in a lot of cases which could be an indication of less order than typically. The fibril-like material therefore shows morphological differences to both fibrils at acidic pH (Figure 19) and fibril-like material remaining after 24 hours of incubation at neutral pH (Figure 24) The material does not absorb negative stain as is the case with the β_2m fibrils and fibril-like fibres that appear in the high salt incubation (Figure 25) and free β_2m incubation (Figure 28) samples. This type of fibril-like fibre has not appeared in any of the previous images taken of fibrils under any of the tested conditions.

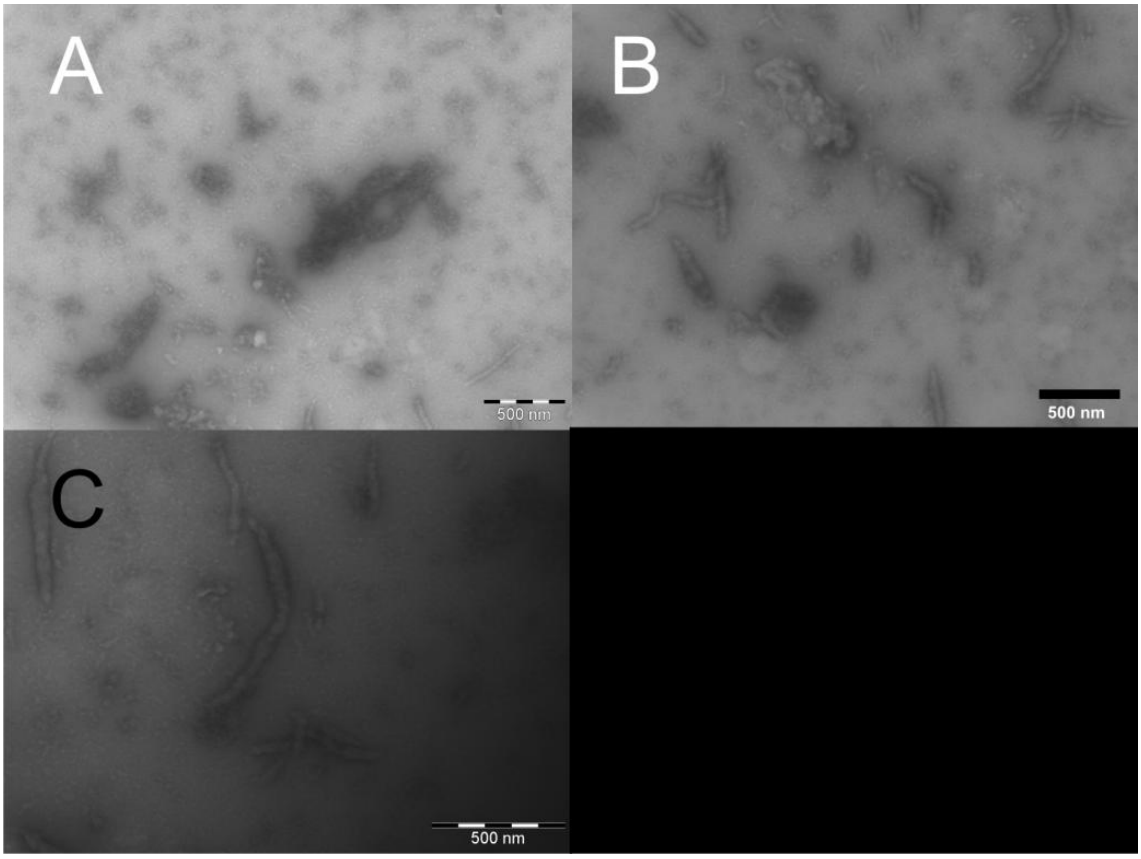

Figure 32 Transmission electron micrograph of fibril sample incubated in neutral pH Bovine Serum Albumin for 24 hours

The TEM data reveal a grid covered in protofibril like material. A) 30000 x magnification, this image is representative of the entire grid. B) Fibril-like material at 30000 x magnification. C) Fibril-like material at 50000 x magnification.

The incubation of β_2m fibrils in BSA unexpectedly resulted in no net decrease in ThT fluorescence over 24 hours. This led to the speculation that a possible molecular crowding effect could be causing the persistence of ThT binding material. In order to investigate this we performed the fibril depolymerisation in the presence of the molecular crowding agent Ficoll 70, an extended polysaccharide chain used extensively for molecular crowding purposes (*108, 114*). Figure 33 shows the ThT intensity against time results from the incubation of fibrils in increasing concentrations of Ficoll 70. In the samples containing 150 mg/ml of Ficoll 70 or less, the ThT fluorescence immediately starts to decay in an exponential manner similar to that of the sample containing no Ficoll 70. In the samples containing between 200 and 300 mg/ml of Ficoll 70 there is a slight concentration

dependent delay before the ThT fluorescence reaches its maximum. In these cases this delay is most probably due to the viscosity of the solution slowing down the binding of ThT and the β_2m fibrils as the starting values of ThT fluorescence in the samples are lower than that of the sample containing no Ficoll 70. This lower ThT fluorescence is negatively correlated with the concentration of Ficoll 70; the higher the concentration of Ficoll 70 the lower the initial ThT fluorescence. The ThT measurements at 24 hours are higher in the Ficoll 70 containing samples but these higher values are a normalisation artefact, normalisation of the data to the maximum fluorescence in each separate experiment would have resulted in the final amplitudes being the same. We can model this behaviour as the sum of two exponentials, the first charactering the initial build-up of fluorescence intensity, the second the decay, using the following relationship:

$$\boldsymbol{f(t) = A_1.(1 - e^{-R_1 t}) + A_2.e^{-R_2 t}}$$

Where *t* is time elapsed, A_1 is the amplitude of the first component, R_1 the rate constant of the first component (corresponding to the build-up of fluorescence intensity), A_2 the amplitude of the second component and R_2 the rate constant of the second component (characterising the subsequent decay of the fluorescence intensity).

The data fits can be seen in Figure 34 and they fit the model well. Figure 35 shows the comparison of the amplitudes and rate constants The amplitudes of the experiments show no definite trend; amplitude does increase up until 150 mg/ml of Ficoll 70 but then decreases at higher concentrations. The rate constants also show no definite trend. There is a decrease in rate of depolymerisation at concentrations higher than 150 mg/ml; this could be due to the viscosity of the solution slowing movement of molecules through the solution. If this was due to a molecular crowding effect it would be more likely that an

increasing rate of depolymerisation would be seen throughout the concentrations. The error bars representing the 95% confidence bounds are for both rate constants up to 150 mg/ml. This is because up until and including 150 mg/ml of Ficoll there is very little fluorescence build up at the start of the experiment and so the uncertainty of the fit is higher for these experiments. The error bars for the rate of the fluorescence decay are high because the two rates are correlated.

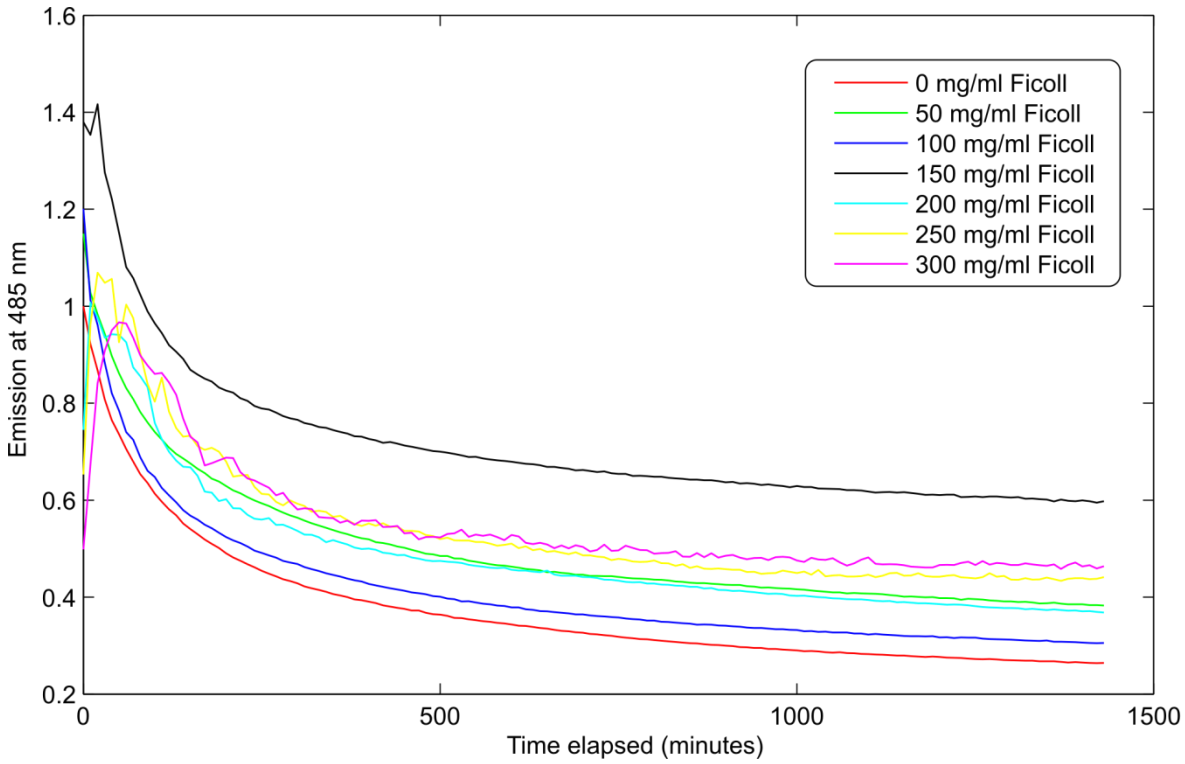

Figure 33 Incubation of β_2m fibrils in Ficoll 70 at neutral pH followed by ThT fluorescence
Above shows the ThT intensity against time results from the incubation of fibrils in increasing concentrations of Ficoll 70. The data are normalised to the first data point of the 0 mg/ml sample which is treated as an intensity of 1.

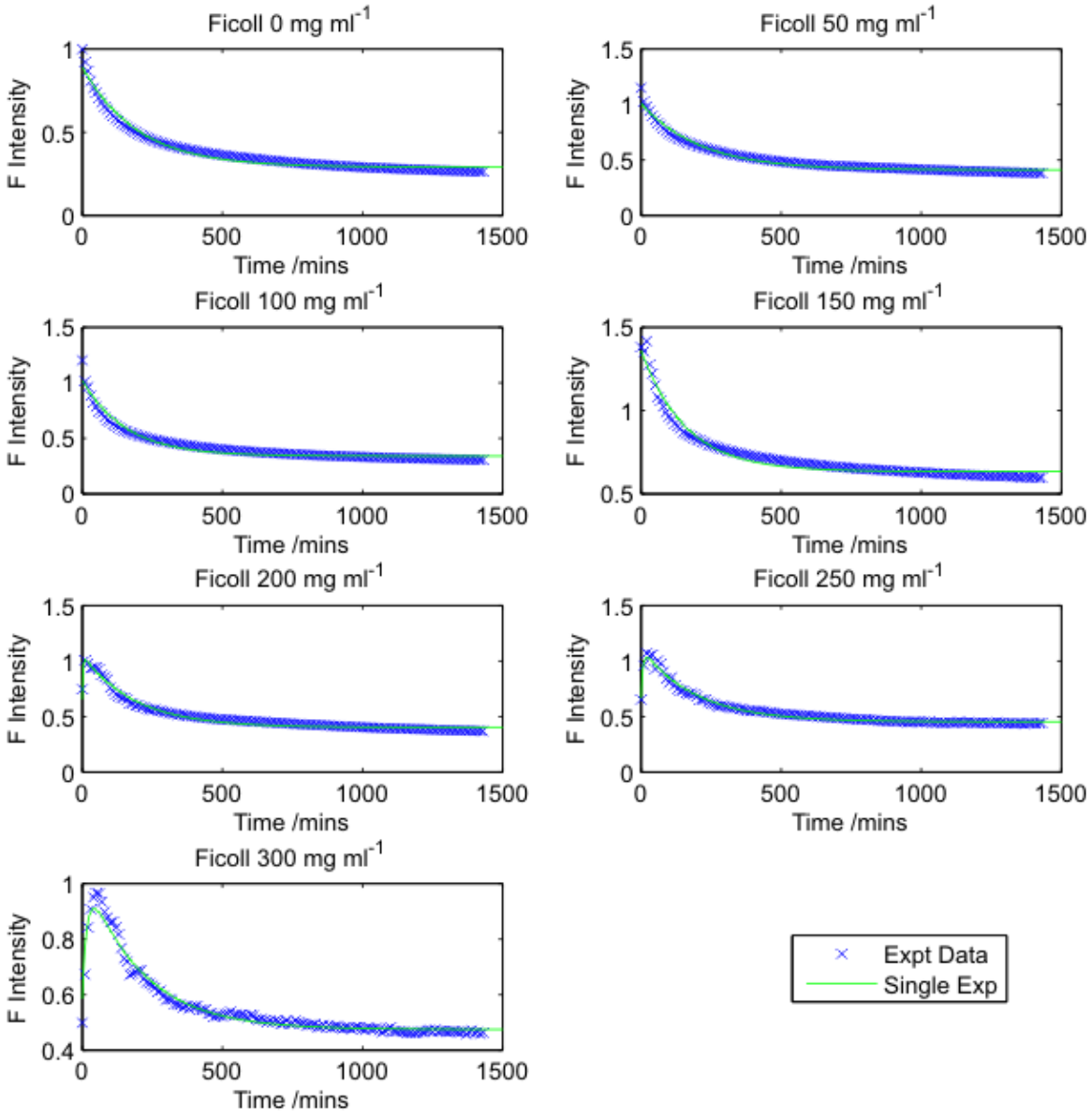

Figure 34 Data fits of ThT fluorescence over 24 hours incubation of β_2m fibrils in Ficoll 70 at neutral pH

These graphs show the data fits (green) of each of the depolymerisation experiments. This can be modelled as $f(\boldsymbol{t}) = \boldsymbol{A_1}.(\boldsymbol{1} - \boldsymbol{e^{-R_1 t}}) + \boldsymbol{A_2}.\boldsymbol{e^{-R_2 t}}$ where t is time elapsed, A_1 is the amplitude of build-up of fluorescence intensity, R_1 the rate constant of the build up of fluorescence intensity, A_2 the amplitude of the decay of fluorescence intensity and R_2 the rate constant of the decay of fluorescence intensity.

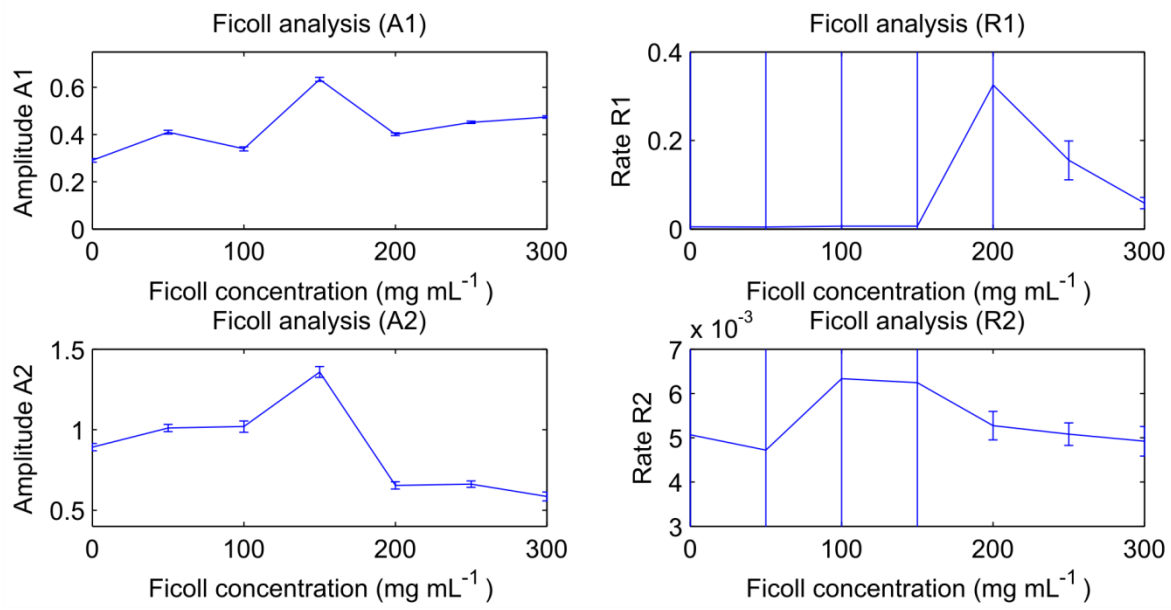

Figure 35 Comparison of amplitudes and rate constants of ThT fluorescence evolution during fibril incubation in different concentrations of Ficoll 70

A1 is the amplitude of the ThT fluorescence growth component. R1 is the rate constant of the ThT fluorescence growth. A2 is the amplitude of the fluorescence decay component. R2 is the rate constant of the fluorescence decay component. Error bars are 95% confidence bounds.

It is difficult to determine what these results show experimentally but there is likely to be one process occurring causing the decay of the ThT fluorescence. The presence of Ficoll 70 does clearly have a dose dependent effect on the experiments but from these results there is no clear correlation. At much higher concentrations a negatively correlated concentration dependent effect can be seen but this could be due to the viscosity of the solutions at these concentrations which causes the process to become diffusion limited (*114*).

2.4 Conclusion

In this chapter we have described the expression and purification, and fibrilisation of β_2m used in all subsequent NMR investigations. Furthermore, we have sought to establish conditions whereby the fibrils produced by acid precipitation are stable in complex with SAP. This has led us to make interesting discoveries regarding the stability of fibrils under a variety of conditions that are described below

SAP and fibrillar β_2m show strong interaction

The interaction between SAP and fibrillar β_2m is well established from clinical studies (*47*) but binding between SAP and *in vitro* acid produced β_2m fibrils had so far not been studied and published. It was essential to prove that there was an interaction between the two proteins if we were to proceed onto NMR studies investigating this interaction. We therefore undertook an SAP pull-down assay using our acid produced fibrils. The results of the pull-down assay show a definite interaction between β_2m fibrils and SAP (Figure 21). SAP is successfully pulled down with the fibrils showing a strong interaction between the two. In the control experiment β_2m was present in supernatant meaning some fibrils turned into soluble species but in the SAP containing sample there was no β_2m present in the supernatant. The only difference between the experiments was the presence of SAP in the buffer so this indicates that over the 1 hour time course of the incubation SAP has prevented or at least reduced the transition of β_2m from insoluble to soluble species.

Ionic strength and not SAP is the prime factor in determining whether ThT binding material is present after 24 hours

In order to determine whether SAP has a stabilising effect on fibrils at neutral pH, fibrils were incubated at neutral pH for 24 hours with and without the presence of SAP. Concurrently experiments were performed on fibrils in low salt and high salt buffers to determine whether the strong ionic strength used in SAP buffers has an effect on stabilising β_2m fibrils. The depolymerisation assays indicate that SAP presence is not the prime factor determining whether there are fibrils present after 24 hours at neutral pH. The persistence of fibrils is better correlated with the buffer conditions than with the presence of SAP. The SAP containing buffer and the calcium buffer were identical except for the presence of SAP and Figure 22 shows that the percentage of maximum ThT fluorescence after 24 hours was almost identical (30 and 33%) for the two conditions.

The high salt conditions had the highest percentage of maximum fluorescence left after 24 hours and it was almost double that of the calcium and SAP experiments (Figure 22). The only difference between the buffer conditions in this case was the addition of 540 mM NaCl. This suggests that it is the ionic strength that is determining how much fibrillar material is left after 24 hours and not the presence of calcium which is at the same concentration in all 3 samples.

The low salt conditions give the lowest fluorescence after 24 hours, this correlates well with ionic strength being the determining factor in the persistence of fibrils in these experiments. The fluorescence decay in the low salt conditions was also distinctly different to that for the other samples. The bi-exponential decay of fluorescence in the low

salt sample is characterised by two relatively rapid rate constants which is in contrast to the other samples that are characterised by a rapid and a very slow rate constant.

TEM studies reveal three different morphologies of fibrils present in all the depolymerisation assays performed.

- Type A: Long and straight helically twisted, ThT binding fibres, less than 20 nm wide that negative stain cannot penetrate. These are the fibrils produced under acidic, low salt conditions and are the fibrils present at the start of the experiment.
- Type B: Highly curved, worm like, ThT binding fibrils that are possibly protofilaments. They are in the region of 400 nm in length and less than 5 nm wide. Negative stain cannot penetrate these fibrils.
- Type C: Short ThT binding fibrils of about 200 nm length and 10 nm width whose exact morphology is difficult to dictate due to diffuse staining of the fibrils by the negative stain.

The low salt sample contains type B fibrils after 24 hours and does not contain the type C fibrils that are characteristic of the buffers with high ionic strength as shown in Figure 25. This suggests a mechanism similar to as displayed in Figure 36. In this proposed mechanism the type A fibrils in the low salt experiment rapidly break up into the type B fibrils which are possibly protofilaments which in turn rapidly depolymerise into non-ThT binding species. In the high salt samples the type A fibrils are rapidly converted into type C fibrils by the presence of high ionic strength and these type C fibrils very slowly depolymerise into non-ThT binding species. All these species may cause ThT to have different quantum yields when it is bound to them.

The evidence thus far points to several possible scenarios:

1. High ionic strength in the suspension forces transformation of type A fibrils into type C. Type C fibrils are stabilised by high ionic strength, and will persist indefinitely if the ionic strength is high enough. The initial decrease in ThT fluorescence is due to type A fibrils breaking down into soluble species, the likelihood of this happening increasing with decreased ionic strength.
2. High ionic strength in the suspension forces transformation of type A fibrils into type C. Type C fibrils are stabilised by high ionic strength and will persist indefinitely if the ionic strength is high enough. The initial decrease in ThT fluorescence is due to a difference in quantum yield between type A and type C fibrils. The total amount of fibrils remains the same.
3. A combination of the two.

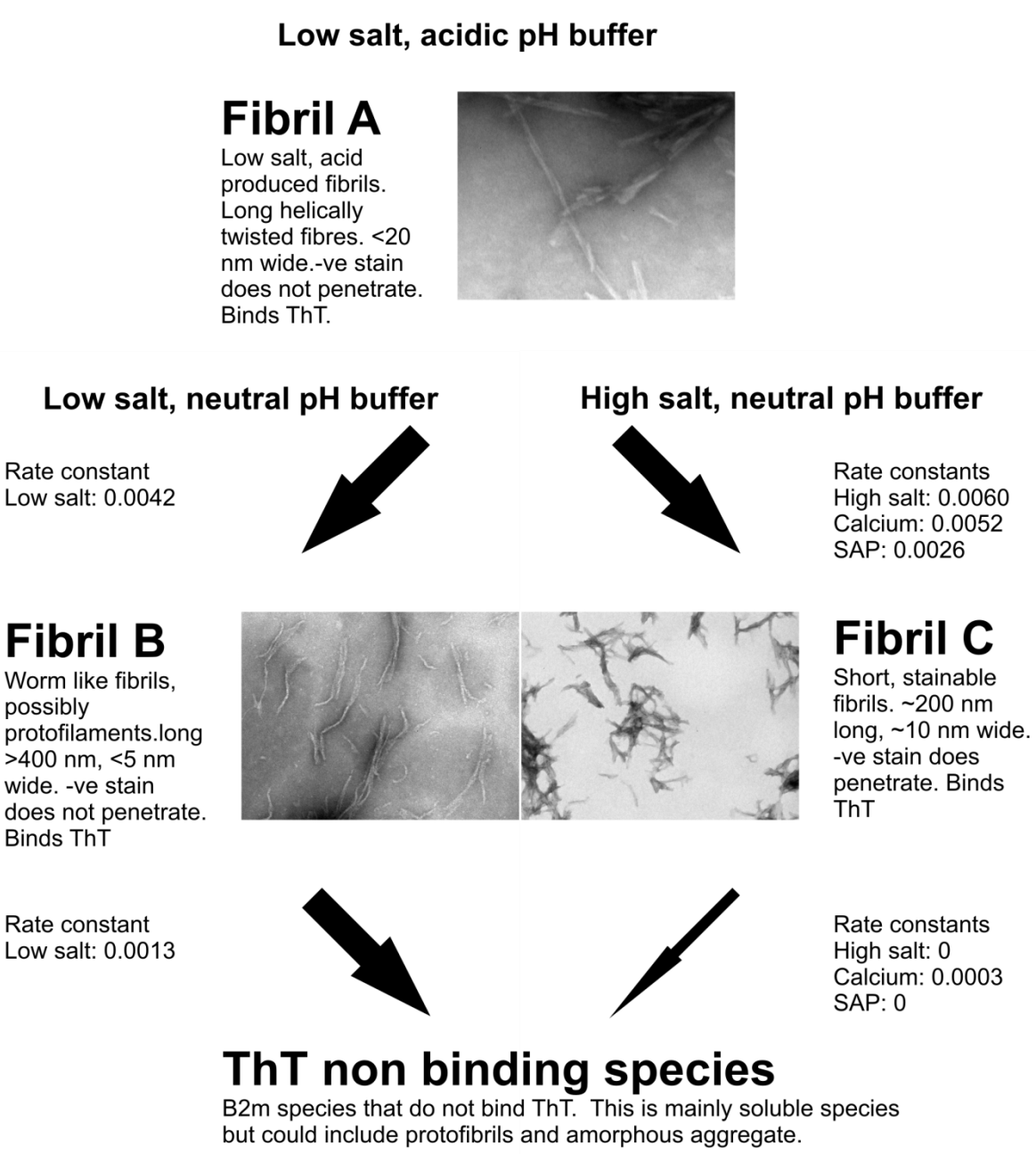

Figure 36 Proposed fibril morphology changes which occur during depolymerisation experiments

This schematic is based upon results from depolymerisation experiments and subsequent TEM of samples. The typical acid produced fibril, type A, rapidly changes morphology under low salt, neutral pH conditions to worm-like, type B fibrils. These type B fibrils undergo rapid depolymerisation to species that are soluble or otherwise do not bind ThT dye. The rate constants of both reactions are within an order of magnitude of each other. Under conditions with at least 200 mM of added salts, the type A fibril undergoes rapid morphology changes to the type C fibril whose stability is then determined by the concentration of salts. The fibrils do not dissociate under the highest salt conditions but slow dissociation does occur in the calcium and SAP buffers.

SAP does not have an appreciable effect on slowing the rate of the fast decay however in the presence of SAP the second slower decay is almost halted whereas in the calcium only buffer the ThT fluorescence is still decaying appreciably. If the experiment had been run for longer, then the models used predict that the ThT fluorescence in the calcium experiment would have become below that of the SAP experiment. It could be that due to their slower rate of depolymerisation, SAP is able to stabilise the type C fibrils.

Quantitative studies now need to be performed in order to quantitate the amount of fibrillar material left after 24 hours and relate this to the ThT fluorescence remaining. This will determine which of the above scenarios is happening.

Presence of free β_2m or BSA increases ThT fluorescence in fibril depolymerisation assays

To investigate the hypothesis earlier formulated that an equilibrium between fibrillar β_2m and free β_2m in fibril pellets prevented depolymerisation of fibrils at neutral pH, we undertook fibril depolymerisation assays in the presence of variable concentrations of free β_2m. It was hypothesised that the high amounts of free β_2m in the buffer would shift the equilibrium towards free β_2m and reduce or prevent fibril depolymerisation resulting in a slower rate of decay in ThT fluorescence. The results of these experiments can be found in Figure 26 and they are not as expected. ThT fluorescence actually showed a net increase during the 24 hour incubation in a non-linear but concentration dependent manner. This increase occurred through a fast exponential growth in ThT fluorescence at the beginning of the experiment; a second process was causing a slow exponential decay of fluorescence. ThT binding free β_2m and causing an increase in fluorescence has been ruled out through the use of a control containing free β_2m and ThT only, and the ThT and free β_2m being pre-

incubated with each other so if there were increased fluorescence due to ThT binding free β_2m it would be present from the start of the experiment. The increase in fluorescence is not due to time taken for all available binding sites on fibrils to be filled with ThT as this was investigated and ruled out by running experiments with fibrils pre-incubated in ThT for 24 hours before being incubated at neutral pH. The rise in fluorescence is still seen under these conditions. Therefore three main factors could be responsible for this increase in ThT fluorescence:

- An increase in fibrillar material would result in more ThT fluorescence (up until all ThT is bound)
- An increase in accessible binding sites for ThT to bind to would result in an increase in ThT fluorescence
- A change of fibril morphology to a species that causes ThT to have a higher quantum yield

With the presence of free β_2m and the β_2m fibrils acting as seeds, an increase in fibrillar material could be possible.

Negative stain TEM of the samples after 24 hours does not rule out any of the above possibilities as there is plenty of material present on the grid and it appears to be of a fibril-like nature. The morphology of the fibrils has definitely changed from typical fibrils described as type A in the SAP depolymerisation experiments (Figure 36) to material which more resembles but is not identical to the type C fibrils identified in the high salt depolymerisation experiments. Further investigation will be needed in order to determine if any or all the above possible reasons for increased ThT fluorescence are responsible for the fluorescence increase in the presence of free β_2m.

In order to investigate further whether an equilibrium between fibrillar and free β_2m causes the persistence of β_2m fibrils at neutral pH the depolymerisation assays were repeated with BSA replacing the free β_2m. Failure of BSA to slow depolymerisation would have been strong evidence for an equilibrium existing between fibrillar and free β_2m. The results in Figure 29 show that the presence of BSA in the buffer causes an increase in ThT fluorescence in the same fashion that free β_2m did. Like the β_2m experiment the increase in ThT fluorescence being caused by ThT binding to BSA was controlled against using BSA and ThT only samples and pre-incubation of the BSA and ThT. This result is really not as expected as BSA is not known to form fibrils and there are no reported cases of amyloid from one type of protein being able to cause fibrillogenesis of a different protein, although there are cases of truncated versions of a protein being able to seed the fibrillogenesis of the full length protein (*83*). Negative stain of the BSA samples after 24 hours reveal a grid covered in protofibril like material but also in places, fibril-like material (Figure 32B & C). This morphology of fibril has so far not been seen in any previous experiments with β_2m and so it cannot be ruled out that these fibril-like structures are formed from BSA; however these fibrils made up only a small percentage of the total material on the grid and so it is unlikely that a large proportion of BSA was converted into fibrils if at all.

The large amount of protofibrils present after 24 hours is unusual; in the low ionic strength experiments material of any nature is sparse and hard to find after 24 hours of incubation at neutral pH; (Figure 19) therefore BSA must be having an effect. The presence of the protofibrils could be explanatory of the high ThT fluorescence after 24 hours; it could also explain the rise in ThT fluorescence as the spherical nature of protofibrils could potentially result in more accessible binding sites for ThT. High concentrations of BSA are known to

cause aggregation in refolding assays (*115*), as β_2m could be partially unfolded as it depolymerises, the BSA could be causing aggregation of the partially folded states. Further investigation is needed to determine the cause of the ThT increase; these will be discussed in the outlook in chapter 6.

Ficoll 70 does not cause a net increase in ThT fluorescence in depolymerisation experiments

The β_2m and BSA results open up the possibility that the conversion of fibrils into a different species or the inhibition of protofibril depolymerisation could be due to a molecular crowding effect. To investigate this we repeated the depolymerisation experiments in the presence of the molecular crowding agent Ficoll 70. At up to 150 mg/ml of Ficoll 70 a simple exponential decay is seen with no rise in ThT fluorescence as seen in the free β_2m and BSA experiments; some rise in fluorescence is seen above 150 mg/ml but unlike the free β_2m and BSA experiments the initial ThT fluorescence is much lower than the 0 mg/ml Ficoll 70 sample and rises up to a similar value to that of the starting value in the 0 mg/ml experiment (Figure 33). This suggests that rather than the increase being caused by increased ThT binding over and above that of the original amount of fibrils, in fact the rate of diffusion of ThT is being slowed so that it takes a while for ThT molecules to bind to all available fibrils. The ThT fluorescence after 24 hours is higher in the Ficoll 70 containing experiments than it is in the 0 mg/ml experiments but this shows no linear concentration dependence and so it is difficult to explain why this happening. The difference between the Ficoll 70 results and the free β_2m and BSA results suggests that a different process is occurring during the experiment and it would be reasonable to postulate that a straight molecular crowding effect is not responsible for the increase in fluorescence seen in the free β_2m and BSA experiments. TEM images need to

be acquired of the 24 hour endpoint of the Ficoll 70 samples; this is difficult because of the extremely high concentrations of Ficoll 70 present which would be difficult to wash off and therefore will interfere with the negative staining of the grids.

At this point it is not possible to say what is happening in the depolymerisation experiments and more investigation is needed. What can be said is that the TEM data demonstrate there is much more insoluble material left after 24 hours in both free β_2m and BSA experiments than in typical low salt and no additives experiments; the amount of material left in each case now needs to be quantified. The addition of additives to the samples does show a concentration dependent effect. It can also be said that the material left in the free β_2m and BSA experiments is not the same morphology, perhaps suggesting that different processes are occurring. A pure molecular crowding effect causing the increase in ThT fluorescence is unlikely due to the Ficoll 70 experiments not showing a net increase over the time course of the experiment however it has before been observed that molecular crowding with proteins affects experiments more than molecular crowding with polysaccharides (*115*).

In summary this chapter has described how β_2m has been successfully expressed, purified and refolded in sufficient quantities for study by biochemical, biophysical and NMR methods. It has described the successful fibrillogenesis of β_2m and the subsequent successful binding of serum amyloid P component to the fibrils. Depolymerisation experiments have shown how ionic strength and addition of SAP to β_2m fibril samples affects the stability and morphology of fibrils under the dilute conditions tested and finally how the addition of free β_2m and BSA causes a large net increase in the ThT fluorescence of β_2m at neutral pH. The change in morphology of β_2m fibrils seen in the presence of free β_2m does open the possibility that β_2m fibrils packed in MAS rotors at neutral pH may

have a different morphology to that of the long and straight fibrils produced under acidic conditions. However the effective concentration of free β_2m in a MAS rotor (which would be unobservable in the spectrum as the cross-polarisation selectively observes solid material) caused by depolymerisation of fibrils would be much more concentrated than in the experimental conditions used here as the excluded volume is much higher. Further investigation into the morphology of acid produced fibrils at neutral pH is needed.

Chapter 3

3 Liquid-State NMR Studies of Beta-2 Microglobulin

3.1 Introduction

In the previous chapter, evidence was presented that SAP and fibrillar β_2m have a strong interaction with each other. *In vivo* evidence from other groups was presented that radiolabelled SAP will associate with β_2m amyloid deposits in dialysis related amyloidosis patients (*47*). *In vitro* fibrillogenesis studies demonstrated that SAP increases β_2m fibrillogenesis at neutral pH (*45*), while our own studies demonstrated that SAP both shows a strong enough interaction with fibrillar β_2m to be pulled down with it in pull-down assays (Figure 21). The interaction of SAP with fibrils is not β_2m specific and has been demonstrated with many fibril types including Aβ fibrils from amyloid deposits found in Alzheimer's disease and serum amyloid A fragments from AA amyloidosis (*89*). Despite the well characterised interaction between SAP and amyloid fibrils, less is known about SAP's interaction with the monomeric precursor proteins of the amyloid fibrils. No previous studies have demonstrated an interaction between SAP and the monomeric species of amyloid forming proteins. Here we use β_2m as a model to establish if there are any interactions between SAP and the monomeric species of amyloid forming proteins.

We have undertaken a series of NMR experiments to answer the following questions:

a. Upon potential binding of SAP are perturbations in chemical shift observed which would be consistent with high-affinity binding,
b. If so which residues do these resonances belong to,
c. If no binding is detected – we wish to know how the resonances compare to the solid-state assignment to identify which regions exhibit a similar or different structure and how this may relate to SAP binding.

To examine whether there is binding between soluble β_2m and SAP, HSQC experiments measuring correlations between β_2m amide protons and nitrogens were undertaken in the presence and absence of a large excess of SAP.

To date the published liquid-state NMR structures of soluble β_2m are based on ^{1}H- NMR spectroscopy. In 2002 Genaro Esposito's group published a full ^{1}H NMR derived structure using TOCSY experiments to extract torsion angle restraints and NOESY experiments to provide internuclear distances required for restraint modelling (*57*). When this project was started there had been no full heteronuclear assignment of soluble β_2m published and in order to achieve the stated goals of comparing the liquid and solid-state data the ^{13}C and ^{15}N assignments are needed. We have used multidimensional heteronuclear correlation experiments to assign the backbone and side-chain resonances of β_2m.

3.2 Liquid-state NMR experiments used for chemical shift assignment and comparison

3.2.1 Sample preparation and experimental parameters

Dually labelled ^{13}C ^{15}N β_2m was expressed in *E.coli* and purified as described in the previous chapter. The final sample compositions and experimental conditions and parameters were as follows:

<u>β_2m/SAP HSQC comparison</u>

β_2m only: 30 μM β_2m, 10 mM Tris-HCl, 600 mM NaCl, 200 mM $CaCl_2$, 10% D_2O, pH 7.4

β_2m with SAP: 30 μM β_2m, 350 μM SAP (wrt monomer), 10 mM Tris-HCl, 600 mM NaCl, 200 mM $CaCl_2$, 10% D_2O, pH 7.4

All experiments were performed on a Varian INOVA 600 MHz spectrometer equipped with a room temperature triple resonance probe and z-gradients at 25˚C.

<u>HSQC, HNCA, HNCO, HNCACB, CBCA(CO)NH, HCCH-TOCSY,H(CCO)NH</u>

1 mM β_2m, 50 mM KCl, 50 mM HEPES, 10% D_2O, pH 7.4

Experiments undertaken on a Varian INOVA 600 MHz spectrometer at 25˚C using the Biopack (Varian Inc, USA) suite of pulse sequences.

1 mM β_2m, 50 mM KCl, 50 mM HEPES, 10% D_2O, pH 7.4

Experiments undertaken on a Varian INOVA 600 MHz spectrometer at 25˚C

Experiment	Acquisition time proton (s)	Acquisition time carbon (s)	Acquisition time nitrogen (s)	Acquisition time 2nd proton (s)	Mixing time (ms)
HSQC (SAP)	0.051	-	0.021	-	-
HSQC	0.051	-	0.021	-	-
HNCA	0.064	0.007	39	-	-
HNCO	0.051	0.013	0.027	-	-
HNCACB	0.051	0.005	0.021	-	-
CBCA(CO)NH	0.064	0.004	0.021	-	-
HCCH-TOCSY	0.051	0.003	-	0.016	14
H(CCO)NH	0.051	0.011	0.021	-	-

Table 5 Experimental parameters used in liquid-state heteronuclear correlation experiments

3.2.2 HSQC NMR experiment

This important experiment records one-bond correlations between protons and ^{15}N by transferring magnetisation from protons onto nitrogen using an INEPT transfer (insensitive nuclei enhanced by polarisation transfer) (*116*). During the evolution period the ^{15}N nuclei acquire a frequency label specific to nitrogen and this labelled magnetisation is transferred back to protons where it is detected. The diagrammatic representation of the pulse sequence is shown in Figure 37.

Proton magnetisation is excited by a 90˚ pulse. An INEPT sequence transfers polarisation from protons to ^{15}N nuclei. The anti-phase magnetisation that this creates evolves under the ^{15}N chemical shift in t_1. J-couplings with the protons are refocused using an 180˚ pulse in the middle of the t_1 period. A reverse INEPT sequence converts magnetisation into in-phase proton magnetisation and proton acquisition is performed under ^{15}N decoupling.

The ^{1}H-^{15}N-HSQC experiment produces a 2D spectrum with the $^{1}H^{N}$ measured in the direct dimension and ^{15}N measured in the indirect dimension. Thus resonances arise that have a proton and nitrogen resonance and correspond to each backbone NH in the protein so

effectively a signal is produced for each amino residue present in the protein; apart from proline which has no free NH due to its side chain terminus being covalently attached to the backbone nitrogen. The NH_2 groups of asparagine and glutamine side chains are also present in the spectrum as are the indole NH correlations from tryptophan.

^{1}H-^{15}N-HSQC spectra are used as "fingerprints" of proteins as spectra are easily interpreted and each protein's HSQC is distinct. Due to their high sensitivity, good quality spectra can be acquired quickly and they easily show whether a protein is unfolded or is degrading due to poorly dispersed peaks in the centre of the spectrum or additional peaks present in the "graveyard" (bottom, right hand side) region of the spectrum respectively.

The INEPT pulse sequence used in the HSQC experiment is a building block that is used in many liquid-state experiments. It allows the efficient and directed transfer of magnetisation between protons, which have a high gyromagnetic ratio, and nuclei with lower gyromagnetic ratios via j-couplings between nuclei. The sensitivity of a nucleus is positively correlated with its gyromagnetic ratio and the sensitivity of heteronuclear experiments is dependent on the product $\gamma_e.\gamma_d^{3/2}$ where γ_e is the gyromagnetic ratio of the excited nucleus and γ_d is the gyromagnetic ratio of the detected nucleus. Clearly for the maximum sensitivity possible from an experiment, excitation and detection should both take place on the nucleus with the highest gyromagnetic ratio; the INEPT sequence makes this possible.

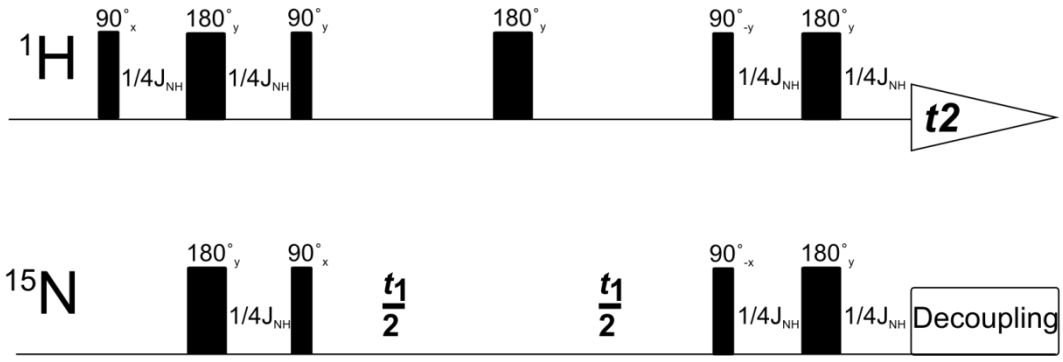

Figure 37 Pulse sequence of HSQC NMR experiment
The top line represents pulses applied on the proton frequency and the bottom line pulses applied on the ^{15}N frequency. The narrow black rectangles represent 90˚ applied pulses. Subscripts are the phase of the pulse. Wide black rectangles represent 180˚ applied pulses. Evolution time on ^{15}N is represented by t_1. The FID is represented by t_2. Decoupling pulses are represented by boxes marked decoupling (*117*).

3.2.3 HNCA NMR experiment

The HNCA is a triple resonance, three-dimensional experiment exploiting the scalar couplings between nuclei to correlate a residue's backbone NH group with the α-carbon of the same (i) and previous residue (i-1). As both α-carbons are correlated to the same nitrogen this gives sequence specific information and the backbone residue sequence can be determined. The correlation occurs through magnetisation transfer from the H^N through to N then through either one or two couplings to the i residue or i-1 residue's α-carbon respectively before the magnetisation is transferred back again along the same route and detected on the proton as can be seen in Figure 38. The peak corresponding to the directly coupled ^{13}Cα will appear relatively more intense than the peak corresponding to the ^{13}Cα of the preceding residue due to the stronger J-coupling between the ^{15}N and directly coupled ^{13}Cα. The proton frequency is then labelled with the chemical shift of the i nitrogen and i and i-1 α-carbons. This leads to resonances occurring twice in the same spectrum at the same carbon shift but correlated to different nitrogens. These carbon resonances can then be aligned as in Figure 45 to give the sequential assignment.

The sequence starts with an INEPT transfer of the magnetisation from the backbone ^{1}H to ^{15}N. A dephasing delay T follows, during which the 1-bond coupling between ^{15}N and $^{13}C\alpha$ leads to an anti-phase ^{15}N magnetisation with respect to $^{13}C\alpha$. This is transferred to $^{13}C\alpha$ magnetisation by a selective ^{13}C 90˚-pulse and labelled by the $^{13}C\alpha$ chemical shift during the t_1-evolution time. It is converted back to ^{15}N anti-phase magnetisation by a ^{13}C 90˚ pulse. The ^{15}N magnetisation becomes in phase again during the delay T and becomes simultaneously labelled by the ^{15}N chemical shift during the constant time-type of t_2 evolution. A reverse INEPT transfer converts the coherences of interest back to the amide protons for observation.

Protons are decoupled by the DIPSI-2 scheme. The ^{13}C-labeled carbonyl carbons are decoupled by a selective 180˚ pulse during the $^{13}C\alpha$ evolution.

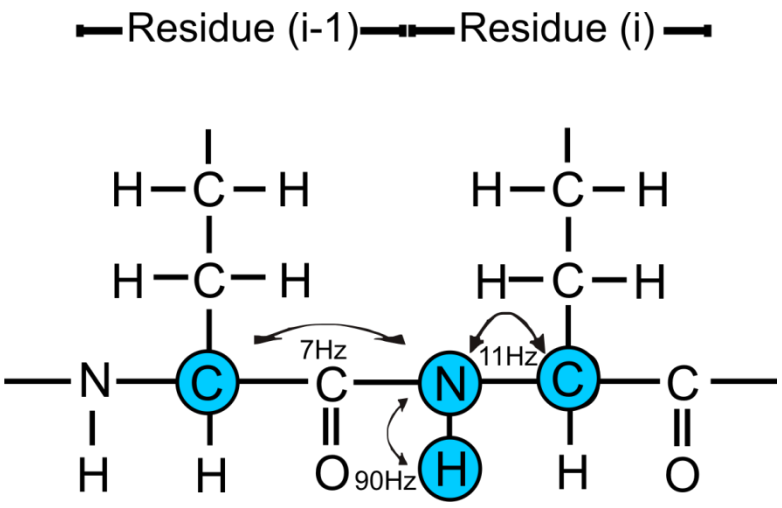

Figure 38 Magnetisation transfer in HNCA NMR experiment
Atoms shaded blue have magnetisation pass through them and are detected. Arrows represent direction of magnetisation transfer and are annotated with the size of the J-couplings between those nuclei. Residue (i) is the residue whose amide proton is being detected and Residue (i-1) is the preceding residue.

Due to the short route of the magnetisation transfer, the HNCA is a highly sensitive experiment, but ambiguity can occur due to the low range of α-carbon chemical shifts leading to several possible choices when aligning resonances. Full and in depth accounts of

the experiment, including full pulse sequences, can be found published in several papers (*118-120*).

3.2.4 HNCACB NMR experiment

The HNCACB experiment is similar to the HNCA except that magnetisation is also transferred to the β-carbons of i and i-1 residues. This experiment therefore gives the chemical shifts of the β-carbons and reduces the ambiguity that is present in the HNCA experiment. The pulse sequence starts with an INEPT transfer of the magnetisation from the backbone ^{1}H to ^{15}N. Another INEPT sequence transfers magnetisation from ^{15}N to $^{13}C\alpha$ and a 90° ^{13}C pulse transfers magnetisation to $^{13}C\beta$. ^{13}C chemical shift evolution follows in the period t_1 followed by transfer of magnetisation back to $^{13}C\alpha$ by a 90° pulse on ^{13}C. A fixed period T allows ^{13}C magnetisation to become anti-phase in respect to ^{15}N and simultaneous 90° pulses on ^{13}C and ^{15}N transfers magnetisation back on to ^{15}N. A period t_2 allows ^{15}N chemical shift evolution. Finally magnetisation is transferred back to the NH protons by a reverse-INEPT sequence and an FID acquired under ^{15}N decoupling.

Magnetisation transfer is shown in Figure 39. In theory a full sequential assignment can be acquired from the HNCACB experiment alone however the longer route that the magnetisation takes means the experiment is less sensitive than the HNCA and ambiguity can arise over which Cβ peak is from i or i-1 as they may be similar sizes or some peaks may not show at all. This can be quite clearly seen in Figure 46. A full and in depth account of the experiment, including pulse sequence, has been published by Wittekind *et al.* in 1993 (*121*).

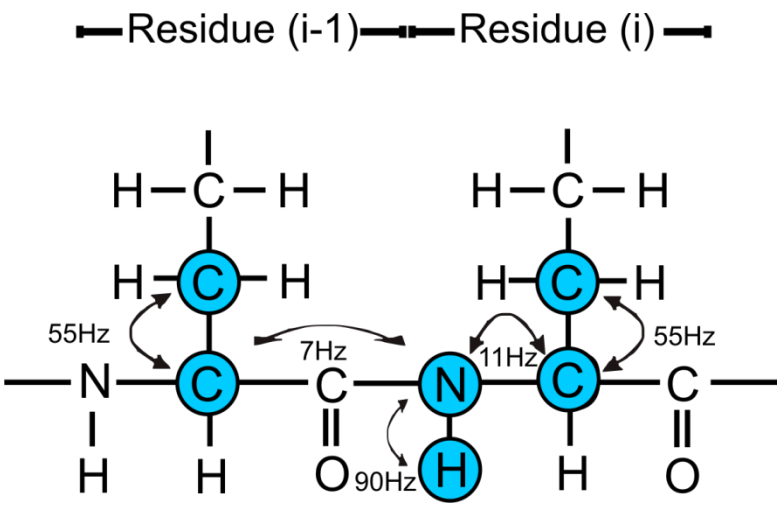

Figure 39 Magnetisation transfer in HNCACB NMR experiment.
Atoms shaded blue have magnetisation pass through them and are detected. Arrows represent direction of magnetisation transfer and are annotated with the size of the J-couplings between those nuclei. Residue (i) is the residue whose amide proton is being detected and Residue (i-1) is the preceding residue.

3.2.5 CBCA(CO)NH NMR experiment

The CBCA(CO)NH experiment differs from the experiments mentioned previously in that the protons attached to the β-carbon and not the protons attached to the backbone nitrogen are excited. The magnetisation is then transferred to the β-carbon followed by the α-carbon. At this point instead of transferring magnetisation directly to the backbone nitrogen, it is transferred to the carbonyl carbon and then directly on to the nitrogen and then the proton. The magnetisation does not undergo an evolution period on the carbonyl carbon and so the proton magnetisation does not get labelled with the carbonyl carbon chemical shift. Exploiting the scalar coupling between the α-carbon and carbonyl carbon results in the magnetisation being transferred in only one direction so only the i-1 carbons are detected.

The direct route of magnetisation transfer means that the CBCA(CO)NH is a sensitive experiment (relative to an experiment with two way transfer such as an HNCACB. The

magnetisation transfer is shown in Figure 40. Used in conjunction with the HNCACB experiment this allows the unambiguous assignment of carbon resonances to either the i or i-1 residue.

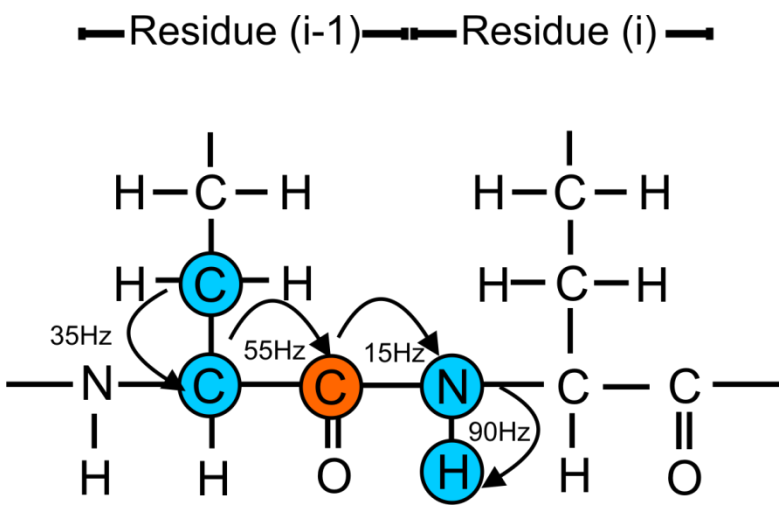

Figure 40 Magnetisation transfer in CBCA(CO)NH NMR experiment
Atoms shaded blue have magnetisation pass through them and are detected. Atoms shaded orange have magnetisation pass through them but are not detected. Arrows represent direction of magnetisation transfer and are annotated with the size of the J-couplings between those nuclei. Residue (i) is the residue whose amide proton is being detected and Residue (i-1) is the preceding residue.

3.2.6 HNCO NMR experiment

The HNCO experiment is completely analogous to the HNCA but magnetisation is transferred to the carbonyl carbon instead of α-carbon. Magnetisation transfer is shown in Figure 41. This experiment allows the chemical shifts of the carbonyl carbon nuclei to be acquired. The short route of magnetisation transfer means that the HNCO is a sensitive experiment. A full account of this experiment has been published by Löhr and Rüterjans in 1995 (*122*).

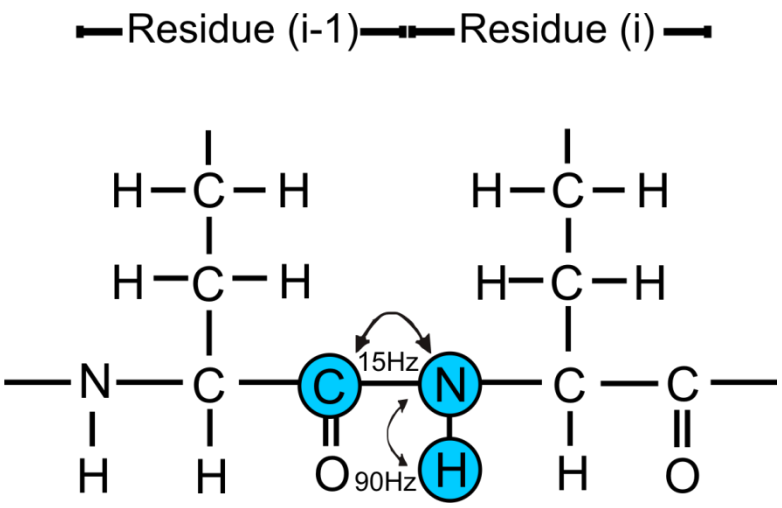

Figure 41 Magnetisation transfer in HNCO NMR experiment
Atoms shaded blue have magnetisation pass through them and are detected. Arrows represent direction of magnetisation transfer and are annotated with the size of the J-couplings between those nuclei. Residue (i) is the residue whose amide proton is being detected and Residue (i-1) is the preceding residue.

3.2.7 H(CCO)NH NMR experiment

The H(CCO)NH experiment is a 3-dimensional experiment that correlates the amide proton and nitrogen of a residue to the aliphatic protons of the previous residue. It allows the sequential assignment of protons when used in combination with an assigned HSQC spectrum due to magnetisation passing through the backbone carbonyl carbon, giving the nitrogen and amide proton chemical shifts of residue i and the aliphatic proton chemical shifts of residue i-1.

The experiment proceeds as follows: Firstly a 90˚ pulse is applied to the aliphatic protons and the magnetisation evolved before being transferred via J-couplings to all connecting aliphatic ^{13}C using an INEPT sequence. Isotropic mixing using ^{13}C-^{13}C DIPSI (Decoupling In Presence of Scalar Interactions) allows the magnetisation to transfer from side-chain ^{13}C resonances to $^{13}C\alpha$. The magnetisation is subsequently transferred via J-couplings to the

carbonyl ^{13}C without a variable evolution period and onto the amide ^{15}N via J-couplings; once again without a variable evolution period. The magnetisation is evolved on the nitrogen and the transferred via a reverse INEPT sequence to the amide proton where it s detected under ^{15}N decoupling. Magnetisation transfer is shown in Figure 42.

The assignment strategy is to have the amide proton chemical shifts in the first dimension, the aliphatic proton chemical shifts in the second dimension with the amide nitrogen chemical shifts in the third dimension. Migrating to the assigned amide shifts obtained from the HSQC will result in the aliphatic protons from the previous residue being displayed along y. The H(CCO)NH is used in conjunction with an HCCH-TOCSY to assign side-chain carbon chemical shifts. The markers shown above will overlay with peaks on the HCCH-TOCSY at the chemical shift of the connected carbon. A full account of the H(CCO)NH experiment along with the related H(CCO)NH-TOCSY has been published by Logan, 1993(*123*).

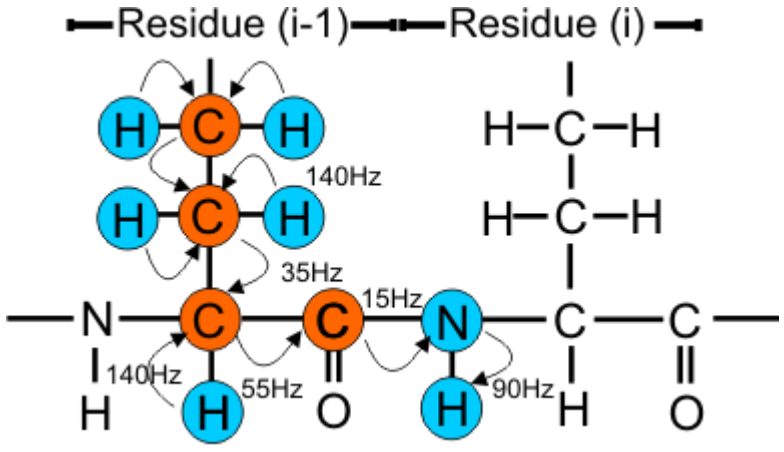

Figure 42 Magnetisation transfer in H(CCO)NH NMR experiment
Atoms shaded blue have magnetisation pass through them and are detected. Atoms shaded orange have magnetisation pass through them but are not detected. Arrows represent direction of magnetisation transfer and are annotated with the size of the J-couplings between those nuclei. Residue (i) is the residue whose amide proton is being detected and Residue (i-1) is the preceding residue.

3.2.8 HCCH-TOCSY NMR experiments

The HCCH-TOCSY experiment is a 3-dimensional double resonance experiment that is used in order to obtain side-chain ^{1}H and ^{13}C assignments. Magnetisation transfer is shown in Figure 43. The experiment proceeds as follows: A 90˚ pulse is applied to the protons and a proton chemical shift evolved for the period t_1. Magnetisation is transferred from protons to connecting carbons via J-couplings using an INEPT like sequence. The magnetisation is then evolved on the ^{13}C nuclei for the period t_2; subsequently an isotropic mixing period (DIPSI) transfers the magnetisation along the ^{13}C side-chain via carbon-carbon J-couplings. The ^{13}C magnetisation is then transferred back to the protons via a reverse INEPT sequence and detected under ^{13}C decoupling. This results in a 3-dimensional spectrum displaying almost all the protons that are attached to the side-chain carbons at their chemical shift.

The assignment strategy is to display the proton chemical shifts in the x and y dimensions and have ^{13}C in the z dimension. Assigned proton chemical shifts are obtained from the H(CCO)NH experiment and marked. The z dimension is then searched until proton resonances align correctly with the marked chemical shifts. The peak belonging to the proton directly connected to the carbon at that shift will appear on the diagonal.

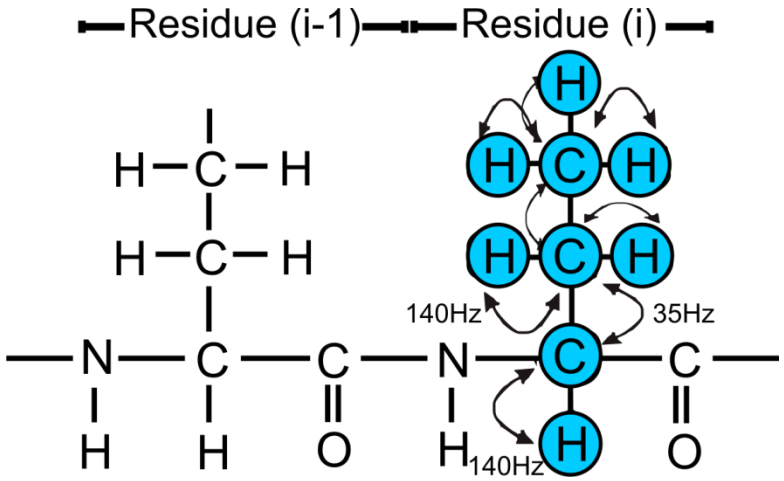

Figure 43 Magnetisation transfer in HCCH-TOCSY NMR experiment
Atoms shaded blue have magnetisation pass through them and are detected. Arrows represent direction of magnetisation transfer and are annotated with the size of the J-couplings between those nuclei. Residue (i) is the residue whose amide proton is being detected and Residue (i-1) is the preceding residue.

3.3 Resonance assignments of soluble beta-2 microglobulin

The HSQC of β_2m gives a spectrum with well dispersed peaks indicative of a correctly folded protein. The HSQC spectrum of soluble β_2m is given in

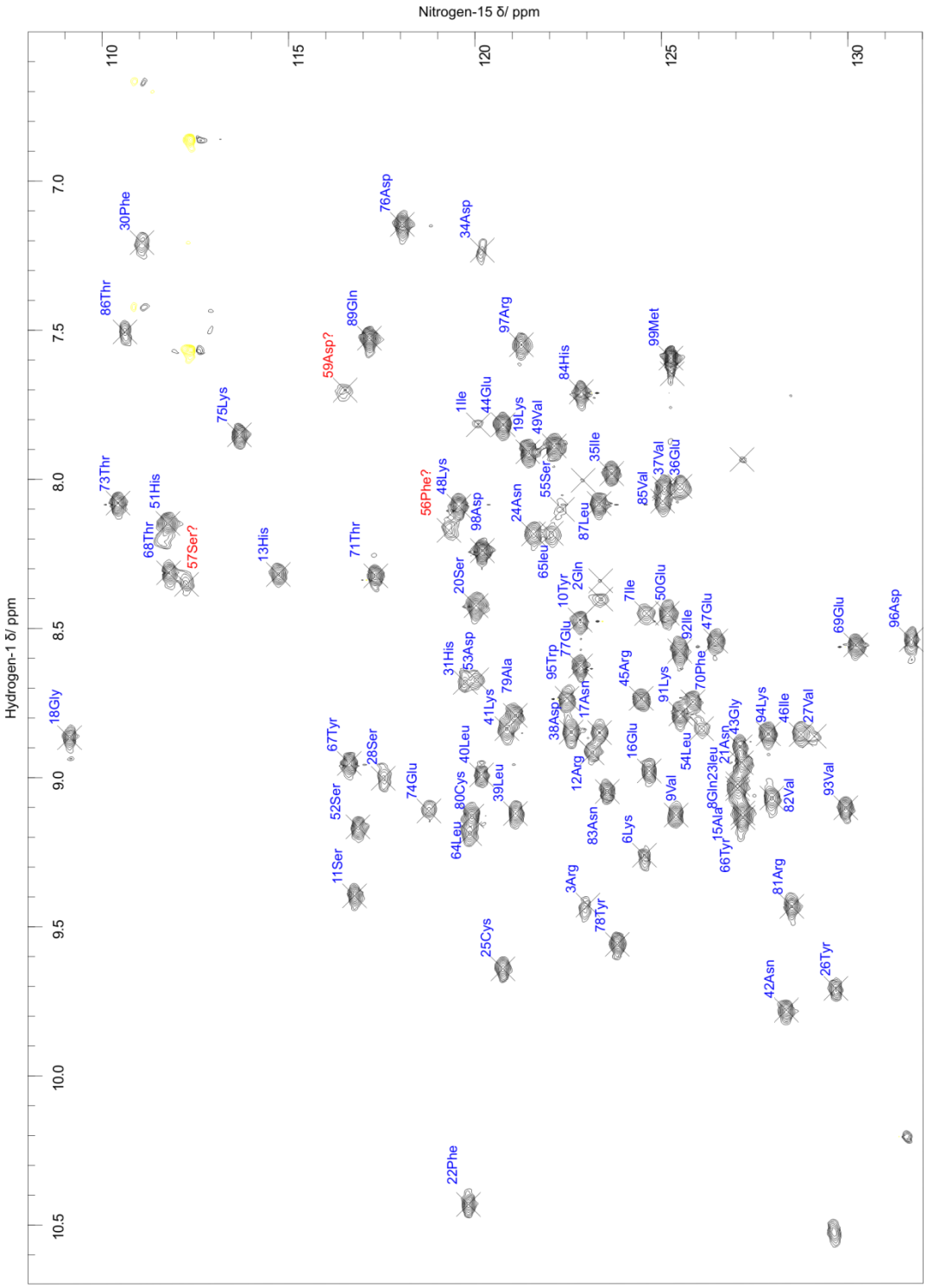

. There

are 88 NH peaks in total, 6 less than the 94 expected NH peaks. The construct used has 100 residues but 5 prolines and 1 N-terminal methionine cannot be observed. Tryptophan indole resonances (bottom left-hand side of HSQC spectrum) were not assigned. The spectrum shows very good signal to noise and therefore it is unlikely that these peaks are missing due to poor signal to noise. The majority of the missing peaks belong to residues that are in or adjacent to the loop region between β-strands V and VI. This is the region that binds with the MHC I alpha domain when β_2m forms the light chain of the MHC I complex as shown by X-ray diffraction data of the MHC I complex with β_2m bound (*59*); these contacts can be seen in Table 3. Three of the missing peaks: Trp-60, Phe-62 and Tyr-63 are all directly involved with binding the MHC I alpha domain through their side-chains. Three of the less intense peaks in the spectrum have all been tentatively assigned to residues that appear in the loop and two of these, Asp-53 and Phe-56, are also directly involved in binding to the alpha chain when in complex. Our spectra and assignments suggest that when not in complex with the MHC I alpha domain the loop region between β-strands V and VI is highly dynamic resulting in signal loss due to fast transverse relaxation leading to broadening of the peaks.

The triple resonance experiments all displayed good signal to noise ratios. HNCA (Figure 45), HNCACB (Figure 46), CBCA(CO)NH (Figure 47) and HNCO (Figure 48) experiments were acquired in order to sequentially assign the backbone resonances. The assignment strategy with these experiments is to primarily use the HNCACB experiment to sequentially align the peaks belonging to the same resonance. Peaks will appear twice in the same spectrum and arranging the spectrum acquired in a HNCACB experiment into a strip plot as shown in Figure 46 allows the sequential assignment of resonances. Each strip displays the Cα and Cβ of that residue plus the Cα and Cβ of the previous residue.

Sequential assignment is achieved by aligning the strong current residue's peak on one strip with the weak peak corresponding to the same nucleus on another strip. The HNCA spectrum is used to remove ambiguity that can arise in the HNCACB due to its lower sensitivity, sequential assignment is achieved in the same manner as the HNCACB by arranging the spectrum into a strip plot as can be seen in Figure 45. Ambiguity can also occur in the HNCACB experiment from not being able to distinguish between which peaks belong to the i residue and the i-1 residue. This ambiguity is removed through the use of the CBCA(CO)NH experiment (Figure 47) which due to the transfer of magnetisation through the $^{13}C'$ will only show the peaks from the i-1 residue. Overlaying the strip plots of the HNCACB and CBCA(CO)NH spectra will result in the superimposition of the i-1 peaks. The HNCA, HNCACB and CB(CO)NH experiments have led to 90 of 100 residues having their Cα and Cβ assigned (where residues have both Cα and Cβ atoms) and 88 of 100 residues having their carbonyl carbon assigned. Excluding prolines, all but one of the unassigned Cα resonances belong to residues 56-62 which form and are adjacent to the loop region between β-strands V and VI. H(CCO)NH (Figure 49) and HCCH-TOCSY (Figure 50) experiments were used to sequentially assign the side-chain proton and ^{13}C resonances. The experiments are used in combination, the H(CCO)NH correlates the i amide nitrogen and proton with the aliphatic protons of the i-1 residue, by displaying the spectrum as seen in Figure 49 and marking the i-1 aliphatic proton peaks, one can then identify the corresponding peaks in the HCCH-TOCSY as seen in Figure 50. The aliphatic ^{13}C that are connected to those protons can then be assigned. Excluding the V-VI loop and ring carbons 80% of the expected side-chain carbons have been assigned. All low gamma nuclei assigned chemical shifts can be found in Table 6 and assigned proton chemical shifts in Table 7.

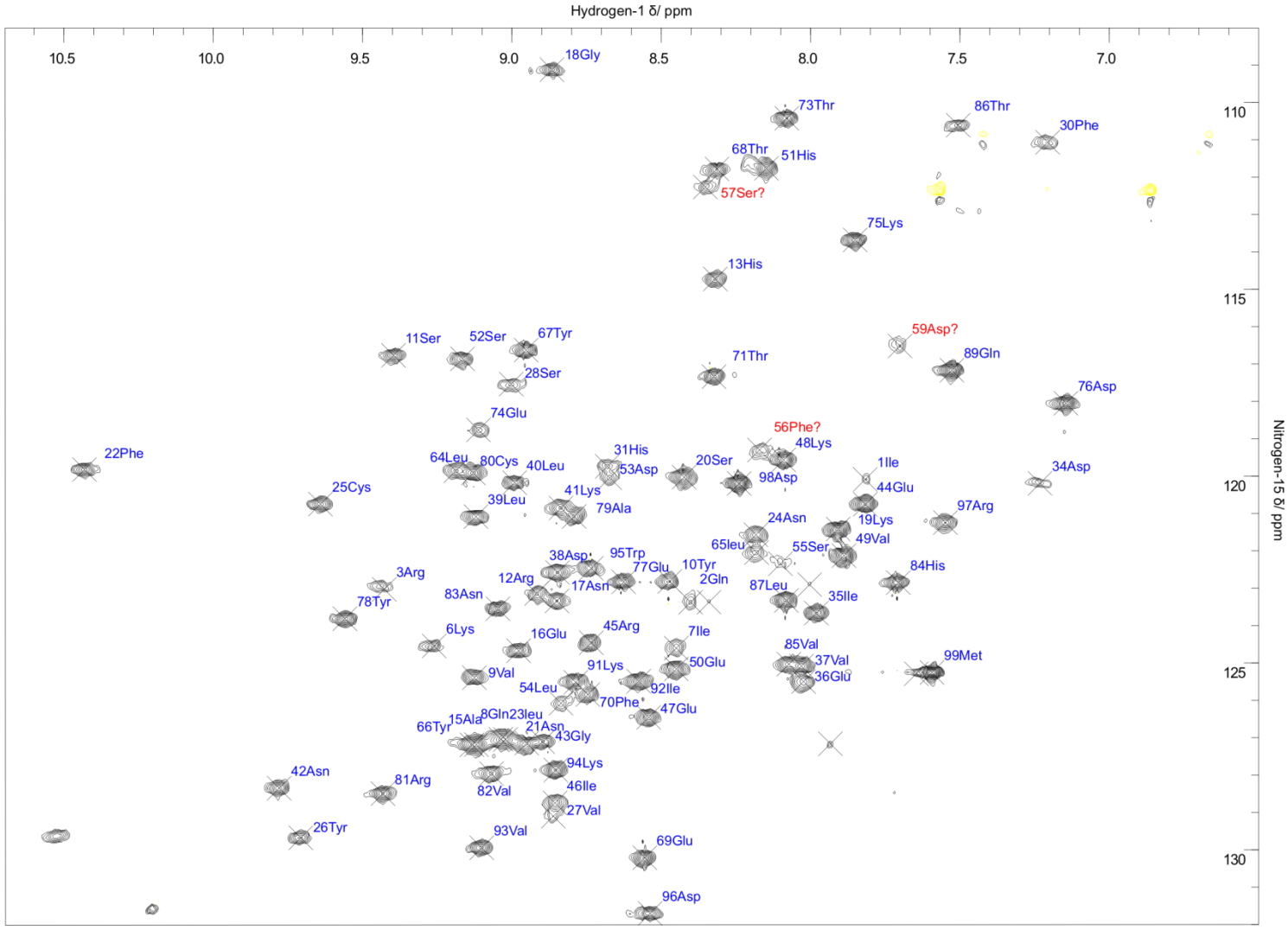

Figure 44 Assigned HSQC of 1 mM beta-2 microglobulin

Black peaks are NH correlations. Confident assignments are in blue. Red assignments are tentative. Yellow peaks are anti-phased NH2 peaks.

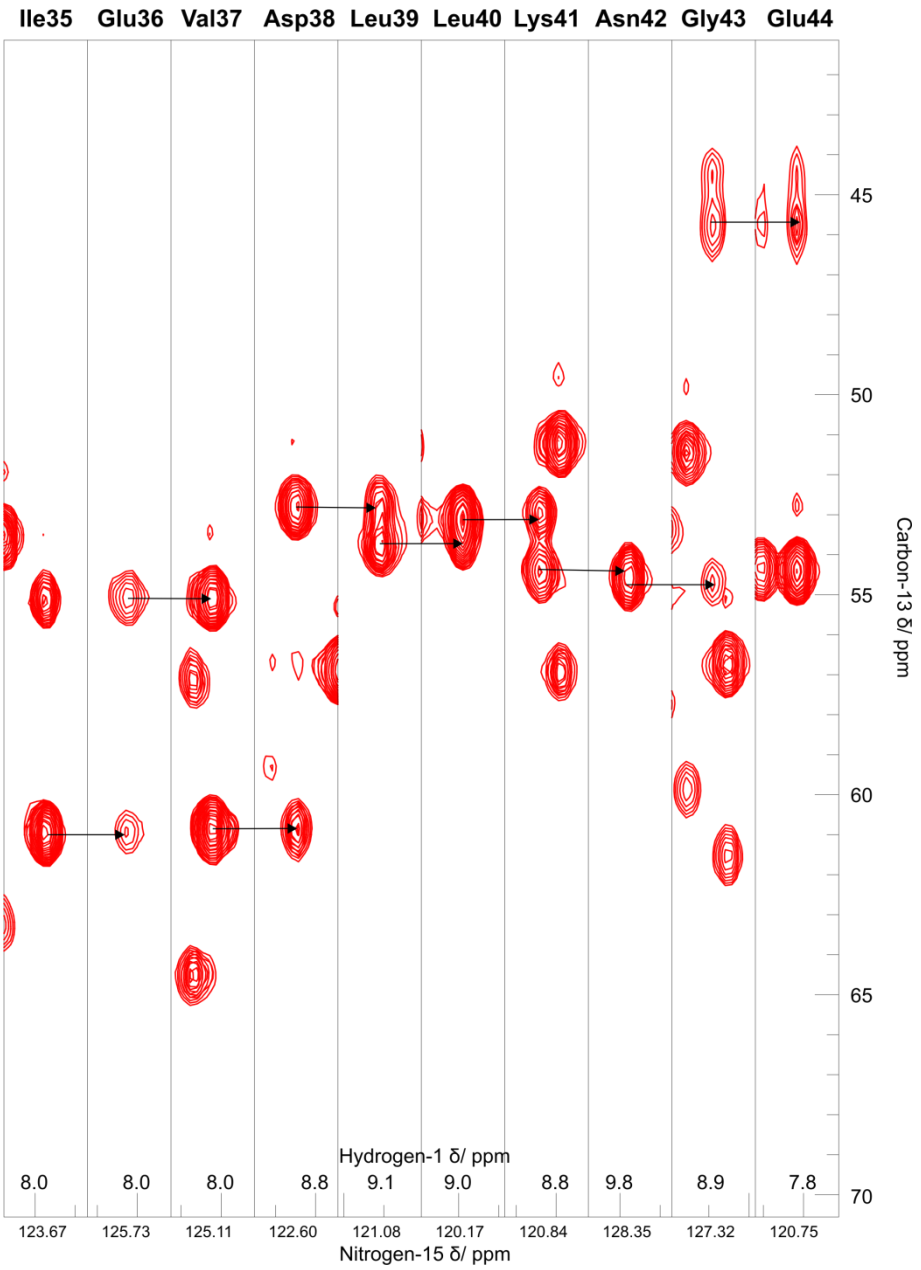

Figure 45 Representative strip plot from HNCA experiment on β_2m
Arranging the spectrum acquired in a HNCA experiment into a strip plot as shown above allows the sequential assignment of resonances. Each strip displays the Cα from the current residue (Stronger red peak) and the Cα from the previous residue (weaker red peak). Sequential assignment is achieved by aligning (shown with arrows) the strong current residue's peak on one peak with the weak peak corresponding to the same nucleus on another strip.

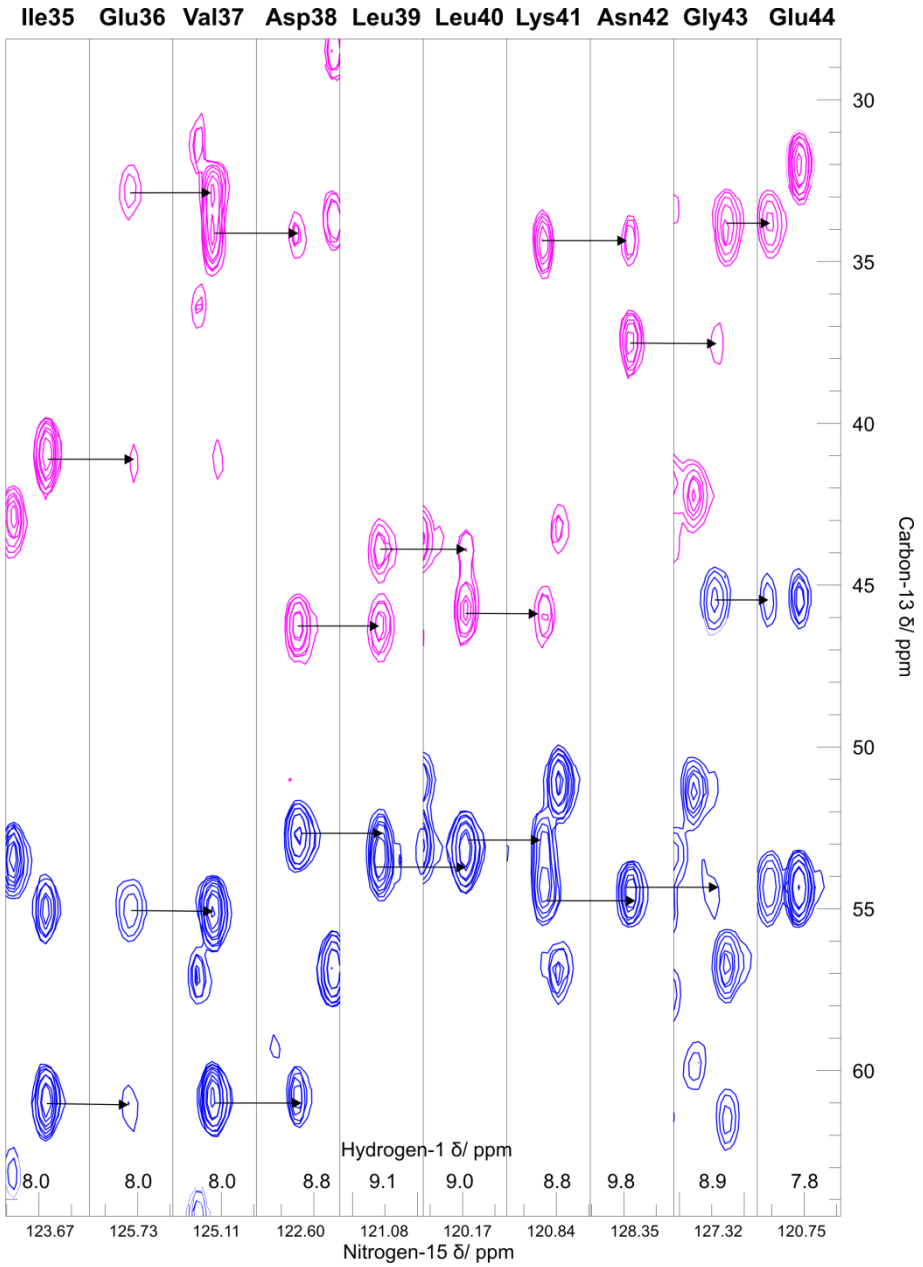

Figure 46 Representative strip plot from HNCACB experiment on β_2m.
Arranging the spectrum acquired in a HNCACB experiment into a strip plot as shown above allows the sequential assignment of resonances. Each strip displays the Cα (Strong blue peak) and Cβ (Strong pink peak) of that residue plus the Cα (weak blue peak) and Cβ(weak pink peak) of the previous residue. Sequential assignment is achieved by aligning (shown with arrows) the strong current residue's peak on one peak with the weak peak corresponding to the same nucleus on another strip.

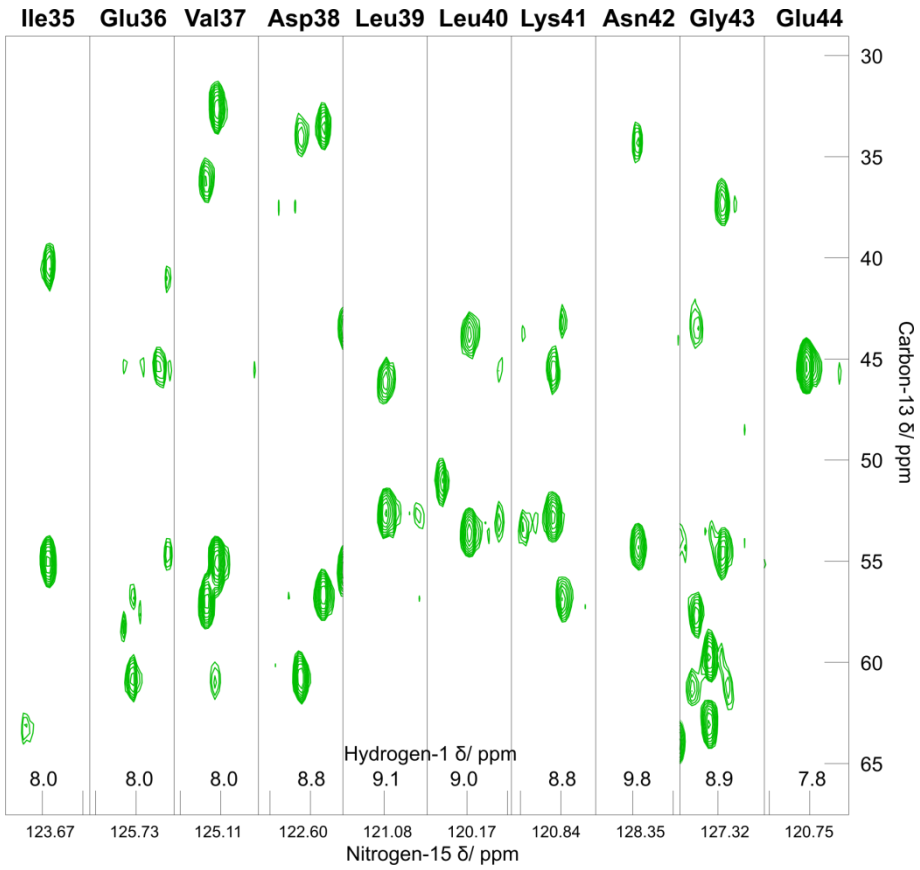

Figure 47 Representative strip plot from CBCA(CO)NH experiment.
Each strip from the CBCA(CO)NH experiment displays the Cα and Cβ peaks from the previous residue.

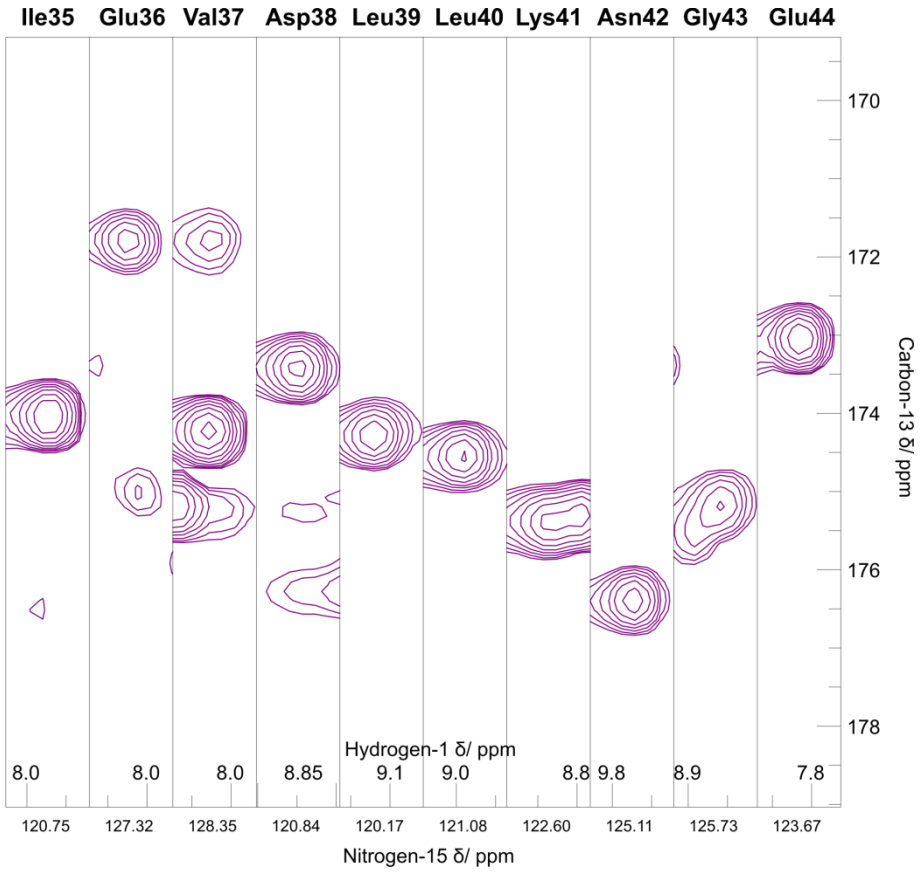

Figure 48 Representative strip plot from HNCO experiment
This experiment is used to determine the main chain carbonyl chemical shifts by correlating with the nitrogen that is shared with the alpha carbon of the same residue. The alpha carbon will be displayed on the corresponding strip of the HNCA experiment at the same nitrogen and proton shifts.

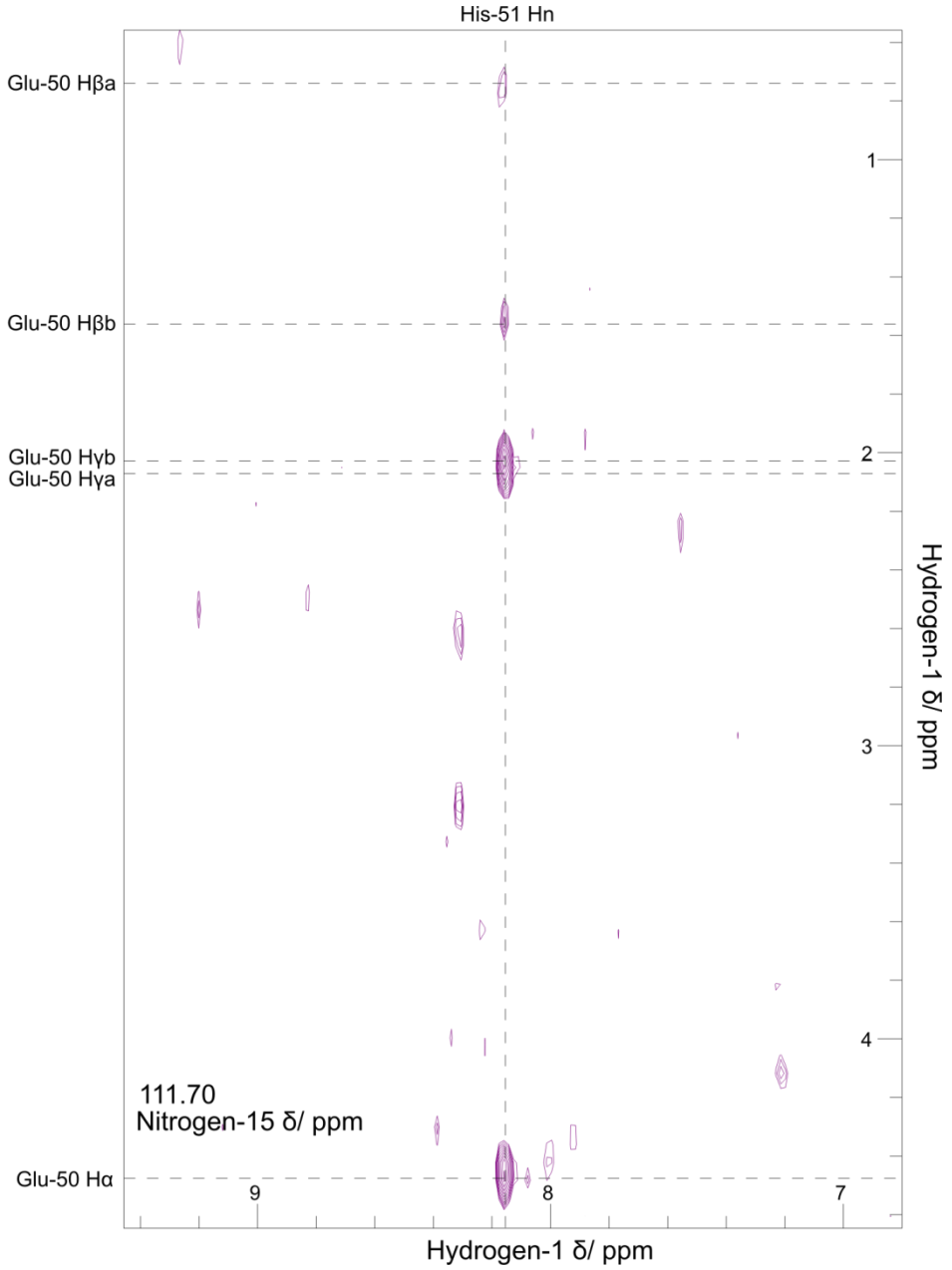

Figure 49 Representative plot from H(CCO)NH spectrum

The H(CCO)NH experiment is used to acquire main-chain and side-chain proton chemical shifts. The markers shown above will overlay with peaks on the HCCH-TOCSY at the chemical shift of the connected carbon.

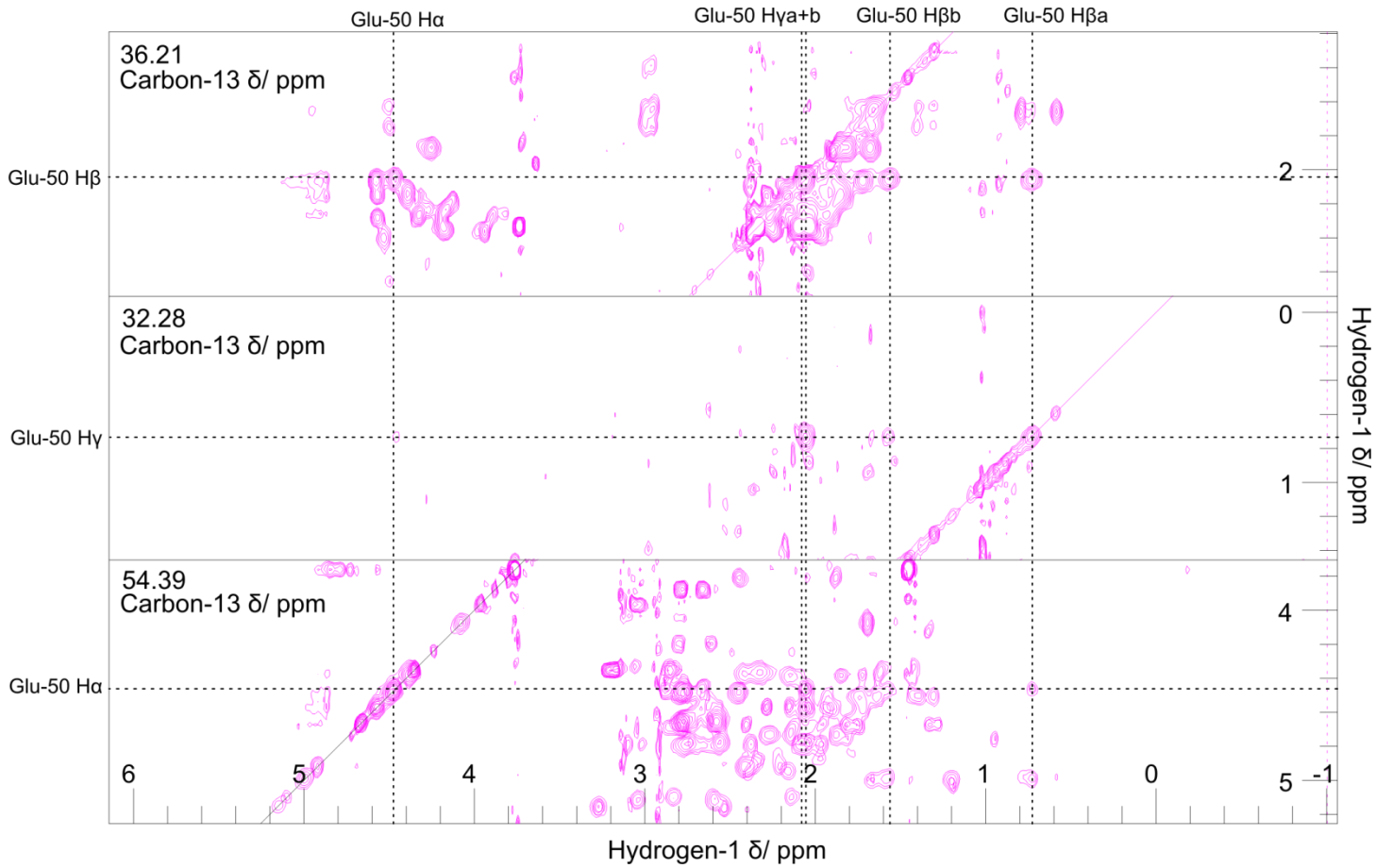

Figure 50 Representative plot of HCCH-TOCSY spectrum

The HCCH-TOCSY experiment is used to obtain the side-chain ^{13}C resonances. The dotted lines represent mark the chemical shifts of Glu-50 protons

Table 6 Chemical shifts of assigned carbon and amine nitrogen nuclei in β_2m at 25˚C

Chemical shifts of ^{15}N and ^{13}C nuclei assigned using 2D and 3D double and triple resonance hetero correlation experiments. Gray shading is used in cases of that nucleus type not being present in the corresponding residue. Pink shading is used for the loop region V-VI which are not expected to be observable in the spectra acquired due to the high mobility of this region when β_2m is not bound to the MHC I heavy chain. Missing chemical shifts were not able to be determined with the data acquired.

Residue	N_{amine}	C'	Cα	Cβ	$C\gamma_1$	$C\gamma_2$	$C\delta_1$	$C\delta_2$	Cε
1Ile	120.09	175.65	61.09	39.18	17.22				
2Gln	123.36	175.83	56.13	30.17	33.78				
3Arg	122.95		55.66	34.68					
4Thr									
5Pro		175.79	62.68	32.09	26.61		49.17		
6Lys	124.53	176.19	56.04	32.86	24.81				41.91
7Ile	124.58	174.88	61.46	41.99	18.71		14.38		
8Gln	126.96	173.81	55.09	33.47	35.82				
9Val	125.37	175.31	60.70	34.15	23.06	21.09			
10Tyr	122.79	173.33	56.30	39.28					
11Ser	116.75	174.72	56.52	65.17					
12Arg	123.11	175.36	59.35	33.55					
13His	114.84		52.65	30.76					
14Pro		176.84	64.06	31.65					
15Ala	127.19	176.84	53.27	20.00					
16Glu	124.64	175.16	55.21	32.76	36.26				
17Asn	123.32	177.38	50.92	56.96					
18Gly	109.11	173.43	45.52						
19Lys	121.38	175.26	54.34	33.79	24.79		28.9		43.08
20Ser	120.01	173.38	59.78	63.05					
21Asn	127.17	173.73	51.34	42.15					
22Phe	119.84	173.48	57.74	43.49					
23Leu	126.94	172.47	53.28	41.62	20.98		27.20	25.90	
24Asn	121.60	173.38	51.77	41.62					
25Cys	120.73	171.55	54.01	41.65					
26Tyr	129.67	174.45	56.33	41.36					
27Val	129.09	174.32	59.86	33.60	23.5	22.25			
28Ser	117.55		57.18	67.57					
29Gly		173.43	46.79						
30Phe	111.03	174.42	54.07	42.12					
31His	119.76		58.08	34.17					
32Pro									
33Ser		173.76	61.01	62.49					
34Asp	120.15	174.02	55.19	40.62					
35Ile	123.67	171.81	60.90	41.18	15.98	28.68	13.48		
36Glu	125.66	174.18	55.08	32.70	36.45				
37Val	125.14	173.44	60.82	34.19	22.10	20.9			

38Asp	122.60	174.28	52.66	46.23					
39Leu	121.08	174.55	53.64	43.86	27.39		26.14	24.89	
40Leu	120.18	175.33	52.96	45.68	26.93		23.18	26.93	
41Lys	120.83	176.39	54.37	34.37	25.25		30.25		42.75
42Asn	128.35	175.49	54.64	37.38					
43Gly	127.29	173.07	45.51						
44Glu	120.75	175.70	54.38	32.00	36.00				
45Arg	124.46	176.28	57.92	30.92	27.81		44.06		
46Ile	128.72	176.02	61.99	38.99	18.25	28.25	13.99		
47Glu	126.45	177.17	58.68	30.75	36.18				
48Lys	119.56	174.49	55.90	31.11	24.50		30.22		43.25
49Val	122.13	174.72	61.02	35.04	21.29	22.54			
50Glu	125.17	174.12	54.39	32.46	36.21				
51His	111.70	175.21	53.76	30.71					
52Ser	116.91		57.65	65.61					
53Asp	120.12	176.81	54.74	40.99					
54Leu	126.06	176.31	56.80	42.91	27.91		26.22	23.72	
55Ser	122.35		57.35						
56Phe									
57Ser									
58Lys									
59Asp									
60Trp									
61Ser									
62Phe									
63Tyr		174.09	56.54	40.43					
64Leu	119.85	173.27	55.86	46.66	27.37		25.80	25.80	
65Leu	122.01	175.03	53.94	46.78	28.50		23.50	26.00	
66Tyr	127.19	174.98	56.97	42.08					
67Tyr	116.61	173.59	55.98	41.47					
68Thr	111.81	171.42	60.22	70.19	18.96				
69Glu	130.21	175.72	56.78	30.05	36.30				
70Phe	125.82	171.74	55.39	41.10					
71Thr	117.32		58.67	70.18					
72Pro		174.93	63.13	32.09	26.87		51.88		
73Thr	110.42	175.22	60.16	72.93	21.67				
74Glu	118.78	177.84	59.07	30.13	37.01				
75Lys	113.68	176.81	56.48	34.02	24.00		30.25		43.29
76Asp	118.05	175.13	55.49	43.62					
77Glu	122.81	174.98	54.93	32.94	37.39				
78Tyr	123.79	175.28	56.94	43.41					
79Ala	121.07	173.65	51.10	24.35					
80Cys	119.89	171.22	53.06	43.67					
81Arg	128.48	174.02	53.77	33.97	26.47		43.97		
82Val	127.97	173.33	60.41	35.99	23.49	20.99			

83Asn	**123.53**	**172.86**	**51.25**	**41.73**					
84His	**122.85**	**175.22**	**57.08**	**36.37**					
85Val	**124.99**	**175.22**	**64.49**	**31.47**	**21.80**	**20.20**			
86Thr	**110.62**	**174.53**	**63.21**	**69.72**	**23.21**				
87Leu	**123.30**		**53.48**	**43.17**					
88Ser		**174.02**	**60.50**	**63.19**					
89Gln	**117.17**		**53.33**	**30.21**					
90Pro		**175.85**	**63.56**	**31.81**					
91Lys	**125.47**	**174.56**	**55.19**	**35.52**					**42.34**
92Ile	**125.49**	**175.82**	**60.42**	**38.97**	**27.67**		**15.89**		
93Val	**129.94**	**175.19**	**61.50**	**34.11**	**20.36**	**22.86**			
94Lys	**127.84**	**176.35**	**56.69**	**33.58**	**25.25**		**29.72**		**43.47**
95Trp	**122.46**	**174.46**	**56.99**	**28.37**					
96Asp	**131.69**	**175.16**	**52.97**	**41.85**					
97Arg	**121.24**	**175.63**	**56.81**	**30.04**	**25.04**		**43.79**		
98Asp	**120.20**	**175.25**	**54.72**	**41.31**					
99Met	**125.23**		**57.43**	**34.35**					

Table 7 Chemical shifts of assigned protons in β_2m at 25˚C

Chemical shifts of protons assigned using 2D and 3D double and triple resonance hetero correlation experiments. Gray shading is used in cases of that nucleus type not being present in the corresponding residue. Pink shading is used for the loop region V-VI which are not expected to be observable in the spectra acquired due to the high mobility of this region when β_2m is not bound to the MHC I heavy chain. Missing chemical shifts were not able to be determined with the data acquired.

Residue	H(N)	Hα	Hβ	Hγ	Hδ	Hε
1Ile	7.82	4.19	1.74	1.04,1.10,0.81	0.77	
2Gln	8.40	4.67	2.07,2.13	2.40,2.52		
3Arg	9.43					
4Thr						
5Pro		4.41	1.53	1.10	3.09,3.65	
6Lys	9.27	4.49	1.50,1.77	1.42,1.75		2.99
7Ile	8.45	4.74	1.65	0.75,1.43	0.74	
8Gln	9.04	4.92	2.37,2.21	2.43		
9Val	9.12	5.33	2.04	0.91,0.97		
10Tyr	8.47	5.30	3.19,3.41			
11Ser	9.39	5.26	4.44,3.66			
12Arg	8.91	3.87	1.97,1.74			
13His	8.32					
14Pro		4.51	1.94,2.43			
15Ala	9.11	4.07	1.67			
16Glu	8.98	4.38	1.85	2.10,2.15		
17Asn	8.84	4.49	2.68,2.78			
18Gly	8.86	3.51,4.19				
19Lys	7.91	4.67	1.75,1.82	1.26,1.32	1.63,1.57	3.07
20Ser	8.42	4.24	3.74,3.70			
21Asn	8.95	4.90	2.76,2.55			
22Phe	10.43	5.42	2.60,2.68			
23Leu	9.02	3.67	0.78,-0.85	-0.59	0.00, 0.66	
24Asn	8.18	5.38	1.42,1.82			
25Cys	9.64	5.15	3.26,2.53			
26Tyr	9.71	5.43	3.20,3.22			
27Val	8.86	5.17	1.92	0.77,0.91		
28Ser	9.00		3.80			
29Gly		3.85, 4.12				
30Phe	7.21	4.88	1.98, 2.34			
31His	8.67					
32Pro						
33Ser		3.50	3.29, 1.79			
34Asp	7.23	4.36	2.43, 2.34			
35Ile	7.97	4.55	1.41	0.67,1.49,0.58	-0.54	
36Glu	8.02	4.56	1.73, 1.91	2.09, 2.03		
37Val	8.13	4.61	0.43	0.48, 0.23		

38Asp	8.85	4.94	2.38, 2.15			
39Leu	9.11	4.99	1.66, 1.21	1.59	0.75, 0.70	
40Leu	8.99	4.98	0.78, 1.55	1.21	0.57, 0.39	
41Lys	8.84	4.37	1.41, 1.72	0.82, 0.56	1.61, 1.76	2.82,2.75
42Asn	9.78	4.35	2.89, 2.82			
43Gly	8.89	4.15, 3.31				
44Glu	7.82	4.56	1.93, 2.04	2.15, 2.28		
45Arg	8.74	4.14	1.62, 1.63	1.54, 1.31	3.05, 3.12	
46Ile	8.85	3.97	1.52	1.03,1.69,0.96	0.85	
47Glu	8.54	4.17	2.09, 2.02	2.23, 2.35		
48Lys	8.09	4.51	1.78, 1.94	1.42, 1.36	1.71, 1.68	3.01
49Val	7.89	4.38	2.11	1.08, 1.01		
50Glu	8.45	4.47	0.73, 1.56	2.05, 2.06		
51His	8.16	5.51	1.97, 2.43			
52Ser	9.18	4.67	4.08, 4.48			
53Asp	8.67	4.78	2.56, 2.76			
54Leu	8.84	4.33	1.67, 1.83	1.70	1.08, 0.86	
55Ser	8.09					
56Phe						
57Ser						
58Lys						
59Asp						
60Trp						
61Ser						
62Phe						
63Tyr		5.49	3.01, 2.84			
64Leu	9.18	4.62	2.01, 1.76	1.76	0.96, 1.04	
65Leu	8.18	5.47	1.54, 1.98	1.57	1.04, 0.80	
66Tyr	9.14	5.35	2.65, 3.05			
67Tyr	8.95	5.97	3.22, 2.61			
68Thr	8.31	4.86	4.09	0.92		
69Glu	8.55	4.26	1.81, 1.69	1.89		
70Phe	8.75	4.79	2.78, 2.68			
71Thr	8.32					
72Pro		4.57	2.41, 2.18	2.00, 1.40	4.00, 2.24	
73Thr	8.08	4.65	4.53	1.30		
74Glu	9.11	4.18	2.06, 2.10	2.25		
75Lys	7.85	4.44	1.83, 1.76	1.39	1.65	2.96
76Asp	7.14	5.10	2.12, 2.82			
77Glu	8.63	4.80	1.97, 2.09	2.37		
78Tyr	9.55	5.59	2.71, 2.80			
79Ala	8.79	5.03	1.17			
80Cys	9.13	5.10	2.59, 3.04			
81Arg	9.43	5.39	1.17, 1.79	1.33, 1.22	3.07, 2.89	
82Val	9.07	4.94	1.65	0.60, 0.78		

83Asn	9.04	5.18	2.41, 2.87			
84His	7.71	4.53				
85Val	8.07	3.97	1.95	0.86, 0.60		
86Thr	7.51	4.16	4.50	1.47		
87Leu	8.08					
88Ser		4.24	3.93, 3.98			
89Gln	7.53					
90Pro		4.47	1.82, 1.49	1.99, 1.78		
91Lys	8.78	4.50	1.74, 1.64	1.38, 1.32	1.66, 1.63	2.98, 2.95
92Ile	8.57	4.82	1.69	0.60,1.42,1.08	0.73	
93Val	9.10	4.30	1.86	0.92, 1.03		
94Lys	8.85	4.42	1.85, 1.80	1.43, 1.54	1.67	2.96, 2.99
95Trp	8.74	4.61	3.51, 2.61			
96Asp	8.54	4.48	2.78, 2.46			
97Arg	7.55	3.43	1.05, 1.41	1.15, 0.92	2.95, 2.90	
98Asp	8.24					
99Met	7.59					

There are many published structures of soluble β_2m in the literature, both in complex with MHC I and when not in complex, therefore a full structure was not required as part of this project. However as Cα and Cβ chemical shifts had already been acquired in order to map chemical shift changes between native and fibrillar β_2m, these could be used to predict the secondary structure of our recombinant β_2m. The chemical shift index (CSI) predicts secondary structure based on deviation of chemical shift from reference random coil values and was first developed to use α-CH proton chemical shifts (*124*) and then later developed to use Cα and Cβ chemical shifts (*125*). The values for the carbon shifts for amino acids measured in urea (the random coil chemical shifts) can be subtracted from carbon shifts gained experimentally for the studied protein. This results in a chemical shift deviation from the random coil value which when plotted against the residue number produces the chemical shift index. Large positive deviations for Cα and negative deviations for Cβ are characteristic of α-helices while negative Cα deviations and positive Cβ deviations are indicative of β-strand secondary structure. The CSI based on the data acquired from the

triple resonance experiments predicts seven regions of β-strands spaced along the length of the molecule (Figure 51). The secondary structure predicted correlates well with the published structures of β_2m (*58, 126*) which also have seven β-strands in the same regions as predicted by our chemical shift index. The good correlation with published structures adds validity to the chemical shifts that we have assigned and further demonstrates that we are working with the correctly folded protein.

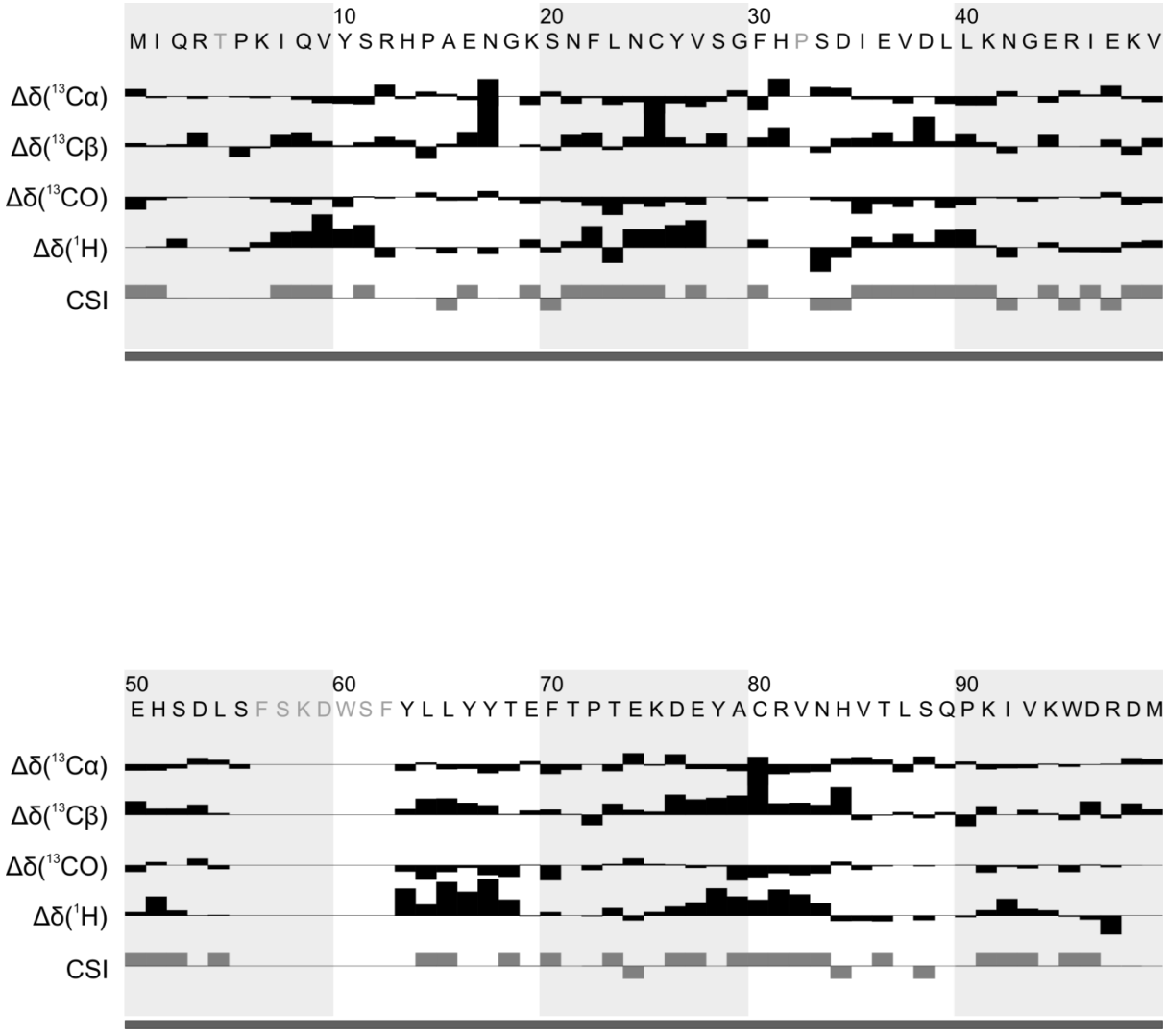

Figure 51 Chemical Shift Index of native β_2m
The chemical shift index predicts secondary structure based on deviation of chemical shift from reference random coil values. Letters at top of the CSI are the single letter code of the residues in the primary structure. Bars extending below the line in the CSI row predict residues in alpha helices while bars extending above the line predict residues in beta strands.

3.4 Soluble β_2m in presence of SAP

To explore whether there is an interaction between soluble β_2m and SAP, HSQC NMR spectra of β_2m in absence and presence of a 10 x SAP (wrt monomeric) excess were acquired. An interaction between SAP and β_2m could result in peak shifts due to changes in electrostatic environment brought about by the binding of SAP. Exchange processes between the SAP bound and free form of β_2m could give rise to changes in the spectra, depending on what timescale these exchange processes take place on. Exchange is a kinetic process between two or more states. These can be conformational exchange in which a molecule exchanges between two or more conformations, such as the *cis*/*trans* state of proline, or chemical exchange where a chemical reaction takes place, such as a SAP binding to β_2m. Exchange is measured in Hertz and is classified according to its rate in respect to the difference in chemical shifts between the different states. In slow exchange the rate of exchange is much smaller than the difference in chemical shift between the two states. Slow exchange leads to two separate peaks each corresponding to the chemical shift of each separate state. The intensities of the peaks are proportional to the population of the states. In fast exchange the rate of exchange is much larger than the difference in chemical shift and leads to one peak that is the average of the two chemical shifts. During cases of intermediate exchange the transition between the signals for fast and slow exchange takes place and broad and often non-observable signals result. Most exchange will lead to an increase in line-width except in cases of very fast exchange or very slow exchange. The perturbations in chemical shift and intensity changes associated with exchange can be easily identified by overlaying HSQC spectra of β_2m with and without SAP (Figure 52). The peaks corresponding to the following residues all reduce in intensity: Arg-12 (60.3% reduction), Phe-22 (32.9% reduction), His-31 (36.4% reduction), Lys-48 (17.9% reduction)

and His-51 (29.3% reduction). The chemical shifts of the following peaks change: Glu-16, Lys-75 and Val-82. The peaks corresponding to Asp-76 and Gln-89 have small secondary peaks appear near them which could be indicative of slow exchange. These perturbations have been mapped out onto a model of β_2m in Figure 53. There is an increase in intensity in the peaks corresponding to the side-chain nitrogens of glutamine and asparagine; this could be due to a slowing of molecular dynamics in these side-chains leading to narrowing of peaks because of decreased transverse relaxation. This decrease in dynamics could be due to steric hindrance of the side-chains by the proximity of SAP if binding is occurring. It can be ascertained from these spectra that there is not a strong interaction between the two proteins as if there were the total correlation time of the molecule would vastly increase leading to severe line broadening (*127*); β_2m's effective molecular weight would increase from ~12 kDa to ~137 kDa almost certainly leading to β_2m's peaks not being visible in the spectrum when bound to SAP.

Figure 52 HSQC of β_2m overlain with β_2m in 10 x excess of SAP

HSQC spectra were acquired of 30 µM ^{13}C ^{15}N β2m (black) and 30 µM ^{13}C ^{15}N β_2m in 300 µM (10 x excess) of unlabelled SAP (red). Buffer conditions: 600 mM NaCl, 200 mM $CaCl_2$, 10 mM Tris-HCl, 0.1% NaN_3. pH 7.0. Spectra acquired on Varian 600 MHz Inova at 25˚C.

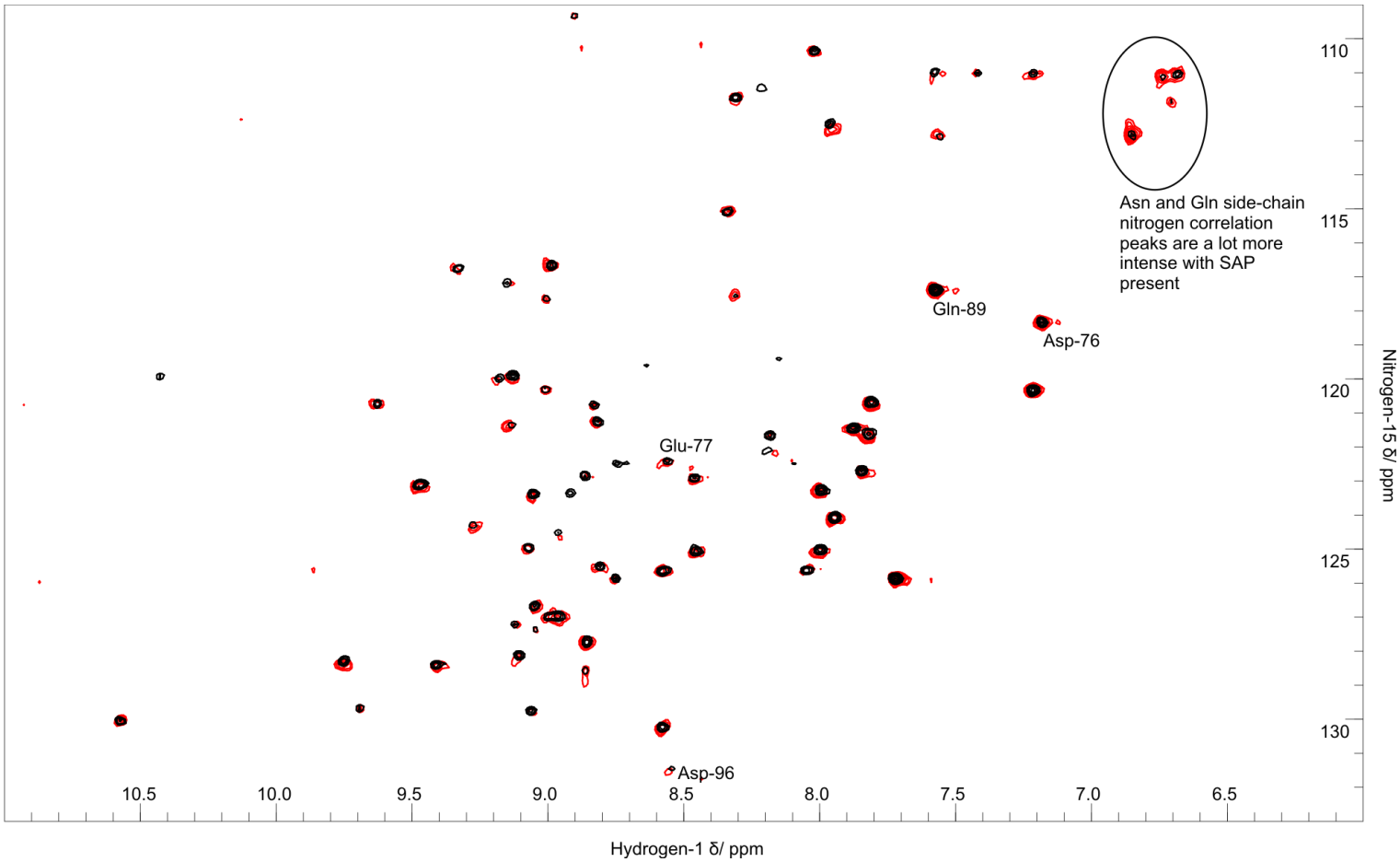

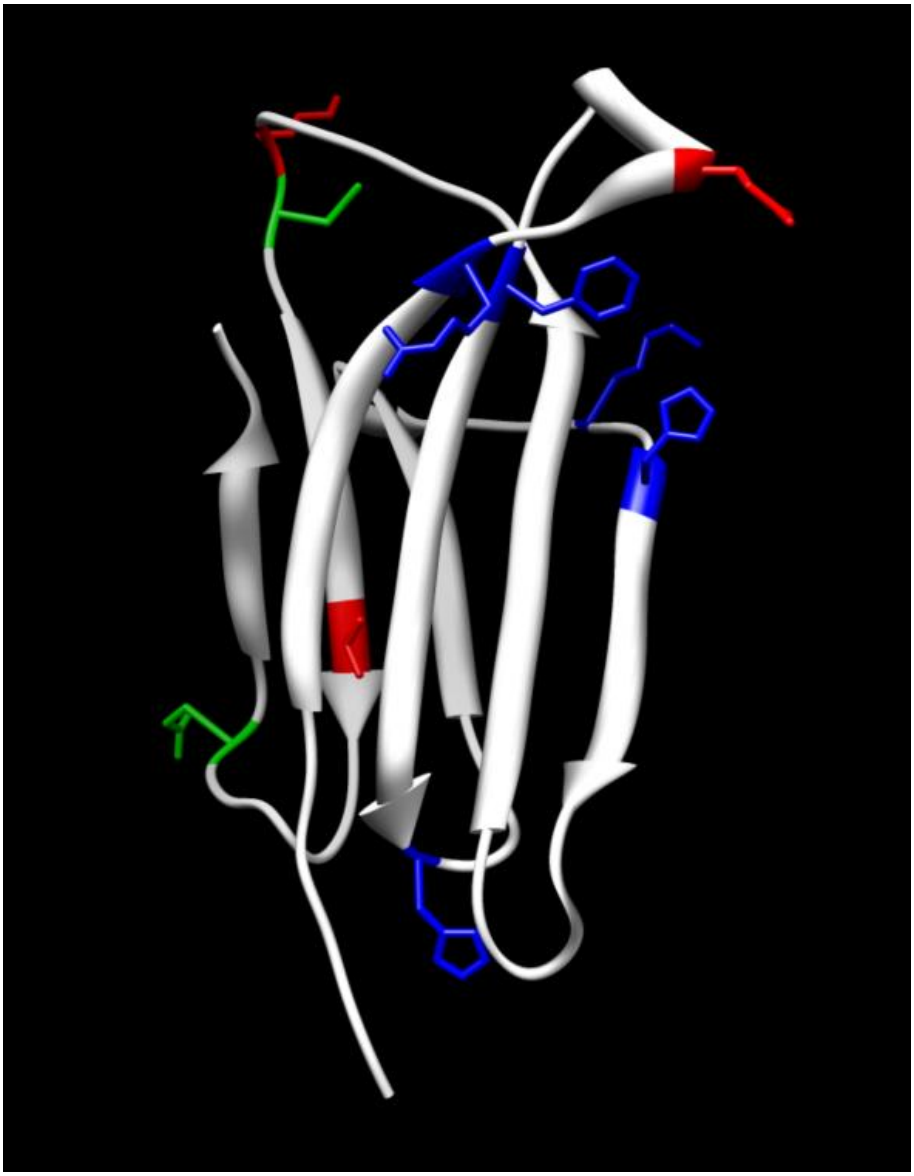

Figure 53 Ribbon diagram of monomeric β_2m showing residues whose resonances display perturbations in the presence of SAP

The HSQC overlay of β_2m only and β_2m with SAP spectra showed few significant differences. Residues displaying a difference in intensity (blue), chemical shift (red) or those that developed secondary peaks near them (green) have been mapped onto the model of monomeric β_2m above (PDB code: 1LDS).

3.5 Conclusion

Liquid state NMR confirms that we have a well folded protein which gives HSQC spectra similar, if not identical, to those acquired by other groups working on β_2m (Jahn, presentation at CCPN conference, 2009).

The experiments conducted have enabled us to identify 85.4% of the resonances arising from the β_2m and of the unassigned resonances 48.6% of them are located in the loop region between β-strands V and VI. This is the loop region that non covalently binds with the alpha 1 domain of the MHC-1 complex(*59*) and our results show that whilst not in complex with MHC 1 this region is likely to be highly mobile resulting in extremely broad peaks that disappear into the noise. Excluding the loop region and ring carbons 80% of the side-chain carbons have been assigned through use of the HCCH-TOCSY experiment. The assignment of the main and side-chain chemical shifts in the liquid state has allowed the direct comparison of native and fibrillar β_2m chemical shifts through the creation of simulated PDSD spectra which will be presented and discussed in chapter 4.

Chemical shift index calculations from our assigned backbone resonances predict that the structure has seven areas corresponding to β-strands and their locations are in good agreement with those in the literature calculated through X-ray diffraction (*58*) and ^{1}H NMR (*57*).

The SAP-β_2m HSQC overlay provides evidence that there is no strong interaction between soluble β_2m and SAP but the possibility of a weak interaction cannot be ruled out at this time and further investigation could be undertaken. However as no interaction between soluble β_2m and SAP has been reported from *in vivo* or *in vitro* studies and following the co-operative binding model that will be discussed later in chapters 5 and 6 there is no reason why an interaction between the two should be suspected.

Chapter 4

4 Solid-state NMR studies of beta-2 microglobulin

4.1 Introduction

In dialysis related amyloidosis natively soluble β_2m undergoes a transition into insoluble amyloid fibrils which then forms a complex with SAP potentially resulting in the persistence of β_2m amyloid within the body. We aimed to characterise the structure of these fibrils and identify the amino residues which interact with SAP when the two proteins are in complex. Lack of long range three dimensional order makes identifying the protein interactions in amyloid fibrils through X-ray diffraction studies difficult, however by monitoring changes in the electrostatic environment of nuclei through NMR we can identify which residues of β_2m come into contact with SAP. In liquid state NMR small (<30 kDa) molecules tumble rapidly in solution. This rapid tumbling averages out interactions that are dependent on the orientation of the molecule with respect to the static magnetic field; so called anisotropic interactions. These anisotropic interactions include chemical shielding and through space dipolar couplings. Due to the insoluble nature of fibrils and subsequent lack of molecular tumbling β_2m fibrils cannot be studied by liquid state NMR; to overcome this size limitation we can employ solid-state NMR methods which allow us to exploit the information the anisotropic interactions contain about the structure and dynamics within the fibrillar structures.

Here we have employed magic-angle spinning NMR as an attractive alternative for studying fibril structure at atomic resolution. By spinning a sample at an angle of 54.7˚ in

a magnetic field anisotropic interactions are averaged, which can reduce line widths to <0.4 ppm. The magic angle spinning was used in combination with multi-dimensional experiments which enabled the correlation of resonances from individual sites within the protein that are in close proximity; this allowed the sequential assignment of resonances. The assignment of peaks has aided in the characterisation of the SAP-fibril interaction site.

The majority of studies in this chapter are a necessary prelude for the characterisation of the fibril-SAP interface described later in chapter 5; studies of β_2m fibrils at low pH increase fibril stability and allow the sample to be hydrated to a greater extent. This greater hydration leads to better resolution and an increase in the amount of assignments possible through use of neutral pH samples alone. As well as for assignment purposes spectra acquired of fibrils at acidic pH were also used for comparative purposes with spectra simulated from the liquid-state data described in chapter 3 and the assignments from β_2m K3 fibrils published by Iwata *et al.* (*84*).

The β_2m fibrils used in this study are produced *in vitro* by lowering the pH of recombinant β_2m which has been refolded from β_2m expressed as bacterial inclusion bodies (As described in chapter 2). It was widely believed that within these inclusion bodies the proteins were misfolded and functionally inactive. However, a number of studies have revealed that for some proteins there is at least a population of proteins within the inclusion bodies which are functionally competent (*128, 129*).

Recent studies have focused on the similarities between inclusion bodies and amyloid fibrils (*130*), such as those found in a number of diseases including localised conditions such as Alzheimer's and Parkinson's through to systemic conditions including reactive systemic amyloidosis and dialysis related amyloidosis (*1, 3*). These studies have revealed

that upon the expression of a diverse range of proteins in *E.coli*, the inclusion bodies formed have many of the properties associated with the formation of amyloid deposits including the characteristic spectral changes associated with the binding of the dyes Congo-Red and Thioflavin T (*1, 3*) and the diffraction patterns characteristic of the cross-β structure typically found in amyloid fibrils (*130*). In the case of the yeast prion, Het-S, a protein with a propensity to form amyloid fibrils, these studies have been complemented by solid-state NMR studies which indicate that at a molecular level within the inclusion bodies the protein adopts an identical conformation with little structural heterogeneity (*131*). These observations have led to the speculation that inclusion bodies and amyloid deposits may share a common functional role, namely the sequestration of misfolded protein to prevent damage to the host.

In the course of this work we have undertaken and published a study (*132*) of β_2m in inclusion bodies that are formed upon expression in *E.coli*, comparing their amyloid properties with β_2m fibrils produced under low salt acidic conditions.

4.2 NMR Experiments

4.2.1 Sample preparation and experimental parameters

Fibrillar β_2m was prepared as described in chapter 2 and the preparation of each sample is summarised in Table 8 below.

Experiment	Labelling scheme	Buffer	Packing	Spectra
Uniformly labelled acidic β_2m fibrils PDSD (20 ms mixing)	U ^{13}C6 D-Glucose ^{15}N Ammonium Chloride	25 mM KCl 25 mM Na-Citrate 5 mM HEPES 0.05% w/v Na-Azide pH 2.5	Centrifuged at 50000 *g*, Pellet loaded into 3.2 mm MAS rotor with spatula and rod	Figure 58
Uniformly labelled acidic β_2m fibrils PDSD (100 ms mixing)	U ^{13}C6 D-Glucose ^{15}N Ammonium Chloride	25 mM KCl 25 mM Na-Citrate 5 mM HEPES 0.05% w/v Na-Azide pH 2.5	Centrifuged at 50000 *g*, Pellet loaded into 3.2 mm MAS rotor with spatula and rod	Figure 59
Uniformly labelled neutral pH β_2m fibrils PDSD (100 ms mixing)	U ^{13}C6 D-Glucose ^{15}N Ammonium Chloride	25 mM KCl 10 mM HEPES pH 7.4	Pellet washed with buffer in filtered tip. Loading pellet into 3.2 mm MAS rotor with spatula and rod	Figure 60
Uniformly labelled acidic β_2m fibrils NCA/NCO	U ^{13}C6 D-Glucose ^{15}N Ammonium Chloride	25 mM KCl 25 mM Na-Citrate 5 mM HEPES 0.05% w/v Na-Azide pH 2.5	Centrifuged at 50000 *g*, Pellet loaded into 3.2 mm MAS rotor with spatula and rod	Figure 61 (NCA) Figure 62 (NCO)
[2-^{13}C] glycerol Selectively and extensively labelled β_2m fibrils PDSD (500 ms mixing)	[2-^{13}C] Glycerol ^{15}N Ammonium Chloride	25 mM KCl 25 mM Na-Citrate 5 mM HEPES 0.05% w/v Na-Azide pH 2.5	Centrifuged at 50000 *g*, Pellet loaded into 3.2 mm MAS rotor with spatula and rod	Figure 64
[1,3-^{13}C] glycerol Selectively and extensively labelled β_2m fibrils PDSD (500 ms mixing)	[1,3-^{13}C] Glycerol ^{15}N Ammonium Chloride	25 mM KCl 25 mM Na-Citrate 5 mM HEPES 0.05% w/v Na-Azide pH 2.5	Centrifuged at 50000 *g*, Pellet loaded into 3.2 mm MAS rotor with spatula and rod	Figure 65
[1,3-^{13}C] glycerol Selectively and extensively labelled β_2m fibrils. NCA/NCO	[1,3-^{13}C] Glycerol ^{15}N Ammonium Chloride	25 mM KCl 25 mM Na-Citrate 5 mM HEPES 0.05% w/v Na-Azide pH 2.5	Centrifuged at 50000 *g*, Pellet loaded into 3.2 mm MAS rotor with spatula and rod	Figure 66 (NCA) Figure 67(NCO)
[2-^{13}C] glycerol Selectively and extensively labelled β_2m fibrils. NCA/NCO	[2-^{13}C] Glycerol ^{15}N Ammonium Chloride	25 mM KCl 25 mM Na-Citrate 5 mM HEPES 0.05% w/v Na-Azide pH 2.5	Centrifuged at 50000 *g*, Pellet loaded into 3.2 mm MAS rotor with spatula and rod	Sample destroyed
[1,3-^{13}C] glycerol Selectively and extensively labelled β_2m fibrils. H/D exchange NCA/NCO	[1,3-^{13}C] Glycerol ^{15}N Ammonium Chloride	25 mM KCl 25 mM Na-Citrate In 100% D_2O pD 2.5	Centrifuged at 50000 *g*, Pellet loaded into 3.2 mm MAS rotor with spatula and rod	Figure 68 (NCA)

Table 8 Composition of fibrillar β_2m samples for solid-state MAS experiments

4.2.2 Proton Driven Spin Diffusion (PDSD) NMR experiments

The Proton Driven Spin Diffusion (PDSD) is one of many broadband recoupling experiments which reintroduce the homonuclear dipolar couplings between low-γ nuclei (such as ^{13}C and ^{15}N) across a broad range of chemical shifts, an interaction which is typically lost when performing magic-angle spinning. In combination with magic angle spinning, PDSD facilitates assignment of proteins, allowing correlations between proximal low-γ nuclei through the transfer of magnetisation via spin-diffusion. Spin-diffusion describes polarisation exchange in a strongly coupled spin system, which under appropriate conditions can resemble a diffusion process. Typically the rate of spin-diffusion is dependent on two properties. Firstly the strength of the dipolar couplings that exist between the labelled sites within the biopolymers, with stronger couplings and more extensive labelling resulting in a higher rate of spin-diffusion and secondly, the distribution of chemical shifts with small variation making the exchange process energy conserving and thereby increasing the rate of spin diffusion. Typically low-γ nuclei, such as carbon-13, have weak couplings and a large distribution of chemical shifts. These conditions make the measurement of spin-diffusion between low-γ nuclei unfavourable, however in the case of proton-driven spin-diffusion, by coupling the low-γ nuclei to an external reservoir such as the surrounding protons with their strong network of dipolar couplings and relatively small chemical shift dispersion the rate spin diffusion is significantly enhanced (*103*). The ^{13}C PDSD spectrum is two- dimensional with carbon chemical shift on both axis and shows through space correlations between carbon-13 nuclei. This means at short mixing times one bond correlations are seen allowing the identification of adjacent atoms. Adjustment of the mixing time and allowing the spins to diffuse further leads to correlations between nuclei of adjoining residues being identified. These factors facilitate

assignment of resonances to specific atoms. For one bond correlations we employed a mixing time of 20 ms and for the complete side-chains we employed a mixing time of 100 ms.

The pulse sequence for a PDSD experiment was implemented as follows; the proton magnetisation was excited with a 3.5 μs pulse. The magnetisation was then transferred to the carbon-13 by means of ramped cross-polarisation, the proton spin lock field centred on 75 kHz and the carbon-13 amplitude was adjusted to fulfil the Hartmann-Hahn condition and ensure optimal magnetisation transfer. The magnetisation on the carbon-13 was then allowed to evolve during t_1 under 85 kHz SPINAL proton decoupling (*102*). A 3.5 μs 90˚ pulse subsequently stores the magnetisation along the z-axis and the proton decoupling is turned off during the mixing period which was varied in order to acquire either short or longer range ^{13}C-^{13}C correlations. At the end of the mixing period a second 3.5μs pulse restores the magnetisation back to the transverse plane and FID is detected during the period t_2 under 85 kHz SPINAL proton decoupling. A schematic of the pulse sequence can be seen in Figure 54. Phase sensitive two-dimensional data sets were acquired with TPPI (*133*).

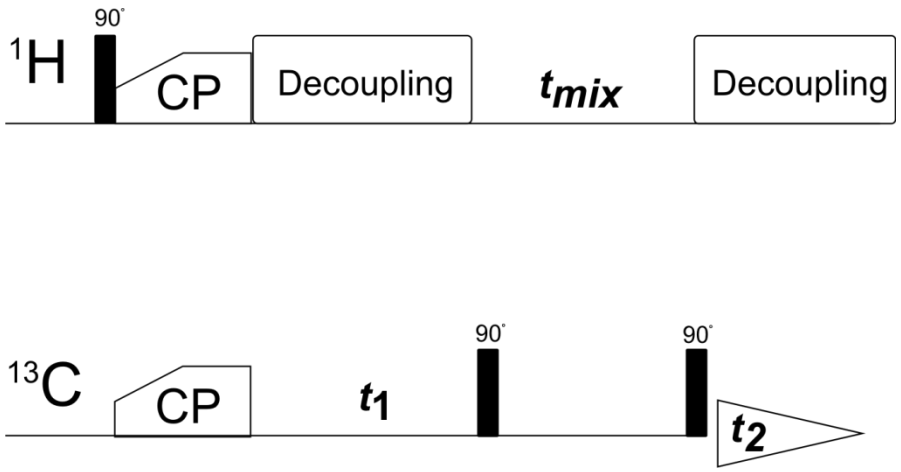

Figure 54 Pulse sequence for cross-polarised Proton Driven Spin Diffusion NMR experiment The top line represents pulses applied on the proton frequency and the bottom line pulses applied on the ^{13}C frequency. The narrow black rectangles represent 90˚ applied pulses. The first evolution period is t_1. Ramped boxes containing 'CP' are contact pulses for cross-polarisation. t_{mix} is themixing time. The FID is represented by t_2. Decoupling pulses are represented by boxes marked decoupling.

4.2.3 HXYCP NMR experiments

The HXYCP experiments are used to correlate different low γ nuclei within a protein. They are analogous to liquid state triple resonance experiments with the exception that they are detected on ^{13}C and not protons due to the resolution issues associated with solid-state ^{1}H NMR of fibrillar proteins. In the NCA/NCO experiments, magnetisation is transferred from the ^{1}H to ^{15}N using a ramped cross polarisation, using a 3.5 μs pulse to excite the proton magnetisation and a proton spin-lock field centred on 75 kHz. The nitrogen magnetisation then evolves under the chemical shift. The chemical shift is evolved on the ^{15}N nuclei in the indirect dimension under proton SPINAL proton decoupling (85 kHz) during the period t_1 and instead of magnetisation being transferred from ^{15}N to all connecting ^{13}C nuclei as in the classic HXY-CP experiment (*134*), it is selectively transferred to either the $^{13}C\alpha$ or $^{13}C'$ using specific cross-polarisation achieved through irradiation of selected areas of the spectrum with a low power (30 kHz) rf contact pulse while other areas dephase; this allows directed transfer of magnetisation and improved signal to noise as magnetisation is not split between both sites (*135*). During

specific cross-polarisation, decoupling is switched from SPINAL to continuous wave (100 kHz), reducing any cross-polarisation to the protons through the presence of phase transients. An FID is then acquired during the period t_2 under SPINAL proton decoupling (85 kHz). A schematic of a HXY-CP two-dimensional experiment can be seen in Figure 55. These experiments are used in conjunction with the PDSD experiment to sequentially assign proteins as in **Error! Reference source not found.**.

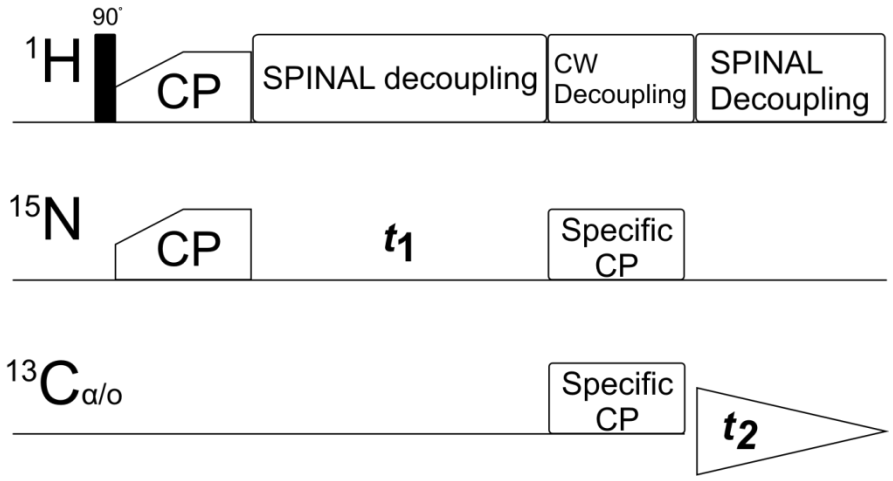

Figure 55 Pulse sequence for specific HXYCP NMR experiment
The top line represents pulses applied on the proton frequency, the middle line ^{15}N and the bottom line pulses applied on either the ^{13}Cα or ^{13}C' frequency depending on the experiment. The narrow black rectangles represent 90˚ applied pulses. Ramped boxes containing 'CP' are contact pulses for cross-polarisation. t_1 is the first evolution period. Decoupling pulses are represented by boxes marked decoupling. Boxes marked 'Specific CP' represent low power contact pulses from specific cross-polarisation. The FID is represented by t_2

4.2.4 NCACX/NCOCX 3D NMR experiments

The NCACX and NCOCX experiments are commonly used for the identification of spin systems and the sequential assignment of resonances. They vastly decrease spectral crowding and therefore are an effective experiment for structure determination of large fibrillar proteins whose spectra in two dimensions are too crowded to yield a substantial assignment. The NCACX experiment correlates the amide nitrogen with the aliphatic

carbons, while the NCOCX experiment correlates the amide nitrogen with intra residue carbonyl carbon and aliphatic carbons of the previous residue, allowing for sequential assignment and disambiguation of resonances. Magnetisation starts on the protons and is put into the transverse plane with a 90˚ pulse. It is transferred from protons to ^{15}N nuclei via Hartmann-Hahn cross polarisation, followed by evolution on the ^{15}N nuclei under proton SPINAL decoupling before being specifically transferred to either ^{13}Cα or ^{13}C' nuclei during which the proton decoupling is switched to continuous wave. This part of the pulse sequence is exactly analogous to a NCA/NCO experiment except that the magnetisation is allowed to evolve on the ^{13}Cα/^{13}C' under SPINAL decoupling. After evolution a PDSD step is used to propagate magnetisation to nearby in space ^{13}C nuclei and an FID is then acquired under SPINAL proton decoupling in the period t_3. Figure 56 shows the pulse sequence for the NCACX/NCOCX experiment. A full an in depth account for the experiment has been published by Jutta Pauli in 2001 (*136*).

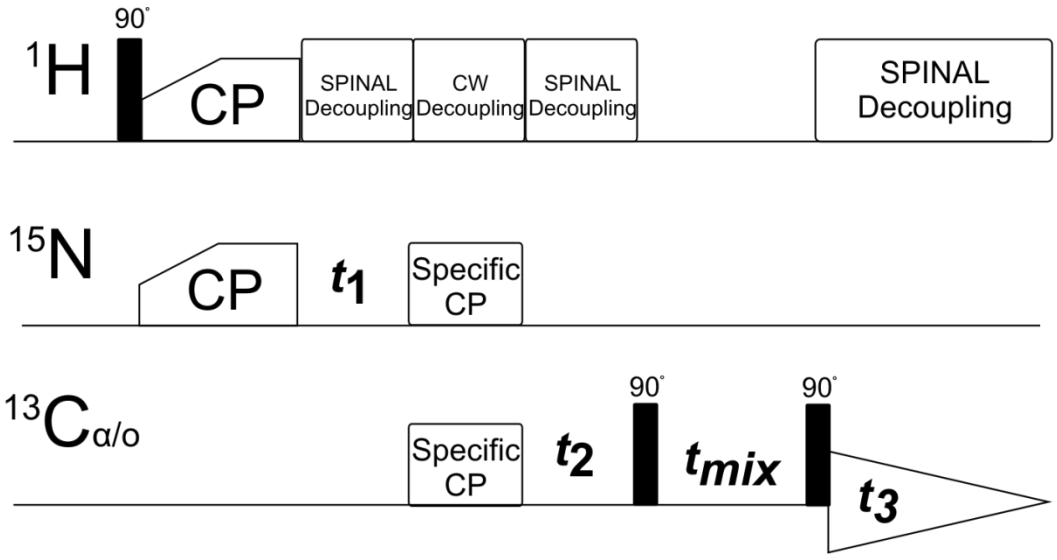

Figure 56 Pulse sequence for NCACX/NCOCX 3D NMR experiment

The top line represents pulses applied on the proton frequency, the middle line ^{15}N and the bottom line pulses applied on either the ^{13}Cα or ^{13}C' frequency depending on the experiment. The narrow black rectangles represent 90˚ applied pulses. Ramped boxes containing 'CP' are contact pulses for cross-polarisation. t_1 is the first evolution period. Decoupling pulses are represented by boxes marked decoupling. Boxes marked 'Specific CP' represent low power contact pulses from specific cross-polarisation. t_2 is the second evolution period. t_{mix} is mixing time The FID is represented by t_3.

4.2.5 PDSD simulations

Chemical shift assignment experiments can be used to create simulated PDSD NMR spectra. This allows a visual comparison of the chemical shifts distributions and correlations to be made between existing published liquid and solid data and newly acquired spectra without the need for a complete assignment. The simulations can be used to identify nuclei whose electrostatic environment has changed by overlaying the simulation onto acquired spectra. In cases where changes have not been observed it could be possible that the simulated peak and the acquired peak represent the same correlation and therefore a tentative assignment of the acquired peak may be possible. PDSD data have been simulated in the frequency domain using custom algorithms in C++ using the GAMMA programme (*137*) and analysed in Matlab (Mathworks). The data are simulated assuming one bond correlations and approximate to short mixing time PDSD spectra. These simulations ignore any motional averaging and differences in polarisation transfer that may experimentally lead to weak signal intensity in experimental spectra.

4.3 Employing selective and extensive isotopic labelling

Homo and heteronuclear two dimensional NMR spectra of uniformly labelled samples are crowded and suffer from spectral overlap in all but the smallest of proteins, making extensive resonance assignment difficult in these spectra. The lack of resolving power from amide proton frequencies which is available in liquid-state NMR means that XXY 3D experiments are desirable. However, 3D experiments have proved difficult on this protein due to limited acquisition time available at 850 MHz compounded by the relatively poor transfer of magnetisation between sites which has limited the acquisition of high quality

three dimensional spectra. In order to address this problem we have used an assignment procedure that both decreases overlap in the spectra and improves resolution.

This assignment procedure is based on the extensive and selective labelling that occurs when samples are prepared with [1,3-^{13}C]and [2-^{13}C]-glycerol as the sole carbon source in the bacterial growth medium. This labelling scheme has been successfully used before by Castellani in the assignment of the α-spectrin Src homology 3 domain (SH3) (*138*) as well as directly on fibrils in 2008 with the CA150.WW2 domain by Johanna Becker (*139*).

The use of selectively labelled glycerol to grow recombinant bacteria results in the site specific labelling of the amino acids produced by those bacteria. The specificity of the labelling depends on how those amino acids are produced. Amino acids derived from either the glycolytic or pentose phosphate pathways (alanine, cysteine, glycine, histidine, leucine, phenylalanine, serine, tryptophan, tyrosine and valine) have each specific site either ^{12}C or ^{13}C labelled in near 100% of cases (Figure 57a, c, d). The remaining amino acids are produced from precursors in the citric acid cycle and give rise to non- random mixtures of isotopomers (Figure 57b, d, e).

The specific labelling of amino acids allows resonances to be assigned due to the unique cross-peaks that will occur between spins within certain residues. For instance valines will be unique in having strong Cα-Cβ crosspeaks in the PDSD spectrum acquired from protein produced with [2-^{13}C]-glycerol. In addition the reduced amount of labelled spins vastly reduces overlap, allowing resonances to be identified which may have otherwise been obscured. The labelling scheme also reduces the number of adjacent carbon atoms, eliminating many of the J-couplings which, although not resolved in a typical solid-state NMR spectra, do contribute to the linewidth, limiting the available resolution. The dilution

of ^{13}C nuclei reduces dipolar truncation effects and enables longer range contacts to be measured. Removal of some ^{13}C-^{13}C dipolar coupling also decreases line-widths and therefore improves resolution, further facilitating assignment.

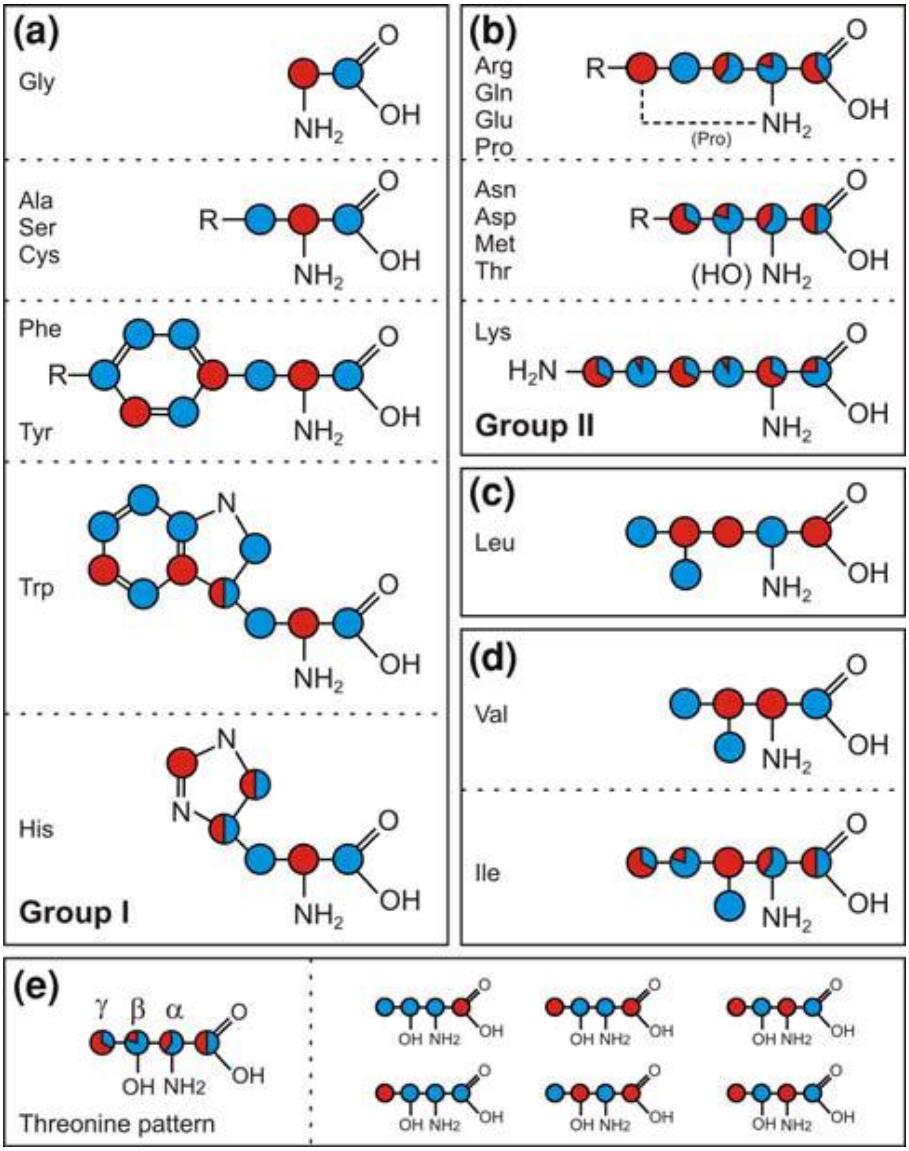

Figure 57 Schematic representation of the effective ^{13}C enrichment of amino acids in the SH3 domain expressed in *E.coli* BL21 (DE3)

Labelling pattern achieved by Oschkinat's group when expressing the SH3 domain. The pattern should be the same for β_2m as the same *E.coli* strain was employed and thus we would expect a similar labelling pattern same. Sites which are ^{13}C labelled by growth on [1,3-^{13}C]-glycerol are shown in blue; sites labelled by growth on [2-13C]-glycerol are shown in red. For residues with mixed labelling, the percentage of labelling is represented using relative blue/red colouring, except for the tryptophan Cδ and histidine Cδ and Cε sites, for which the percentages could not be determined and a half/half distribution is displayed. (a) Group I residues have ^{13}C-labelled C' and Cβ sites in the [1,3-^{13}C]-glycerol sample and ^{13}C-labelled Cα sites in the [2-^{13}C]-glycerol sample. (b) Group II residues have mixed labelling patterns arising from different isotopomers as shown for threonine in (e). (c) Leucine is the only residue with a backbone labelling pattern exactly opposite to that of the Group I residues. (d) Valine and isoleucine residues present exceptions from Groups I and II, respectively, as their Cβ sites are only ^{13}C-labelled in the [2-^{13}C]-glycerol sample. e Illustration of the fractional labelling pattern seen for Group II residues and isoleucine, using threonine as an example. Figure modified from Higman 2009 (*140*).

4.4 Hydrogen-Deuterium exchange of β_2m fibrils

Unprotected amide protons of amino acids undergo exchange with the exchangeable protons of water when proteins are in solution. This phenomenon can be exploited to give structural information about proteins by replacing the H_2O of aqueous solution with D_2O. Amide protons which are part of a hydrogen bond are not easily exchangeable; amide protons that are not part of a hydrogen bond but are located within the proteins core and have reduced solvent accessibility will exchange at a slower rate than those amide protons that are fully solvent accessible on the protein surface. The rate of exchange of amide protons is highly dependent on the protein and the experimental conditions; temperature, pH and ionic conditions all markedly affect the rate of amide proton exchange which ranges from minutes to years (*141*). In liquid-state NMR this is often exploited by running a series of HSQC experiments of proteins in a deuterated aqueous solution, in the case of protonated proteins, or in protonated aqueous solution in the case of deuterated proteins. In the case of protonated proteins, the peaks corresponding to rapidly exchangeable amide protons will disappear from the spectra early on in the series while the peaks corresponding to less solvent accessible amides will remain to later in the series. The peaks corresponding to hydrogen bonded amides will usually remain throughout the series of experiments. As the buffer conditions experienced by the amide protons are all the same within a single experiment, rate of exchange is determined by the hydrogen bonding and solvent accessibility of the amide and hence a map of the hydrogen bonding/solvent accessibility of the protein can be made when used in conjunction with an assigned HSQC.

Hydrogen-deuterium exchange NMR has recently been applied to many fibril types including β_2m in order to try and elucidate which parts of the protein form the core of the fibril and which parts are on the surface (*142-144*). However in all cases the fibrils

underwent H/D exchange and then were dissolved in DMSO back to a monomeric denatured form before HSQC measurements were acquired using liquid-state NMR.

As mentioned above Hoshino *et al.* subjected β_2m fibrils to H/D exchange and subsequently dissolved the fibrils in DMSO at different time points. The lack of exchangeable protons in DMSO means that the amides retain the proton or deuterium that was bound when the β_2m was in its fibrillar state. The DMSO denatured β_2m was then studied by liquid-state NMR and HSQC spectra acquired. The study identifies amides of β_2m fibrils that are rapidly exchangeable and therefore highly likely to form part of the solvent exposed surface of the fibril or not participating in a hydrogen bond. It was not therefore necessary to acquire H/D exchange data for the purpose of identifying the fibril core. However as 25 residues have amides that are shown to be susceptible to exchange and show substantial signal decay over a 24 hour period, it was decided that H/D exchange could provide an effective method for further de-crowding of NCA/NCO spectra already partially decrowded through specific glycerol based labelling schemes. Decrowding of the spectra in this manner could have two possible beneficial outcomes, the facilitation of the sequential assignment of the NCA/NCO spectra and the confirmation of residues that are solvent accessible in the fibrils.

For the hydrogen-deuterium exchange, selectively and extensively labelled β_2m was produced and underwent acid fibrillogenesis as previously described in chapter 2.2.1. The selectively and extensively labelled fibrils were then buffer exchanged into pH 2.5 sodium citrate buffer made with D_2O (25 mM sodium citrate, 25 mM KCl, D_2O, pD*[1] 2.5) by centrifuging the fibrils, removing the H_2O based supernatant and replacing with the D_2O

[1] pD* is the pH meter electrode reading without correction for the isotope effect

sodium citrate buffer. The fibrils were resuspended and left to incubate for 24 hours. Afterwards the fibrils were pelleted by ultracentrifugation at 50000 *g*, the supernatant removed and the pellet loaded into a 3.2 mm MAS rotor using a spatula and rod. The exchange was not quenched by lyophilisation as the experiments were to be carried out at 0˚C and the acidic pD* of the samples should reduce the exchange rate of any but the most solvent accessible amides to a level where few exchange over the time course of the experiment; the solvent accessible amides should already have exchanged in the incubation period.

4.5 NMR spectra of fibrillar beta-2 microglobulin

Initial spectra of fibrillar β_2m were acquired on a 600 MHz spectrometer; this gave good line-widths (~0.5 ppm) but due to the size of β_2m (100 residues) spectral crowding was a significant issue and assignment of the protein would be challenging. This problem was partially overcome by using higher field magnets available through national and European facilities. At 850 MHz, far better resolved spectra were acquired with line-widths averaging 0.7 ppm and as low as 0.6 ppm being achieved on PDSD spectra of fibrillar β_2m at pH 2.5 (Figure 58 and Figure 59). This allowed the assignment of many peaks but spectral crowding became the dominant problem in preventing substantial assignments to be made.

Attempts were made to overcome the spectral overlap, which is particularly bad in the NCA and NCO spectrum due to the low dispersion of ^{15}N and ^{13}Cα chemical shifts, by running three-dimensional experiments, however signal to noise became the dominant issue as conventionally prepared β_2m fibrils are substantially hydrated with up to 75% of the sample being water. This signal to noise problem was eventually overcome with a change in sample preparation technique as discussed in chapter 2, however the reduction in water content and the higher packing led to a reduction in dynamics that decreased resolution from an average of 0.7 ppm in the spectra from uniformly labelled, conventionally prepared fibrils to an average of 1 ppm in the spectra of the more densely packed fibrils; attention has been brought to this in Figure 60. This combined with the prohibitively long acquisition times that are essential when running three dimensional experiments in the solid-state meant that the three dimensional approach was abandoned.

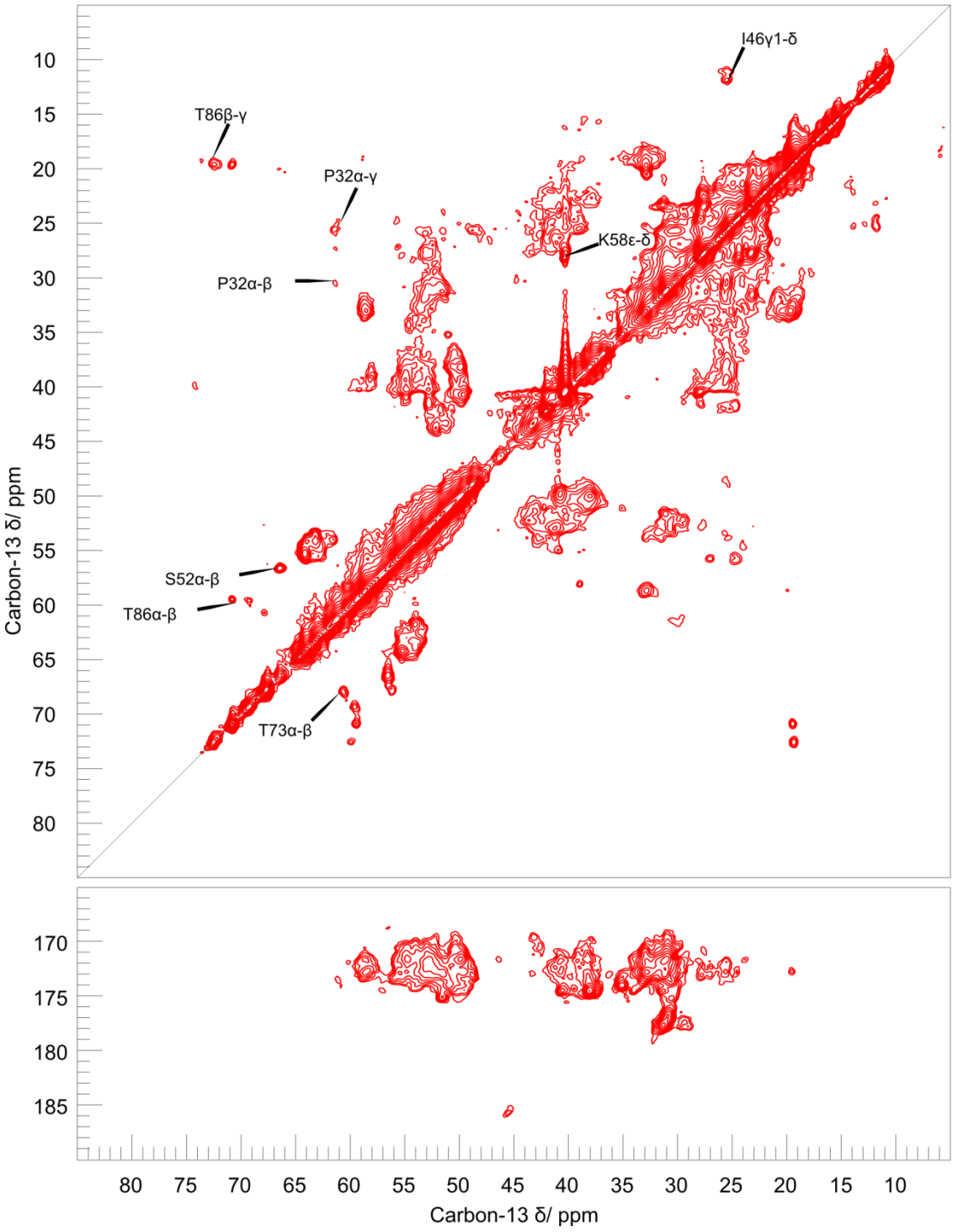

Figure 58 PDSD (20 ms mixing time) spectrum of fibrillar β_2m at pH 2.5
The PDSD experiment makes use of the densely coupled proton network in proteins to enable spin diffusion amongst the low gamma carbon-13 nuclei of the protein. The PDSD spectrum is two dimensional with carbon chemical shift on both axis and shows through space correlations between carbon-13 nuclei. Spectrum acquired on Bruker 850 MHz WB US_2 with 100 ms mixing time at -1˚C and pH 2.5. 15000 Hz spinning.

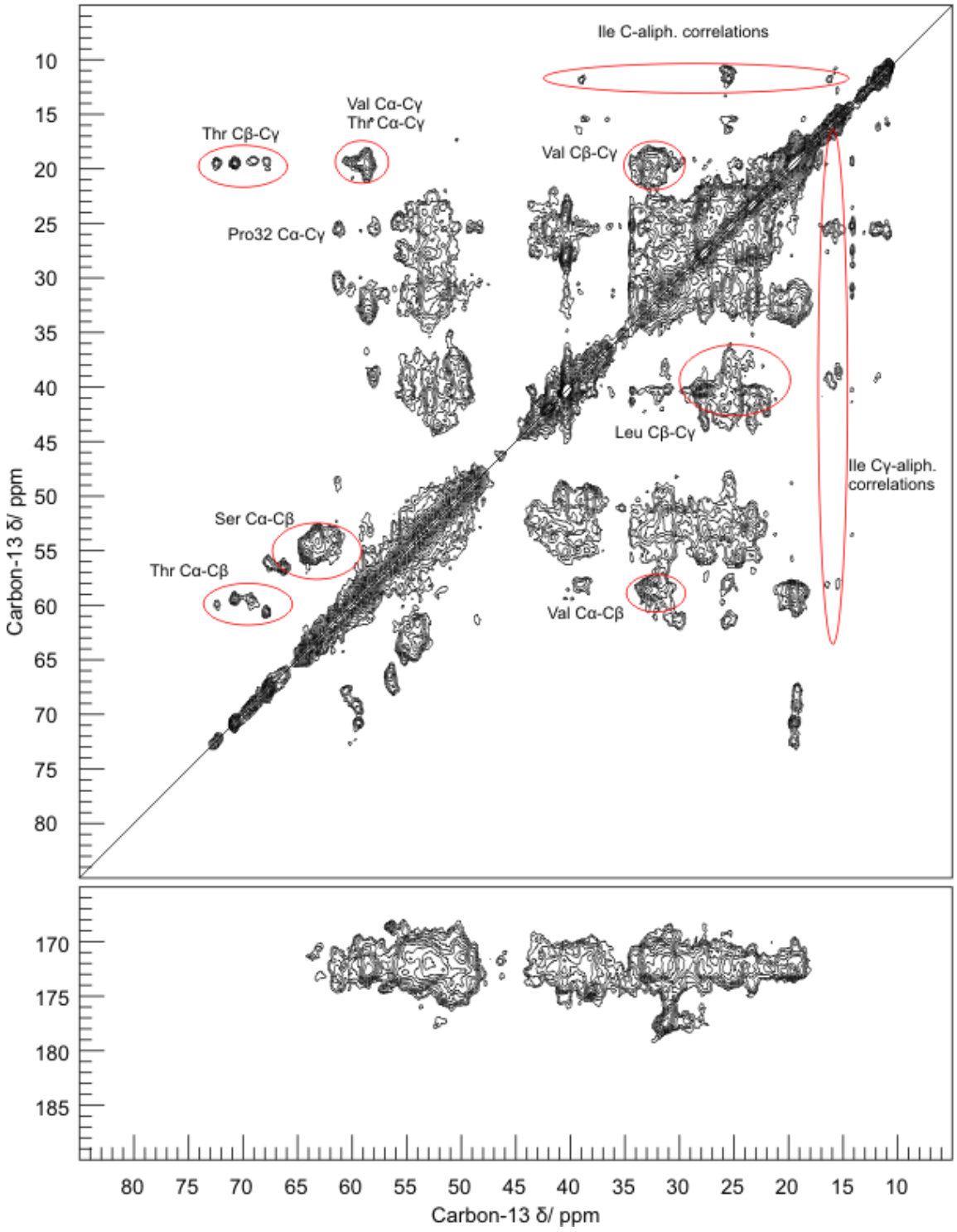

Figure 59 PDSD (100 ms mixing time) spectrum of fibrillar β_2m at pH 2.5
Circled in red are prominent envelopes that contain mainly just one or two correlation types. Marked on the spectrum is also the ^{13}Cα-^{13}Cγ correlation of proline 32. The chemical shifts of proline 32's ^{13}Cγ and ^{13}Cβ can be used to determine if it is in its *cis* or *trans* configuration. Spectrum acquired on Bruker 850 MHz WB US_2 with 100 ms mixing time at a sample temperature of ~-1˚C and pH 2.5, 15000 Hz spinning.

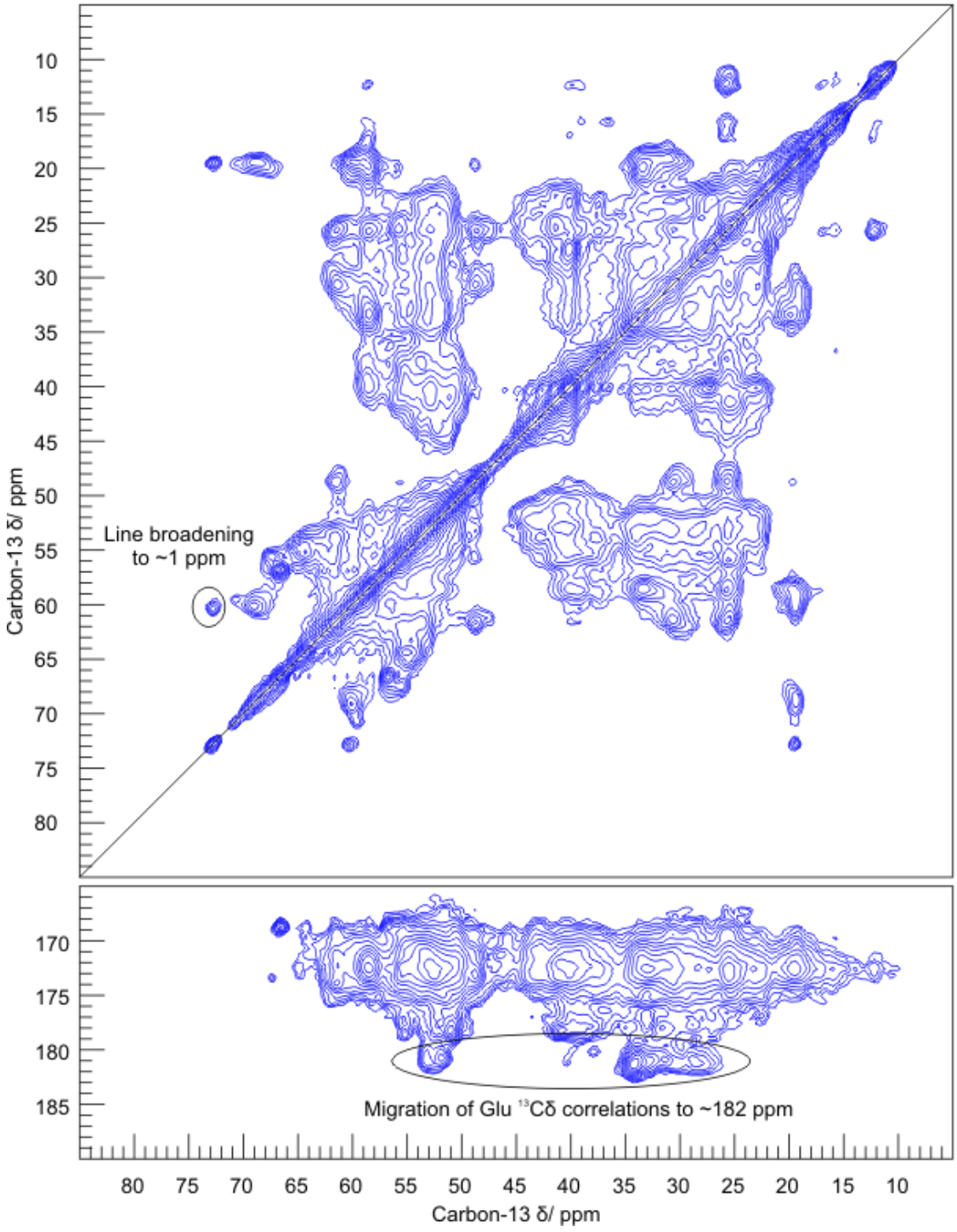

Figure 60 PDSD spectrum (100 ms mixing time) of fibrillar β_2m at pH 7.4
Circled in the lower section of the spectrum is the migration of the glutamate ^{13}Cδ correlations from ~178 ppm in the acidic spectrum to ~182 ppm at neutral pH can be clearly seen when comparing the β_2m spectra at different pHs. Spectrum acquired on Bruker 850 MHz WB US_2 with 100 ms mixing time at -1˚C. 15000 Hz spinning.

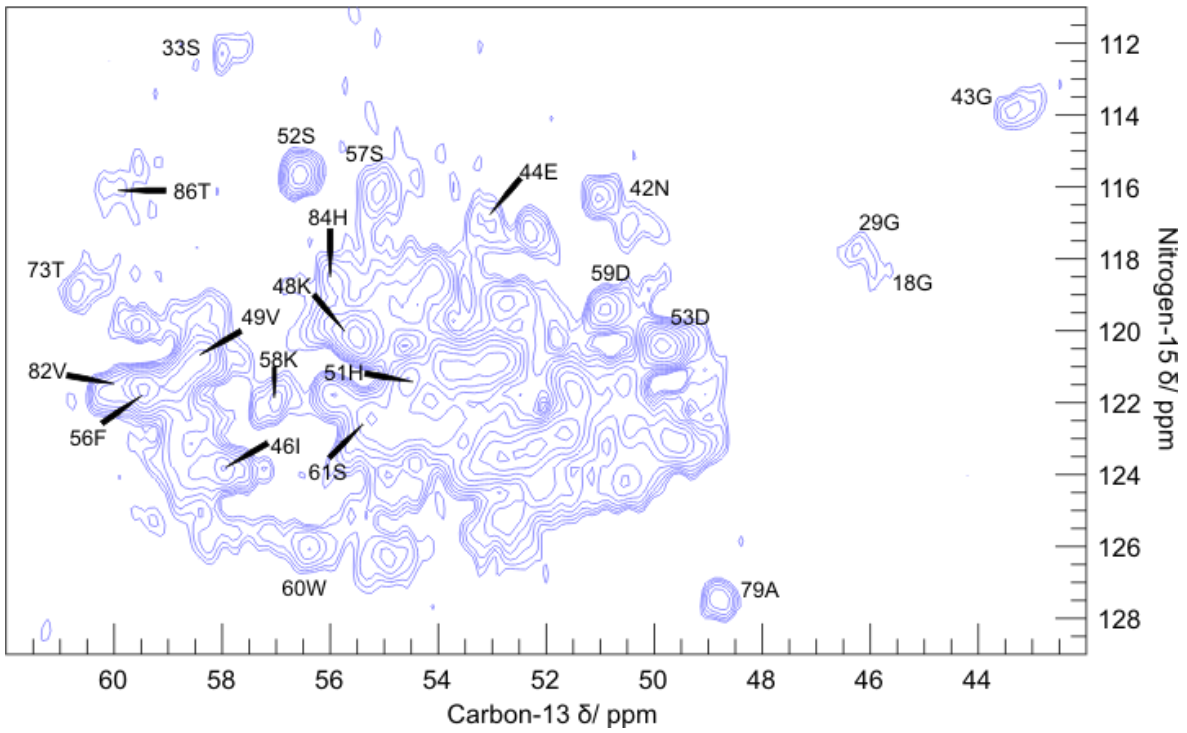

Figure 61 Two dimensional NCA spectrum of fibrillar β_2m at pH 2.5

The NCA spectrum was acquired using β_2m expressed in *E.coli* whose sole carbon source was uniformly ^{13}C labelled glucose. Their nitrogen source was fully ^{15}N enriched ammonium chloride. Assignments are shown. The number and letter refer to the residue number and single letter code for the (i) nitrogen and α-carbon. Spectrum acquired on Bruker 850 MHz WB US_2 at a sample temperature of ~ -1˚C and pH 2.5. 15000 Hz spinning.

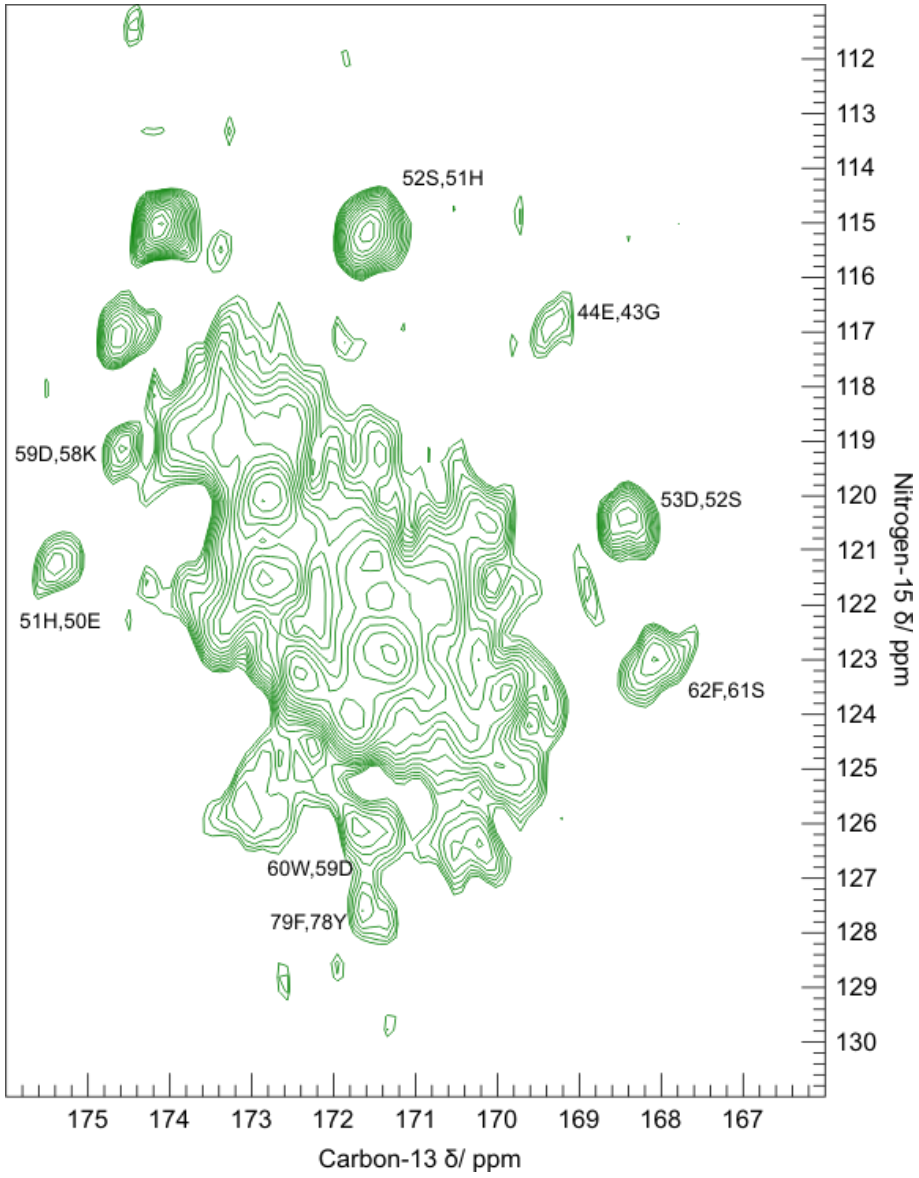

Figure 62 Two dimensional NCO of uniformly labelled ^{13}C ^{15}N fibrillar β_2m
The NCO spectrum was acquired using β_2m expressed in *E.coli* whose sole carbon source was uniformly ^{13}C labelled glucose. Their nitrogen source was fully ^{15}N enriched ammonium chloride. Assignments are shown. The first number and letter refer to the residue number and single letter code for the (i) nitrogen. The second number and letter refer to the residue number and single letter code for the (i-1) carbonyl carbon. Spectrum acquired on Bruker 850 MHz WB US_2 at a sample temperature of ~ -1˚C and pH 2.5. 15000 Hz spinning.

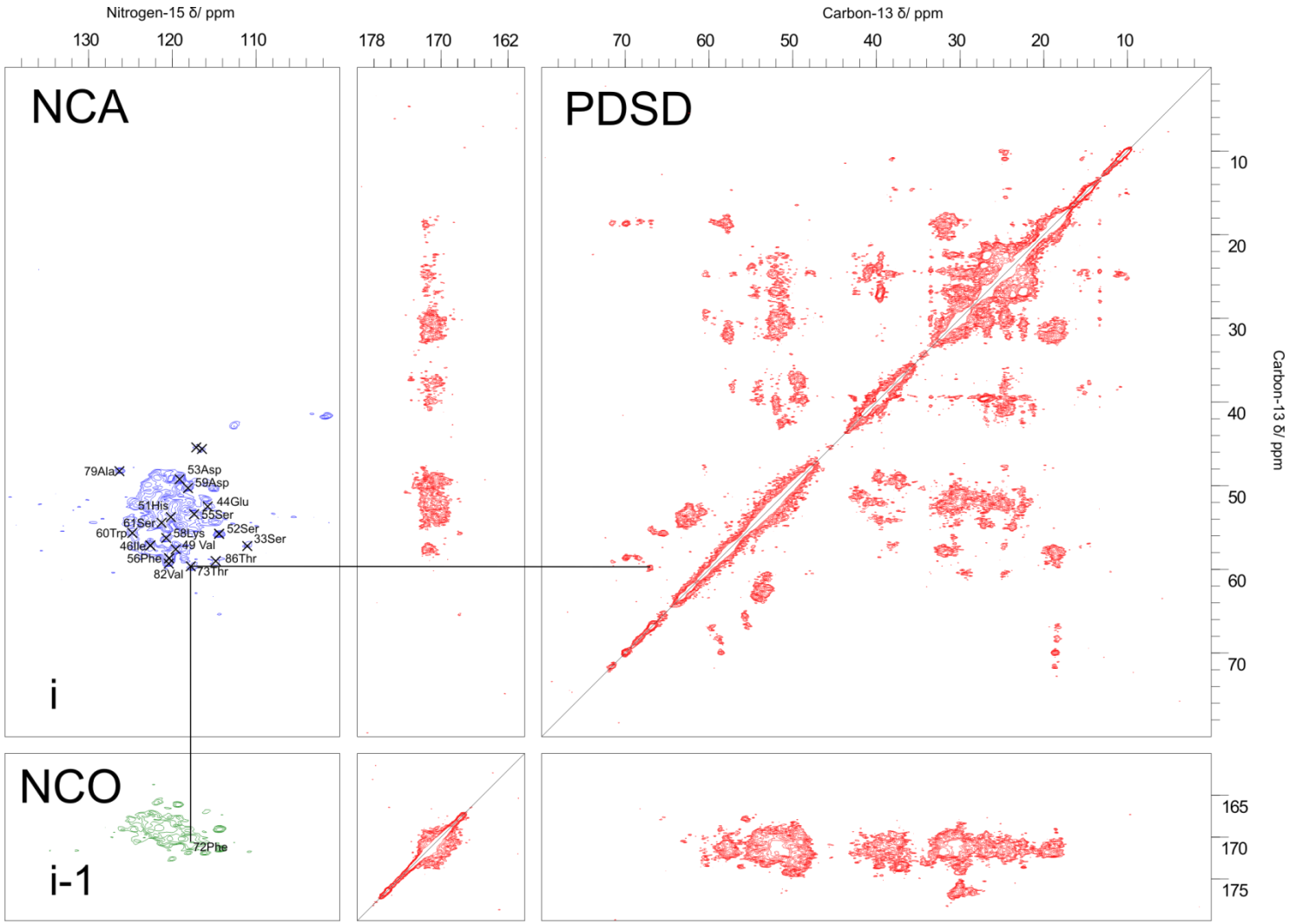

Figure 63 PDSD, NCA, and NCO experiments juxtaposed to allow sequential assignment Sequential assignment in the solid-state can be achieved through a combination of PDSD, NCA and NCO experiments. The PDSD gives atom type through unique correlations and then sequential assignment proceeds through aligning peaks based on their carbon and nitrogen correlations. Due to the magnetisation passing between the residues in the NCO experiment, sequential assignments can be made through the shift shared between the peaks in both NCA and NCO experiments. Spectra acquired on Bruker 850 MHz WB US_2. 15000 Hz spinning. PDSD acquired with 100 ms mixing time. All spectra acquired at a sample temperature of ~-1˚C and pH 2. 5.

Selective and extensive labelling of β_2m for resolution improvement

Selective and extensive labelling of β_2m was chosen as a necessary alternative method to decrease spectral overlap and facilitate assignment. In the first instance PDSD spectra were acquired of [2-^{13}C] (Figure 64) and [1,3-^{13}C] -glycerol (Figure 65) prepared β_2m. Using these labelling schemes a massive simplification of the PDSD spectra is seen, particularly in the [2-^{13}C]-glycerol spectrum due to the removal of substantial amounts of ^{13}C-^{13}C cross-peaks. This greatly facilitated identification of resonances within the same spin system, particularly, valines and leucines in the [2-^{13}C]-glycerol spectrum due to both having adjacent 100% ^{13}C labelled aliphatic nuclei. Longer mixing times had to be employed with the labelled samples in order to transfer magnetisation between all the intra-residue nuclei.

Selective and extensive labelling was not as effective in simplifying the NCA and NCO spectra (Figure 66 &Figure 67) as was hoped for, especially as only [1,3-^{13}C]-glycerol samples were measured due to the loss of the [2-^{13}C]-glycerol sample. The [2-^{13}C]-glycerol sample would have given a more informative NCO spectrum due to the extent of de-crowding predicted from the labelling patterns in Figure 57. A more fully assigned NCO would have facilitated sequential assignment of the backbone resonances.

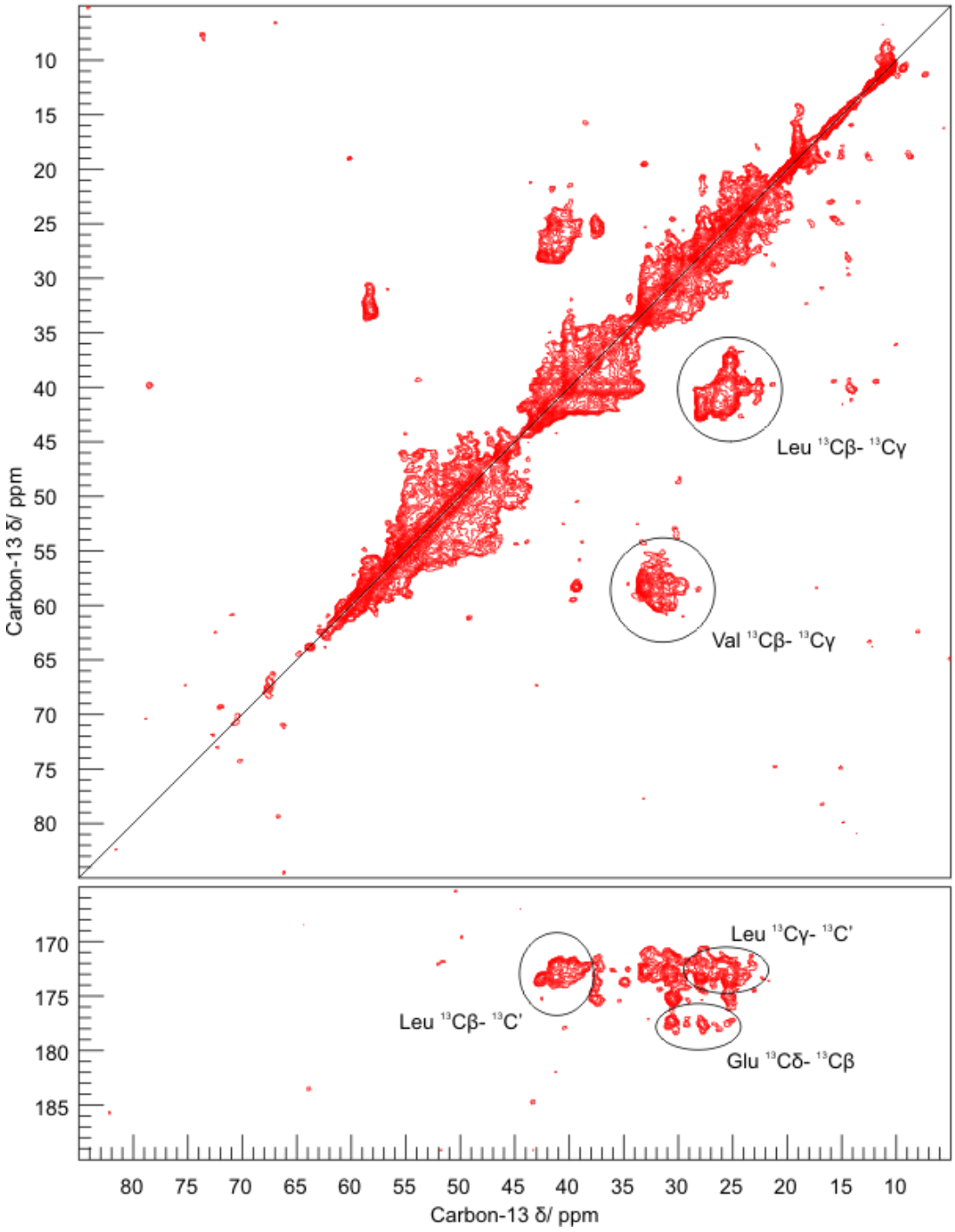

Figure 64 PDSD (500 ms mixing) spectrum of [2-^{13}C]-glycerol selectively and extensively labelled β_2m fibrils

Circled are correlations that are predicted to have 100% labelling with this labelling scheme. Spectrum acquired on Bruker 850 MHz WB US_2 at a sample temperature of ~ -1˚C and pH 2.5. 15000 Hz spinning.

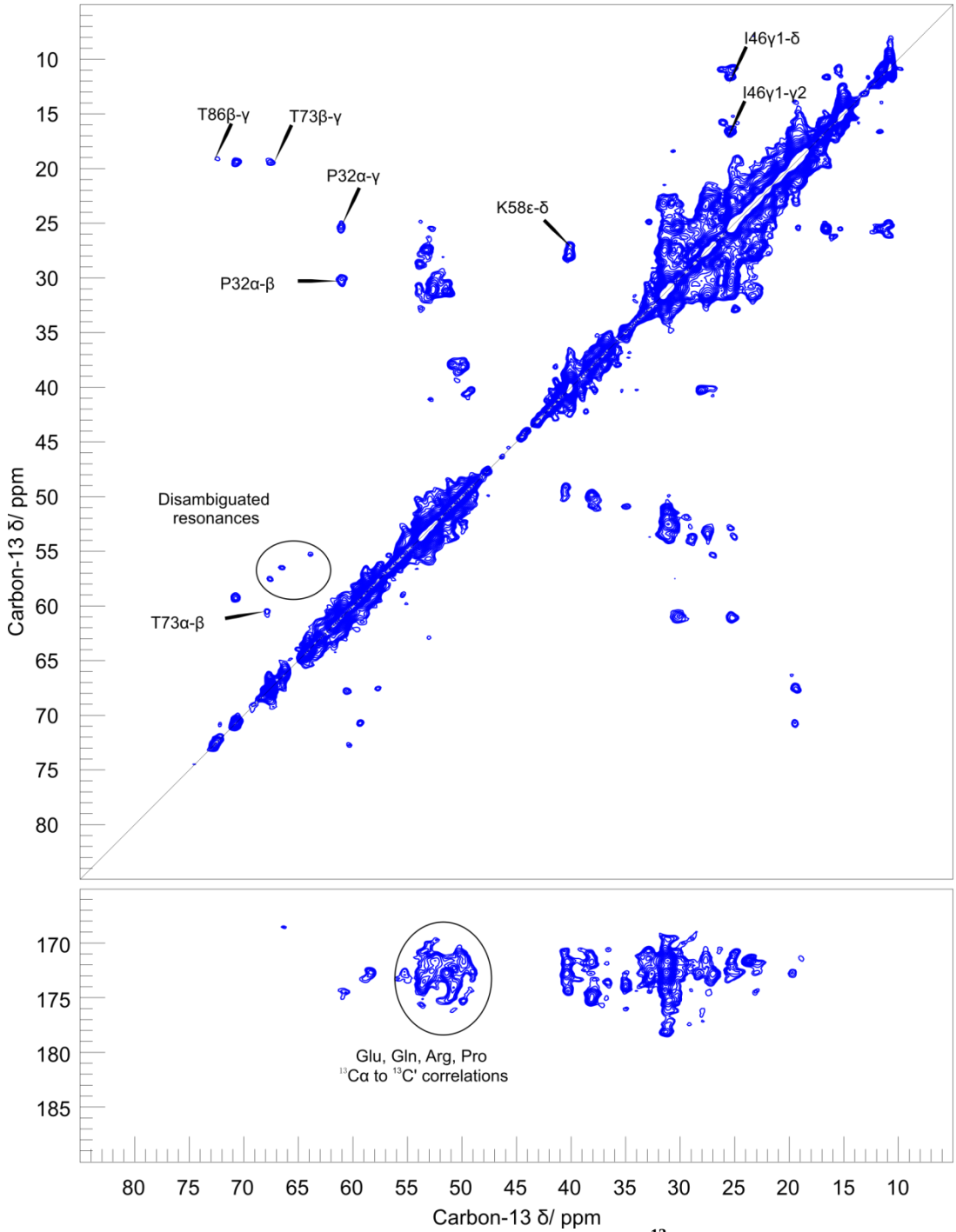

Figure 65 PDSD (500 ms mixing time) spectrum of [1,3-^{13}C]-glycerol selectively and extensively labelled β_2m fibrils

The circled peaks in the C' region of the spectrum are most likely to be Glu, Gln, Arg and Pro ^{13}Cα to ^{13}C'correlations as they are the only residues which have the most significant proportion of both Cα and C' ^{13}C labelled in the same molecules. The circled area in the aliphatic region of the spectrum contains peaks that in a uniformly labelled spectrum would be assumed to be serine ^{13}Cα-^{13}Cβ correlations, however they cannot be as serine has no ^{13}Cα labelling in this scheme. Spectrum acquired on Bruker 850 MHz WB US_2 at a sample temperature of ~ -1˚C and pH 2.5. 15000 Hz spinning.

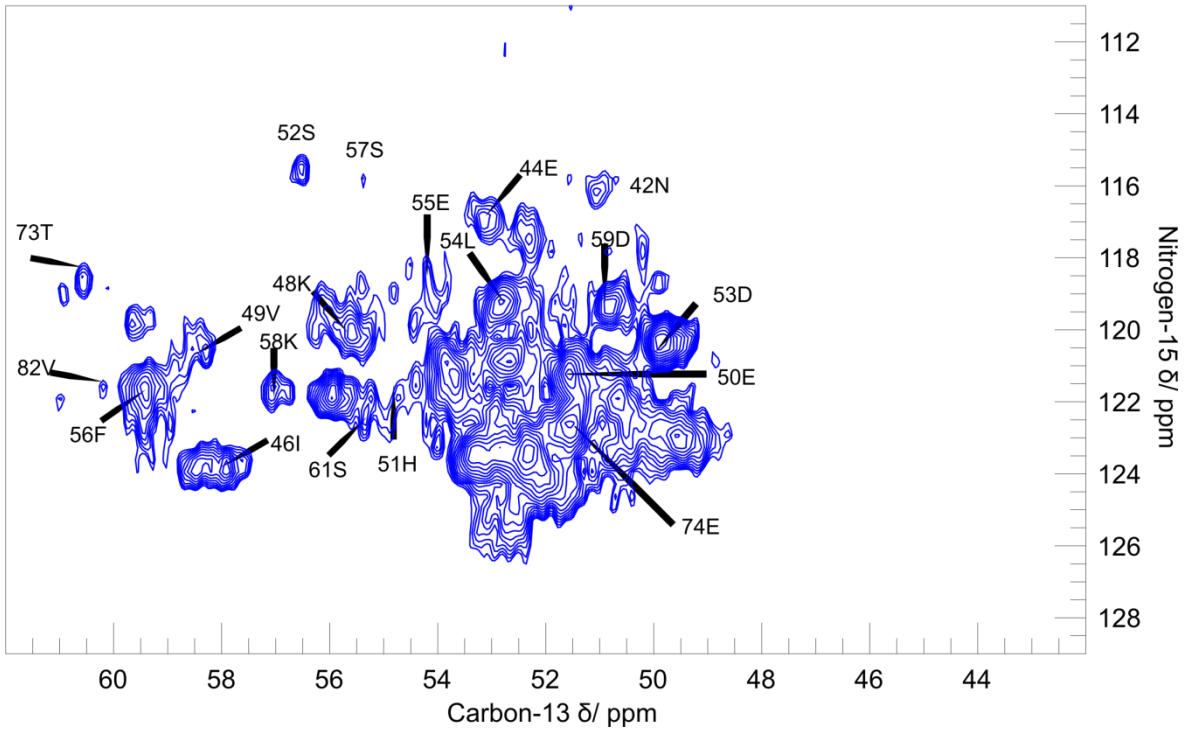

Figure 66 NCA spectrum of [1,3-^{13}C]-glycerol selectively and extensively labelled β_2m fibrils
The above spectrum shows an NCA spectrum of β_2m fibrils that have been selectively and extensively labelled using the [1,3-^{13}C]-glycerol labelling scheme. Prominent assignments have been marked. Assignments are shown. The number and letter refer to the residue number and single letter code for the (i) nitrogen and α-carbon. Spectrum acquired on Bruker 850 MHz WB US_2 at a sample temperature of ~ -1˚C and pH 2.5. 15000 Hz spinning.

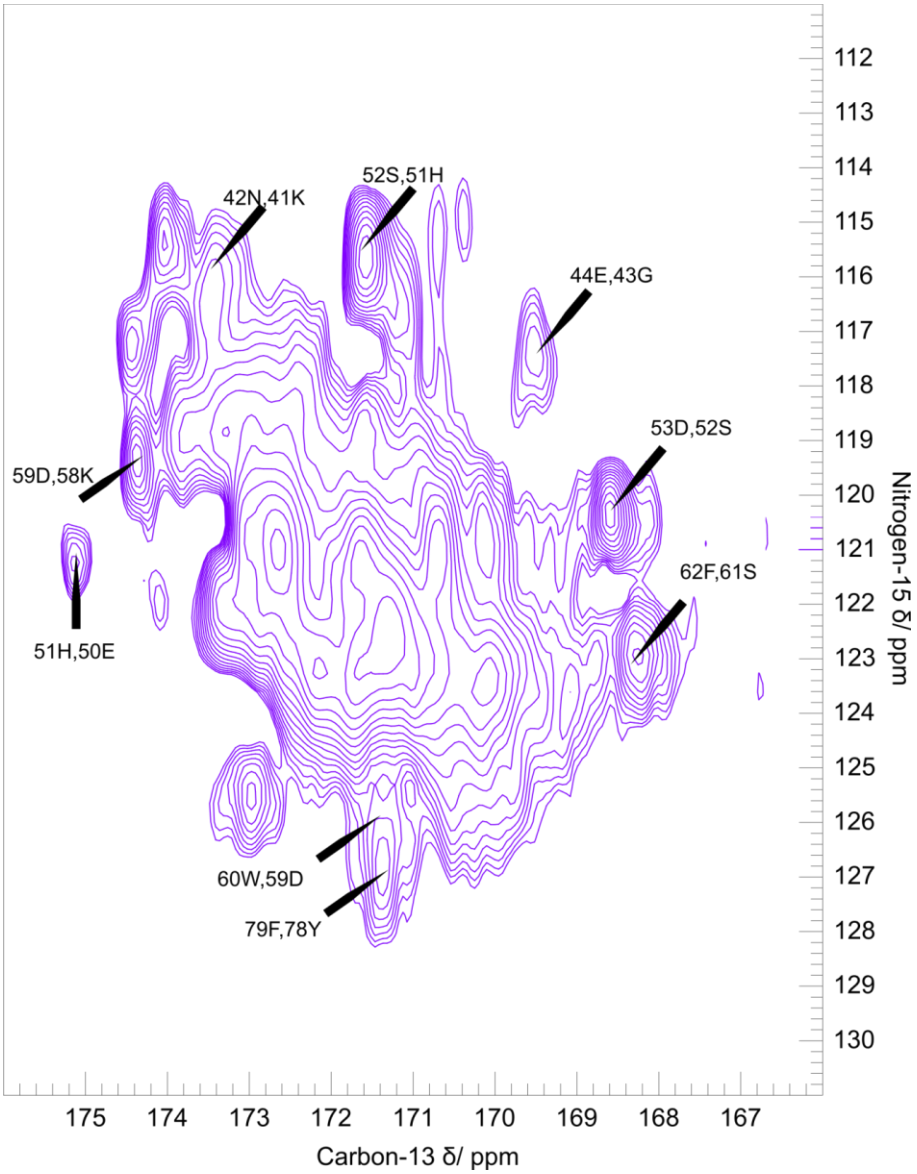

Figure 67 NCO spectrum of [1,3-^{13}C]-glycerol selectively and extensively labelled β_2m fibrils
The NCO spectrum was acquired using β_2m expressed in *E.coli* whose sole carbon source was [1,3-^{13}C]-labelled glycerol. Their nitrogen source was fully ^{15}N enriched ammonium chloride. Assignments are shown. The first number and letter refer to the residue number and single letter code for the (i) nitrogen. The second number and letter refer to the residue number and single letter code for the (i-1) carbonyl carbon. Spectrum acquired on Bruker 850 MHz WB US_2 at a sample temperature of ~ -1˚C and pH 2.5. 15000 Hz spinning.

Deuteration of selectively and extensively labelled β_2m for resolution improvement

Only the [1,3-^{13}C]-glycerol sample was deuterated before NCA and NCO spectra were acquired due to the loss of the [2-^{13}C]-glycerol sample. Signal to noise was vastly decreased in both the NCA (Figure 68) and NCO spectra but especially the latter and the spectrum from the NCO was not of sufficient quality to be of use. This decrease in signal to noise can be accounted for by the lack of magnetisation being cross-polarised from the solvent as normally happens when ^1H_2O is the solvent (*145*). The specificity of the ^{15}N to ^{13}Cα transfer was reduced in the deuterated experiment, with a significant amount of signal coming through on the ^{13}C'. This is surprising as both deuterated and non-deuterated samples were irradiated at the same carrier frequencies. Despite lower signal to noise, the majority of the peaks are still present and spectral crowding is not significantly reduced; this informs us that a significant proportion of the amide residues are in environments that are not conducive to H/D exchange. This fits with previous findings that 75% of amide residues are protected (*144*), presumably due to the high beta-strand content of the β_2m fibrils and subsequent high degree of hydrogen bonding.

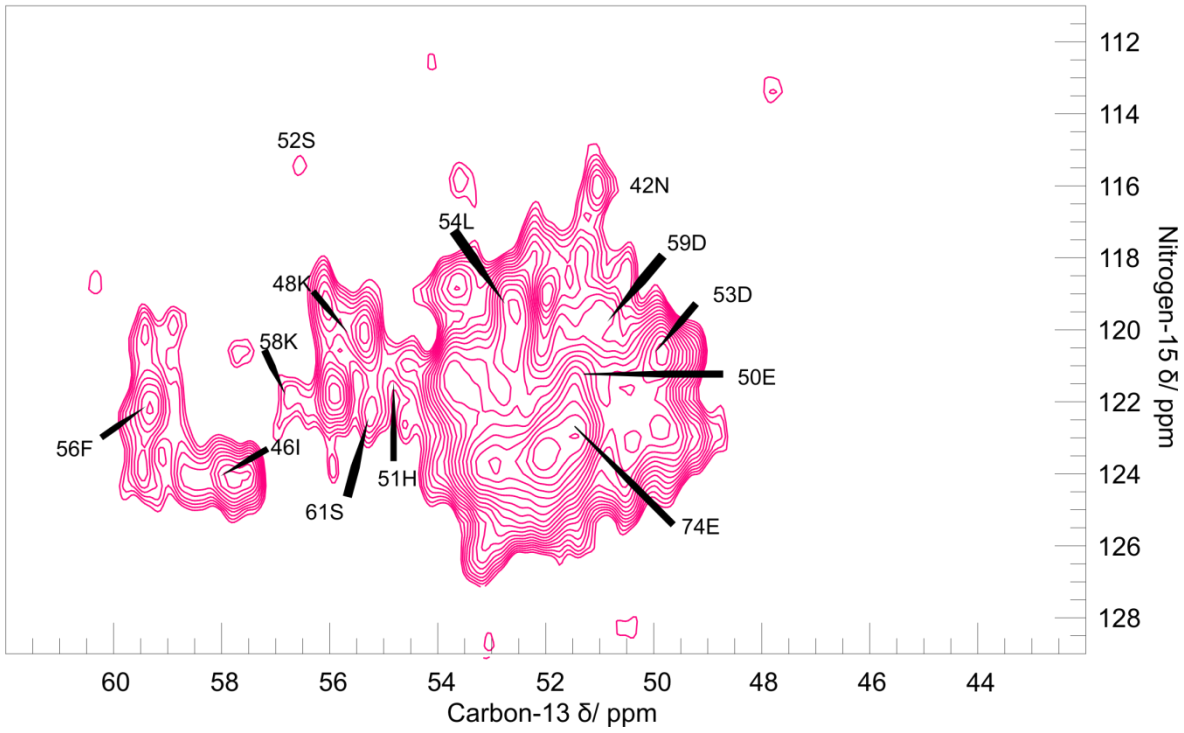

Figure 68 NCA spectrum of [1,3-^{13}C]-glycerol selectively and extensively labelled β_2m fibrils after H/D exchange

The above spectrum is of fibrillar β_2m labelled with the [1,3-^{13}C]-glycerol scheme and then subjected to H/D exchange. Assigned peaks are shown. The number and letter refer to the residue number and single letter code for the (i) nitrogen and α-carbon. Spectrum acquired on Bruker 850 MHz WB US_2 at a sample temperature of ~ -1˚C and pH 2.5. 15000 Hz spinning.

NMR Assignment of fibrillar β_2m

The identification of cross-peaks belonging to the same spin system using the PDSD spectra and subsequent sequential assignment using the NCX experiments has allowed the assignment of 137 resonances from 39 different spin-systems; the assignments can be found in Table 9. Previous research has shown that the 16 residues at the N-terminus and the 13 residues at the C-terminus are likely to be mobile regions and not be observable using dipolar coupling through space experiments such as the PDSD and NCX experiments (*146*, *147*). Therefore approximately 54% of the residues that are expected to appear in the spectra have at least one of their nuclei assigned. Another 16 residues have been tentatively assigned or have at least 3 resonances identified as belonging to their spin

system; making a total of 84 residues accounted for as either being present in the spectra or not expected to be in it. Alanine has a distinctive cross-peak on PDSD spectra and there are only 2 alanines in β_2m, both alanines should therefore be assignable; interestingly only one cross peak either side of the diagonal appeared for alanine and this was assigned to Ala-79. The ^{13}Cα-^{13}Cβ cross-peak for Ala-15 was not present in any of the PDSD spectra; this lends evidence to previous findings that the first 16 residues of β_2m do not appear in through-space spectra due to high mobility. Glycines have a distinctive ^{13}Cα-^{13}C' cross-peak on PDSD spectra and all three present in β_2m have been fully assigned; Gly-18 is very close to the proposed mobile region on β_2m fibrils and its peaks are extremely weak in all spectra, it is the nearest residue to the N-terminus that is fully assignable, again supporting evidence of the proposed mobile N-terminus. Pro-32 and Pro-72 are the only two prolines that do not fall within the non-observable termini regions; these were both fully assigned. From a search of the BioMagRes database the average ^{13}Cβ chemical shift for proline in the *cis* conformation is 34.16 ppm, while for *trans* it is 31.75 ppm; for ^{13}Cγ, *cis* is 24.52 ppm and *trans* is 27.26 ppm. The average difference between the chemical shifts in the *trans* conformation is 4.51 ppm, whilst in the *cis* conformation the difference is 9.64 ppm (*148*). In our spectra the difference between the ^{13}Cβ & γ in Pro-32 is 4.67 ppm; in Pro-72 it is 5.3 ppm. This informs us that both prolines are more likely to adopt the *trans* conformation; this is in contrast with native monomeric β_2m where the His-31-Pro-32 bond is *cis* (*58*). The transformation of Pro-32 from *cis* to *trans* is thought to be a necessary step in β_2m fibrillogenesis (*58*). There are five threonines in β_2m and four of these are easily identifiable from the PDSD spectrum. The fifth again falls within the N-terminus and has in fact been shown to be observable using INEPT-TOBSY experiments by Debelouchina *et al.* in 2010 (*147*). Only Thr-73 and Thr-86 have been unambiguously

assigned due to the others falling within regions that we were not able to sequentially assign due to spectral crowding in the NCX spectra.

An interesting finding of the data collected is that one of the areas that was substantially assigned was the region corresponding to the loop between β-strands V and VI which we were unable to assign in the liquid state. This suggests that during the transition from native to fibrillar form this region becomes a lot less mobile. Chemical shift index calculations performed on the assigned resonances predict this area to be β-strands (Figure 71). This is an important finding as if confirms that residues that were previously located in flexible loop regions are forming β-strands in fibrillar β_2m. This shows that β_2m must undergo significant structural changes in transition from native to fibrillar forms, which is consistent with the EM studies of Helen Saibil that concluded that the β_2m monomer must undergo significant structural rearrangement in order fit with the cryo-EM data that she had collected (*13*).

Comparison of fibrillar β_2m PDSD with PDSD simulated from native β_2m assignments

The PDSD data that we have acquired can be compared with the liquid state assignments that were presented in the previous chapter by creating a simulated PDSD (Figure 69). All ^{13}C chemical shifts acquired using liquid-state NMR triple resonance experiments have been used here to simulate a PDSD spectrum. This has then been overlain over our experimental 20 ms mixing time PDSD spectrum of fibrillar β_2m. There are a significant number of differences between the simulated and experimental spectra. Although peaks arise in similar regions indicating the contribution of similar amino acids (e.g. Thr/Ser/Val etc.), the distribution of resonances within these regions is frequently different suggesting

that the electrostatic environment of each amino acid is most often different. It must also be considered that the pH of the two samples was different, so in the very least glutamate and aspartate side-chain ^{13}C resonances will appear at different chemical shifts. The simulated alanine cross-peaks appear in areas where no peaks are present in the 20 ms spectrum. However at longer mixing times, Ala-79 does appear in this area; Ala-15 however is conspicuous by its absence from all the solid-state spectra and this could well be because it is located within the first twenty residues of β_2m which have been shown in several papers to be difficult to detect when dipolar couplings are used to transfer coherence and are suspected of being highly solvent exposed (*146, 147*). The poor superimposition between the simulated spectrum and the 20 ms PDSD spectrum reinforces the chemical shift data that we have predicting the formation of extra β-strands in the transition between native and fibrillar forms of β_2m. We note though that the presence of cross-peaks in the PDSD spectra is sensitive to a number of factors including cross-polarisation and recoupling efficiency which may lead to the absence of peaks in the spectra.

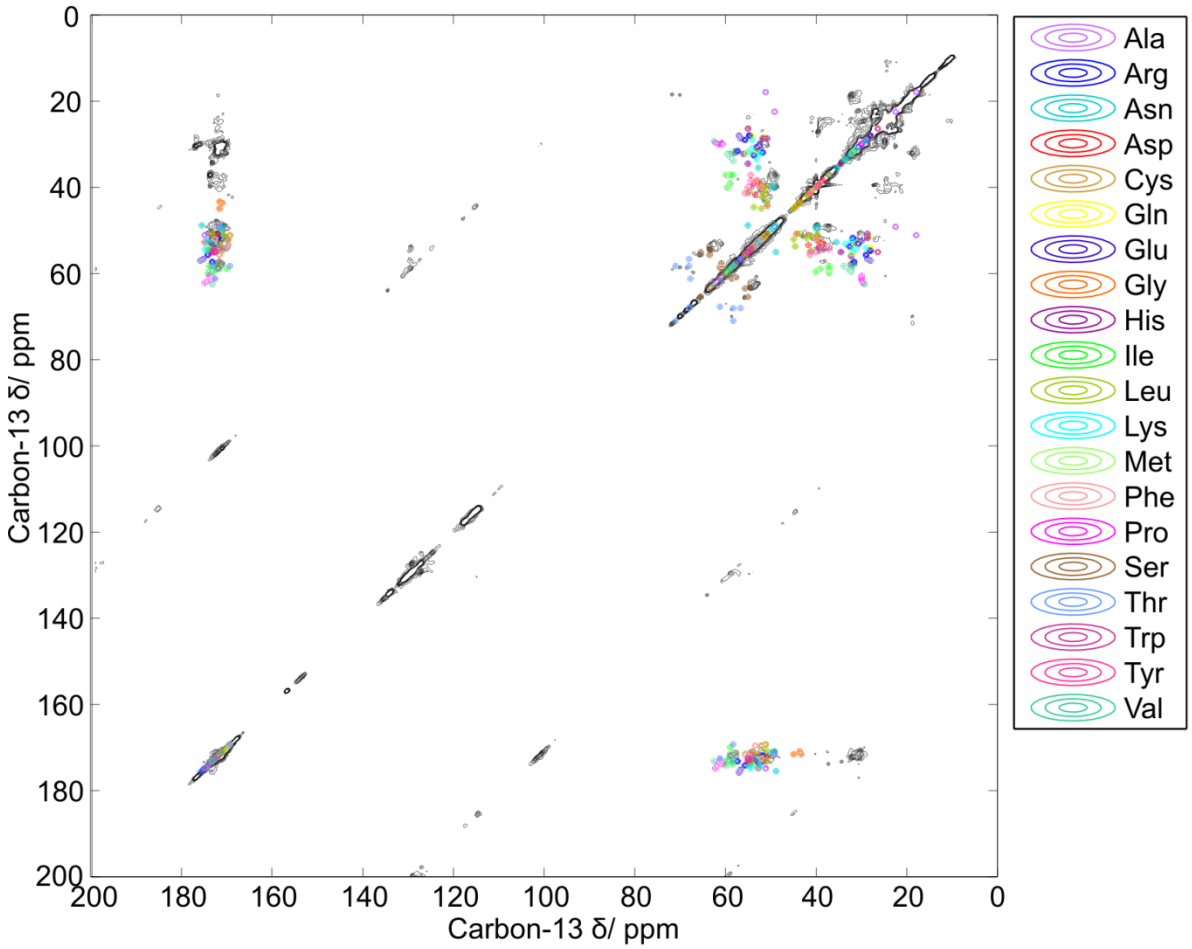

Figure 69 PDSD simulated from chemical shifts of soluble β_2m overlain on PDSD of full length fibrillar β_2m

Our $^{13}C\alpha$, $^{13}C\beta$ and $^{13}C'$ chemical shifts acquired using liquid state NMR triple resonance experiments have been used here to simulate a PDSD spectrum. Coloured peaks are simulated from liquid-state data. The black spectrum is a 20 ms mixing time PDSD of β_2m fibrils at pH 2.5.

Comparison with fibrillar β_2m PDSD with PDSD simulated from β_2m K3 assignments

A simulated PDSD (Figure 70) has also been created using the chemical shift data published by Iwata (*84*) for the fibrils they created using the K3 fragment of β_2m. This fragment of β_2m was discussed in chapter 1; to recall it is the twenty-two residue section of β_2m whose N-terminus is Ser-20 and C-terminus is Lys-41. K3 is created from lysyl endopeptidase digestion of monomeric β_2m and is the third of nine peptides produced by this digestion. Under acidic conditions it forms fibrils and the structure of these fibrils has been solved by solid-state NMR; the structure can be seen in Figure 7. Some of the simulated peaks correlate extremely well with those of the full length β_2m PDSD with resonances from Valine 27 and Serine 28 peaks superimposable with peaks in the PDSD. In contrast a number of peaks do not match at all including those belonging to the residues S20, C25, G29, H31, S33 and K41. S20 and K41 are at the termini of the fragment, in full length fibrils these residues would not be terminal residues suggesting the shifts would be extensively perturbed as is expected for residues at the N and the C termini. C25 forms a disulphide bond in full length β_2m which is absent in the K3 fragment as C80 is not being present. G29, H31 and S33 all form loop regions in Iwata's structure but are found within β-strands within full length soluble β_2m. It is possible because of the extended structure in full length fibrils that they remain in β-strands due to increased electrostatic interactions. All other peaks are either superimposable or very similar. This is suggestive that the residues found in K3 adopt a similar structure in fibrils of the full length protein. The simulated peaks from the K3 fibril match much better than the soluble β_2m peaks match in Figure 69; however the superimposition of the peaks is not proof that the peaks belong to the same resonances. Where there are assignments available for superimposable peaks of both K3 and our full length fibrils, the assignments do not match. For example, the Ser-28

$^{13}C\alpha$-$^{13}C\beta$ cross-peak from K3 lies directly over the cross-peak assigned as Ser-61 in the PDSD spectrum of the full length β_2m fibrils; it is possible that the cross-peak in the PDSD contains contributions from more than one residue, in which case the peaks could correspond to each other; however it's also equally possible that the peaks do not correspond at all and that is just co-incidence that they superimpose. The same situation also occurs with the K3 Val-27 which overlays with a peak assigned to Val-49 in the full length fibrils and the same caveats apply.

It is difficult to make definitive conclusions about the similarity between the structures of the two fibril types. The majority of K3 peaks, with the exceptions outlined above, do appear in very similar envelopes as the peaks in the 20 ms PDSD which is indicative of similar environments; however there are too many caveats associated with the comparison in order to be confident that the residues share very similar environments within the two fibril types. What is clear from this comparison is that care should be taken if using the K3 assignments in order to try and facilitate assignment of the full length β_2m spectrum as the currently assigned peaks do not correspond to the superimposed K3 assignments.

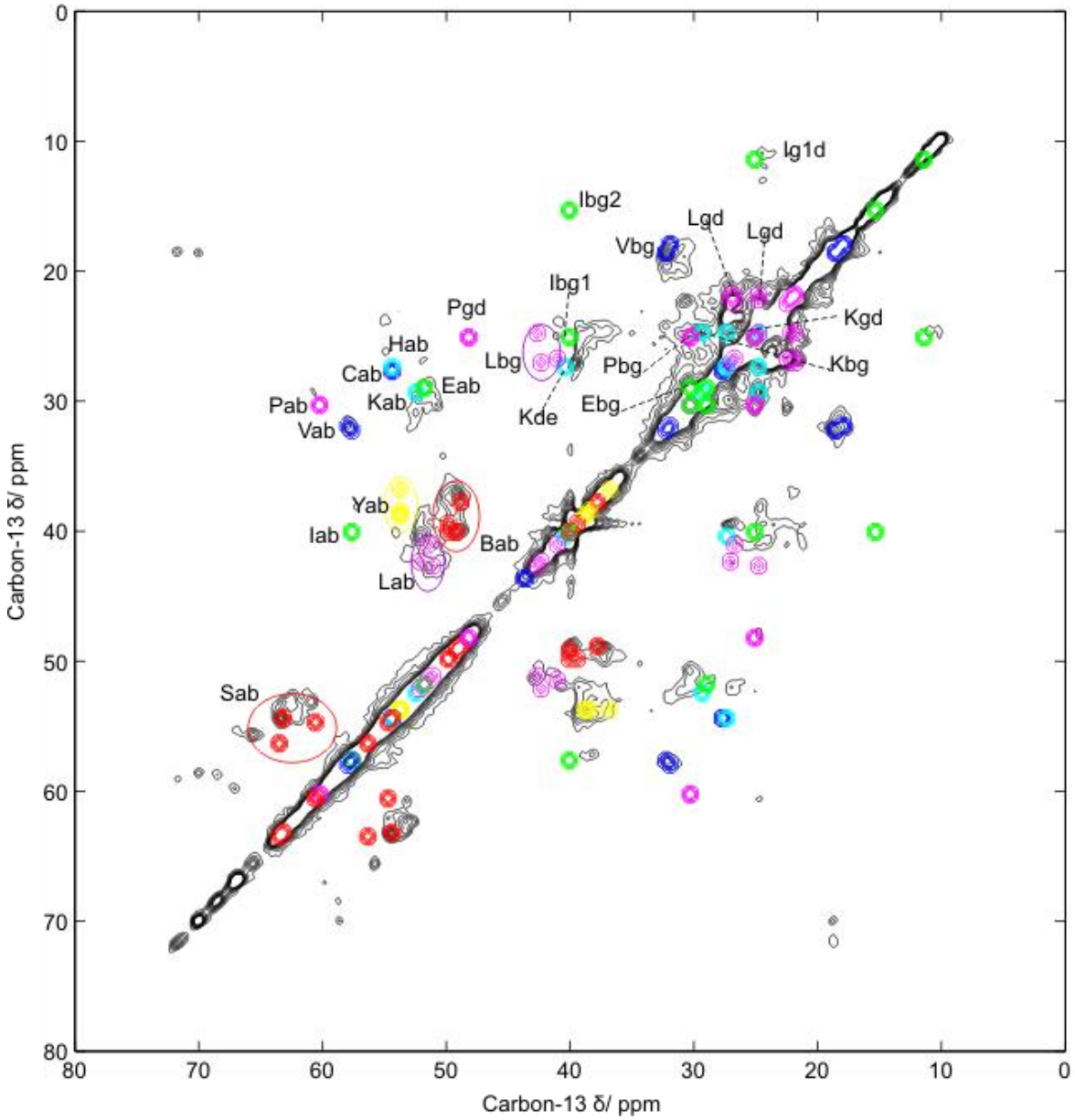

Figure 70 Simulated PDSD spectrum of fibrillar K3 fragment overlain on PDSD (20 ms) spectrum of full length fibrillar β_2m

K3 fibrils PDSD (in colour) simulated from chemical shifts published by Iwata *et al.* in 2006 (*84*) are overlain on PDSD of full length β_2m. Correlations are identified through single letter code followed by correlation type i.e. Ibg2 is isoleucine β to γ2 correlation.

Table 9 Chemical shifts of assigned carbon and amine nitrogen nuclei in fibrillar β_2m at pH 2.5

Chemical shifts of ^{15}N and ^{13}C nuclei assigned using 2D triple resonance hetero correlation experiments. Gray shading is used in cases of that nucleus type not being present in the corresponding residue. Pink shading is used for the areas of the N and C termini that are not expected to appear in dipolar mediated solid-state spectra which are not expected to be observable in the spectra acquired due to high mobility Missing chemical shifts were not able to be determined with the data acquired.

Residue	N_{amine}	C'	Cα	Cβ	$C\gamma_1$	$C\gamma_2$	$C\delta_1$	$C\delta_2$	Cε
1Ile									
2Gln									
3Arg									
4Thr									
5Pro									
6Lys									
7Ile									
8Gln									
9Val									
10Tyr									
11Ser									
12Arg									
13His									
14Pro									
15Ala									
16Glu									
17Asn		172.24							
18Gly	118.28	170.87	45.97						
19Lys									
20Ser									
21Asn									
22Phe									
23Leu									
24Asn									
25Cys									
26Tyr									
27Val									
28Ser		172.53		61.31					
29Gly	117.56	171.79	46.31						
30Phe									
31His		167.66	51.26						
32Pro	128.35	174.2	61.28	30.15	25.48		48.41		
33Ser	112.2	170.26	58.2	66.41					
34Asp									
35Ile									
36Glu									

37Val								
38Asp								
39Leu								
40Leu								
41Lys		173.47						
42Asn	116.29	173.89	51.01	35.21				
43Gly	113.84	169.47	43.43					
44Glu	117.24		53.01	30.99				
45Arg		171.73						
46Ile	123.86		58.00	39.09	25.53	16.39	12.05	
47Glu		172.69						
48Lys	120.12		55.55					
49Val	120.84	172.71	58.48	32.93	19.67			
50Glu	121.23	175.07	51.58	31.12	34.91		177.6	
51His	121.33	171.55	54.49					
52Ser	115.64	168.62	56.51	66.37				
53Asp	120.37	171.44	49.88	38.12	174.43			
54Leu	119.28	173.21	52.8	41.24	25.26			
55Ser	118.45	168.48	54.09	63.68				
56Phe	121.64		59.45					
57Ser	116.31	170.33	55.10	61.69				
58Lys	121.95	174.35	56.98	31.37	23.29		27.62	40.39
59Asp	119.35	171.62	50.83	38.19				
60Trp	125.91	173.17	56.39				127.33	
61Ser	122.51	168.35	55.29	64.15				
62Phe	122.9							
63Tyr								
64Leu								
65Leu								
66Tyr								
67Tyr								
68Thr								
69Glu								
70Phe								
71Thr								
72Pro		174.32	61.06	30.72	25.42		49.10	
73Thr	118.89	171.78	60.63	67.92	19.22			
74Glu	122.64	172.59	51.58	30.65	34.93			
75Lys								
76Asp								
77Glu								
78Tyr		171.54						
79Ala	127.28		48.78	19.75				
80Cys								
81Arg								

82Val	121.8	172.67	60.11	30.69	20.58
83Asn					
84His	118.63		55.92		
85Val	119.67	173.19	58.75	32.18	19.18
86Thr	116.01		59.9	72.41	19.48
87Leu					
88Ser					
89Gln					
90Pro					
91Lys					
92Ile					
93Val					
94Lys					
95Trp					
96Asp					
97Arg					
98Asp					
99Met					

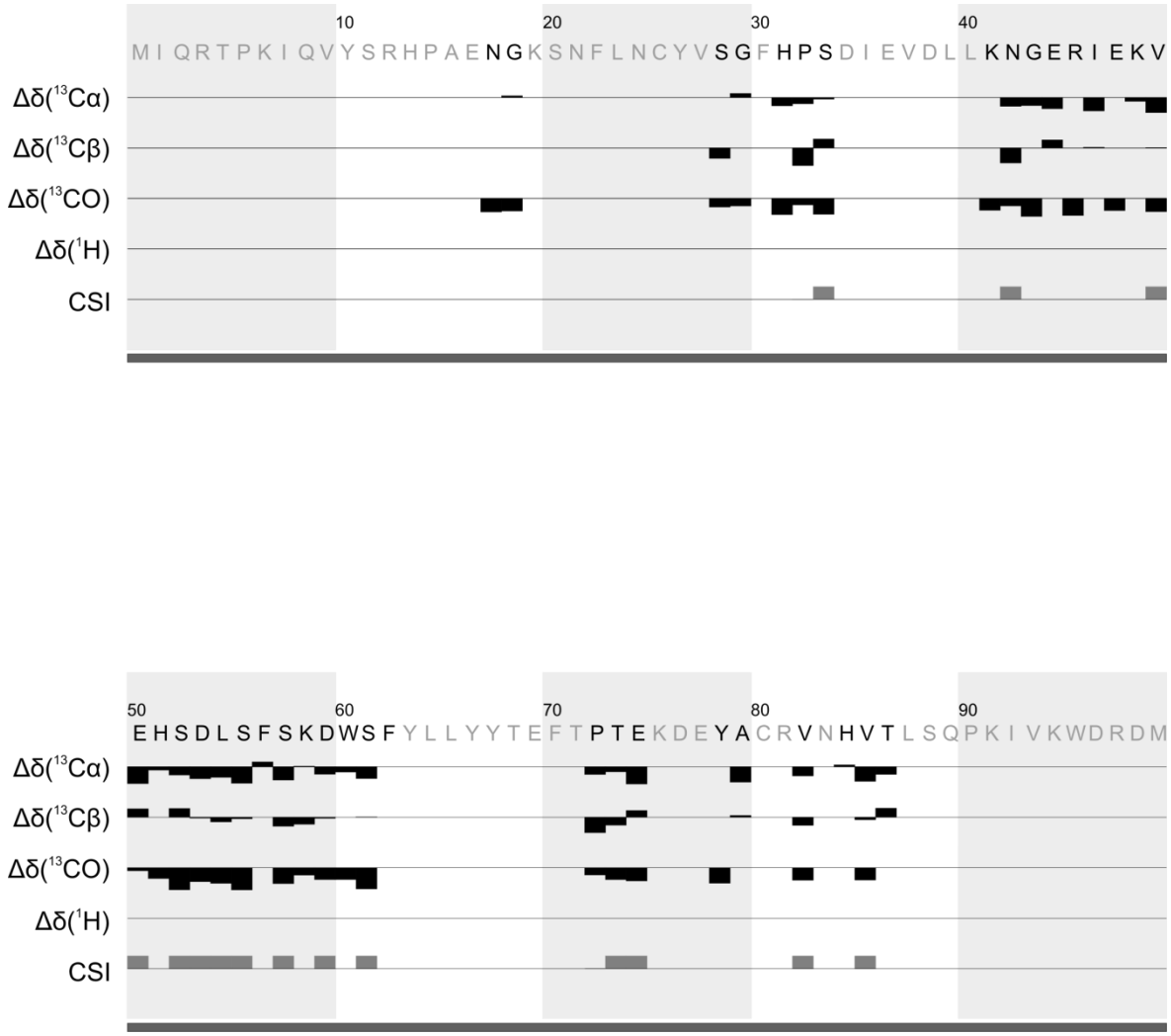

Figure 71 Chemical Shift Index of assigned fibrillar β_2m resonances
The chemical shift index predicts secondary structure based on deviation of chemical shift from reference random coil values. Bars extending below the line in the CSI row predict residues in alpha helices while bars extending above the line predict residues in beta strands.

4.6 Comparison between fibrillar beta-2 microglobulin and beta-2 microglobulin inclusion bodies

To ascertain as to whether β_2m in inclusion bodies have the same structure as β_2m in fibrils we used a range of methods to identify any similarities or differences between the two. The fluorescence emission spectra of thioflavin T (ThT) is widely used as an indicator for the formation of amyloid fibrils (*149*). To ascertain if β_2m inclusion bodies possess the necessary structural properties to bind ThT, emission spectra were recorded in the presence of inclusion bodies, β_2m fibrils created by acid precipitation and soluble monomeric β_2m (Figure 72). Both the β_2m fibrils and inclusion bodies showed enhanced fluorescence at 485nm compared with the soluble β_2m. Interestingly, ThT fluorescence for the inclusion bodies was only 11% of that of the fibrillar material (*132*). This suggests that within the inclusion bodies either only a fraction of the protein exists in its fibrillar form capable of enhancing fluorescence or that the β_2m adopts a conformation that results in a lower enhancement of fluorescence than when bound to fibrillar structures.

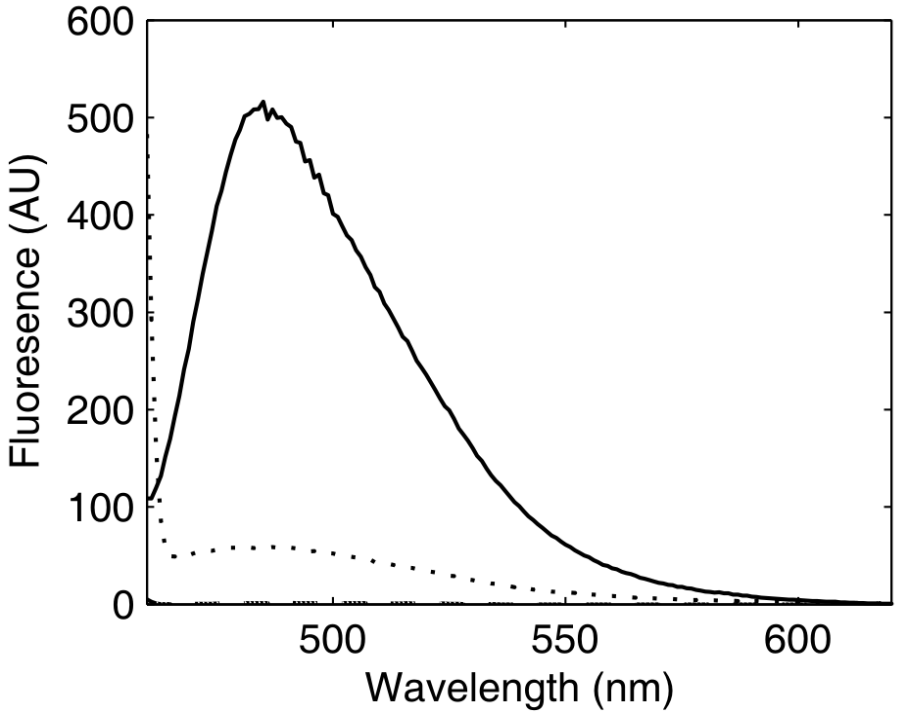

Figure 72 ThT emission spectra in different morphologies of β_2m
1 mg mL^{-1} solutions of β_2m fibrils (-), inclusion bodies (. . .) and monomeric β_2m (- - -). ThT excited at a wavelength of 440 nm and emissions measured at 485 nm.

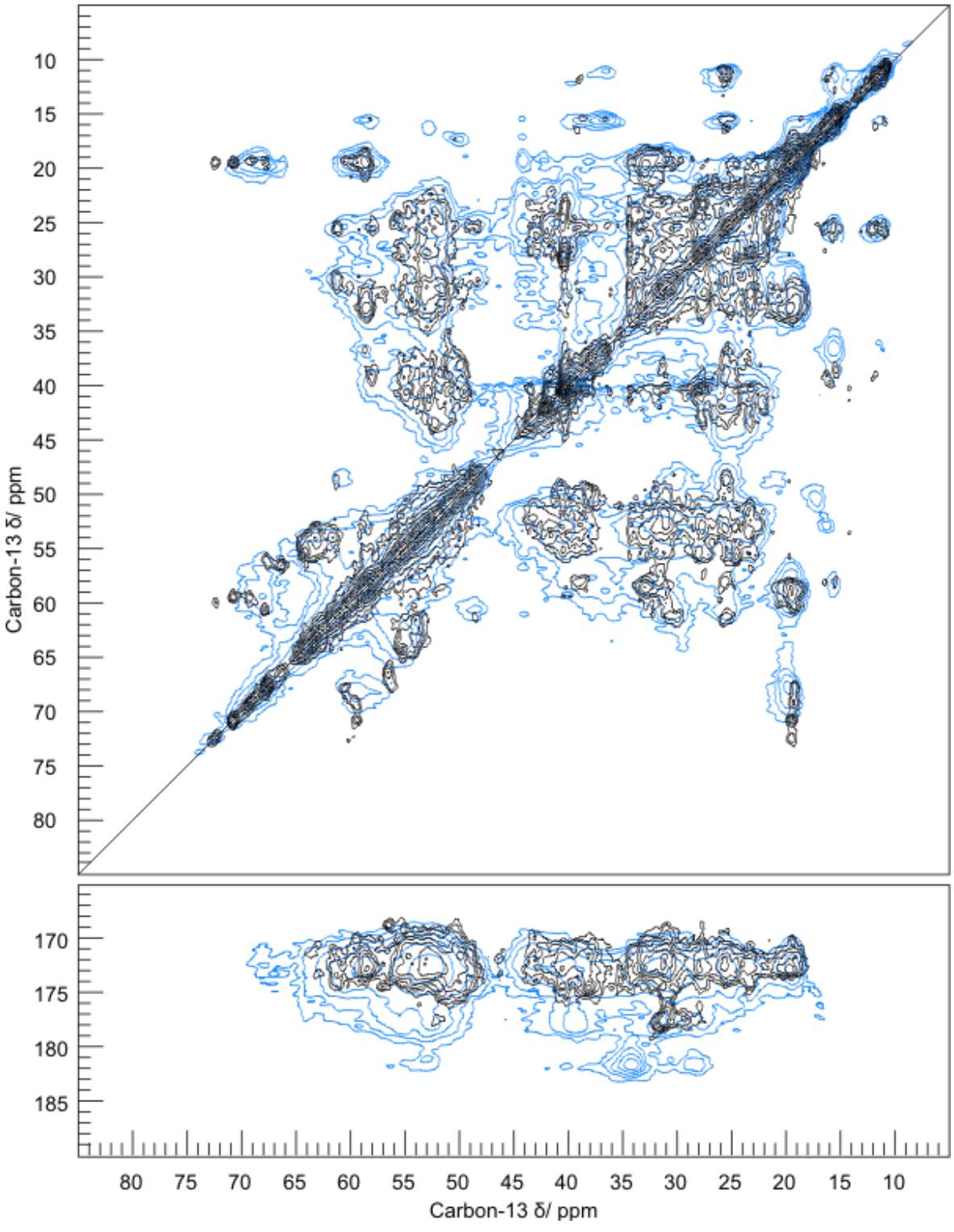

Figure 73 Overlain PDSD spectra from fibrils and inclusion bodies.
Black spectrum is β_2m in fibrils, blue spectrum is β_2m in inclusion bodies Spectra acquired on Bruker 850 MHz WB US_2, 15000 Hz spinning with 30 (IB) or 100 (Fibrils) ms mixing time. IB are at pH 7, fibrils are at pH2.5. Both spectra acquired at -1˚C (*132*).

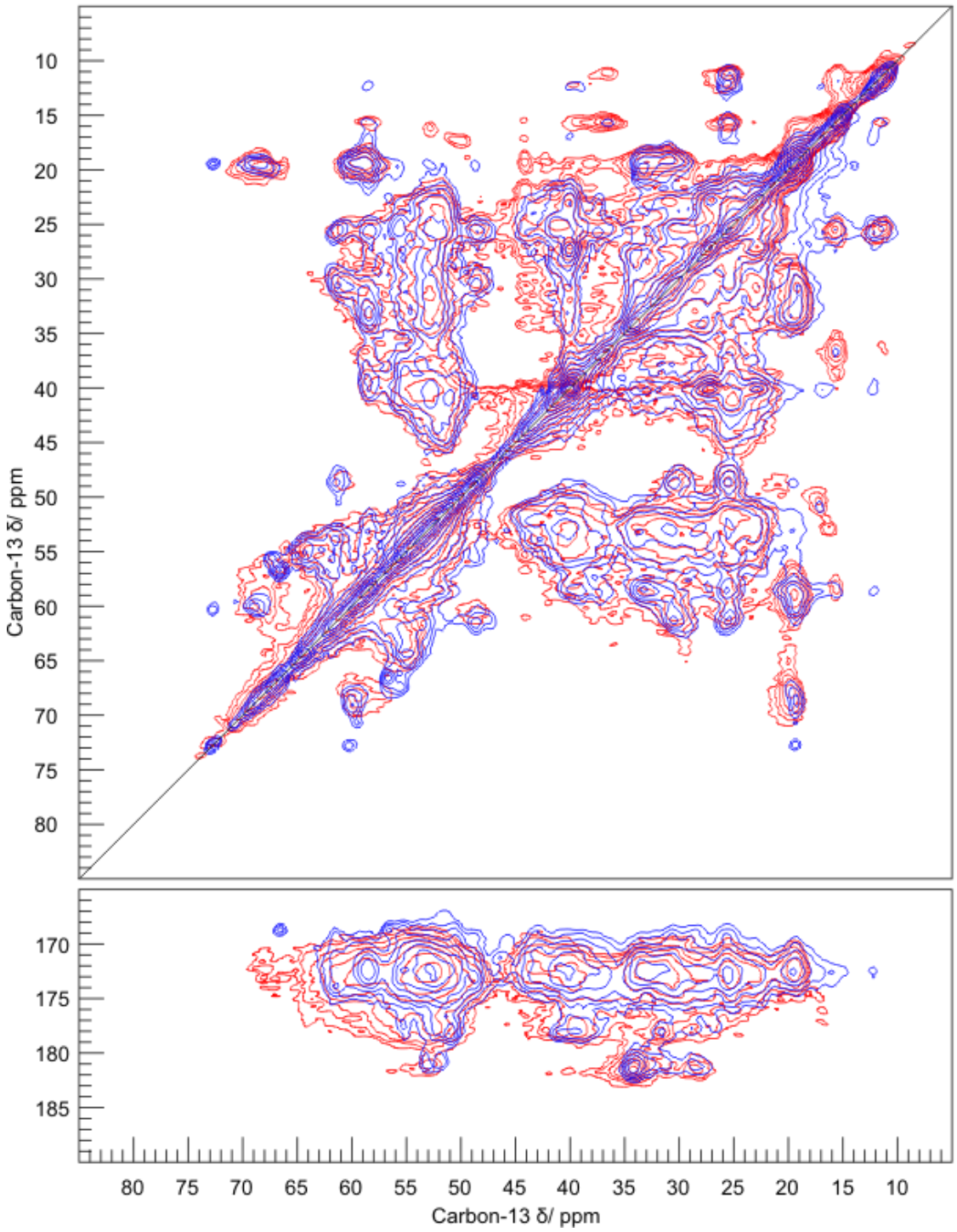

Figure 74 Overlain PDSD spectra from fibrils (blue) and inclusion bodies (red) both at neutral pH

Blue spectrum is β_2m in fibrils, red spectrum is β_2m in inclusion bodies. Spectra acquired on Bruker 850 MHz WB US_2, 15000 Hz spinning with 30 (IB) or 100 (Fibrils) ms mixing time. IB and fibrils are both at pH 7. Both spectra acquired at -1˚C.

The spectrum of β_2m inclusion bodies is dominated by intense protein resonances that arise from β_2m within the inclusion bodies (Figure 73). There is no evidence of other material such as oligosaccharides, DNA and lipids as previously observed in inclusion body preparations of other systems (*131*). The spectrum of inclusion bodies is again dominated by intra-residue cross-peaks; however in contrast to the fibrillar β_2m these are significantly more intense. The efficient proton driven spin diffusion and cross polarisation throughout the spectra suggests that the dipolar couplings within the inclusion body sample are stronger than those in the fibrillar material suggesting the protein exhibits less mobility. This efficient proton driven spin-diffusion also leads to a number of additional cross-peaks within the inclusion body spectrum compared to the fibrillar material. In particular significant intensity is apparent at sites which correspond to correlations between sites in the sidechains containing carboxylic/carboxamide groups (Asp/Glu/Asn/Gln) at (58-25, 175-185 ppm) and correlations between the aromatic sidechains (Phe/Tyr) and the corresponding Cβ's at (~130, 30 ppm) (*150*). In addition, correlations between resonances attributed to aliphatic sidechains show significantly enhanced intensity, in particular Ile (*132*).

The resonances observed in the inclusion body spectrum are significantly broader than those observed in the fibrillar spectrum. This increase in linewidth can be attributed to the lower mobility within the inclusion bodies resulting in an increase in the homogeneous linewidth. This is consistent with the enhanced spin-diffusion observed throughout the PDSD spectra of the inclusion bodies due to reduced motional scaling of dipolar interactions. The observed increase in homogeneous linewidth is further supported by inspection of resonances along the diagonal. It is expected that inhomogeneous broadening would lead to a distribution of resonances along the diagonal whilst an increase

in the homogeneous linewidth would result in a broadening of the diagonal (*132*). Comparison of the diagonal resonances in the fibrillar and inclusion body spectra show a clear increase in linewidth from ~0.7 ppm to 1.2 ppm consistent with an increase in homogeneous linewidth.

Further evidence still that the increased linewidth is homogenous and due to a change in dynamics comes from the comparison of the inclusion body PDSD spectrum with that of fibrils at neutral pH (Figure 74). In order to maintain fibril stability at neutral pH the fibrils in neutral pH buffer are more densely packed into the MAS rotor in order exclude water and increase molecular crowding which we have shown increases fibril stability. The higher packing of the fibrils leads to increased linewidths in the neutral pH spectrum, which results in increased similarity between the neutral pH fibril and inclusion body spectra. Despite the increased similarity due to line broadening there are still clear differences. The width of the diagonal in the inclusion body spectra is still wider than the neutral pH fibrils indicating that the inclusion bodies still have higher packing than the fibrils. The inclusion bodies were pelleted at 16000 *g* and loaded into the MAS rotor with a spatula and rod while the fibrils were pelleted at 16000 *g* using the filter method described on page 232. This method vastly decreases the amount of water in the fibril sample which can be up to 75% of the sample; the removal of the water allows for higher packing of the fibrils into the MAS rotor. The higher packing of the inclusion bodies despite no attempt to remove water from the sample is most probably due to the spherical morphology of the bodies they form as can be seen in Figure 75. Inclusion bodies were negatively stained with uranyl acetate and then studied using a transmission electron microscope (Hitachi) in exactly the same manner as acid produced fibrils (Chapter 2.2.2) The images produced quite clearly show huge differences between the aggregate

morphology of β_2m fibrils and inclusion bodies. As opposed to the classical long, straight and helical morphology of β_2m fibrils of about 20 nm diameter and varying length up to and in excess of 1 μm; inclusion bodies are spherical in nature. These spheres of β_2m aggregate vary greatly in size from less than 40 nm in diameter to nearly 200 nm in diameter. The negative stain does not pool around the outside of the inclusion bodies as with low salt acid produced fibrils but gets absorbed into them. This could be indicative of less densely arranged β_2m within the inclusion bodies themselves, although the spherical nature of the bodies would allow denser packing of inclusion bodies into MAS rotors leading to increased signal to noise from solid-state NMR samples.

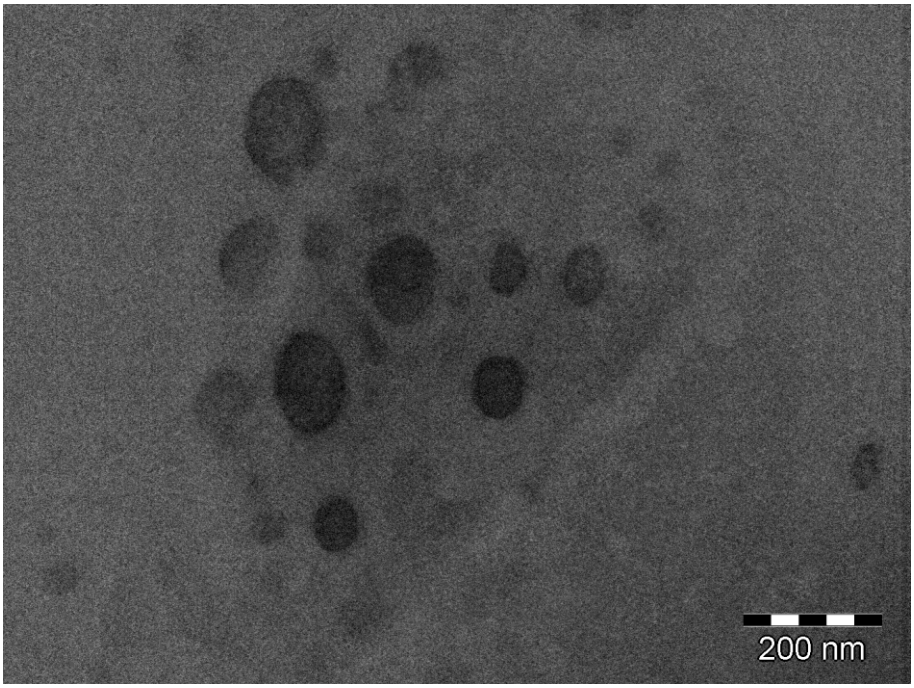

Figure 75 Negative stained TEM image of inclusion bodies at 80000 x magnification
This image is of β_2m inclusion bodies stained with uranyl acetate (2%). Image taken on a Hitachi transmission electron microscope operated at 120 kV.

Peaks in the fibril spectrum are generally better resolved and there are peaks that appear alone and well resolved that do not appear in the inclusion body spectrum such as that

corresponding to the alpha-beta correlation of Thr- 86. In addition to this within the crowded envelopes corresponding to the side-chain correlations peak maxima are not superimposable in all cases indicating differences in electrostatic environment and hence structure between the two forms of β_2m.

4.7 Conclusion

In chapter 2 it was demonstrated that fibrillar β_2m interacts with Serum Amyloid P component (SAP). It was decided to undertake a study investigating the binding site between fibrillar β_2m and SAP. In order to attain this goal, atomic level structural information was needed for β_2m while it is in its fibrillar state. Solid-state Magic Angle Spinning NMR was chosen as an attractive method in which chemical shift data, reflecting the electrostatic environment of the nuclei within β_2m, could be used to monitor changes in environment in later experiments with SAP bound.

Substantial assignment of β_2m in fibrils

A range of homo and heteronuclear experiments were therefore run, spectra acquired and a heteronuclear chemical shift assignment was undertaken. Initial experiments at 600 MHz were promising but the large size of β_2m meant that spectral crowding was a problem. Uniformly ^{13}C and ^{15}N labelled PDSD (Figure 58 and Figure 59) and NCX (Figure 61 and Figure 62) spectra were therefore acquired at 850 MHz; this increase in field strength led to sufficient resolution in order to make site-specific assignments and the combination of experiments used allowed sequential assignments to be made as demonstrated in **Error! Reference source not found.**. Recombinant β_2m is 100 residues in size, this far exceeds the size of any fibrillar protein that has been published; at the time of writing HET-s (218-219) is the largest solved structure. This 71 residue fragment of the full length HET-s fungal prion protein structure has been determined but even so only 56 out its 71 residues have been sequentially assigned (*20*). The size of β_2m means that two-dimensional spectra of uniformly labelled samples are extremely crowded and due to this, the amount of sequential assignments that could be made in two dimensions was limited. Attempts to run

three-dimensional experiments resulted in spectra with such poor signal to noise that they were unable to be used for assignment purposes. Due to machine time constraints it was not possible to increase the number of scans and increments used therefore selective and extensive labelling was used as an alternative method to simplify the two-dimensional spectra. As can be seen in Figure 64 and Figure 65, the labelling schemes used were effective at reducing spectral overlap in PDSD spectra and as a consequence of the [2-^{13}C] –glycerol labelling scheme many leucine and valine resonances were identified as belonging to the same spin system. The [1,3^{13}C]-glycerol labelling scheme was useful for determining which ^{13}C'-^{13}Cα cross-peaks did not belong to certain residue types and the general improved resolution in this spectra made peak-picking much more reliable. Despite the usefulness of the PDSD spectra, the labelling schemes did not simplify the NCX spectra (Figure 66 and Figure 67) to the extent that was hoped; some additional sequential assignments were however able to be made. Deuteration of the labelled samples did not result in substantial simplification of NCX spectra and the poor signal to noise that resulted meant that no additional assignments were made using this method. Despite the obvious problems with spectral crowding some large sections of fibrillar β_2m were sequentially assigned and structural and dynamic information was able to be inferred. Resonances were assigned from 39 different spin systems with the longest stretch of sequential assignment being 14 residues. No resonances were assigned in the first 16 N-terminus residues or the last 13 C-terminus residues. This finding corroborates previous findings that these sections of the termini are mobile and are not observable in the dipolar coupled spectra (*146, 147*). When this is taken into account approximately 54% of the residues expected to appear in the spectra have at least one resonance assigned to them. The assigned chemical shifts can be found in Table 9.

Beta-strand structure increases in fibrillar β_2m

Chemical Shift Index (CSI) analysis (Figure 71) of the assigned resonances gives an interesting result, that is, the residues that form the loop region between β-strands V and VI in native β_2m are predicted to form β-strand secondary structure in fibrillar β_2m. This finding is corroborated in other work recently published (*147*). This strongly suggests that β-strand secondary structure increases during the transition from native to fibrillar β_2m. This means that there are large structural transitions occurring in the formation of fibrils and it can be speculated that it is not solely the β-strands that exist in the native form which contribute to the cross-β structure present in β_2m fibrils. The occurrence of large structural transitions fits with previous cryo-EM data which demonstrated that native β_2m monomers could not fit into the dimensions of fibrils without structural rearrangement (*13*). Another finding of note is that Pro-32 and Pro-72 were both fully assigned and from their ^{13}Cβ & γ chemical shifts it can be confidently predicted that they are both in the *trans* conformation which is in contrast to native β_2m and in fact most soluble proteins where the *cis* conformer of proline is present. The transformation of Pro-32 from *cis* to *trans* is thought to be a necessary step in β_2m fibrillogenesis (*58*).

Significant progress has therefore been made towards the assignment of chemical shifts within fibrillar β_2m. However, it is clear that in order to get a full assignment other techniques will need to be used in order to decrease spectral overlap and assign chemical shifts to specific residues' nuclei.

Extensive differences in electrostatic environment occur between native β_2m and β_2m in fibrils

In chapter 3 a full heteronuclear assignment was completed for native monomeric β_2m; the goal of this was to obtain chemical shifts so that they could be compared with the chemical shifts of fibrillar β_2m. This would allow the identification of areas of the protein that undergo structural transition between the native and fibrillar states. As previously mentioned in this conclusion, CSI analysis has already predicted a structural transition in the V-VI loop region of native β_2m to β-strands in fibrillar β_2m. The loop region is unobservable in our liquid-state spectra of native β_2m; but in the fibrillar form it is contained within the longest uninterrupted series of sequential assignments. This demonstrates that as well as gaining β-strand secondary structure, the dynamics of the region slow down enough to allow efficient coherence transfer through dipolar couplings. In order to be able to draw comparisons between our liquid-state data a short mixing time PDSD spectra was simulated from the data using the programs GAMMA and Matlab. This simulated spectrum was then overlain on the 20 ms mixing time PDSD of uniformly labelled β_2m which roughly corresponds to the mixing of magnetisation between adjacent ^{13}C nuclei. More general conclusions about whether β_2m undergoes structural transitions between the native and fibrillar form can be drawn when the two spectra are compared Figure 69). The cross-peaks in the spectra are not directly superimposable which immediately suggests that the electrostatic environments of the nuclei are not identical. Many peaks easily assignable to a particular residue type such as the threonine ^{13}Cβ correlations to ^{13}Cα and γ and serine ^{13}Cα-β have clearly substantial chemical shift differences, implying that they are in significantly different environments. The majority of simulated cross-peaks do not superimpose upon corresponding peaks in the 20 ms mixing time PDSD spectrum suggesting that most residues are in different environments within

the native and fibrillar forms of β_2m. These results do have to be considered with the caveats discussed in the results section, such as increased coupling efficiency in the liquid-state experiments and the pH of the samples being different. The simulated peaks are also all of the same intensity irrespective of the intensity of peaks in the original data they were simulated from.

Nuclei experience different environments within β_2m fibrils and β_2m K3 fibrils

The 22 residue K3 fragment of β_2m forms fibrils at acidic pH, and the structure of fibrillar K3 has been solved by Iwata *et al.* (*84*). It has been proposed that the residues contained within the K3 fragment may form the amyloidogenic core of fibrils formed from full length β_2m and therefore, there was the possibility that the residues within the K3 fibril experienced a similar environment to those found within full length β_2m fibrils. If this was the case then it would inform us a lot about the structure of β_2m fibrils and may even have facilitated assignment. The chemical shift data from the published structure of K3 fibrils was therefore taken and a PDSD spectrum simulated as with the liquid-state data previously described. The simulated K3 spectrum was overlain on the 20 ms PDSD spectrum of the fibrillar β_2m to allow comparison of the chemical shifts (Figure 70). The cross-peaks from the simulated K3 PDSD show much better superimposition with the cross-peaks of the 20 ms spectrum than the simulated liquid-state data do. Most simulated peaks fall within the same envelope as the β_2m peaks they correspond to, with the exception of those belonging to peaks at the termini of K3 and the Cys-25 which in K3 does not form a disulphide bridge. Only the peaks corresponding to Val-27 and Ser-28 α-β correlations were directly superimposable on peaks from β_2m but these peaks have already been confidently assigned to Val-49 and Ser-61. The data therefore suggest that although the environments experienced by the nuclei may be similar, as determined by similar

envelopes, they are not the same. Apart from at the termini the peaks that superimpose least well are Gly-29 to Asp-34; in K3 these are situated in the loop region between the two β-strands. This could suggest that these residues may form a different secondary structure within the β_2m fibrils, most likely β-strand.

Differences in morphology between β_2m in inclusion bodies and fibrils

Bacterial inclusion bodies are formed when protein is over-expressed in recombinant bacteria. Traditionally it was thought that the protein within these inclusion bodies was amorphous and functionally inactive. However, a number of studies have revealed that for some proteins there is at least a population of proteins within the inclusion bodies which are functionally competent (*128, 129*).

Recent studies have focused on the similarities between inclusion bodies and amyloid fibrils (*130, 131, 151*). These studies have revealed that upon expression of a diverse range of proteins in *E.coli*, the inclusion bodies formed have many of the properties associated with the formation of amyloid deposits. These observations have led to the speculation that inclusion bodies and amyloid deposits may share a common functional role, namely the sequestration of misfolded protein to prevent damage to the host.

In order to investigate whether this is the case with β_2m inclusion bodies we undertook a comparison of the properties of β_2m in inclusion bodies and of β_2m in fibrils. This study compared ThT fluorescence in the presence of inclusion bodies or fibrils (Figure 72); used Transmission Electron Microscopy (TEM) to study the macroscopic structure (on the nanometre scale) (Figure 75); and PDSD spectra of the two forms (Figure 73 and Figure 74) to study differences in electrostatic environment and dynamics. ThT fluorescence in the presence of inclusion bodies was only 10% of that in the presence of the equivalent amount

of fibrils (Figure 72). This could indicate several possibilities: 10% of the β_2m within inclusion bodies is of a fibrillar nature; in the presence of β_2m inclusion bodies ThT has a different quantum yield than in the presence of fibrils; ThT can bind to β_2m within inclusion bodies but has a reduced affinity; or the packing of inclusion bodies prevents the access of ThT to any β_2m that is not on the surface of the inclusion body.

The ThT fluorescence data quite clearly show that there are differences between β_2m in inclusion bodies and β_2m in fibrils. If the structure and morphology were exactly the same the ThT fluorescence of the two samples would be similar. The results also show that increasing ThT fluorescence at 485 nm is not a generic property of β_2m as ThT does not show increased fluorescence in the presence of native β_2m (*132*).

The fluorescence data are supported by the TEM data in Figure 75. Inclusion bodies were negatively stained; the images produced quite clearly show large differences between the aggregate morphology of inclusion bodies and fibrils. As opposed to the classical long, straight and helical morphology of β_2m fibrils, inclusion bodies are spherical in nature. The negative stain does not pool around the outside of the inclusion bodies as with fibrils but gets absorbed into them. This could be indicative of less densely arranged β_2m within the inclusion bodies themselves, although the spherical nature of the bodies would allow denser packing of inclusion bodies into MAS rotors leading to increased signal to noise from solid-state NMR samples. The absorbance of the stain is an important factor as it effectively rules out the possibility that the ThT emission is reduced because of ThT not being able to access fibril-like inclusion bodies with the core of the inclusion body. This leaves the possibilities that ThT fluorescence is different because of a difference in quantum yield or binding affinity, which are both related to molecular structure, or that a sub population of β_2m within the inclusion bodies is fibrillar in nature.

The morphologies of the two types of β_2m aggregate are irrefutably different, but only solid-state NMR spectra would be able to prove whether they show identical molecular structures as found with other proteins (*131, 151*). The PDSD spectrum acquired of β_2m in inclusion bodies shows large differences with the PDSD spectrum of β_2m fibrils at acidic pH when overlain as in Figure 73. The intensities of the cross-peaks in the inclusion body spectrum are significantly larger than in the fibril spectrum; this suggests more efficient proton driven spin diffusion and cross-polarisation due to stronger dipolar coupling in the inclusion body sample which in turn suggests less mobility. This efficient proton driven spin-diffusion also leads to a number of additional cross-peaks within the inclusion body spectrum compared to the fibrillar material. Notably, correlations between sites in aspartate, glutamate, asparagine, and glutamine side-chains; correlations between aromatic side-chains and their corresponding ^{13}Cβ's; and isoleucine side-chain site correlations showed particularly enhanced intensity (*132*).

The resonances observed in the inclusion body spectrum are significantly broader than those observed in the fibrillar spectrum. This increase in linewidth can be attributed to the lower mobility within the inclusion bodies resulting in an increase in the homogeneous linewidth. This is consistent with the enhanced spin-diffusion observed throughout the PDSD spectra of the inclusion bodies. Based on the earlier perception that inclusion bodies are composed of misfolded protein it was expected that significant inhomogeneous broadening would have been observed due to the structural heterogeneities within the sample. However, resonances can be resolved in the inclusion body spectrum with linewidths of 1.0 ppm, similar to those observed in other non-crystalline yet structurally homogeneous fibrillar systems (*152*). The observed increase in homogeneous linewidth is further supported by inspection of resonances along the diagonal. It is expected that

inhomogeneous broadening would lead to a distribution of resonances along the diagonal whilst an increase in the homogeneous linewidth would result in a broadening of the diagonal. Comparison of the diagonal resonances in the fibrillar and inclusion body spectra show a clear increase in linewidth from ~0.5 ppm to 1.2 ppm consistent with an increase in homogeneous linewidth.

The enhanced cross peak intensity and larger line width observed in the inclusion body spectrum suggests significant dynamical differences between the acidic fibrillar and inclusion body forms of β_2m. In addition, there are noticeable differences in the position of a number of resonances suggesting differences in local structure or environments. These may be responsible for the lower ThT fluorescence that is observed upon the binding of ThT to the inclusion bodies (*132*).

The PDSD spectrum of fibrils at neutral pH (Figure 74) also shows an increase in homogenous linewidth due to a change in dynamics. As discussed in the results section the neutral pH fibrils have had water excluded from them leading to higher packing. The higher packing of the fibrils and exclusion of water leads to increased linewidths in the neutral pH spectrum, which results in increased similarity between the neutral pH fibril and inclusion body spectra, evidence that the increase in line-width in the inclusion body spectrum is due to decreased dynamics caused by higher packing/less hydration. Despite the increased similarity due to line broadening there are still clear differences. The width of the diagonal in the inclusion body spectra is still wider than in the spectrum of the neutral pH fibrils indicating that the inclusion bodies still have higher packing than the fibrils; this higher packing of the inclusion bodies despite no attempt to remove water from the sample is most probably due to the spherical morphology of the bodies they form as can be seen in Figure 75. Peaks in the fibril spectrum are generally better resolved and

there are peaks that appear alone and well resolved that do not appear in the inclusion body spectrum such as that corresponding to the alpha-beta correlation of Thr-86. In addition to this, within the crowded envelopes corresponding to the side-chain correlations, peak maxima are not superimposable in all cases indicating differences in electrostatic environment and hence structure between the two forms of β_2m.

Chapter 5

5 Identifying the β_2m fibril-SAP interface

5.1 Introduction

The main goal of this project is to identify how β_2m fibrils and SAP interact. Identifying this interaction will not only give insight into the pathogenesis of DRA but also a variety of other amyloid diseases in which SAP may stabilise fibrils and prevent amyloid load being cleared by the body. There is an increasingly large amount of evidence that SAP is causative in amyloidosis. Firstly SAP is found associated with all types of amyloid deposits (*99*). In addition *in vivo* studies demonstrate that progression of amyloidosis is linked to SAP; in experimental murine reactive systemic amyloidosis, deposition of serum amyloid A protein as amyloid was found to correlate better with levels of SAP than that of serum amyloid A protein (*86*). In studies in the Syrian hamster females developed reactive systemic amyloidosis much more readily than males. The relevant difference between males and females in this case being that SAP is under female sex hormone control (*87*). SAP knockout mice show retarded and reduced induction of experimental reactive systemic amyloidosis (*90*) demonstrating that SAP definitely does contribute to at the very least this type of amyloidosis

Catabolism of SAP only occurs in the hepatocytes and so when associated with amyloid deposits no degradation of SAP takes place. This has been demonstrated by Pepys by using radiolabelled ^{125}I-SAP as it persists in the deposits for prolonged periods. SAP from both blood and amyloid deposits are indistinguishable from each other. These findings

support the concept that SAP provides a protein coating to the fibrils masking them from the body's protein scavenging mechanisms (*1*). SAP itself is also highly resistant to proteolysis (*88*). It has been demonstrated that SAP binding to Aβ deposits from Alzheimer's, and AA fibrils from reactive systemic amyloidosis, conferred resistance to proteolysis during *in vitro* tests. SAP could only prevent the degradation while bound to the fibrils, and when the SAP was dissociated from the fibrils using cyclic pyruvate acetal the proteinases cleaved the fibrils to the same extent as with no SAP present. This demonstrates that SAP prevents proteolysis through steric hindrance and it is not a protease inhibitor (*89*).

Mouse studies of the drug R-1-[6-[R-2-carboxy-pyrrolidin-1-yl]-6-oxohexanoyl] pyrrolidine-2-carboxylic acid (CPHPC) resulted in the clearance of both SAP and amyloid from animals tested with the drug (*90*). CPHPC's mechanism of action is by blocking ligand binding sites on SAP whilst cross linking pairs of pentameric SAP molecules forming a decameric molecule which is rapidly cleared from the body by the liver. This rapid depletion of SAP from the plasma leads to SAP dissociating from amyloid deposits into the plasma as SAP in the two components are in dynamic equilibrium. CPHPC is now undergoing human trials for the treatment of amyloidosis.

This evidence has so far been corroborated by our own studies which show that SAP binds β_2m fibrils strongly *in vitro* (Figure 21). Having demonstrated that SAP and fibrillar β_2m do interact the work in this chapter describes the efforts to characterise that interaction and identify the motif that must be common to all amyloid types that allows SAP to bind to each of them, irrespective of precursor protein. We employed solid-state NMR methods to study the differences between spectra of uniformly ^{13}C & ^{15}N labelled β_2m fibrils with and

without non-labelled SAP bound. This led to the identification of acidic residues of fibrillar β_2m as candidate molecules for involvement in binding with SAP.

Subsequently we chemically modified these acidic residues via an N-methylation protocol based on that of Hoare and Koshland (1966) (*153*); this removed their negative charge and then performed an SAP pull-down assay to see what effect the modification of acidic residues has on SAP binding.

The potential involvement of acidic residues of β_2m fibrils in SAP binding was further investigated using saturation transfer difference (STD) NMR. STD NMR is a technique becoming increasingly popular to study ligand-protein interaction and in particular which ligands and what part of them show an interaction with the protein. The experiment works through the principal of transferring saturation from a protein to a ligand: a sufficiently long period of irradiation of a resonance will result in the populations of the high energy and low energy spins contributing to that resonance becoming equal, this resulting in no NMR signal as NMR signal intensity is proportional to the population difference between energy levels (*127*). This phenomenon is called *saturation*; saturation of one part of a protein spectrum will result in propagation of saturation throughout the whole molecule via spin diffusion and hence the whole protein will be saturated. When a protein becomes saturated, ligands that are in exchange between a bound and free form with the ligand become saturated by *transfer* of the saturation from the protein to the ligand. When the ligand leaves the binding site that saturation is carried into solution. These saturated ligands will no longer contribute to the signal when a spectrum is acquired of the ligand in solution; a spectrum is also acquired of the ligand without the protein being saturated and in this experiment all the ligand in the sample will contribute to the signal. Subtraction of saturated spectrum from the non-saturated spectrum results in a *difference* spectrum which

will only show the resonances of the ligands that have come into contact with the protein (*154*).

Saturation of protein and bound ligand occurs in the region of 100 ms. A fast off rate will rapidly transfer information about saturation into solution; combined with a large excess of ligand a fast off rate will result in one binding site saturating many ligands in several seconds. Small molecules relax via T_1 and T_2 mechanisms in the order of 1 second in solution and so the proportion of saturated molecules increases throughout the saturation period. This results in the amplification of the signal arising from molecules that had been bound to the protein during the course of the experiment (*155*).

Conversely, if a ligand were to bind tightly to the protein and subsequently have a slower off rate then less ligands would have the opportunity to become saturated by contact with the protein during the saturation period; consequently the signal from these ligands would be attenuated due to smaller total amount being saturated and free in solution. Due to this, STD experiments are well suited to characterising ligand-protein interactions which have a K_D of 100 nM or more.

A series of Saturation-Transfer-Difference (STD) NMR experiments was carried out in order to determine if the glutamic sidechains show the weak interaction with SAP necessary for the strips of glutamates on fibrils to be the motif recognised by SAP when it binds to amyloid fibrils. A weak interaction could suggest that the co-operative action of many glutamates is needed in order to bind SAP. The side-chain carboxylate of glutamate was suspected as being the probable primary binding partner with SAP and so interactions of the free backbone carboxylate (which would not occur in the protein) had to be prevented. For this reason glutamic acid amide was used as the primary ligand as it has

only the side-chain carboxylate free to interact. Although aspartate side-chains are also candidates for binding with SAP, neither aspartic acid amide nor aspartate methyl ester were commercially available during the time of the study. The methyl esters of other amino acids were used as a control to determine if any STD effect seen with glutamic acid amide was specific and not a general low affinity interaction with SAP shown by all amino acids.

This chapter describes the methods used to identify the β_2m/SAP interaction site, the results from those experiments and the subsequent conclusions drawn.

5.2 Materials and Methods

5.2.1 Solid-State NMR studies of SAP bound β_2m fibrils

Two dimensional homonuclear correlation cross-polarised magic angle spinning experiments with $^{13}C/^{15}N$ enriched β_2m fibrils in the presence of isotopically non-enriched serum amyloid P component were run in order to identify the β_2m residues that are involved in SAP binding.

Fibrils (~20 mg) were produced as on page 79 and the supernatant removed by pipette and absorbent paper. The fibril pellet was then resuspended in 1 ml SAP (0.334 μM SAP, 200 mM $CaCl_2$, 200 mM Tris-HCl, pH 7.8) for 30 minutes. The sample was centrifuged for 30 minutes at 16000 *g* and supernatant removed and retained for analysis. The pellet was then washed with a low calcium buffer while keeping the pellet intact (in order to keep the fibrils in a crowded environment to reduce depolymerisation at neutral pH). This was achieved by transferring the pellet with a spatula to the top of a filtered pipette tip, which in turn was placed in a 1.5 ml reaction tube (Eppendorf) and this was subsequently centrifuged for 10 minutes at 16000 *g*. Low calcium buffer (200 μl of 10 mM $CaCl_2$, 25 mM KCl, 10 mM HEPES, pH 7.4) was added to the pellet in the filtered tip and the sample centrifuged for 1 minute at 16000 *g*. The pellet was transferred into a 3.2 mm rotor (Bruker) with a spatula.

Experiments were run on a Bruker advance 850 MHz wide bore, Ultra Shield 2. The probe used was an E^{free} 3.2 mm 850 MHz HCN CP-MAS probe. Magic angle spinning at 15000 Hz was used and the probe temperature was set to -10˚C for a sample temperature of ~0˚C once sample heating from spinning was taken into account. The PDSD experiments were run with a 100 ms mixing time, 128 scans and 631 increments in the indirect dimension.

5.2.2 N-methylation of acidic carboxylates

To ascertain the role and importance of fibrillar β_2m acidic side-chains in binding SAP we N-methylated the side-chains in order to remove their negative charge. The modification protocol used is based on that of Hoare and Koshland (1966) (*153*). The carboxyl group is first activated by the water soluble carbodiimide 1-Ethyl-3-(3-dimethylaminopropyl) carbodiimide hydrochloride (EDAC). The nucleophilic modifying reagent, methylamine-HCl, then attacks the activated carboxyl groups to yield the N-methylated carboxylate. N-hydroxysuccinimide has been shown to improve coupling efficiency of EDAC mediated protein-carboxylate conjugations (*156*) and so has been included to improve the efficiency of modification and to reduce side reactions such as modification of tyrosines (*157*).

A suspension of β_2m fibrils (1430 µl of 59 µM β_2m fibrils, 25 mM Citric acid, 25 mM KCl, 5 mM HEPES, 0.05% w/v sodium azide, pH 2.5, final conc. 8.4 µM β_2m) was centrifuged and the supernatant removed. The fibril pellet was resuspended in 15 ml MES buffer (50 mM pH 4.0). The suspension was repelleted, the supernatant removed and the pellet subsequently resuspended in 1430 µl MES buffer. EDAC (3750 µl of 23.5 mM, pH 4.0) was added to the fibril suspension and left to incubate at ambient temperature for 2 hours. The pH was monitored after the addition of EDAC and adjusted to 4.0 with dilute NaOH/HCl if necessary. N-Hydroxysuccinimide (2500 µl of 33.6 mM, pH 4.0) was added to the reaction tube and the pH again checked and readjusted to 4.0 if necessary. The reaction was allowed to proceed for a further 2 hours at ambient temperature. Finally methylamine-HCl (2500 µl of 40 mM, pH 4.0) was added to the reaction tube and the pH checked and readjusted to 4.0 if necessary. The reaction was allowed to proceed to completion overnight at ambient temperature. The fibrils were harvested and the supernatant removed. The pellet was then resuspended in 1430 µl distilled H_2O.

5.2.3 Mass spectrometry of depolymerised N-methylated fibrils

The successful N-methylation of β_2m fibrils will result in a mass increase of the β_2m molecules that make up the fibrils. Each carboxylate that is N-methylated should result in an increase in mass of 13 Da. Mass spectrometry is an analytical technique that can measure the mass of soluble molecules to the resolution of ~1 Da. Although fibrils are insoluble they can be dissolved down to their monomeric units through incubation in DMSO. Electrospray ionisation mass spectrometry of DMSO dissolved N-methylated fibrils was therefore used in order to determine the success of the above N-methylation experiment. The N-methylated β_2m fibrils samples were centrifuged (20 min, 17000 *g*), the supernatant removed and the pellet allowed to dissolve in 80% DMSO and 20% H_2O for 24 hours. Mass spectrometry was carried out on a Quattro II mass spectrometer (Micromass) fitted with a nano-ESI source. Samples were electrosprayed from gold-coated glass capillaries prepared in house, with an applied capillary voltage of 1.45-2.2 kV, a cone voltage of 75 V and a source temperature of 70˚C. The same procedure was applied to unmodified β_2m fibrils as a control.

5.2.4 Isoelectric focussing of depolymerised N-methylated fibrils

Removal of the negative charges of β_2m acidic residues will result in an overall increase in the pI of the β_2m within the fibrils; this change in pI can be detected by isoelectric focussing (IEF). In IEF the inclusion of ampholytes within a low density polyacrylamide gel means that any proteins added to the gel will migrate to their pI. The gel is then fixed with 10% TCA and stained with a method of choice for band visualisation; changes in pI as small as 0.01 pH unit can be detected. The theoretical maximum pI of a protein can be calculated using the tool ProtParam on the ExPASy bioinformatics portal (Swiss institute

for bioinformatics). The theoretical pI of unmodified β_2m is 6.05 and the theoretical pI of β_2m with all its side-chain negative charges removed is 10.39; accordingly IEF is a very good method for determining whether or not the N-methylation has been successful which should be readily detectable on an IEF gel.

IEF gels and buffers were supplied pre-made by Invitrogen and used in the XCell *Surelock*™ Mini-Cell. β_2m fibril suspension (1000 µl of 59 µM β_2m fibrils, 25 mM Citric acid, 25 mM KCl, 5 mM HEPES, 0.05% w/v sodium azide, pH 2.5, final conc. 8.4 µM β_2m) either modified or unmodified were centrifuged and supernatants removed. Sample buffer (40 µl of 225 mM Tris-HCl pH 6.8, 50% glycerol, 0.4 mM DTT) was added directly to each pellet and heated to 95˚C for 5 minutes. The pellets were incubated for 24 hours to allow dissolution and subsequently heated to 95˚C for 5 minutes again. The samples were centrifuged (20 min, 13000 rpm) and 20 µl of each added to a well of the IEF gel. The upper buffer chamber of the Mini-Cell was filled with 200 ml of 4˚C IEF cathode buffer (Invitrogen) and the lower buffer chamber filled with 600 ml of 4˚C IEF anode buffer (Invitrogen)

5.2.5 Pull down assay SAP with N-methylated β_2m fibrils

Fibrils were produced in low pH, low salt conditions (reaction composition: 49.3 µM β_2m, 50 mM sodium citrate, 25 mM KCl, 5 mM HEPES, pH 2.5). Fibrils were spun down for 10 minutes at 17000 *g* and supernatant removed. At this point they were either left as is or N-methylated as described on page 233. The fibrils were resuspended in 100 µl of either SAP solution (300 µM SAP, 200 mM $CaCl_2$, 100 mM Tris-HCl, pH 8.0) or the buffer minus SAP (control). The fibrils were left to incubate for 30 minutes at ambient temperature and then spun down at 17000 *g* for 20 minutes. The supernatant was removed

by pipette and the excess removed with absorbent paper. SDS PAGE was run on the final pellets and supernatants.

5.2.6 Saturation-Transfer-Difference NMR of acidic side-chains versus SAP

Saturation-Transfer-Difference (STD) NMR spectroscopy allows ligands with a weak binding affinity for a protein to be identified. Amino acids can be screened against proteins to identify any that have a weak binding affinity for a particular protein; in this case SAP. Several amino acids can be run together in the same experiment as long as their signals do not overlap; this allows the rapid identification of any amino acids that show an interaction. Residues that are involved in SAP binding should have at least a weak affinity for SAP and these have been identified using STD experiments.

Preparation of samples for Saturation-Transfer-Difference NMR

Serum Amyloid P component solution (300 µl of 300 µM SAP, 200 mM Tris-HCl, 200 mM $CaCl_2$, pH 8.0) was buffer exchanged by dialysis using a 10000 MWCO slyde-a-lyser (Thermo Scientific) into a deuterated Tris buffer (500 ml of 200 mM $CaCl_2$, 200 mM NaCl, 10 mM deuterated Tris, D_2O, pH 7.4, 4˚C) over 6 hours. The buffer was then replaced with 100 ml of fresh buffer and the SAP left to dialyse overnight. Once dialysed the SAP was diluted to a concentration of 45 µM in fresh deuterated Tris buffer, leaving the protonated Tris at a concentration of less than 400 nM and the SAP concentration 100 x in excess of this, removing the possibility of the protonated Tris interfering with the experiment.

Glutamic acid amide and all amino methyl ester HCl controls were made up in a stock concentration of 1M with the exception of tryptophan methyl ester HCl which due to poor solubility was kept at a stock concentration of 100 mM. 2 µl of each of these stocks (20 µl

for tryptophan) were then mixed with up to three other amino methyl esters and the mixture made up to 50 µl. The 50 µl of each mixture was added to 450 µl of SAP solution to make the final NMR samples. See Table 10 for final sample compositions.

Sample	Ligands	Buffer
CPHPC	CPHPC 4 mM	Tris D11 100 mM $CaCl_2$ 200 mM NaCl 600 mM D_2O (SAP 44 μM)
E amide	Glutamic acid amide 4 mM	Tris D11 100 mM $CaCl_2$ 200 mM NaCl 600 mM D_2O (SAP 44 μM)
WISK	Tryptophan methyl ester HCl 4 mM Isoleucine methyl ester HCl 4 mM Serine methyl ester HCl 4 mM Lysine methyl ester di-HCl 4 mM	Tris D11 100 mM $CaCl_2$ 200 mM NaCl 600 mM D_2O (SAP 44 μM)
YAGT	Tyrosine methyl ester HCl 4 mM Alanine methyl ester HCl 4 mM Glycine methyl ester HCl 4 mM Threonine methyl ester HCl 4 mM	Tris D11 100 mM $CaCl_2$ 200 mM NaCl 600 mM D_2O (SAP 44 μM)
HMRV	Histidine methyl ester di-HCl 4 mM Methionine methyl ester 4 mM Arginine methyl ester di-HCl 4 mM Valine methyl ester HCl 4 mM	Tris D11 100 mM $CaCl_2$ 200 mM NaCl 600 mM D_2O (SAP 44 μM)
FPC	Phenylalanine methyl ester HCl 4 mM Proline methyl ester HCl 4 mM Cysteine methyl ester HCl 4 mM	Tris D11 100 mM $CaCl_2$ 200 mM NaCl 600 mM D_2O (SAP 44 μM)

Table 10 Sample compositions for Saturation Transfer Difference NMR experiments

5.3 Results

5.3.1 Fibril/SAP complex spectra

In chapter 2 it is described how fibrillar β_2m and SAP show a strong interaction with each other. In an attempt to characterise this interaction at an atomic level we employed Cross-Polarised Magic Angle Spinning Proton Driven Spin Diffusion experiments (CPMAS-PDSD) of ^{13}C ^{15}N labelled fibrillar β_2m at neutral pH with or without non-isotopically enriched SAP. PDSD spectra show the ^{13}C-^{13}C dipolar connectivities within a molecule. For nearest neighbour connectivities (~one bond) short isotropic mixing times are used (~20 ms at the used field for β_2m fibril samples at 20 Tesla), and for longer connectivities that correlate all the aliphatic and carbonyl ^{13}C within one residue, longer isotropic mixing times are used (~100 ms for β_2m fibril samples at 20 Tesla). Inter-residue connectivities can be observed by using even longer mixing times; up to 1000 ms are not uncommon. A mixing time of 100 ms was chosen for these experiments so that all intra residue connectivities could be observed without leading to further overcrowding of the spectra through the observation of inter-residue cross-peaks. The purpose of these experiments was to identify chemical shift perturbations or changes in peak width that occur between spectra of the bound and non-bound β_2m to allow identification of β_2m residues that SAP binds at or near. To achieve this, the spectra from both experiments were overlain on each other to allow the easy identification of differences between the spectra.

Figure 76 shows the overlain PDSD spectra from β_2m fibrils in low calcium buffer (red) and fibrils with SAP bound (blue) both at neutral pH in identical buffers. Buffer conditions between the spectra are identical with the exception of the presence of SAP in one. Signal to noise in both spectra is good and both spectra are presented on the same scale, so that

any differences between the spectra can therefore be attributed to the presence of SAP. Clear differences are observable between the spectra; immediately apparent are the isoleucine $^{13}C\gamma$ and $^{13}C\delta$ cross-peaks to the rest of the isoleucine side-chain ^{13}C nuclei that become significantly more intense in the SAP-bound spectrum. The $^{13}C\delta$ to $^{13}C\alpha$ peaks are unusually intense and even ^{13}C' to $^{13}C\alpha$ cross-peaks are observable which are four nuclei away from each other. Peaks appear in the region of the spectrum corresponding to the usual envelope for Alanine $^{13}C\alpha$-$^{13}C\beta$ correlations; the peak assignment prediction tool of the CCPN analysis programme (*158*) predicts with 98% certainty that one of the peaks belongs to an alanine residue, assuming that the peak is an intra-molecular correlation. As Ala-79 has been unambiguously assigned already, this peak could belong to Ala-15. Ala-15 is usually unobservable in dipolar coupling based spectra (*147*) as it appears in the first 16 N-terminus residues of β_2m which is usually highly mobile and difficult to observe in solid-state through-space homonuclear dipolar recoupling experiments. The observation of peaks potentially belonging to residues within the first 16 N-terminus residues could indicate that the binding of SAP is decreasing the mobility of the N-terminus enough that dipolar interactions can be observed. In the region which is typically assigned to glycine ^{13}C'-$^{13}C\alpha$ correlations a very prominent new peak appears. As there are only 3 glycine residues in β_2m this could be indicative of a proportion of glycines being in a different electrostatic environment when SAP is bound to fibrillar β_2m. The envelope corresponding to the usual range of glutamic acid $^{13}C\delta$ and aspartic acid $^{13}C\gamma$ correlations to their respective side-chains shows significant differences with new peaks appearing. These chemical shifts are distinctive of free carboxylic acids; it is therefore unlikely that the new cross-peaks appearing belong to any other types of correlations. The only other correlations nearby would be those of the corresponding nuclei of the amide equivalents, glutamine and asparagine. Many of the resonances that show intensity changes or chemical

shift perturbations potentially belong to residues that are proximal to each other; Gly-43 is located adjacent to Glu-44, Ile-46 is proximal to Glu-47 and Glu-44 is also proximal. Ile-35 is flanked by Asp-34 and Glu-36 with Asp-38 only 3 residues away. It therefore could be that nuclei belonging to residues that are close to acidic residues are experiencing losses in mobility due to SAP binding at the acidic residues.

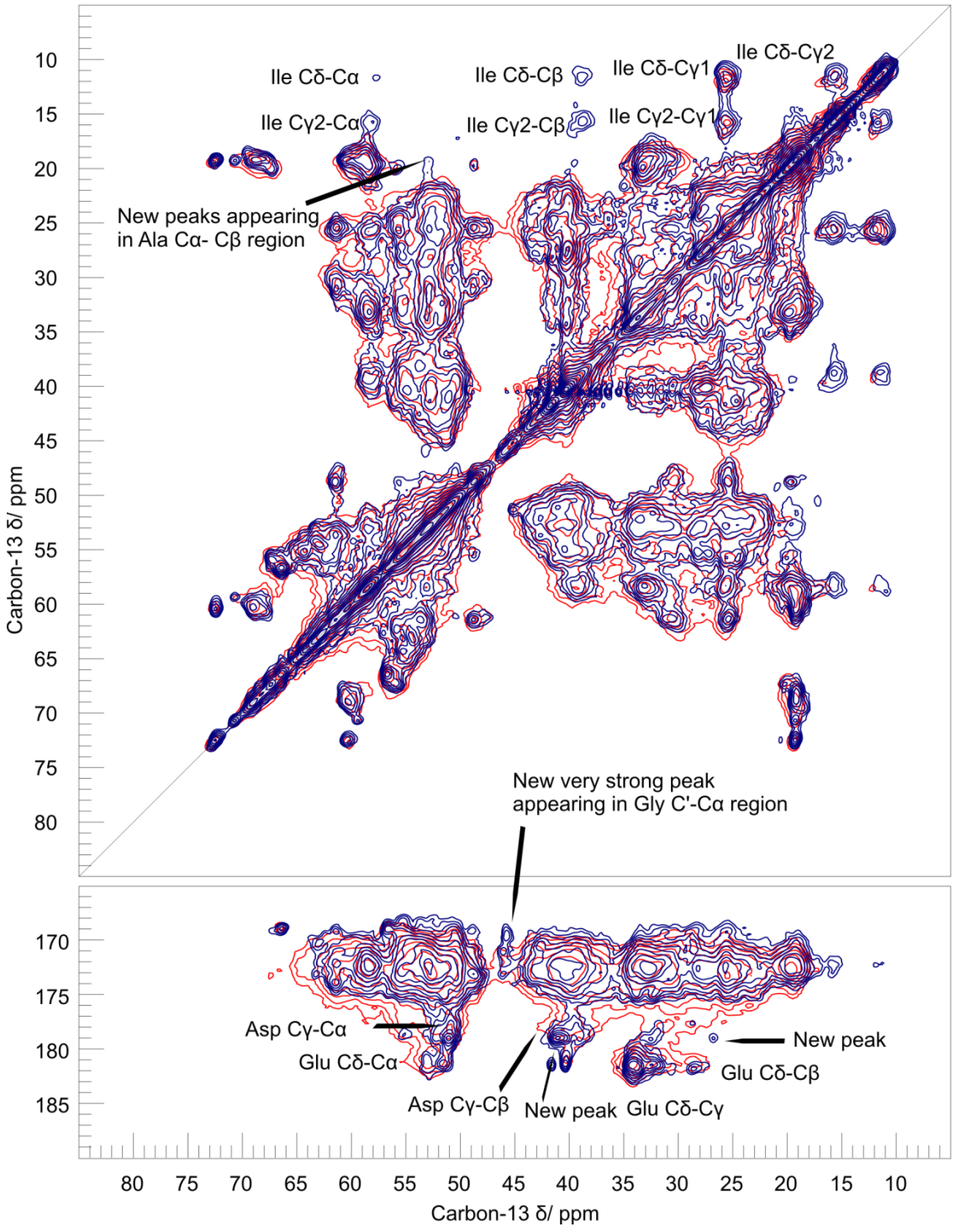

Figure 76 Overlain PDSD spectra from fibrils in low calcium buffer (red) and fibrils with SAP bound (blue) both at pH 7.4

Experiments were performed under identical buffer conditions. Areas of prominent change between the spectra have been marked on the spectra. Spectra acquired on Bruker 850 MHz WB US_2, 15000 Hz spinning with 30 100 ms mixing time. Both samples are at pH 7.4. Both spectra acquired at a sample temperature of ~ -1˚C.

5.3.2 Functional role of acidic residues in the binding of SAP to β_2m fibrils

In order to investigate the functional role of fibrillar β_2m acidic residues in the binding of SAP, pull-down experiments were carried out with β_2m fibrils whose acidic residues were N-methylated to remove their acidic charge. For the experiments to be valid N-methylation of the fibrils had to be proven and characterised.

ElectroSpray Ionisation Mass Spectrometry (ESI-MS) was undertaken on DMSO dissolved β_2m fibrils that had undergone N-methylation (described on page 233) and DMSO dissolved β_2m fibrils from the same batch that had not undergone N-methylation in order to determine whether the N-methylation protocol had worked and to determine to what extent the fibrils had been N-methylated. ESI-MS of the unmodified fibrils (Figure 77A) yielded the unexpected finding that a proportion of the fibrils from this batch were in fact truncated. As well as the full length protein of 11860 Da, species of 10764 Da and 10502 Da were detected; analysis of the primary structure reveal these species to have truncations of the first 9 and first 11 N-terminal residues respectively. Investigation into what may have caused these truncations took place. The dissolution in DMSO and mass spectrometry procedure were ruled out as running full length native β_2m under the same conditions did not result in truncation of the protein (data not shown). The fibrillogenesis procedure was ruled out by undertaking mass spectrometry of fibrils at different time points during the fibrillogenesis procedure; at no point were truncations detected (data not shown). This meant that the truncations were most probably caused by either proteolysis of the native β_2m species used to make that batch of β_2m fibrils or proteolysis of that particular batch of β_2m post-fibrillogenesis; whatever the case no truncations were detected in any other batch of β_2m fibrils tested.

Analysis of the spectrum from the ESI-MS of the N-methylated fibrils (Figure 77B) reveals several different molecular weight species, however the two most prominent peaks in the spectrum correspond to 10901 Da and 10639 Da. These weights are both exactly 137 Da heavier than the 10764 Da and 10507 Da weights of the truncated proteins from the unmodified experiments. The expected mass gain for each successful N-methylation of a carboxylate group is 13 Da. This is though the addition of one nitrogen, one carbon and three hydrogens, and the removal on one oxygen (14 Da + 12 Da + (3 x 1 Da) – 16 Da = 13 Da). The increase in mass of 137 Da by both these species is best explained by the addition of 10 N-methyl groups to the carboxylates of the β_2m in its fibrillar form. There are 8 glutamate side-chain carboxylates, 7 aspartate side-chain carboxylates and 1 C-terminus main-chain carboxylate that make a theoretical total of 16 carboxylates per β_2m unit that could be N-methylated. Some side-chains of aspartate and glutamate residues might be expected to be within the fibril core and therefore may not be accessible for chemical modification during the reaction process. The addition of N-hydroxysuccinimide during the reaction process should also have minimised side-reactions but they cannot be ruled out, therefore there could in theory be less than 10 N-methylations of carboxylates per β_2m unit. Despite these caveats it can be assumed that most solvent exposed carboxylates were N-methylated and hence the preparation was successful when the results are taken in conjunction with those of the isoelectrofocussing gel (Figure 78) and SAP pull-down experiment (Figure 79) which are described in the following sections.

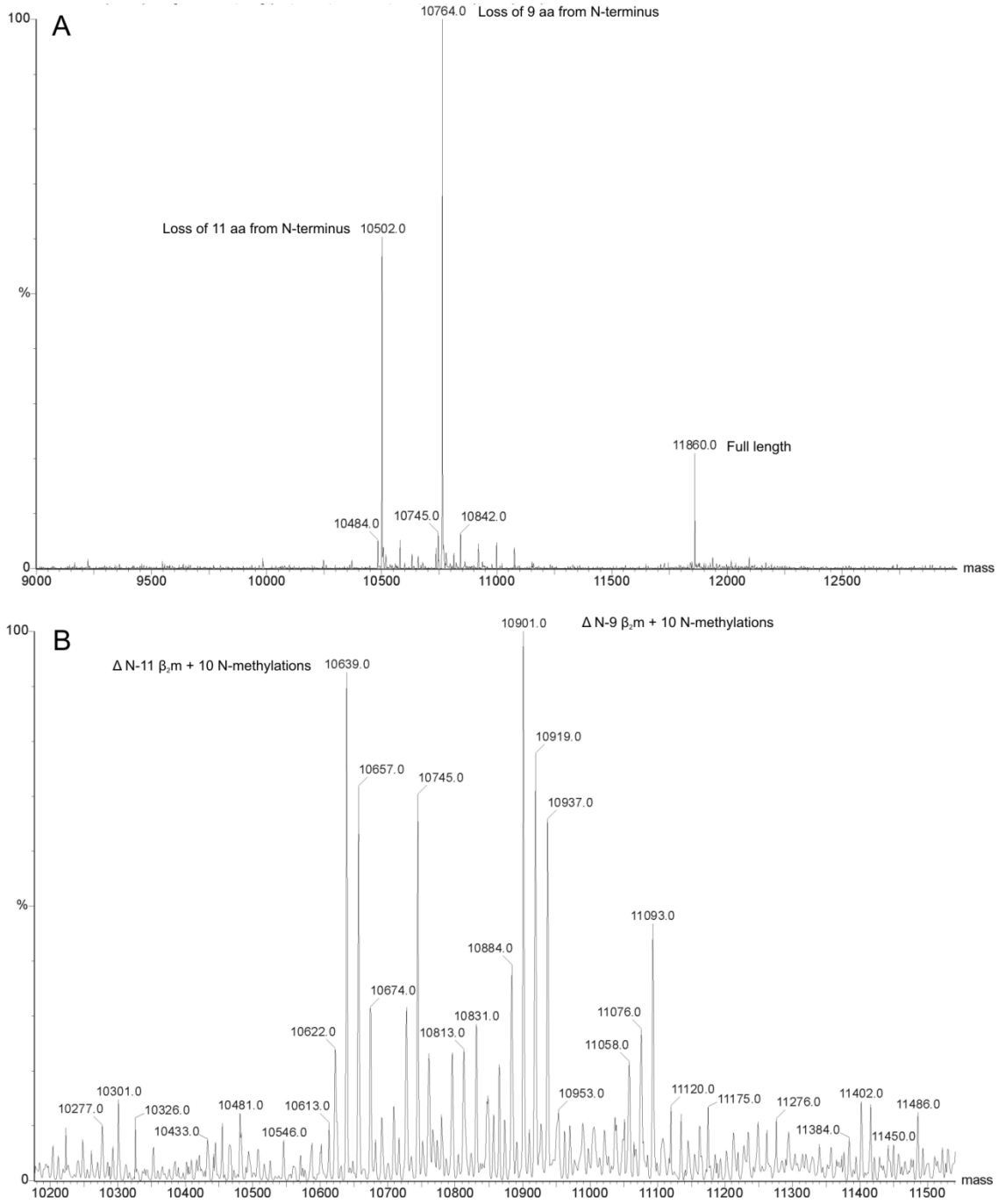

Figure 77 N-methylation of β_2m analysed by ESI-Mass spectrometry

ElectroSpray Ionisation mass spectrometry was undertaken on β_2m fibrils that had and had not undergone N-methylation in order to determine the successfulness and to what extent the fibrils had been N-methylated. A) Maximum entropy spectrum of unmodified fibrils. B) Maximum entropy spectrum of modified fibrils. Mass spectrometry was carried out on a Quattro II mass spectrometer (Micromass) fitted with a nano-ESI source. Samples were electrosprayed from gold-coated glass capillaries prepared in house, with an applied capillary voltage of 1.45-2.2 kV, a cone voltage of 75 V and a source temperature of 70˚C.

Isoelectric focussing (IEF) allows the separation of proteins according to their isoelectric point; small changes in pI can be detected by IEF. As N-methylation of carboxylates will remove their negative charge, the pI of N-methylated β_2m should be higher to that of non N-methylated β_2m; isoelectric focussing can therefore be used to confirm if the N-methylation of proteins has been successful. The gel in Figure 78 shows the results of isoelectric focussing both N-methylated and non N-methylated β_2m fibrils. The fibrils have been depolymerised by incubation in native gel loading buffer for 24 hours prior to loading onto the gel with periodic heating to 95˚C. Lane 1 contains a control of soluble non-modified β_2m, lane 2 a non-modified fibrillar β_2m, lane 3 is empty and in lane 4 contains a modified fibrillar β_2m. A large shift towards a basic pI can quite clearly be seen between the non-modified and modified fibrils, clearly demonstrating that the N-methylation has been successful. The pI of the unmodified fibrils is slightly more acidic than that of the soluble β_2m; this can be accounted for by the discovery that the fibrils used in this experiment were N-terminus truncated as shown by mass spectrometry and that 2 positively charged residues are present in the truncated N-terminus (Figure 77).

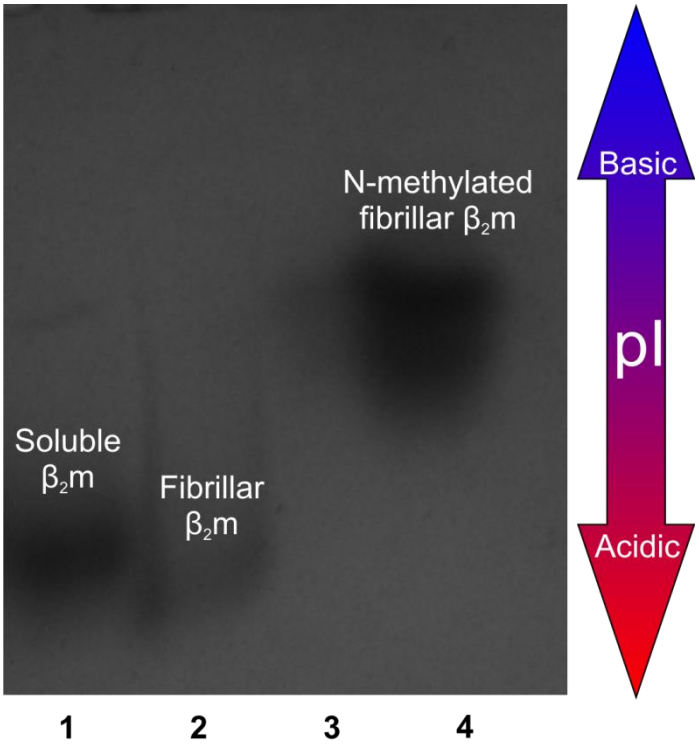

Figure 78 Isoelectric focussing gel of depolymerised N-methylated and non-N-methylated β_2m fibrils

Isoelectric focussing allows the separation of proteins according to their isoelectric point. In lane 1 is a control of soluble non-modified β_2m, lane 2 is non-modified fibrillar β_2m, lane 3 is empty and in lane 4 is modified fibrillar β_2m.

5.3.3 SDS-PAGE results of SAP pull down assays

We have previously described in this chapter how perturbations in chemical shift, corresponding to the acidic side-chains of glutamate and aspartate, can be detected in PDSD spectra of SAP-bound β_2m fibrils (section 5.3.1 Fibril/SAP complex spectra). We have then gone on to describe how these side-chains can be modified by N-methylation of the carboxylate, as confirmed by ESI-MS (Figure 77); which subsequently removes the acidic charge associated with the side-chain, as confirmed by isoelectrofocussing (Figure 78). We postulate that if the acidic side-chains are essential for binding then removal of their charge, and hence their ability to interact with SAP electrostatically, should compromise the ability of the fibrils to bind SAP. In order to investigate this we undertook

SAP pull-down assays with the N-methylated fibrils to see if the modified fibrils would still bind SAP. Figure 79 is the SDS PAGE gel from the pull-down experiment; pull-downs of unmodified fibrils, N-methylated fibrils and a control experiment of unmodified fibrils with no SAP were undertaken. Samples of the pellet and supernatant were taken for SDS-PAGE in each case; if there is a strong interaction between the fibril and SAP then the SAP will appear in the pellet along with the β_2m.

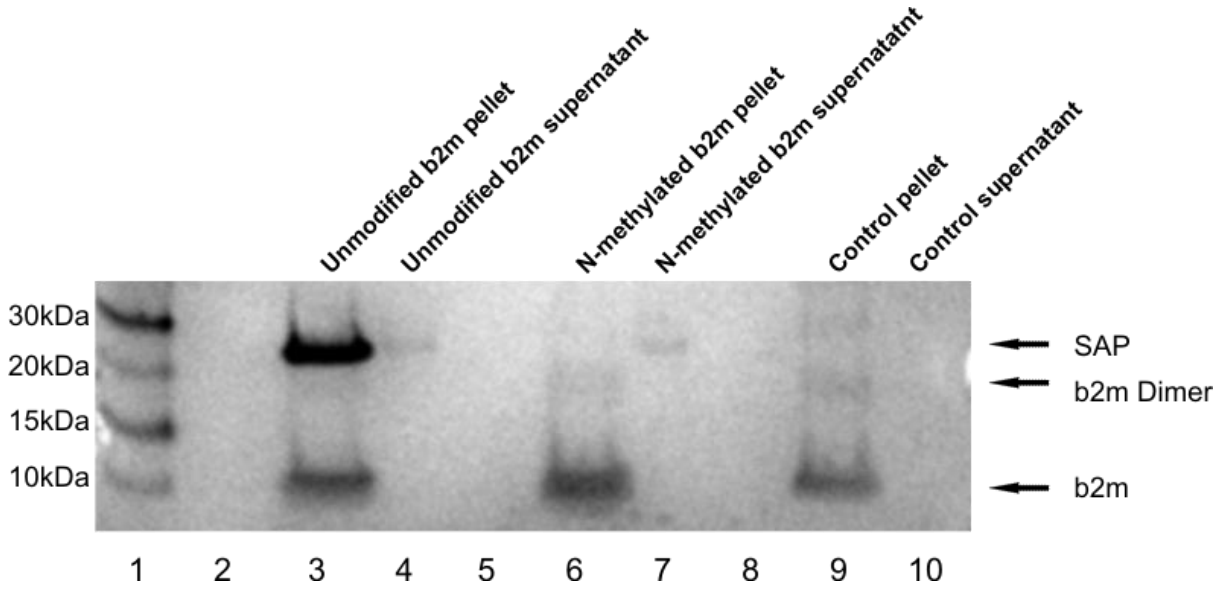

Figure 79 SDS PAGE of SAP pull down with unmodified and N-methylated β_2m fibrils
Unmodified fibrils and N-methylated fibrils were incubated with SAP and then centrifuged to separate the soluble and insoluble fractions. 1) MW marker. 3) Pellet of unmodified β_2m-SAP pull-down 4) Supernatant of unmodified β_2m-SAP pull-down. 6) Pellet of N-methylated β_2m-SAP pull-down. 7) Supernatant of N-methylated β_2m-SAP pull-down. 9) Pellet from control experiment. 10) supernatant from control experiment.

Lane 1 of the gel contains a broad-range molecular marker (Invitrogen) appropriate for all potentially expected protein species. Lane 3 of the gel is the pellet from the unmodified fibril pull-down experiment; bands corresponding to the molecular weights of both β_2m and the SAP monomer are present in this lane, demonstrating that the SAP did bind to the unmodified fibrils as would be expected. Lane 4 is the supernatant from the unmodified experiment. A faint band corresponding to the molecular weight of SAP can be seen in this lane as an excess of SAP was used but no β_2m which is as expected. Lane 6 shows the constituents of the pellet from the N-methylated fibril pull-down experiment. In this lane there is a strong band corresponding to the molecular weight of β_2m but no band at all corresponding to the molecular weight of the SAP monomer; this means that SAP was not pulled down with the fibrils and that binding of SAP to the N-methylated fibrils did not take place or was substantially weakened. Lane 7 shows the supernatant from the same experiment, there is a faint band corresponding to the molecular weight of SAP; as no SAP has been pulled down with the N-methylated fibrils, it would be expected that more SAP should be in the supernatant, roughly equivalent to the combined amounts of lane 3 and 4. This inconsistency can be explained by the presence of precipitated SAP in the LDS sample buffer (Invitrogen) used. When prepared for SDS-PAGE, a final concentration of 1 x LDS buffer was used in the supernatant, this concentration of sample buffer is not enough to solubilise the SAP which precipitates when the buffer is added. Conversely, the SAP does solubilise in the pellet samples as concentrated 4 x LDS gel loading buffer is added directly to the fibrils and does not get diluted as in the case of the supernatant. Lane 9 contains the pellet of unmodified fibrils that were incubated in the calcium buffer used in the other experiments but without the presence of SAP. A strong band corresponding to the monomeric β_2m can be seen; also visible are bands corresponding to the molecular weight of dimeric β_2m and trimeric β_2m which are often present in SDS-PAGE gels of β_2m

fibrils. Lane 10 contains the supernatant from that experiment and no bands can be seen. The control experiment demonstrates that the bands present in the other experiments correspond to SAP and not another component present in the buffer.

The SAP pull-down experiments demonstrate that N-methylation of the acidic side-chain carboxylates prevents SAP binding to β_2m fibrils.

5.3.4 Saturation-Transfer-Difference NMR of glutamic acid amide and SAP

Saturation transfer difference NMR experiments can be used to determine low affinity binding between molecules. We tested a range of amino acid derivatives to determine if they have affinity for SAP; glutamic acid amide was of particular interest as it has the same side-chain as glutamate which we propose help form the SAP binding site in fibrillar β_2m. The STD spectrum is in fact created from two experiments, one 'off-resonance' which would produce a normal spectrum and one 'on-resonance' which saturates SAP and any ligands that bind to it. The ligands that are saturated will not contribute to the ligand signal in the on-resonance spectrum. The on-resonance spectrum is subtracted from the off-resonance spectrum. In cases where there is no ligand binding and therefore all ligands contribute to the on-resonance spectrum the two spectra will cancel each other out and no peaks will be present in the spectrum. In cases where there is binding and hence the ligand's signals are attenuated through saturation, the subtraction of the spectra will result in the signals from saturated nuclei being observable. A schematic diagram demonstrating this principle is shown in Figure 80. The spectra in Figure 81 show some of the results of the STD experiments that were undertaken. A) is a 1 dimensional proton spectrum of SAP, B) shows SAP being saturated by a train of Gaussian pulses. This is performed at a carrier frequency that does not also saturate the ligand. C) is a 1-dimensional proton spectrum of glutamic acid amide showing Hα, β and γ peak; the experiment is undertaken in ~100%

D_2O and so NH and COOH protons will be exchanged for deuterium and not observable. D) is an STD spectrum of glutamic acid amide against SAP. Subtraction of the on-resonance experiment from the off-resonance experiment has resulted in signal still being present in the spectrum demonstrating that glutamic acid side-chains do have affinity for SAP. The vertical scale in D is 300 times that in C.

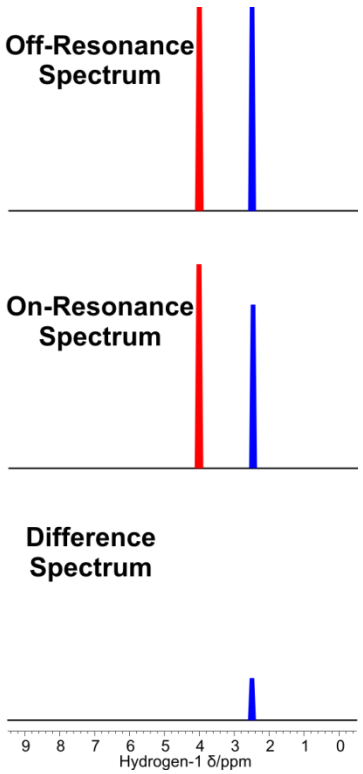

Figure 80 Example of production of STD difference spectrum
This schematic demonstrates the principle behind an STD difference spectrum. In the off-resonance experiment the irradiation frequency is set at a frequency far from any signal, neither from protein nor ligand, and a spectrum is recorded yielding a normal spectrum of ligand 1 (red) and ligand 2 (blue). In the on-resonance experiment the irradiation frequency is set so the protein is selectively irradiated and becomes saturated. This saturation is passed on to any ligand that comes into contact with the protein; the saturated ligand dissociates and does not contribute to the ligand signal when the spectrum is recorded. Subtracting the on-resonance spectrum from the off-resonance spectrum leads to a difference spectrum in which only the signals of protons that were attenuated by saturation transfer (ligand 2, blue) remain. Signals from protons that did not come into contact with the protein (ligand 1, red) are cancelled out and do not appear in the spectrum.

The spectra in Figure 82 show 1 dimensional and STD spectra of amino methyl ester mixes. The purposes of these experiments were to dually act as controls for the glutamic acid amide experiment to make sure that any STD effect was not just a generic binding effect seen between all amino acids and SAP, and also to identify other amino acids that potentially have affinity for SAP. A) is the 1D spectrum of the methyl esters of histidine, methionine, arginine and valine. B) is the STD spectrum of the mix. An STD effect can be seen on the histidine ring protons, histidine Hβs, Valine Hγs and potentially valine Hβ, Arginine Hβs and the methyl ester protons**.** There is a relatively large STD effect seen for the methionine Hδs; it is roughly 5 times larger than the STD effect seen for the above mentioned nuclei. C) is a 1D spectrum of the methyl esters of tryptophan, isoleucine, serine and lysine. D) is the STD spectrum of C, some STD effects can be seen, particularly intense relative to the other peaks are those protons belonging to the tryptophan ring, this is despite these peaks being of lower intensity than most other peaks in the 1D spectrum. This could be suggestive that the aromatic protons are interacting more specifically than the protons of the other amino methyl esters but at this cannot be determined without further experiments.

When interpreting the STD-NMR data it must be taken into account that only one concentration of ligand was used in the STD experiments; this makes it difficult to rule out the possibility that the STD effects seen could be due to non-specific interactions, especially when taking into account the high ligand concentrations used. In order to rule out non-specific interactions caused by high ligand concentration the experiments need to be repeated with lower ligand concentrations. Repeating the amino derivative mix STD experiments at increasingly lower concentrations until the majority of the STD effects are not seen and then repeating the glutamic acid amide experiment at that concentration will

be informative as to whether glutamic acid amide has a more specific interaction with SAP than other amino acids. Concurrently it has to be considered that other amino acids may have specific interaction sites with SAP that have nothing to do with fibril binding. From these experiments it can however be determined that glutamic acid amide side-chains do show an interaction with SAP at high concentrations.

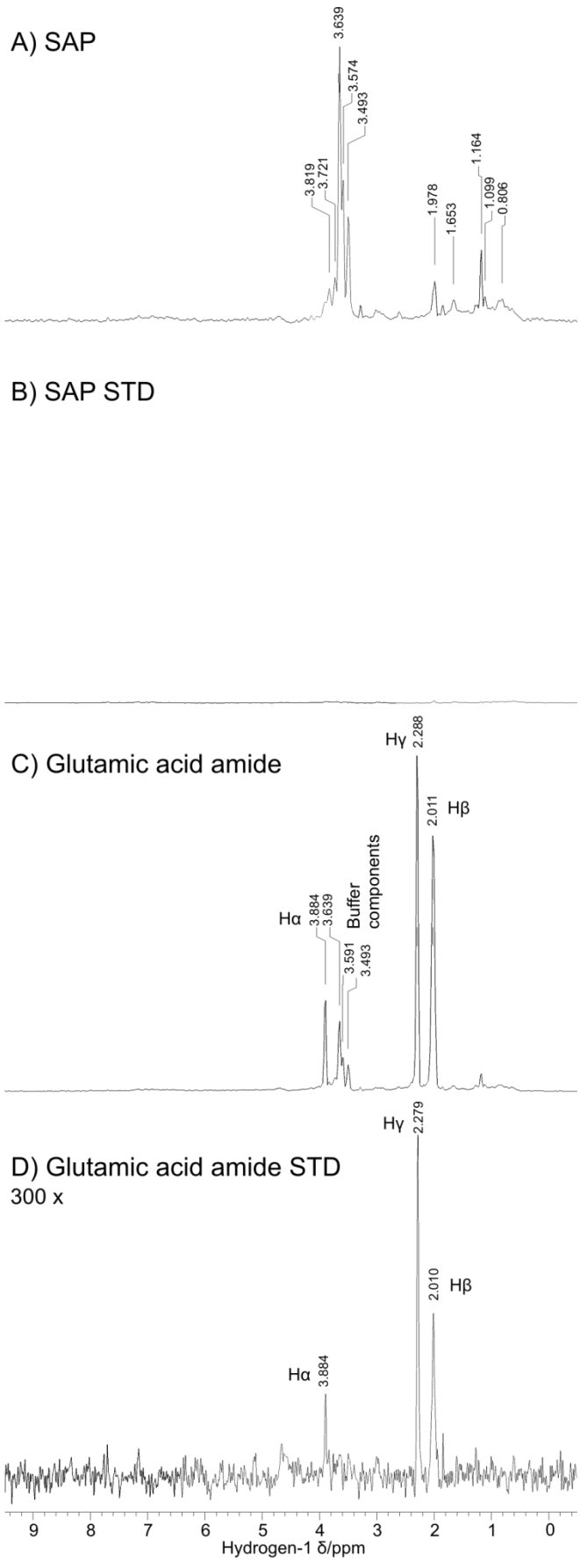

Figure 81 Saturation Transfer Difference Spectra of SAP and glutamic acid amide

A) is a 1 dimensional proton spectrum of SAP. B) shows SAP being saturated at 10.3 ppm by a train of Gaussian pulses. This is performed at a carrier frequency that does not also saturate the ligand. C) is a 1-dimensional proton spectrum of glutamic acid amide showing Hα, β and γ peak; the experiment is undertaken in ~100% D_2O and so NH and COOH protons will be exchanged for deuterium and not observable. D) is an STD spectrum of glutamic acid amide against SAP. The vertical scale in D is 300 times that in C.

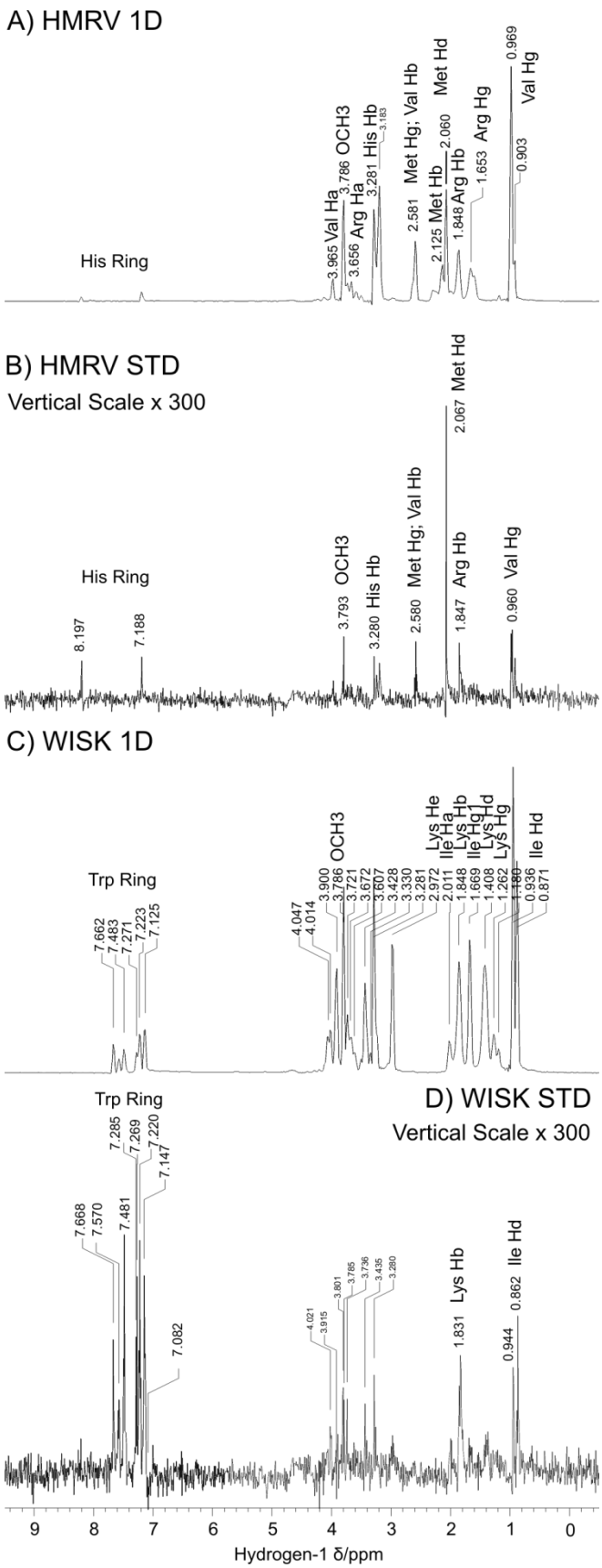

Figure 82 Saturation Transfer Difference Spectra of amino methyl ester mixes 1 + 2

The spectra to the right show 1 dimensional and STD spectra of amino methyl ester mixes. A) is the 1D spectrum of the methyl esters of histidine, methionine, arginine and valine. B) is the STD spectrum of the mix. C) is a 1D spectrum of the methyl esters of tryptophan, isoleucine, serine and lysine. D) is the STD spectrum of C.

5.4 Conclusion

Work in previous chapters had established that fibrillar β_2m and SAP show a strong interaction with each other and also that SAP is able to stabilise β_2m fibrils at neutral pH. It was deemed that this interaction could be important for the persistence of amyloid load in dialysis related amyloidosis patients and therefore it was deemed important that the interaction was characterised. The aim of the work within this chapter was to identify sites of interaction between fibrillar β_2m and serum amyloid P component. This was undertaken by using solid-state NMR methods; CPMAS-PDSD spectra (Figure 76) were acquired of fibrillar uniformly labelled ^{13}C ^{15}N β_2m at neutral pH with or without isotopically non-enriched SAP being present. The objective of this was to compare the spectra and identify chemical shift perturbations or line-width changes; in doing so residues or areas of the protein that come into contact with SAP may be identified.

Upon comparing the spectra immediate and obvious differences could be identified; major differences between the spectra are the appearance of peaks in the SAP bound spectrum at sites corresponding to the correlations between the resonances between aspartate $^{13}C\gamma$ nuclei and the rest of the aspartate side-chain and also at sites corresponding to the correlations between glutamate $^{13}C\delta$ nuclei and the rest of the glutamate side-chain. In the SAP-bound spectrum cross-peaks corresponding to correlations between the resonances of ^{13}C nuclei of the isoleucine side-chains become much more intense. Another prominent peak appears at a site corresponding to glycine $^{13}C'$-$^{13}C\alpha$, this makes a total of 4 glycine peaks in that area despite only being 3 glycines in β_2m. It is therefore likely that this peak is from a proportion of glycines that are experiencing a different environment caused by proximity of SAP. The common feature linking the changes in environment of the

isoleucines and glycines is that they can either be assigned or potentially assigned to residues in close proximity to one or more glutamate or aspartate residue. It therefore could be that nuclei belonging to residues that are close to acidic residues are experiencing changes in electrostatic environment and/or losses in mobility due to SAP binding at the acidic residues.

The functional relevance of the proposed interaction between SAP and negatively charged amino acids on the surface of the fibril were tested using chemical modification to remove the charge. These inhibited the interaction of SAP with β_2m fibrils as determined by a fibril pull down assay

Acidic residues are amenable to chemical modification so that they lose their charge, this brought about the opportunity to see if the acidic residues of β_2m are essential for SAP binding. Using a procedure modified from that of Koshland and Hoare (*153*), we undertook N-methylation of the free carboxylates of β_2m fibrils in order to remove their negative charges and determine the effect that this has on binding with SAP. N-methylation of the fibrils was proven to be successful through electrospray ionisation mass spectrometry (Figure 77) and isoelectric focussing (Figure 78) which together proved that β_2m units within fibrils had a maximum of 10 carboxylates N-methylated and that this caused a large shift towards a basic pI.

We then undertook an SAP pull-down assay with the N-methylated fibrils (Figure 79). Unlike unmodified fibrils that bind with SAP and pull it down into the fibril pellet when centrifuged, the N-methylated fibrils do not pull down SAP with them. This demonstrates that the N-methylation of acidic residues prevents fibril binding to SAP and consequently that the acidic residues form an essential part of the binding site.

Solid-state NMR studies identified glutamate and aspartate residues of fibrillar β_2m as candidate residues for being involved in binding with SAP. The N-methylation studies described above subsequently showed that removal of the negative charge of these side-chains prevents fibrillar β_2m from binding with SAP. If glutamates and aspartates are forming part of the binding site for SAP then it follows that they must have some affinity for SAP. In order to determine this we used saturation transfer difference (STD) experiments testing glutamic acid amide against SAP; glutamic acid amide was used as its side-chain carboxylate has been protected to prevent its charge from interacting with SAP. Aspartate derivatives were not tested as they were not available at the time of the study. The STD experiments show conclusively that glutamic acid amide side-chains have affinity for SAP. The experiments show that the interaction is very specific for the side-chains with the Hγ showing the highest level of saturation followed by Hβ and finally by Hα. This pattern of saturation is suggestive of the end of the side-chain, i.e. the carboxylate group, binding with SAP and then the saturation propagating down the side-chain. Most other amino derivatives tested showed some degree of STD effect and therefore at this stage it cannot be ruled out that any STD effect seen with any of the ligands is unspecific binding due to the high concentration of ligands used. Follow up experiments should include running a series of experiments at lower ligand and protein concentrations to see if the STD effect of the amino acid derivatives disappears; if the majority of the STD signals from the controls disappear before the glutamic acid amide then a specific interaction between the glutamic acid side-chain and SAP can be inferred. Efforts should also be made to undertake STD experiments with an aspartic acid derivative as aspartates of β_2m fibrils are also candidates for binding with SAP.

When taken together with the pull-down results on the N-methylated fibrils it is a likely possibility that the interaction seen with glutamic acid amide is specific but it cannot be ruled out at this time that it is solely the aspartate residues that are responsible for fibrils binding with SAP. More high resolution studies of SAP bound fibrillar β_2m are needed; specific labelling of the protein with either labelled glutamic acid or aspartic acid will help determine exactly which residues are binding and if both types are involved. It would also be of value to determine exactly how the negative charges interact with SAP; some evidence points towards this being through the SAP Ca^{2+} binding sites as Ca^{2+} is necessary for fibril binding and crystal structures exist of glutamate co-ordinating with the Ca^{2+} in the binding sites.

Chapter 6

6 Conclusion

The results from this thesis can be broadly split into three categories; those pertaining to the characterisation of fibrillar β_2m and its transition from and back to the native state, those pertaining to the differences between β_2m in inclusion bodies and fibrils, and those results pertaining to the identification of sites of interaction between fibrillar β_2m and serum amyloid P component. The conclusions drawn from the three categories as well as suggestions for future research on the project are made below.

6.1 Characterisation of fibrillar β_2m and its transition from and to the native state

The main aim of the work in this thesis was to characterise the interaction between fibrillar beta-2 microglobulin and serum amyloid P component thereby adding to the literature valuable evidence towards SAP's role in amyloidosis. In the process it was a necessity to characterise fibrillar β_2m so that comparisons could be made between SAP-bound and non-bound fibrils. Another aim of the project was to characterise transitions that occur between native β_2m and fibrillar β_2m. To achieve these aims we successfully produced recombinant native β_2m and fibrillar β_2m and undertook chemical shift assignments of both forms.

Using three-dimensional heteronuclear double and triple resonance experiments, 90 out of 100 residues had their Cα and Cβ assigned and ~80% of expected side-chain resonances were assigned. The majority of missing assignments fell within the loop region between strands V & VI, the binding site between β_2m and the MHC I heavy chain, confirming previous findings that this region is highly mobile in dissociated β_2m (*54, 57*). The

virtually complete assignment of native β_2m's backbone allowed prediction of secondary structure using a chemical shift index; this predicted that the recombinant native β_2m we were using had 7 beta-strands as with other published structures (*54, 57, 58*).

Solid-state assignment of fibrillar β_2m was more challenging than with the native form. Cross-polarised two-dimensional homo and heteronuclear experiments were used at high field in order to attempt to resolve peaks and assign them. This technique met with partial success and substantial assignments were made, however, in terms of study by solid-state NMR, β_2m is a large protein and two-dimensional spectra of uniformly labelled β_2m were spectrally crowded; a full assignment therefore using these methods alone was not possible. To further these assignments, alternative methods were sought. The first of these was to undertake three-dimensional experiments; this met with little success due to the poor efficiency with which magnetisation could be transferred between sites within the protein and the limited acquisition time available. The second method used was extensive and selective labelling of the sample using specifically labelled glycerol samples as the sole carbon source for *E.coli* expressing the protein. This technique led to massive simplification of PDSD spectra allowing the assignment of resonances to atom types, but NCA and NCO spectra were not decrowded enough to allow substantially more site specific assignments; however more site-specific assignments were actually made using this technique. A third technique of using hydrogen-deuterium exchange on extensively and selectively labelled samples to further decrease crowding failed due to poor signal to noise, possibly due to polarisation from hydrogens in water not contributing to the cross-polarisation (*145*).

Through the combination of techniques ~50% of expected assignments were made and concur with findings from other groups that large portions of the N and C-termini are not

observable using dipolar based experiments (*146, 147*). The assignments that were made allowed secondary structure predictions to be made using the chemical shift index. These predictions were compared with the liquid-state predictions and it was found that the loop area between β-strands V & VI, which is highly mobile and unobservable in liquid-state experiments, had become observable and predicted to have β-strand secondary structure. This finding is also corroborated by Debelouchina *et al.* (*147*) who published the same findings during the writing of this thesis. This finding adds evidence to the general community opinion that β-strand secondary structure becomes enhanced during fibrillogenesis.

Comparison of assigned fibrillar PDSD spectra and PDSD spectra simulated from the liquid-state assignments suggests that extensive transitions must occur between native and fibrillar forms of β_2m as very few peaks are superimposable on each other due to differences in chemical shift; differences in chemical shift are indicative of changes in electrostatic environment and hence structure.

Fibril depolymerisation assays

Experiments measuring the rate and extent of depolymerisation using ThT fluorescence confirmed findings from other groups (*76*) that incubation of acid produced β_2m fibrils at neutral pH results in their depolymerisation. In addition to this, depolymerisation experiments under several conditions found several factors that affect the rate and extent of depolymerisation, including ionic strength, the presence of high concentrations of free β_2m and BSA and a low concentration of SAP.

The dual observation that low concentrations of SAP were able to inhibit depolymerisation of dilute suspensions of β_2m fibrils, and that fast to ultra fast centrifugation of fibrils at

neutral pH did not result in the rapid depolymerisation of fibrils, led to the successful creation of a sample preparation protocol that enabled the fibrils to be maintained at neutral pH. This was for periods of at least months, exceeding the time needed to run a full range of successful solid-state NMR experiments both with and without the presence of SAP. This made possible the characterisation of the interaction between fibrillar β_2m and SAP at atomic resolution.

6.2 Inclusion bodies of β_2m show morphological differences from fibrillar β_2m

During the course of this project there was speculation from several groups that protein within inclusion bodies was in fact fibrillar in nature (*131, 151*). Our high-resolution solid-state NMR studies of β_2m in inclusion bodies revealed that contrary to the other published studies, β_2m in inclusion bodies was unlikely to be completely fibrillar in nature (*132*). The studies did reveal however that inclusion bodies did have structure and were not amorphous aggregates as was generally thought previously. The study concluded that the morphology that protein adopts in inclusion bodies is dependent on the precursor protein and that naturally amyloidogenic proteins such as Het-s and Aβ1-42 are more likely to adopt fibril-like structure in inclusion bodies due to their natural propensity to form such structures, contrasting with β_2m which is primarily found complexed in the MHC-I complex or free in solution.

6.3 Acidic carboxylates of fibrils are primary binding site for SAP

The ultimate goal of this project was to map the interaction sites between SAP and fibrillar β_2m. We aimed to achieve this by identifying perturbations in chemical shift in spectra of fibrillar β_2m with SAP bound through comparison with spectra of fibrillar β_2m with no SAP bound. The first challenge in achieving this was the necessity to carry out the

experiments at neutral pH; conditions under which acid-produced β_2m fibrils were thought to be unstable. This was overcome through the use of sample preparation techniques that stabilised the fibrils at neutral pH. The second challenge to be overcome was the necessity of SAP to contain high concentrations of calcium chloride and/or sodium chloride in order to remain stable at the concentrations required to decorate all the fibrils in a solid-state NMR sample; the high concentrations of ions in the sample originally made collection of spectra impossible. This was first overcome through the use of a newly available E_{free} probe (Bruker) allowing low quality spectra to be acquired; subsequently a carefully planned sample preparation protocol ensuring that SAP always had its ligand binding site occupied meant that high concentrations of salts were no longer required and high quality spectra of fibrillar β_2m bound with SAP bound were acquired. These spectra allowed the identification of perturbations in chemical shift which notably appeared in the region of the spectra corresponding to the side-chain carboxylates of glutamate and aspartate.

Acidic carboxylates would be able to interact with the positively charged calcium binding sites of SAP and there is a crystal structure of SAP with a glutamate residue ligated at the calcium binding site (*98*), so the acidic carboxylates of β_2m fibrils made a good putative binding site for SAP. To investigate this finding further, β_2m fibrils were modified so that the acidic carboxylates were N-methylated and no longer carried a negative charge. If, as suspected, the SAP and fibrillar β_2m were binding through electrostatic interactions mediated through acidic carboxylates and the calcium ions in the calcium binding sites of SAP, then removal of the negative charges should inhibit the interaction. Removal of the charges completely inhibited SAP binding to modified fibrils as shown by pull-down assays.

Most naturally occurring fibril types contain acidic residues, due to the cross-beta structure that defines amyloid fibrils; these acidic residues frequently form strips along the long axis of the fibril. Figure 83 shows four currently published fibril structures all showing strips of acidic residues. This arrangement of acidic strips is not unique to amyloid fibrils but also appears in DNA and carboxymethyl cellulose (CMC) fibres, both of which bind SAP (*93, 159*). Preliminary studies within the group have shown N-methylation of carboxylates of several fibril types as well as CMC fibres prevents SAP binding (*160*).

Due to the above experimental evidence gathered and the observations made throughout the literature we propose that acidic strips common to all fibril types, nucleic acids and CMC fibres are the motif that SAP recognises, explaining its ability to recognise all fibril types tested irrespective of the primary sequence of those fibrils. The arrangement of acidic charges in strips could allow the co-operative action of several acidic groups to bind at multiple sites on SAP so that even with a low binding affinity of individual acidic sites, fibrils could still bind to SAP.

If SAP has the ability to bind acidic strips for the purpose of binding necrotic DNA as suspected (*91*), it explains why humans have conserved a protein that binds to and protects pathogenic amyloid fibrils. In the majority of cases of amyloid disease the patients are elderly. From an evolutionary perspective anyone who lived long enough for amyloid disease to affect them would already have passed child-bearing age and potentially had many children. On the other hand an autoimmune response to self DNA would likely cause death before sexual maturity; therefore the gene for SAP would be conserved even if it did eventually contribute to amyloid disease.

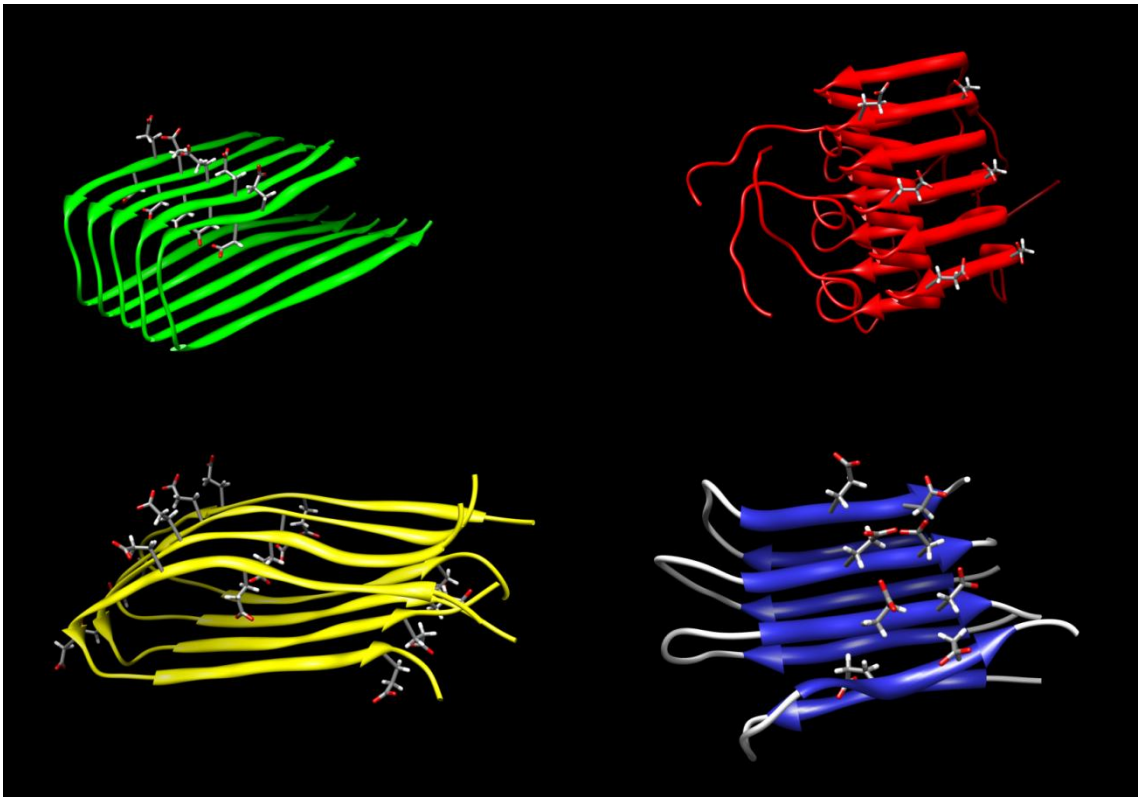

Figure 83 Currently published amyloid high resolution fibril structures showing acidic strips
In green: Aβ(1-42) by Luhrs *et al.* (*161*). In red: HET-S (218-289) by Van Melckebeke *et al.* (*20*). In yellow: Human CA150 by Ferguson *et al.* (*19*). In blue: K3 fragment of β_2m by Iwata *et al.(84).*

6.4 Outlook

Despite significant progress being made towards the identification of the motif that SAP recognises in fibrils there still remains a lot of scope for further research on this project. Firstly a complete assignment of β_2m would be desirable; this would allow each specific site which has an interaction with β_2m to be identified.

A promising technique to achieve this goal would be to use double selective labelling. In this technique combinations of labelled amino acids are added to unlabelled growth medium. The combinations of amino acid are carefully chosen so that only cross-peaks belonging to specific residues appear in spectra. For example, if uniformly labelled glutamate, valine and isoleucine were used then, from an NCO spectrum, unambiguous assignments of Ile-35, Glu-36, Val-37, Val-49, Glu-50 (and also Ile-92 and Val-93 if they showed up at all in the spectrum due to being in the C-terminus) could be made. In an NCA spectrum there would be only a maximum of 20 cross-peaks, significantly simplifying the spectrum and almost certainly allowing the assignment of the amide ^{15}N and ^{13}Cα nuclei from all observable glutamates, valines and isoleucines when used in combination with existing assignments. The PDSD would show all ^{13}C-^{13}C correlations for the 3 residue types but would be significantly simplified in respect to the PDSD of uniformly labelled β_2m and using all the spectra in unison should allow for complete assignment of all observable residues. The drawback of this labelling technique is its cost but this can be kept to a minimum by careful planning of the combinations of amino acids to be used in order for key residues to be assigned.

The assignment procedure should be repeated with samples at neutral pH so as to be directly comparable with spectra of β_2m bound.

The results of the ThT monitored depolymerisation experiments were extremely interesting and need to be followed up. TEM of different time points from the samples of the BSA and free β_2m experiments should be carried out, especially during the period when ThT fluorescence is rising rapidly. This should determine if the rise in fluorescence is due to a conversion of typical fibrils to a different fibril type or protofibrils.

In the case of the free β_2m experiments especially, the solid material should be determined before and after the depolymerisation; this should determine if fibrillogenesis of the free β_2m is occurring. The depolymerisation experiments in the presence of SAP should be repeated both with higher concentrations of SAP and with the addition of molecular crowding agents to see if under these conditions SAP stabilises β_2m fibrils.

The N-methylation experiments should be expanded to many more different fibril types so as to widen the conclusions and prove beyond doubt that the acidic carboxylates are the common motif that SAP recognises and the SAP pull-down experiments could be repeated with bacterial inclusion bodies so as to improve the importance of the strip formation of the acidic residues.

Appendices

Appendix 1-Minimal media

M9 Minimal media preparation per L

100ml M9 medium x10

1ml 1M $MgSO_4$

0.3ml 1M $CaCl_2$

pH 7.4

Autoclave

1g $^{(15)}NH_4Cl$ & 2g $^{(13)}C_6$ glucose in 10ml H_2O 0.2µm filter sterilised

10ml trace elements 0.2µm filtered

1ml 100mg/ml Ampicillin

M9 medium x10 per L		Trace Elements solution x100 per L	
60g	Na_2HPO_4	5g	EDTA in 800ml H_2O pH →7.5
30g	KH_2PO_4	0.83g	$FeCl_3.6H_2O$
5g	NaCl	84mg	$ZnCl_2$
		13mg	$CuCl_2.2H_2O$
		10mg	$CoCl_2.6H_2O$
		10mg	H_3BO_3
		1.6mg	$MnCl_2.6H_2O$
		make up to 1L, 02um filter.	

References

1. Pepys, M. (2001) Pathogenesis, diagnosis and treatment of systemic amyloidosis, *Phil. trans. R. Soc. B 356*, 203-211.

2. Divry, P., and Florkin, M. (1927) Sur les proprietes optiques de l'amyloide, *C. R. Soc. Biol. 97*, 1808-1810.

3. Chiti, F., and Dobson, C. M. (2006) Protein misfolding, functional amyloid, and human disease, *Annu. Rev. Biochem. 75*, 333-366.

4. Glabe, C. G. (2006) Common mechanisms of amyloid oligomer pathogenesis in degenerative disease, *Neurobiol. Aging 27*, 570-575.

5. Glabe, C. G., and Kayed, R. (2006) Common structure and toxic function of amyloid oligomers implies a common mechanism of pathogenesis, *Neurology 66*, S74-S78.

6. Chimon, S., and Ishii, Y. (2005) Capturing Intermediate Structures of Alzheimer's β-Amyloid, Aβ(1−40), by Solid-State NMR Spectroscopy, *J. Am. Chem. Soc. 127*, 13472-13473.

7. Hawkins, P., and Pepys, M. (1995) Imaging amyloidosis with radiolabelled SAP, *Eur. J. Nucl. Med. Mol. Imaging 22*, 595-599.

8. Dubrey, S. W., Cha, K., Skinner, M., LaValley, M., and Falk, R. H. (1997) Familial and primary (AL) cardiac amyloidosis: echocardiographically similar diseases with distinctly different clinical outcomes, *Heart 78*, 74-82.

9. Lorenzo, A., and Yanker, B. A. (1996) Amyloid Fibril Toxicity in Alzheimer's Disease and Diabetesa, *Ann. N.Y. Acad. Sci. 777*, 89-95.

10. Lambert, M. P., Barlow, A. K., Chromy, B. A., Edwards, C., Freed, R., Liosatos, M., Morgan, T. E., Rozovsky, I., Trommer, B., Viola, K. L., Wals, P., Zhang, C., Finch, C. E., Krafft, G. A., and Klein, W. L. (1998) Diffusible, nonfibrillar ligands derived from Aβ1–42 are potent central nervous system neurotoxins *Proc. Natl. Acad. Sci. U.S.A. 95*, 6448-6453.

11. Hartley, D. M., Walsh, D. M., Ye, C. P., Diehl, T., Vasquez, S., Vassilev, P. M., Teplow, D. B., and Selkoe, D. J. (1999) Protofibrillar Intermediates of Amyloid beta - Protein Induce Acute Electrophysiological Changes and Progressive Neurotoxicity in Cortical Neurons, *J. Neurosci. 19*, 8876-8884.

12. Shirahama, T., and Cohen, A. S. (1967) High resolution electron microscopic analysis of the amyloid fibril, *J. Cell. Biol. 33*, 679-708.

13. White, H. E., Hodgkinson, J. L., Jahn, T. R., Cohen-Krausz, S., Gosal, W. S., Müller, S., Orlova, E. V., Radford, S. E., and Saibil, H. R. (2009) Globular Tetramers of [beta]2-Microglobulin Assemble into Elaborate Amyloid Fibrils, *J. Mol. Biol. 389*, 48-57.

14. Eanes, E. D., and Glenner, G. G. (1968) X-Ray diffraction studies on amyloid filaments, *J. Histochem. Cytochem. 16*, 673-677.

15. Sunde, M., Serpell, L. C., Bartlam, M., Fraser, P. E., Pepys, M. B., and Blake, C. C. F. (1997) Common core structure of amyloid fibrils by synchrotron X-ray diffraction, *J. Mol. Biol. 273*, 729-739.

16. Balbach, J. J., Petkova, A. T., Oyler, N. A., Antzutkin, O. N., Gordon, D. J., Meredith, S. C., and Tycko, R. (2002) Supramolecular Structure in Full-Length Alzheimer's [beta]-Amyloid Fibrils: Evidence for a Parallel [beta]-Sheet Organization from Solid-State Nuclear Magnetic Resonance, *Biophys. J. 83*, 1205-1216.

17. Antzutkin, O. N., Balbach, J. J., Leapman, R. D., Rizzo, N. W., Reed, J., and Tycko, R. (2000) Multiple quantum solid-state NMR indicates a parallel, not antiparallel, organization of β-sheets in Alzheimer's β-amyloid fibrils *Proc. Natl. Acad. Sci. U.S.A. 97*, 13045-13050.

18. Petkova, A. T., Ishii, Y., Balbach, J. J., Antzutkin, O. N., Leapman, R. D., Delaglio, F., and Tycko, R. (2002) A structural model for Alzheimer's β-amyloid fibrils based on experimental constraints from solid state NMR, *Proc. Natl. Acad. Sci. U.S.A. 99*, 16742-16747.

19. Ferguson, N., Becker, J., Tidow, H., Tremmel, S., Sharpe, T. D., Krause, G., Flinders, J., Petrovich, M., Berriman, J., Oschkinat, H., and Fersht, A. R. (2006) General structural motifs of amyloid protofilaments, *Proc. Natl. Acad. Sci. U.S.A. 103*, 16248-16253.

20. Van Melckebeke, H., Wasmer, C., Lange, A., Ab, E., Loquet, A., Bockmann, A., and Meier, B. H. (2010) Atomic-Resolution Three-Dimensional Structure of HET-s(218-289) Amyloid Fibrils by Solid-State NMR Spectroscopy, *J. Am. Chem. Soc. 132*, 13765-13775.

21. Andronesi, O. C., Bergen, M. v., Biernat, J., Seidel, K., Griesinger, C., Mandelkow, E., and Baldus, M. (2008) Characterization of Alzheimer's-like Paired Helical Filaments from the Core Domain of Tau Protein Using Solid-State NMR Spectroscopy, *J. Am. Chem. Soc. 130*, 5922-5928.

22. Yamamoto, S., and Gejyo, F. (2005) Historical background and clinical treatment of dialysis-related amyloidosis, *BBA-Proteins Proteom. 1753*, 4-10.

23. Garbar, C., Jadoul, M., Noel, H., and Van Ypersele De Strihou, C. (1999) Histological characteristics of sternoclavicular beta-2-microglobulin amyloidosis and clues for its histogenesis, *Kidney Int. 55*, 1983-1990.

24. Rashid, G., Korzets, Z., and Bernheim, J. (2006) Advanced glycation end products stimulate tumor necrosis factor-alpha and interleukin-1 beta secretion by peritoneal macrophages in patients on continuous ambulatory peritoneal dialysis, *Israel Med. Assoc. J. 8*, 36-39.

25. Miyata, T., Oda, O., Inagi, R., Iida, Y., Araki, N., Yamada, N., Horiuchi, S., Taniguchi, N., Maeda, K., and Kinoshita, T. (1993) Beta 2-Microglobulin Modified with Advanced Glycation End Products Is a Major Component of Hemodialysis-associated Amyloidosis, *J. Clin. Invest. 92*, 1243-1252.

26. Miyata, T., R. I., Iida, Y., Sato, M., Yamada, N., Oda, O., Maeda, K. and Seo, H. (1994) Involvement of beta 2-microglobulin modified with advanced glycation end products in the pathogenesis of hemodialysis-associated amyloidosis. Induction of human monocyte chemotaxis and macrophage secretion of tumor necrosis factor-alpha and interleukin-1., *J. Clin. Invest. 93*, 521-528.

27. Deforges-Lasseur, C., Combe, C., Cernier, A., Vital, J. M., and Aparicio, M. (1993) Destructive spondyloarthropathy presenting with progressive paraplegia in a dialysis patient. Recovery after surgical spinal cord decompression and parathyroidectomy, *Nephrol. Dial. Transplant. 8*, 180-184.

28. Farhad, R. D., Jens, K., Hidejiro, Y., and Peter, I. (1999) Fatal cervical spondyloarthropathy in a hemodialysis patient with systemic deposition of beta-2-microglobulin amyloid, *Am. J. Kid. Dis. 33*, 563-566.

29. Allard, J. C., Artze, M. E., Porter, G., Ghandur-Mnaymneh, L., Velasco, R. d., and Perez, G. O. (1992) Fatal destructive cervical spondyloarthropathy in two patients on long-term dialysis, *Am. J. Kid. Dis. 19*, 81-85.

30. Bardin, T., Zingraff, J., Shirahama, T., Noel, L.-H., Droz, D., Voisin, M.-C., Drueke, T., Dryll, A., Skinner, M., S. Cohen, A., and Kuntz, D. (1987) Hemodialysis-associated amyloidosis and beta-2 microglobulin : Clinical and immunohistochemical study, *Am. J. Med. 83*, 419-424.

31. Lutz, A. E., Schneider, U., Ehlerding, G., Frenzel, H., Koch, K. M., and Kuhn, K. (1995) Right ventricular cardiac failure and pulmonary hypertension in a long-term dialysis patient--unusual presentation of visceral {beta}2-microglobulin amyloidosis, *Nephrol. Dial. Transplant. 10*, 555-558.

32. E.R. Maher, S. H. D., R.A. Baillod, P. Sweny, J.F. Moorhead. (1988) Gastrointestinal complications of dialysis related amyloidosis, *Brit. Med. J. 297*, 265-266.

33. Drueke, T. (2000) Beta 2 Microglobulin and amyloidosis, *Nephrol. Dial. Transplant. 15 (suppl. 1)*, 17-24.

34. Schoels, M., Jahn, B., Hug, F., Deppisch, R., Ritz, E., and Hansch, G. M. (1993) Stimulation of Mononuclear-Cells by Contact with Cuprophan Membranes - Further Increase of Beta(2)-Microglobulin Synthesis by Activated Late Complement Components, *Am. J. Kid. Dis. 21*, 394-399.

35. Zaoui, P. M., Stone, W. J., and Hakim, R. M. (1990) Effects of Dialysis Membranes on Beta-2-Microglobulin Production and Cellular Expression, *Kidney Int. 38*, 962-968.

36. Messner, R. P. (1984) Beta-2-Microglobulin - an Old Molecule Assumes a New Look, *J. Lab. Clin. Med. 104*, 141-145.

37. Sonikian, M., Gogusev, J., Zingraff, J., Loric, S., Quednau, B., Bessou, G., Siffert, W., Drueke, T. B., Reusch, H. P., and Luft, F. C. (1996) Potential effect of metabolic acidosis on beta 2-microglobulin generation: In vivo and in vitro studies, *J. Am. Soc. Nephrol. 7*, 350-356.

38. Lee, S. H., Huang, T. S., and Hsieh, S. J. (1996) Changes of bone markers during long-term intravenous calcitriol therapy in maintenance dialysis patients, *Miner. Electrol. Metab. 22*, 219-223.

39. Morgan, C. J., Gelfand, M., Atreya, C., and Miranker, A. D. (2001) Kidney dialysis-associated amyloidosis: A molecular role for copper in fiber formation, *J. Mol. Biol. 309*, 339-345.

40. Gejyo, F., Odani, S., Yamada, T., Honma, N., Saito, H., Suzuki, Y., Nakagawa, Y., Kobayashi, H., Maruyama, Y., Hirasawa, Y., Suzuki, M., and Arakawa, M. (1986) [beta]2-microglobulin: A new form of amyloid protein associated with chronic hemodialysis, *Kidney Int. 30*, 385-390.

41. Kessler, M., Hestin, D., Aymard, B., Mainard, D., Claudon, M., Netter, P., and Gaucher, A. (1995) Carpal-tunnel syndrome with {beta}2-microglobulin amyloid deposits and erosive arthropathy of the wrist and spine in a uraemic patient before chronic haemodialysis, *Nephrol. Dial. Transplant. 10*, 298-299.

42. Vorbeck-Meister, I., Sommer, R., Vorbeck, F., and Horl, W. (1999) Quality of water used for haemodialysis: bacteriological and chemical parameters, *Nephrol. Dial. Transplant. 14*, 666-675.

43. Barbour, B. H., Bischel, M. & Abrams, D. E. . (1971) Copper accumulation in patients undergoing chronic hemodialysis. The role of cuprophan, *Nephron 8*, 455-462.

44. De Strihou, C. v. Y., Jadoul, M., Malghem, J., Maldague, B., and Jamart, J. (1991) Effect of dialysis membrane and patient's age on signs of dialysis-related amyloidosis, *Kidney Int. 39*, 1012-1019.

45. Myers, S., Jones, S., Jahn, T., Morten, I., Tennent, G., Hewitt, E., and Radford, S. (2006) A Systematic Study of the Effect of Physiological Factors on Beta 2-Microglobulin Amyloid Formation at Neutral pH, *Biochemistry-U.S. 45*, 2311-2321.

46. Mourad, G., and Argiles, A. (1996) Renal transplantation relieves the symptoms but does not reverse beta 2- microglobulin amyloidosis, *J. Am. Soc. Nephrol. 7*, 798-804.

47. Nelson, S. R., Hawkins, P. N., Richardson, S., Pepys, M. B., Lavender, J. P., Sethi, D., Gower, P. E., Pugh, C. W., Winearls, C. G., and Oliver, D. O. (1991) Imaging of haemodialysis-associated amyloidosis with 123I-serum amyloid P component, *Lancet 338*, 335-339.

48. Bardin, T., Lebail-Darné, J. L., Zingraff, J., Laredo, J. D., Voisin, M. C., Kreis, H., and Kuntz, D. (1995) Dialysis arthropathy: Outcome after renal transplantation, *Am. J. Med. 99*, 243-248.

49. Kutsuki, H. (2005) [beta]2-Microglobulin-selective direct hemoperfusion column for the treatment of dialysis-related amyloidosis, *BBA- Proteins Proteom. 1753*, 141-145.

50. Gorevic, P., Casey, T., Stone, W., DiRaimondo, C., Prelli, F., and Frangione, B. (1985) Beta-2 microglobulin is an amyloidogenic protein in man, *J. Clin. Invest. 76*, 2425-2429.

51. Gejyo, F., Yamada, T., Odani, S., Nakagawa, Y., Arakawa, M., Kunitomo, T., Kataoka, H., Suzuki, M., Hirasawa, Y., Shirahama, T., Cohen, A. S., and Schmid, K. (1985) A New Form of Amyloid Protein Associated with Chronic-Hemodialysis Was Identified as Beta-2-Microglobulin, *Biochem. Biophys. Res. Commun. 129*, 701-706.

52. Theaker, J. M., Raine, A. E., Rainey, A. J., Heryet, A., Clark, A., and Oliver, D. O. (1987) Systemic amyloidosis of beta 2-microglobulin type: a complication of long-term haemodialysis, *J. Clin. Pathol. 40*, 1247-1251.

53. Saper, M. A., Bjorkman, P. J., and Wiley, D. C. (1991) Refined structure of the human histocompatibility antigen HLA-A2 at 2.6 Å resolution, *J. Mol. Biol. 219*, 277-319.

54. Okon, M., Bray, P., and Vucelic, D. (1992) Proton NMR assignments and secondary structure of human .beta.2-microglobulin in solution, *Biochemistry-U.S 31*, 8906-8915.

55. Becker, J. W., and Reeke, G. N. (1985) Three-dimensional structure of beta 2-microglobulin, *Proc. Natl. Acad. Sci. U.S.A. 82*, 4225-4229.

56. Rosano, C., Zuccotti, S., and Bolognesi, M. (2005) The three-dimensional structure of 2 microglobulin: Results from X-ray crystallography, *BBA-Proteins Proteom. 1753*, 85-91.

57. Verdone, G., Corazza, A., Viglino, P., Pettirossi, F., Giorgetti, S., Mangione, P., Andreola, A., Stoppini, M., Bellotti, V., and Esposito, G. (2002) The solution structure of human {beta}2-microglobulin reveals the prodromes of its amyloid transition, *Protein Sci. 11*, 487-499.

58. Trinh, C. H., Smith, D. P., Kalverda, A. P., Phillips, S. E. V., and Radford, S. E. (2002) Crystal structure of monomeric human beta-2-microglobulin reveals clues to its amyloidogenic properties, *Proc. Natl. Acad. Sci. U.S.A. 99*, 9771-9776.

59. Tysoe-Calnon, V. A., Grundy, J. E., and Perkins, S. J. (1991) Molecular comparisons of the beta 2-microglobulin-binding site in class I major-histocompatibility-complex alpha-chains and proteins of related sequences, *Biochem. J. 277*, 359-369.

60. Smith, D. P., Jones, S., Serpell, L. C., Sunde, M., and Radford, S. E. (2003) A systematic investigation into the effect of protein destabilisation on beta 2-microglobulin amyloid formation, *J. Mol. Biol. 330*, 943-954.

61. Kardos, J., Okuno, D., Kawai, T., Hagihara, Y., Yumoto, N., Kitagawa, T., Zavodszky, P., Naiki, H., and Goto, Y. (2005) Structural studies reveal that the diverse morphology of beta(2)-microglobulin aggregates is a reflection of different molecular architectures, *BBA-Proteins Proteom. 1753*, 108-120.

62. Kozhukh, G. V., Hagihara, Y., Kawakami, T., Hasegawa, K., Naiki, H., and Goto, Y. (2002) Investigation of a Peptide Responsible for Amyloid Fibril Formation of beta 2-Microglobulin by Achromobacter Protease I, *J. Biol. Chem. 277*, 1310-1315.

63. M Chicurel, E. G., and F Goodsaid. (1988) Modulation of macrophage lysosomal pH by Mycobacterium tuberculosis-derived proteins, *Infect. Immun. 56*, 479-483.

64. Morten, I. J., Gosal, W. S., Radford, S. E., and Hewitt, E. W. (2007) Investigation into the role of macrophages in the formation and degradation of beta(2)-microglobulin amyloid fibrils, *J. Biol. Chem. 282*, 29691-29700.

65. Garcia-Garcia, M., Argiles, A., Gouin-Charnet, A., Durfort, M., Garcia-Valero, J., and Mourad, G. (1999) Impaired lysosomal processing of beta-2-microglobulin by infiltrating macrophages in dialysis amyloidosis, *Kidney Int. 55*, 899-906.

66. Eakin, C. M., Knight, J. D., Morgan, C. J., Gelfand, M. A., and Miranker, A. D. (2002) Formation of a copper specific binding site in non-native states of beta-2-microglobulin, *Biochemistry-U.S. 41*, 10646-10656.

67. Miura, T., Suzuki, K., Kohata, N., and Takeuchi, H. (2000) Metal Binding Modes of Alzheimer's Amyloid beta-Peptide in Insoluble Aggregates and Soluble Complexes, *Biochemistry-U.S. 39*, 7024-7031.

68. Brown, D. R. (2001) Copper and prion disease, *Brain Res. Bull. 55*, 165-173.

69. Calabrese, M. F., and Miranker, A. D. (2007) Formation of a stable oligomer of beta-2 microglobulin requires only transient encounter with cu(II), *J. Mol. Biol. 367*, 1-7.

70. Jahn, T., Parker, M., Homans, S., and Radford, S. E. (2006) Amyloid formation under physiological conditions proceeds via a native-like folding intermediate *Nat. Struct. Mol. Biol. 13*, 195-201.

71. Athanasou, N. A., Puddle, B., and Sallie, B. (1995) Highly Sulfated Glycosaminoglycans in Articular-Cartilage and Other Tissues Containing Beta(2) Microglobulin Dialysis Amyloid Deposits, *Nephrol. Dial. Transplant. 10*, 1672-1678.

72. Naiki, H., Yamamoto, S., Hasegawa, K., Yamaguchi, I., Goto, Y., and Gejyo, F. (2005) Molecular interactions in the formation and deposition of beta(2)-microglobuhn-related amyloid fibrils, *Amyloid 12*, 15-25.

73. Mahley, R. W. (1988) Apolipoprotein E: cholesterol transport protein with expanding role in cell biology, *Science 240*, 622-630.

74. Namba, Y., Tomonaga, M., Kawasaki, H., Otomo, E., and Ikeda, K. (1991) Apolipoprotein E immunoreactivity in cerebral amyloid deposits and neurofibrillary tangles in Alzheimer's disease and kuru plaque amyloid in Creutzfeldt-Jakob disease, *Brain Res. 541*, 163-166.

75. Yamada, T., Kakihara, T., Gejyo, F., and Okada, M. (1994) A monoclonal antibody recognizing apolipoprotein E peptides in systemic amyloid deposits, *Ann. Clin. Lab. Sci. 24*, 243-249.

76. Yamaguchi, I., Hasegawa, K., Takahashi, N., Gejyo, F., and Naiki, H. (2001) Apolipoprotein E inhibits the depolymerization of beta 2-microglobulin-related amyloid fibrils at a neutral pH, *Biochemistry-U.S. 40*, 8499-8507.

77. Giorgetti, S., Rossi, A., Mangione, P., Raimondi, S., Marini, S., Stoppini, M., Corazza, A., Viglino, P., Esposito, G., Cetta, G., Merlini, G., and Bellotti, V. (2005) beta 2-microglobulin isoforms display an heterogeneous affinity for type I collagen, *Protein Sci. 14*, 696-702.

78. Relini, A., Canale, C., De Stefano, S., Rolandi, R., Giorgetti, S., Stoppini, M., Rossi, A., Fogolari, F., Corazza, A., Esposito, G., Gliozzi, A., and Bellotti, V. (2006) Collagen plays an active role in the aggregation of beta(2)-microglobulin under physiopathological conditions of dialysis-related amyloidosis, *J. Biol. Chem. 281*, 16521-16529.

79. Bellotti, V., Stoppini, M., Mangione, P., Sunde, M., Robinson, C., Asti, L., Brancaccio, D., and Ferri, G. (1998) β 2-microglobulin can be refolded into a native state from ex vivo amyloid fibrils, *Eur. J. Biochem. 258*, 61-67.

80. Cummings, N. A., and Nordby, G. L. (1966) Measurement of synovial fluid pH in normal and arthritic knees, *Arthritis Rheum. 9*, 47-56.

81. Ward, T. T., and Steigbigel, R. T. (1978) Acidosis of synovial fluid correlates with synovial fluid leukocytosis, *Am. J. Med. 64*, 933-936.

82. Geborek, P., Saxne, T., Pettersson, H., and Wollheim, F. (1989) Synovial fluid acidosis correlates with radiological joint destruction in rheumatoid arthritis knee joints., *J. Rheumatol. 16*, 468-472.

83. Eichner, T., Kalverda, A. P., Thompson, G. S., Homans, S. W., and Radford, S. E. (2011) Conformational Conversion during Amyloid Formation at Atomic Resolution, *Mol. Cell 41*, 161-172.

84. Iwata, K., Fujiwara, T., Matsuki, Y., Akutsu, H., Takahashi, S., Naiki, H., and Goto, Y. (2006) 3D structure of amyloid protofilaments of Beta 2-microglobulin fragment probed by solid-state NMR, *Proc. Natl. Acad. Sci. U.S.A. 103*, 18119-18124.

85. Ivanova, M. I., Sawaya, M. R., Gingery, M., Attinger, A., and Eisenberg, D. (2004) An amyloid-forming segment of beta 2-microglobulin suggests a molecular model for the fibril, *Proc. Natl. Acad. Sci. U.S.A. 101*, 10584-10589.

86. Baltz ML, G. K., Davies AJ, Evans DJ, Klaus GG, Pepys MB. (1980) Differences in the acute phase responses of serum amyloid P-component (SAP) and C3 to injections of casein or bovine serum albumin in amyloid-susceptible and -resistant mouse strains. , *Clin. Exp. Immunol. 39*, 355-360.

87. Coe, J. E., and Ross, M. J. (1990) Amyloidosis and female protein in the Syrian hamster. Concurrent regulation by sex hormones, *J. Exp. Med. 171*, 1257-1267.

88. Kinoshita, C. M., Gewurz, A. T., Siegel, J. N., Ying, S. C., Hugli, T. E., Coe, J. E., Gupta, R. K., Huckman, R., and Gewurz, H. (1992) A protease-sensitive site in the proposed Ca(2+)-binding region of human serum amyloid P component and other pentraxins, *Protein Sci. 1*, 700-709.

89. Tennent, G. A., Lovat, L. B., and Pepys, M. B. (1995) Serum Amyloid P Component Prevents Proteolysis of the Amyloid Fibrils of Alzheimer Disease and Systemic Amyloidosis, *Proc. Natl. Acad. Sci. U.S.A. 92*, 4299-4303.

90. Pepys, M. B., Herbert, J., Hutchinson, W. L., Tennent, G. A., Lachmann, H. J., Gallimore, J. R., Lovat, L. B., Bartfai, T., Alanine, A., Hertel, C., Hoffmann, T., Jakob-Roetne, R., Norcross, R. D., Kemp, J. A., Yamamura, K., Suzuki, M., Taylor, G. W., S. Murray, Thompson, D., Purvis, A., Kolstoe, S., Wood, S. P., and Hawkins, P. N. (2002) Targeted pharmacological depletion of serum amyloid P component for treatment of human amyloidosis, *Nature 417*, 254-259.

91. Pepys, M. B., and Butler, P. J. G. (1987) Serum amyloid P component is the major calcium-dependent specific DNA binding protein of the serum, *Biochem. Biophys. Res. Commun. 148*, 308-313.

92. Bickerstaff, M. (1999) Serum amyloid P component controls chromatin degradation and prevents antinuclear autoimmunity, *Nat. Med. 5*, 694-697.

93. Sørensen, I. J., Nielsen, E. H., Schrøder, L., Voss, A., Horváth, L., and Svehag, S.-E. (2000) Complexes of Serum Amyloid P Component and DNA in Serum from Healthy Individuals and Systemic Lupus Erythematosus Patients, *J. Clin. Immunol. 20*, 408-415.

94. Hind, C. R., Collins, P. M., Baltz, M. L., and Pepys, M. B. (1985) Human serum amyloid P component, a circulating lectin with specificity for the cyclic 4,6-pyruvate acetal of galactose. Interactions with various bacteria, *Biochem. J. 225*, 107-111.

95. Noursadeghi, M., Bickerstaff, M. C. M., Gallimore, J. R., Herbert, J., Cohen, J., and Pepys, M. B. (2000) Role of serum amyloid P component in bacterial infection: Protection of the host or protection of the pathogen, *Proc. Natl. Acad. Sci. U.S.A. 97*, 14584-14589.

96. Mikolajek, H., Kolstoe, S. E., Pye, V. E., Mangione, P., Pepys, M. B., and Wood, S. P. (2011) Structural basis of ligand specificity in the human pentraxins, C-reactive protein and serum amyloid P component, *J. Mol. Recognit. 24, 371-377*

97. Thompson, D., Pepys, M. B., Tickle, I., and Wood, S. (2002) The Structures of Crystalline Complexes of Human Serum Amyloid P Component with Its Carbohydrate Ligand, The Cyclic Pyruvate Acetal of Galactose, *J. Mol. Biol. 320*, 1081-1086.

98. Emsley, J., White, H. E., O'Hara, B. P., Oliva, G., Srinivasan, N., Tickle, I. J., Blundell, T. L., Pepys, M. B., and Wood, S. P. (1994) Structure of pentameric human serum amyloid P component, *Nature 367*, 338-345.

99. Pepys, M. B., Dyck, R. F., De Beer, F. C., Skinner, M., and Cohen, A. S. (1979) Binding of Serum Amyloid P-component (SAP) by amyloid fibrils, *Clin. Exp. Immunol. 38*, 284-293.

100. Levitt, M. (2008) *Spin Dynamics: Basics of Nuclear Magnetic Resonance*. 2nd ed., John Wiley & Sons Ltd, Chichester.

101. Andrew, E. R., Bradbury, A., and Eades, R. G. (1958) Nuclear Magnetic Resonance Spectra from a Crystal rotated at High Speed, *Nature 182*, 1659-1659.

102. Fung, B. M., Khitrin, A. K., and Ermolaev, K. (2000) An Improved Broadband Decoupling Sequence for Liquid Crystals and Solids, *J. Mag. Res.142*, 97-101.

103. Szeverenyi, N. M., Sullivan, M. J., and Maciel, G. E. (1982) Observation of spin exchange by two-dimensional fourier transform 13C cross polarization-magic-angle spinning, *J. Mag. Res. (1969) 47*, 462-475.

104. Ohhashi, Y., Hagihara, Y., Kozhukh, G., Hoshino, M., Hasegawa, K., Yamaguchi, I., Naiki, H., and Goto, Y. (2002) The Intrachain Disulfide Bond of Beta-2-Microglobulin Is Not Essential for the Immunoglobulin Fold at Neutral pH, but Is Essential for Amyloid Fibril Formation at Acidic pH, *J. Biochem. 131*, 45-52.

105. Zimmerman, S. B., and Trach, S. O. (1991) Estimation of macromolecule concentrations and excluded volume effects for the cytoplasm of Escherichia coli, *J. Mol. Biol. 222*, 599-620.

106. Allen P, M. (2000) Implications of macromolecular crowding for protein assembly, *Curr Opin. Struc. Biol. 10*, 34-39.

107. Lansbury, P. T. (1999) Evolution of amyloid: What normal protein folding may tell us about fibrillogenesis and disease, *Proc. Natl. Acad. Sci. U.S.A. 96*, 3342-3344.

108. Uversky, V. N., M. Cooper, E., Bower, K. S., Li, J., and Fink, A. L. (2002) Accelerated Î±-synuclein fibrillation in crowded milieu, *FEBS Lett. 515*, 99-103.

109. Hatters, D. M., Minton, A. P., and Howlett, G. J. (2002) Macromolecular Crowding Accelerates Amyloid Formation by Human Apolipoprotein C-II, *J. Biol. Chem. 277*, 7824-7830.

110. Eichner, T., and Radford, S. E. (2011) Understanding the complex mechanisms of β2-microglobulin amyloid assembly, *FEBS J. 278*, 3868-3883.

111. Biancalana, M., and Koide, S. Molecular mechanism of Thioflavin-T binding to amyloid fibrils, *BBA-Proteins Proteom. 1804*, 1405-1412.

112. Levine, H. (1993) Thioflavine T interaction with synthetic Alzheimer's disease β-amyloid peptides: Detection of amyloid aggregation in solution, *Protein Sci. 2*, 404-410.

113. Kad, N. M., Myers, S. L., Smith, D. P., Smith, D. A., Radford, S. E., and Thomson, N. H. (2003) Hierarchical assembly of beta(2)-microglobulin amyloid in vitro revealed by atomic force microscopy, *J. Mol. Biol. 330*, 785-797.

114. Bokvist, M., and Grobner, G. (2007) Misfolding of Amyloidogenic Proteins at Membrane Surfaces: The Impact of Macromolecular Crowding, *J. Am. Chem. Soc. 129*, 14848-14849.

115. Van den Berg, B., Ellis, R. J., and Dobson, C. M. (1999) Effects of macromolecular crowding on protein folding and aggregation, *EMBO J. 18*, 6927-6933.

116. Morris, G. A., and Freeman, R. (1979) Enhancement of nuclear magnetic resonance signals by polarization transfer, *J. Am. Chem. Soc. 101*, 760-762.

117. Hore, P. J., Jones, J. A., and Wimperis, S. (2000) *NMR: The Toolkit*, Oxford University Press, Oxford, United Kingdom.

118. Kay, L. E., Ikura, M., Tschudin, R., and Bax, A. (1990) Three-dimensional triple-resonance NMR spectroscopy of isotopically enriched proteins, *J. Mag. Reson. (1969) 89*, 496-514.

119. Farmer, B. T., Venters, R. A., Spicer, L. D., Wittekind, M. G., and Müller, L. (1992) A refocused and optimized HNCA: Increased sensitivity and resolution in large macromolecules, *J. Biomol. NMR 2*, 195-202.

120. Grzesiek, S., and Bax, A. (1992) Correlating backbone amide and side chain resonances in larger proteins by multiple relayed triple resonance NMR, *J. Am. Chem. Soc. 114*, 6291-6293.

121. Wittekind, M., and Mueller, L. (1993) HNCACB, a High-Sensitivity 3D NMR Experiment to Correlate Amide-Proton and Nitrogen Resonances with the Alpha- and Beta-Carbon Resonances in Proteins, *J. Mag. Reson. Ser. B 101*, 201-205.

122. Löhr, F., and Rüterjans, H. (1995) A new triple-resonance experiment for the sequential assignment of backbone resonances in proteins, *J. Biomol. NMR 6*, 189-197.

123. Logan, T. M., Olejniczak, E. T., Xu, R. X., and Fesik, S. W. (1993) A general method for assigning NMR spectra of denatured proteins using 3D HC(CO)NH-TOCSY triple resonance experiments, *J. Biomol. NMR 3*, 225-231.

124. Wishart, D. S., Sykes, B. D., and Richards, F. M. (1992) The chemical shift index: a fast and simple method for the assignment of protein secondary structure through NMR spectroscopy, *Biochemistry-U.S 31*, 1647-1651.

125. Wishart, D. S., and Sykes, B. D. (1994) The 13C Chemical-Shift Index: A simple method for the identification of protein secondary structure using 13C chemical-shift data, *J. Biomol. NMR 4*, 171-180.

126. Esposito, G., Corazza, A., Viglino, P., Verdone, G., Pettirossi, F., Fogolari, F., Makek, A., Giorgetti, S., Mangione, P., Stoppini, M., and Bellotti, V. (2005) Solution structure of [beta]2-microglobulin and insights into fibrillogenesis, *BBA-Proteins Proteom. 1753*, 76-84.

127. Levitt, M. H. (2001) *Spin Dynamics: Basics of nuclear magnetic resonance*, 1st ed., John Wiley and sons Ltd, Chichester.

128. De Groot, N. S. n., and Ventura, S. (2006) Effect of temperature on protein quality in bacterial inclusion bodies, *FEBS Lett. 580*, 6471-6476.

129. García-Fruitós, E., González-Montalbán, N., Morell, M., Vera, A., Ferraz, R. M., Arís, A., Ventura, S., and Villaverde, A. (2005) Aggregation as bacterial inclusion bodies does not imply inactivation of enzymes and fluorescent proteins, *Microb. Cell Fact. 4*, 27.

130. Wang, L., Maji, S. K., Sawaya, M. R., Eisenberg, D., and Riek, R. (2008) Bacterial Inclusion Bodies Contain Amyloid-Like Structure, *PLoS Biol. 6*, e195.

131. Wasmer, C., Benkemoun, L., Sabaté, R., Steinmetz, M. O., Coulary-Salin, B., Wang, L., Riek, R., Saupe, S. J., and Meier, B. H. (2009) Solid-State NMR Spectroscopy Reveals that E. coli Inclusion Bodies of HET-s(218–289) are Amyloids, *Angew. Chem. Int. Ed. Engl. 48*, 4858-4860.

132. Taylor, G. F., Wood, S. P., Mörs, K., Glaubitz, C., Werner, J. M., and Williamson, P. T. F. (2011) Morphological Differences between β2-Microglobulin in Fibrils and Inclusion Bodies, *ChemBioChem 12*, 556-558.

133. Marion, D., and WÃ¼thrich, K. (1983) Application of phase sensitive two-dimensional correlated spectroscopy (COSY) for measurements of 1H-1H spin-spin coupling constants in proteins, *Biochem. Biophys. Res. Commun. 113*, 967-974.

134. Baldus, M., Geurts, D. G., Hediger, S., and Meier, B. H. (1996) Efficient 15N-13C Polarization Transfer by Adiabatic Passage Hartmann-Hahn Cross Polarization (APHH-CP), *J. Mag. Reson Ser. A 118*, 140-144.

135. Baldus, M., Petkova, A., Herzfeld, J., and Griffin, R. (1998) Cross polarization in the tilted frame: assignment and spectral simplification in heteronuclear spin systems, *Mol. Phys. 95*, 1197-1207.

136. Pauli, J., Baldus, M., van Rossum, B., de Groot, H., and Oschkinat, H. (2001) Backbone and Side-Chain 13C and 15N Signal Assignments of the α-Spectrin SH3 Domain by Magic Angle Spinning Solid-State NMR at 17.6 Tesla, *ChemBioChem 2*, 272-281.

137. Smith, S., Levante, T., Meier, B., and Ernst, R. (1994) Computer simulations in magnetic resonance. An object-oriented programming approach., *J. Mag. Reson. 106A*, 75-105.

138. Castellani, F., van Rossum, B., Diehl, A., Schubert, M., Rehbein, K., and Oschkinat, H. (2002) Structure of a protein determined by solid-state magic-angle-spinning NMR spectroscopy, *Nature 420*, 98-102.

139. Becker, J., Ferguson, N., Flinders, J., van Rossum, B.-J., Fersht, A. R., and Oschkinat, H. (2008) A Sequential Assignment Procedure for Proteins that have Intermediate Line Widths in MAS NMR Spectra: Amyloid Fibrils of Human CA150.WW2, *ChemBioChem 9*, 1946-1952.

140. Higman, V., Flinders, J., Hiller, M., Jehle, S., Markovic, S., Fiedler, S., van Rossum, B.-J., and Oschkinat, H. (2009) Assigning large proteins in the solid state: a MAS NMR resonance assignment strategy using selectively and extensively 13C-labelled proteins, *J. Biomol. NMR 44*, 245-260.

141. Tadeo, X., Castaño, D., and Millet, O. (2007) Anion modulation of the 1H/2H exchange rates in backbone amide protons monitored by NMR spectroscopy. *Protein Sci. 16*, 2733-2740.

142. Whittemore, N. A., Mishra, R., Kheterpal, I., Williams, A. D., Wetzel, R., and Serpersu, E. H. (2005) Hydrogen-Deuterium (H/D) Exchange Mapping of A-Beta1-40 Amyloid Fibril Secondary Structure Using Nuclear Magnetic Resonance Spectroscopy. *Biochemistry-U.S. 44*, 4434-4441.

143. Vilar, M. a., Chou, H.-T., Luhrs, T., Maji, S. K., Riek-Loher, D., Verel, R., Manning, G., Stahlberg, H., and Riek, R. (2008) The fold of alpha-synuclein fibrils, *Proc. Natl. Acad. Sci. U.S.A. 105*, 8637-8642.

144. Hoshino, M., Katou, H., Yamaguchi, K.-I., and Goto, Y. (2007) Dimethylsulfoxide-quenched hydrogen/deuterium exchange method to study amyloid fibril structure, *BBA-Biomembranes 1768*, 1886-1899.

145. Lesage, A., and Bockmann, A. (2003) Water-Protein Interactions in Microcrystalline Crh Measured by 1H-13C Solid-State NMR Spectroscopy, *J. Am. Chem. Soc. 125*, 13336-13337.

146. Skora, L., Becker, S., and Zweckstetter , M. (2010) Characterization of Amyloid Fibrils of Human beta-2-Microglobulin by High-Resolution Magic-Angle Spinning NMR, *ChemBioChem 11*, 1829-1832.

147. Debelouchina, G. T., Platt, G. W., Bayro, M. J., Radford, S. E., and Griffin, R. G. (2010) Magic Angle Spinning NMR Analysis of Beta-2-Microglobulin Amyloid Fibrils in Two Distinct Morphologies, *J. Am. Chem. Soc. 132*, 10414-10423.

148. Schubert, M., Labudde, D., Oschkinat, H., and Schmieder, P. (2002) A software tool for the prediction of Xaa-Pro peptide bond conformations in proteins based on 13C chemical shift statistics, *J. Biomol. NMR 24*, 149-154.

149. Eisert, R., Felau, L., and Brown, L. R. (2006) Methods for enhancing the accuracy and reproducibility of Congo red and thioflavin T assays, *Anal. Biochem. 353*, 144-146.

150. Wishart, D., Bigam, C., Holm, A., Hodges, R., and Sykes, B. (1995) 1H, 13C and 15N random coil NMR chemical shifts of the common amino acids 1 Investigations of nearest-neighbor effects, *J. Biomol. NMR 5*, 67-81.

151. Dasari, M., Espargaro, A., Sabate, R., Lopez del Amo, J. M., Fink, U., Grelle, G., Bieschke, J., Ventura, S., and Reif, B. Bacterial Inclusion Bodies of Alzheimer's Disease β-Amyloid Peptides Can Be Employed To Study Native-Like Aggregation Intermediate States, *ChemBioChem 12*, 407-423.

152. Tycko, R. (2006) Molecular structure of amyloid fibrils: insights from solid-state NMR, *Q. Rev. Biophys. 39*, 1-55.

153. Hoare, D. G., and Koshland, D. E. (1966) A procedure for selective modification of carboxyl groups in proteins, *J. Am. Chem. Soc. 88*, 2057-2058.

154. Mayer, M., and Meyer, B. (1999) Characterization of Ligand Binding by Saturation Transfer Difference NMR Spectroscopy, *Angew. Chem. Int. Ed. Engl. 38*, 1784-1788.

155. Meyer, B., and Peters, T. (2003) NMR Spectroscopy Techniques for Screening and Identifying Ligand Binding to Protein Receptors, *Angew. Chem. Int. Ed. Engl. 42*, 864-890.

156. Staros, J. V., Wright, R. W., and Swingle, D. M. (1986) Enhancement by N-hydroxysulfosuccinimide of water-soluble carbodiimide-mediated coupling reactions, *Anal. Biochem. 156*, 220-222.

157. Carraway, K. L., and Koshland Jr, D. E. (1968) Reaction of tyrosine residues in proteins with carbodiimide reagents, *BBA-Protein Struct. M. 160*, 272-274.

158. Vranken, W. F., Boucher, W., Stevens, T. J., Fogh, R. H., Pajon, A., Llinas, M., Ulrich, E. L., Markley, J. L., Ionides, J., and Laue, E. D. (2005) The CCPN data model for NMR spectroscopy: Development of a software pipeline, *Proteins 59*, 687-696.

159. Haupt, H., Heimburger, N., Kranz, T., and Baudner, S. (1972) Human serum proteins with affinity for carboxymethyl cellulose. 3. Physico-chemical and immunological characterization of a metal-binding 9.5S- 1-glycoprotein (CM-protein 3), *Hoppe-Seyler's Z. Physiol. Chem. 353*, 1814-1819.

160. Tsoutsoukis, M. (2006) Amyloid recognition by serum amyloid P component, *Unpublished*.

161. Luhrs, T., Ritter, C., Adrian, M., Riek-Loher, D., Bohrmann, B., Dobeli, H., Schubert, D., and Riek, R. (2005) 3D structure of Alzheimer's amyloid-beta(1-42) fibrils, *Proc. Natl. Acad. Sci. U.S.A. 102*, 17342-17347.